REPUBLIC OF IRAQ
MINISTRY OF HIGHER EDUCATION
AND SCIENTIFIC RESEARCH
UNIVERSITY OF BABYLON
COLLAGE OF ENGINEERING

Optical Compensation for Optical Fiber Nonlinearity in Ultra High-Capacity System

A Dissertation

Submitted to the Faculty of Engineering, University of Babylon in Partial Fulfillment of the Requirements for the Degree of Doctorate of Philosophy in Engineering/ Electrical Engineering/ Electronics and Communications

By

Ali Hayder Abdul Kareem Abdul Reda

Supervised by

Prof. Dr. Ibrahim Abdullah Murdas

October 2023 ***Rabi Al-Awal 1445***

بِسۡمِ ٱللَّهِ ٱلرَّحۡمَٰنِ ٱلرَّحِيمِ

قَالُواْ سُبۡحَٰنَكَ لَا عِلۡمَ لَنَآ إِلَّا مَا
عَلَّمۡتَنَآۖ
إِنَّكَ أَنتَ ٱلۡعَلِيمُ ٱلۡحَكِيمُ

صَدَقَ اللهُ العَلِيُ العَظِيمْ

﴿البقرة ٣٢﴾

Supervisor Certification

I certify that this thesis entitled "***Optical Compensation for Optical Fiber nonlinearity in Ultra High-Capacity System***" was prepared by ***Ali Hayder Abdul Kareem Abdul Reda*** under my supervision at the Department of Electrical Engineering, Collage of Engineering, University of Babylon, as a partial fulfillment of the requirements for the degree of Doctorate of Philosophy in Electronics and Communications Engineering.

Signature:

Name: **Prof. Dr.**

Ibrahim Abdullah Murdas

(Supervisor)

Date: 18 / 7 / 2023

In view of the above recommendation, I forward this thesis for discussion by the Examination Committee.

Signature:

Name: **Prof. Dr.**

Qais Kareem Omran

(Head of Electrical Engineering Department)

Date: / / 2023

Examining Committee Certificate

We certify that we have read this thesis entitled "***Optical Compensation for Optical Fiber Nonlinearity in Ultra High-Capacity System***" and as an examining committee, examined the student, "**Ali Hayder Abdul Kareem Abdul Reda**", in its contents and that in our opinion it meets the standard of a thesis for the degree of Doctorate of Philosophy in Engineering/ Electrical Engineering/ Electronics and Communications.

Signature:

Name: **Prof. Dr. Ehab A. Hussein**
(Member)
Date: / 10 / 2023

Signature:

Name: **Prof. Dr. Thamir R. Saeed**
(Member)
Date: / 10 / 2023

Signature:

Name: **Prof. Dr. Haider J. Abd Nasar**
(Member)
Date: / 10 / 2023

Signature:

Name: **Assist. Prof. Dr. Moneer Ali Lil**
(Member)
Date: / 10 / 2023

Signature:

Name: **Prof. Dr. Laith Ali Abdul-Rahaim**
(Chairman)
Date: / 10 / 2023

Signature:

Name: **Prof. Dr. Ibrahim Abdullah Murdas**
(Supervisor)
Date: / 10 / 2023

Signature:

Name: **Prof. Dr. Qais Kareem Omran**
(Head of Electrical Engineering Department)
Date: / 10 / 2023

Signature:

Name: **Prof. Dr. Laith Ali Abdul-Rahaim**
(Dean of College of Engineering)
Date: / 10 / 2023

Dedication

To

My Parents

Without whom none of my success would be possible

My Wife

Who has supported me in all my endeavors

Lovely Children "Zainab & Zahraa"

whom have been constant source of inspiration

Researcher

Acknowledgement

First of all, praise and thanks to Allah (SWT) who gave me the strength and courage to complete this work.

I appreciate the inspirations and guideline that I have received from my supervisor Prof. Dr. Ibrahim A. Murdas for his precious advice and guidance during this work.

I would like to thanks the staff of Electrical Engineering Department at University of Babylon, for providing the support needed to complete this dissertation.

Finally, I would like to express my gratitude and sincere thanks to my family for their daily prayers, invocation, continuous care and generous support during my years of study.

Abstract

Optical communications have grown significantly due to high data rates and long transmission distances. Existing fiber infrastructure limits performance, requiring new technology to meet future demand. A fiber impairment mitigation strategy can increase an optical communication network's capacity and decrease the bit error rate.

This thesis focused on the compensation in multichannel nonlinearity using a dense wavelength division multiplexing technique with 50 GHz channel spacing.

The thesis is divided into two main parts based on the compensation technique used. In the first part, phase conjugation in the highly nonlinear fiber was studied for two different configurations; mid and multiple Optical Phase Conjugation (OPC) process. This work investigated using three methods; conventional, hybrid with dispersion compensation fiber, and hybrid with Raman amplifier. In the second part, a machine learning approach was used based on two different neural algorithms; Convolution Neural Network (CNN) and Nonlinear Auto Regressive with Exogenous (NARX) input.

Results reveal that hybrid OPC with Raman amplifier is optimal over 800 km and multiple OPC is better than mid approach for 16 channels. With 800 Gb/s on (DP-NRZ-OOK), the Q-factor can reach 12.29 dB. Using (SP-8QAM) with a 1.72 Tb/s data rate increased signal quality, attaining 1.3×10^{-3} BER. Lastly, the compensation method (DP-16QAM) with 3.58 Tb/s achieved a 5 dBm increase in launch power and a 13 dB Q factor.

In contrast, the results of neural networks show that the NARX algorithm outperforms CNN in processing, performance, and training ease over 5000

km at (16×120) Gb/s data rate. NARX improved Q-factor and BER to 11.15 dB and 10^{-6} on SP-16 QAM and in SP-64 QAM to 10.29 dB and 10^{-4} surpassing Hard Decision Forward Error Correction (HD-FEC).

The simulation was carried out using the Optisys program (V.19) and the artificial intelligence algorithms were implemented and simulated using MATLAB (V.2022b). The two programs were linked using co-simulations to ensure the validity of the results obtained.

List of Contents

Abstract ……... I

List of Contents ……... III

List of Abbreviations ……... IX

List of Symbols ……... XIII

List of Figures …… XV

List of Tables ……. XX

List of publications ……..... XXI

Chapter One: General Introduction

1.1 Overview ……. 1

1.2 Fundamental Limits …… 3

1.3 Problem Statement ……. 4

1.4 Scope of Study ……. 5

1.5 Literature Survey ...……... 6

1.5.1 Mitigation of Fiber Impairments Based Optical Methods 7

1.5.2 Mitigation of Fiber Impairments Based Machine Learning Methods …… 10

1.6 Thesis Objective …… 14

1.7 Thesis Contributions ……. 14

1.8 Thesis Organization …… 15

Chapter Two: Theoretical Background of Optical System

2.1 Introduction …… 16

2.2 Fiber Channel Modelling ……. 16

2.3 Linear Effects …… 17

2.3.1 Optical Fiber Attenuation ……. 17

2.3.2 Optical Fiber Dispersion …… 18

2.4 Nonlinear Optic Effect …… 20
2.4.1 Self-Phase Modulation (SPM) ……. 22
2.4.2 Cross Phase Modulation (XPM) ...…… 23
2.4.3 Four Wave Mixing (FWM) ……...…… 24
2.5 Ultra High-Capacity Optical Transmission Techniques ...……. 26
2.5.1 Overview of Optical Modulation Formats …… 27
2.5.2 Channel Multiplexing Techniques …… 28
2.5.2.1 Polarization Division Multiplexing (PDM) ... 28
2.5.2.2 Dense Wavelength Division Multiplexing (DWDM) …… 29
2.6 Overcoming Linear Impairments …… 30
2.6.1 Optical Amplification ……. 30
2.6.1.1 Erbium Doped Fiber Amplifiers (EDFAs) …. 31
2.6.1.2 Raman Amplifier …… 31
2.6.2 Dispersion Compensation Fiber (DCF) ….…… 32
2.7 Overcoming Nonlinear Impairments ……. 33
2.8 Optical Phase Conjugation Technique …… 33
2.8.1 Analytical Model for OPC …… 34
2.8.2 Four Wave Mixing in High Nonlinear Fiber (HNLF) …. 38
2.8.3 Fiber Optical Parametric Amplifier (FOPA) …… 38
2.8.3.1 Single Pumped Fiber Optical Parametric Amplifier …… 39
2.8.3.2 Dual Pumped Fiber Optical Parametric Amplifier ……. 40
2.8.4 Implementation of Optical Phase Conjugation …… 41
2.8.4.1 Symmetric OPC Placement …… 41

2.8.4.2 In Line Optical Phase Conjugation …… 42
2.9 Fiber Impairments Compensation Using Machine Learning Techniques …… 42
2.9.1 Learning Algorithms …… 45
2.9.1.1 Supervised Machine Learning …… 45
2.9.1.2 Unsupervised Machine Learning …… 45
2.9.1.3 Reinforcement Machine Learning …… 46
2.9.2 Neural Network (NN) …… 46
2.9.2.1 Activation Function …… 47
2.10 Structure of Neural Network ……... 49
2.10.1 Convolution Neural Network (CNN) …… 49
2.10.1.1 Solver Algorithms …… 52
2.10.2 Recurrent Neural Network (RNN) …… 53
2.10.2.1 NARX Architecture …… 54

Chapter Three: The Proposed Compensation Systems Based on Phase Conjugation

3.1 Introduction ……. 57
3.2 OPC System Design ……..... 58
3.2.1 Transmitter Part ……. 59
3.2.1.1 DP-NRZ-OOK ……... 59
3.2.1.2 SP-mQAM …… 60
3.2.1.3 DP-mQAM ……. 61
3.2.2 DWDM System ……. 62
3.2.3 Fiber Optic Channel Link ……. 63
3.2.4 DeMux DWDM System …… 63
3.2.5 Receiver Part ……. 64

3.2.5.1 DP-NRZ-OOK ……. 64
3.2.5.2 SP-mQAM …… 65
3.2.5.3 DP-mQAM ……... 66
3.3 Optical Compensation Method Using FOPA Based HNLF …… 67
3.4 Mid Span OPC with Proposed System …… 69
3.5 Multiple Span OPC with Proposed System …… 71

Chapter Four: The Proposed Compensation Systems Based on Machine Learning

4.1 Introduction ……. 73
4.2 Machin Learning System Model ……. 73
4.2.1 Transmitter Part …… 74
4.2.2 Channel Multiplexing/ DE Multiplexing and Fiber Links 76
4.2.3 Filtering and Receivers Side ……. 77
4.3 Machine Learning Based Convolutional Neural Network 79
4.3.1 Proposed M-QAM IQ Maps and Targets ……. 80
4.3.2 CNN-ML System Design ……. 81
4.3.3 Training of Network ……. 84
4.4 Machine Learning Based NARX Time Series Network ……. 86
4.4.1 Data Preparation …… 86
4.4.2 Network Architecture …… 88
4.4.3 Training Network ……. 90

Chapter Five: Simulation Results and Discussion

5.1 Introduction ……. 93
5.2 Nonlinearity Compensation of 800 Gb/s DP-NRZ-OOK ……... 95
5.2.1 Mitigation of Fiber Impairments Using Mid OPC …… 96
5.2.2 Fiber Nonlinearity Compensation Based Multiple OPC ... 104

5.2.3 Performance Evaluation Between Mid and Multiple Approach …… 110
5.3 Improvement and Mitigation of Kerr Effects on SP-8QAM Communication Systems …… 117
5.3.1 Mid Way OPC with and without Raman Amplifier …… 118
5.3.2 Multiple OPC with and without Raman Amplifier ……. 123
5.4 Enhanced Mitigation of Nonlinearity Signal Distortion of 3.58 Tb/s for DP-16QAM Communication System …… 129
5.4.1 Compensation of Fiber Impairments Using Mid OPC …. 131
5.4.2 Compensation of Fiber Impairments Using Multiple OPC ……... 135
5.5 Summarization and Contributions of OPC Technique …… 140
5.6 Mitigation and Compensation of Linear and Nonlinear Effects Based Convolutional Neural Network …… 142
5.6.1 CNN-NLC for Single Polarization 16QAM …… 142
5.6.1.1 Five CNN Layers …… 146
5.6.1.2 Six CNN Layers …… 147
5.6.2 Results of Implementation CNN-16QAM …… 150
5.6.3 CNN-NLC for Single Polarization 64QAM ……. 154
5.6.4 Results of Implementation CNN-64QAM …… 158
5.7 Fiber Impairment Compensation Using NARX Time Series Network ……. 163
5.7.1 Mitigation Fiber Impairment for Single Polarization-16QAM …… 163
5.7.2 Results of Implementation NARX-16QAM …… 169

5.7.3 Compensation of Fiber Impairment for Single Polarization 64QAM 173
5.7.4 Results of Implementation NARX-64QAM 178
5.8 Summarization and Contributions of Machin Learning Method Based on Neural Network Algorithms 182
Chapter Six: Conclusions and Future Works
6.1 Conclusion 184
6.2 Recommendations for Future Works 185
References 187
Appendix A A-1
Appendix B B-1

List of Abbreviations

Term	Meaning
AI	Artificial Intelligence
ANN	Artificial Neural Network
ASE	Amplified Spontaneous Emission
ASK	Amplitude Shift Keying
ATM	Automated Teller Machine
BER	Bit Error Rate
BSG	Bit Sequence Generator
CD	Chromatic Dispersion
CNN	Convolution Neural Network
CO-OFDM	Coherent Optical Orthogonal Frequency Division Multiplexing
CW	Continues Wave
DBP	Digital Back Propagation
DCF	Dispersion Compensation Fiber
DCM	Dispersion Compensating Module
DEMUX	Demultiplexer
DFG	Difference Frequency Generation
DFWM	Degenerate Four Wave Mixing
DNN	Deep Neural Network
DP	Dual Polarization
DQPSK	Differential Quadrature Phase Shift Keying
DRA	Distributed Raman Amplifiers
DSP	Digital Signal Processing
DWDM	Dense Wavelength Division Multiplexing
EDFA	Erbium Doped Fiber Amplification
EVM	Error Vector Magnitude
FBG	Fiber Bragg Grating

Term	Meaning
FKVNE	Full Kernel Volterra Nonlinear Equalizer
FOPA	Fiber Optical Parametric Amplifier
FSK	Frequency Shift Keying
FSO	Free Space Optics
FWM	Four Wave Mixing
GVD	Group Velocity Dispersion
HD-FEC	Hard Decision Forward Error Correction
HNLF	Highly Nonlinear Fiber
ICS	Integrated Communication and Sensing
IFWM	Intra Four Wave Mixing
IOT	Internet of Things
I/Q	In phase / Quadrature phase modulator
ISI	Inter Symbol Interference
IXPM	Intra Cross Phase Modulation
LE	Linear Equalization
LM	Levenberg Marquardt
LPF	Low Pass Filter
LSTM	Long Short-Term Memory
ML	Machine Learning
MLPC	Mid-Link Phase Conjugation
MPs	Memory Polynomials
MSE	Mean Square Error
MSSI	Mid Span Spectral Inversion
MUX	Multiplexer
MZI	Mach Zehnder interferometer
MZM	Mach-Zehnder Modulator
NAR	Nonlinear Autoregressive
NARX	Nonlinear Auto Regressive with Exogenous
NDFWM	Non Degenerate Four Wave Mixing

Term	Meaning
NF	Noise Figure
NFT	Nonlinear Fourier Transform
NIO	Nonlinear Input-Output
NLC	Nonlinear Compensation
NLE	Nonlinear Equalizers
NLF	Nonlinear Fourier Transform
NLSE	Nonlinear Schrodinger Equation
NN	Neural Network
NRZ	Non-Return to Zero
OA	Optical Amplifier
OBF	Optical Bandpass Filter
OBP	Optical Back Propagation
OF	Optical Filter
OFDM	Orthogonal Frequency Division Multiplexing
OFS	Optical Fiber Systems
OOK	On Off Keying
OPC	Optical Phase Conjugation
OSNR	Optical Signal to Noise Ratio
OTR	Optical to RF down converter
PAPR	Peak-to-Average Power Ratio
PC	Polarization Combiner
PCA	Principal Component Analysis
PCTW	Phase Conjugated Twin Wave
PD	Photo Detector
PDM	Polarization Division Multiplexing
PIN	P-N Diode
PMD	Polarization Mode Dispersion
PRBS	Pseudo Random Bit Sequence
PSA	Parametric Sensitive Amplifier

Term	Meaning
PSK	Phase Shift Keying
QAM	Quadrature Amplitude Modulation
Q_OT	Quality of Transmission
ReLu	Rectified Linear Unit
RMS	Root Mean Square
RNN	Recurrent Neural Network
RTO	RF to Optical up converter
SBS	Simulated Brillion Scattering
SDM	Space Division Multiplexing
SGD	Stochastic Gradient Descent
SI	Spectral Inversion
SMF	Single Mode Fiber
SOA	Semi-Conductor Optical Amplifier
SP	Single Polarization
SPF	Sample Per Frame
SPM	Self-Phase Modulation
SPS	Sample Per Sample
SRS	Simulated Raman Scattering
SSMF	Standard Single Mode Fiber
SVM	Support Vector Machine
TNN-SL	Triplet-input Neural Network Supervised Learning
TNN-UL	Triplet-input Neural Network Unsupervised Learning
VMM	Vector Matrix Multiplication
VNLE	Volterra Nonlinear Equalizer
WDM	Wavelength Division Multiplexing
XPM	Cross Phase Modulation

List of Symbols

Symbol	Meaning
A_{eff}	Effective mode area
α	Fiber attenuation constant
$\sigma(.)$	Nonlinear activation function
$\beta(w)$	Propagation constant at the optical carrier frequency
β_1	First order dispersion parameter
β_2	Second order dispersion parameter
β_3	Third order dispersion parameter
b_k	Bias or threshold
c	Light velocity in vacuum
D	Dispersion parameter
E	Optical field
ϵ_0	Vacuum permittivity
f_P	Photon frequency
f_S	Signal frequency
f_i	Idler wave frequency
G	Optical amplifier gain
I	Optical intensity
L	Optical fiber length
L_{NL}	Nonlinear length
L_{eff}	Effective length of the fiber
L_{DCF}	Dispersion compensating fiber length
L_{SMF}	Single mode fiber length
$n\ (w)$	Refractive index of the silica fiber
$\tilde{n}_2$	Nonlinear index coefficient
n_2	Nonlinear Kerr index
$\emptyset_{NL}$	Nonlinear phase shift
$\tilde{P}$	Medium polarization

Symbol	**Meaning**
P_{in}	Input optical power
P	Propagating wave's power
S	Dispersion slope
T	Matrix transpose
v_g	Group velocity dispersion parameter
v_p	Phase velocity
w_{km}	Weight of neuron
w_o	Angular frequency of the optical carrier
x_m	Input signal of neuron
X_{eff}	Effective susceptibility
y_k	Signal output of neuron
γ	Nonlinear coefficient
λ	Optical signal wavelength
λ_{ZDW}	Zero dispersion wavelength

List of Figures

Figure	Name	Page
Figure (1.1)	Evolution of commercial optical transmission systems	2
Figure (1.2)	(a) Quality of the received signal with constellation spots. (b) The central idea of this study is based on fiber mitigation in three areas: the number of DWDM channels, modulation type, and data rate	4
Figure (1.3)	Block diagram the scope of study	6
Figure (2.1)	Relationship between optical wavelength and fiber attenuation	18
Figure (2.2)	Signal power as a function of the transmission distance	22
Figure (2.3)	(a) Schematic energy level diagrams and (b) spectra of FWM, the arrows show the energy transfer directions	26
Figure (2.4)	Degenerate and non-degenerate FWM components. Input fields are blue	26
Figure (2.5)	Optical transmission capacity enhancement in six dimensions	27
Figure (2.6)	Polarization division multiplexing with polarization controller and optical modulator	28
Figure (2.7)	Block diagram for dense wavelength division multiplexing system	29
Figure (2.8)	Fiber optic amplifier configurations (a)booster amplifiers, (b) pre-amplifiers, (c) in-line type A amplifiers, and (d) in-line type B amplifiers	30
Figure (2.9)	Three dispersion compensation techniques using DCF	32
Figure (2.10)	Two spans of transmission with (OPC); left is the original signal and right is conjugate (idler)	35
Figure (2.11)	Concept of OPC with single pumped FOPA	39
Figure (2.12)	Concept of OPC with dual pumped FOPA	40
Figure (2.13)	Schematic representation of mid-span spectral inversion (MSSI) optical phase conjugation	41
Figure (2.14)	Schematic representation of in line optical phase conjugation	42
Figure (2.15)	Fiber optic communications systems using AI techniques	44
Figure (2.16)	Structures of supervised learning, unsupervised learning, and reinforcement learning	45
Figure (2.17)	Basic neural network structure	47
Figure (2.18)	(a) tanh and sigmoid functions (b) ReLu function	48
Figure (2.19)	Architecture of CNN neural network	50

Figure	Name	Page
Figure (2.20)	A graphical illustration of (a) artificial recurrent neural network (b)RNN 'unfolded' in time	54
Figure (2.21)	NARX neural network architecture	55
Figure (3.1)	The proposed system based OPC	58
Figure (3.2)	Block diagram of the transmitter part for DP-OOK	59
Figure (3.3)	Block diagram of the transmitter part for SP-mQAM system	60
Figure (3.4)	Block diagram of the transmitter part for DP-mQAM system	61
Figure (3.5)	Block diagram of the receiver part for DP-OOK	64
Figure (3.6)	Block diagram of the receiver part for SP-mQAM system	66
Figure (3.7)	Block diagram of the receiver part for DP-mQAM system	66
Figure (3.8)	Polarization fiber optic parametric amplifier configuration with two pumps and HNLF	68
Figure (3.9)	Proposed system model of Mid OPC with three scenarios	70
Figure (3.10)	Proposed system model of Multiple OPC with three scenarios	72
Figure (4.1)	The proposed compensation system based neural network	74
Figure (4.2)	QAM transmitter signal	75
Figure (4.3)	Multiplexer and De multiplexer with fiber links	77
Figure (4.4)	QAM receiver signal	78
Figure (4.5)	Subsystem with MATLAB component and received bits producing	79
Figure (4.6)	16QAM reference target and classes	80
Figure (4.7)	64 QAM reference target and classes	81
Figure (4.8)	The proposed CNN layers architecture	83
Figure (4.9)	Flow chart of NARX model	87
Figure (4.10)	Training structure of the NARX model	89
Figure (4.11)	NARX neural network configuration	91
Figure (5.1)	Optical system under study	94
Figure (5.2)	Optical spectrum analyzer (a) before OA (b) before GOF (c) after GOF	96
Figure (5.3)	Optical spectrum output for 16 channels	97
Figure (5.4)	Optical spectrum analyzer of the output signal from SMF	97

Figure	Name	Page
Figure (5.5)	Optical spectrum analyzer of pump1 and pump 2	98
Figure (5.6)	Optical spectrum analyzer (a) input of HNLF (b) output of HNLF	98
Figure (5.7)	The optical spectrum analyzer of the idler conjugated the OPC's output	99
Figure (5.8)	Eye diagram and Q-factor for conventional OPC (a) Ch.1 (b) Ch.8 (c) Ch.16	100
Figure (5.9)	Eye diagram and Q-factor for hybrid (OPC + DCF) (a) Ch.1 (b) Ch.8 (c) Ch.16	102
Figure (5.10)	Eye diagram and Q-factor for hybrid (OPC + Raman amplifier) (a) Ch.1 (b) Ch.8 (c) Ch.16	103
Figure (5.11)	Optical spectrum analyzer of second OPC (a) before HNLF (b) after HNLF (c) received optical signal	105
Figure (5.12)	Eye diagram and Q-factor for conventional multiple OPC (a) Ch.1 (b) Ch.8 (c) Ch.16	106
Figure (5.13)	Eye diagram and Q-factor for hybrid multiple OPC with DCF (a) Ch.1 (b) Ch.8 (c) Ch.16	108
Figure (5.14)	Eye diagram and Q-factor for hybrid multiple OPC with Raman amplifier (a) Ch.1 (b) Ch.8 (c) Ch.16	109
Figure (5.15)	Q-factor versus signal input power for conventional mid OPC and mid OPC with DCF	110
Figure (5.16)	Q-factor versus signal input power for conventional mid OPC and mid OPC with Raman amplifier	111
Figure (5.17)	Q-factor versus signal input power for hybrid mid OPC+DCF and Raman amplifier	112
Figure (5.18)	Q-factor versus signal input power for conventional mid and multiple OPC	113
Figure (5.19)	Q-factor versus signal input power for hybrid mid OPC and multiple OPC with DCF	114
Figure (5.20)	Q-factor versus signal input power for hybrid mid OPC and multiple OPC with Raman amplifier	115
Figure (5.21)	Q-factor versus signal input power for mid OPC with three cases (conventional, DCF, and Raman amplifier)	116
Figure (5.22)	Q-factor versus signal input power for multiple OPC with three cases (conventional, DCF, and Raman amplifier)	116
Figure (5.23)	Constellation diagram of the received 8QAM signal transmission back-to-back for (a) Ch.1 (b) Ch.8 (c) Ch.16	117
Figure (5.24)	Constellation diagram of the received 8QAM signal over 800 km SMF (a) Ch.1 (b) Ch.8 (c) Ch.16	118

Figure	Name	Page
Figure (5.25)	Optical spectrum analyzer (a) input of HNLF (b) output of HNLF	119
Figure (5.26)	Constellation diagram for channels (1, 8, and 16)	119
Figure (5.27)	Q-factor and constellation diagram for mid OPC with and without Raman amplifier for (a) Ch.1 (b) Ch.8 (c) Ch.16	122
Figure (5.28)	Q-factor for conventional mid and multiple OPC for (a) Ch.1 (b) Ch.8 (c) Ch.16	124
Figure (5.29)	Q-factor and constellation diagram for multiple OPC with and without Raman amplifier for (a) Ch.1 (b) Ch.8 (c) Ch.16	127
Figure (5.30)	Q-factor for mid OPC and multiple OPC with Raman amplifier for (a) Ch.1 (b) Ch.8 (c) Ch.16	129
Figure (5.31)	Constellation diagram of the received 16QAM signal transmission back-to-back for the middle channel	130
Figure (5.32)	Constellation diagram of the received 16QAM signal over 800 km SMF for the middle channel	131
Figure (5.33)	Q-factor versus signal input power for mid OPC with and without DCF (a) Ch.1 (b) Ch.8 (c) Ch.16	132
Figure (5.34)	Q-factor versus signal input power for mid OPC with three cases (conventional, DCF, and Raman amplifier) (a) Ch.1 (b) Ch.8 (c) Ch.16	134
Figure (5.35)	Q-factor and constellation diagram for conventional mid and multiple OPC for (a) Ch.1 (b) Ch.8 (c) Ch.16	136
Figure (5.36)	Q-factor and constellation diagram for hybrid OPC with DCF for mid and multiple methods for (a) Ch.1 (b) Ch.8 (c) Ch.16	138
Figure (5.37)	Q-factor and constellation diagram for hybrid OPC with Raman amplifier for mid and multiple method for (a) Ch.1 (b) Ch.8 (c) Ch.16	140
Figure (5.38)	16QAM-DWDM optical spectrum output for 16 channels	143
Figure (5.39)	Constellation diagram of the received 16QAM signal over 1000 km SMF for the middle channel	144
Figure (5.40)	Final training progress of 5 CNN @1e-3 (a) accuracy (b) loss	147
Figure (5.41)	Final training progress of 6 CNN @1e-3 (a) accuracy (b) loss	149
Figure (5.42)	BER patterns in 16QAM-CNN for (a) Ch.1 (b) Ch.8 (c) Ch.16	152
Figure (5.43)	Q-factor in 16QAM-CNN for three channels	153
Figure (5.44)	Error vector magnitude (EVM) in 16QAM-CNN for three channels	153
Figure (5.45)	Constellation diagram in 16QAM-CNN for (a) Ch.1 (b) Ch.8 (c) Ch.16	154

Figure	Name	Page
Figure (5.46)	Constellation diagram of the received 64QAM signal over 5000 km SMF for the middle channel	155
Figure (5.47)	Final training progress of six CNN at 1e-3 learning rate for 64QAM (a) accuracy (b) loss	157
Figure (5.48)	BER patterns in 64QAM-CNN for (a) Ch.1 (b) Ch.8 (c) Ch.16	160
Figure (5.49)	Q-factor in 64QAM-CNN for channels 1, 8, and 16	161
Figure (5.50)	Error vector magnitude (EVM) in 64QAM-CNN for channels 1, 8, and 16	162
Figure (5.51)	Constellation diagram in 64QAM-CNN for (a) Ch.1 (b) Ch.8 (c) Ch.16	162
Figure (5.52)	NARX performance for 16QAM after the end of training for (a) real part (b) imaginary part	166
Figure (5.53)	MSE vs. number of epochs for (a) real part (b) imaginary part	167
Figure (5.54)	Error histogram with 20 Bins (a) real training (b) imaginary training	168
Figure (5.55)	BER patterns in 16QAM-NARX algorithm for (a) Ch.1 (b) Ch.8 (c) Ch.16	171
Figure (5.56)	Q-factor in 16QAM based on NARX algorithm for three channels	172
Figure (5.57)	Error vector magnitude (EVM) in 16QAM based on NARX algorithm for three channels	172
Figure (5.58)	Constellation diagram in 16QAM based on NARX algorithm for (a) Ch.1 (b) Ch.8 (c) Ch.16	173
Figure (5.59)	NARX performance for 64QAM after the end of training for (a) real part (b) imaginary part	175
Figure (5.60)	MSE vs. number of epochs for (a) real part (b) imaginary part	176
Figure (5.61)	Error histogram with 20 Bins (a) real training (b) imaginary training	177
Figure (5.62)	BER patterns in 64QAM-NARX algorithm for (a) Ch.1 (b) Ch.8 (c) Ch.16	179
Figure (5.63)	Q-factor in 64QAM based on NARX algorithm for three channels	180
Figure (5.64)	Error vector magnitude (EVM) in 64QAM based on NARX algorithm for three channels	181
Figure (5.65)	Constellation diagram in 64QAM based on NARX algorithm for (a) Ch.1 (b) Ch.8 (c) Ch.16	181

List of Tables

Table	Name	Page
Table (3.1)	DWDM system optical multiplexer and demultiplexer simulation parameters	62
Table (3.2)	Parameters of fiber optic link	63
Table (3.3)	Simulated parameter of OPC with the proposed system	68
Table (4.1)	M-QAM main parameter of NN proposed system	76
Table (5.1)	Comparison of proposed work with previously published work	141
Table (5.2)	Performance of 16QAM for 5 CNN layers @learning rate 1e-4	146
Table (5.3)	Performance of 16QAM for 5 CNN layers @learning rate 1e-3	146
Table (5.4)	Performance of 16QAM for 6 CNN layers @learning rate 1e-4	148
Table (5.5)	Performance of 16QAM for 6 CNN layers @learning rate 1e-3	148
Table (5.6)	Performance of 64QAM for 6 CNN layers @learning rate 1e-4	156
Table (5.7)	Performance of 64QAM for 6 CNN layers @learning rate 1e-3	156
Table (5.8)	Comparison of proposed work with previously published work	183

List of Publications

1- Kareem, Ali Hayder Abdul, and Ibrahim A. Murdas. "**A Comprehensive Survey of Fiber Impairment Mitigation Technologies in High Capacity Systems**." *2022 Muthanna International Conference on Engineering Science and Technology (MICEST)*. IEEE, 2022.

2- Ali Hayder Abdu Kareem and Ibrahim A. Murdas. "**Optical Phase Conjugation Technique for Fiber Nonlinearity Compensation in DWDM Transmission Systems**." *4th International Scientific Conference of Alkafeel University (ISCKU 2022)*, AIP Conference Proceedings.

3- Kareem, A. H. A., and I. A. Murdas. "**Investigation of Fiber Impairment Mitigation Based on Optical Phase Conjugation Technique**." *International Journal of Microwave and Optical Technology* 18.2 (2023): 184-194.

4- Kareem, Ali Hayder Abdul, and Ibrahim A. Murdas. "**Performance evaluation of fiber impairment mitigation for high capacity communication systems using optical compensation method**." *Results in Optics* 11 (2023): 100399.

5- Kareem, Ali Hayder Abdul, and Ibrahim A. Murdas. "**Improvement and Mitigation of Kerr Effects on Multichannel Communication Systems Using Efficient Optical Method**." *Journal of University of Babylon for Engineering Sciences* (2023): 72-91.

6- Hayder, Ali, and Ibrahim Abdullah. "**Raman Amplification for Nonlinearity Compensation in a Fiber Optic Link by Optical Phase Conjugation System**." *Kerbala Journal for Engineering Science* 3.2 (2023): 62-78.

7- Kareem, Ali Hayder Abdul, and Ibrahim A. Murdas. "**Enhanced Mitigation of Nonlinearity Signal Distortion by Hybrid Optical Compensation Technique**." *Przeglad Elektrotechniczny* 2023.8 (2023).

8- Ali Hayder Abdul Kareem and Ibrahim A. Murdas. "**Machine Learning Technique Based on Advanced Neural Network Algorithms to Mitigate Fiber Impairments in Optic Channels**." *Engineering Journal* (Under Review).

Chapter One

General Introduction

1.1 Overview

The demand for network capacity has been increasing in recent decades due to the growth of new digital applications and services. The communication infrastructure relies on optical fiber networks, which are under unprecedented strain from bandwidth intensive applications [1]. Every day, there are more people utilizing the internet with more internet connected devices and applications. Globally, the total number of Internet users is expected to increase by 6% every year, from 3.9 billion in 2018 to 5.3 billion in 2023. This resulted in an average of 2.4 devices and connections per capita increasing to 3.6 by 2023 [2]. Optical fiber networks carry most internet traffic. Fiber-optic communication innovations have enabled these data traffic demands [3]. WDM technology was the first to improve fiber capacity. After reintroducing coherent detection, multi-level modulation and polarization-multiplexing transmission increased capacity to reach 100 Gb/s [4]. Researchers have concentrated on more spectrally efficient technologies to enhance available capacity at low cost and low complexity. Next-generation WDM communication systems proposed use space division multiplexing (SDM) techniques like multi-core fibers and multi-mode fibers [5]. The data rate increases with the number of modes/cores in multi-mode/core fibers. Recently, few-mode fiber technology has advanced. SDM technique still needs to build the optical amplifier for long-haul transmission. SDM techniques require replacing single-mode fibers (SMF) with multi-mode/core

fibers, making them expensive for near-term implementation. Thus, SMF remains the technology of choice for long-haul WDM communication networks of the future. Figure 1.1 Illustrated the development of commercial optical transmission systems over the past 37 years and extrapolations for the coming 15 years [6]. Fiber-optic communication technology, which carries data across thousands of kilometers, lies at the core of this global infrastructural network known as the backbone. Despite the tremendous growth in the capabilities of optical fiber communications technology, it faces many challenges posed by the continuous increase in the demand for bandwidth and communication services around the world such as the Internet of Things (IoT) [7], which poses challenges to the present infrastructure and available response times.

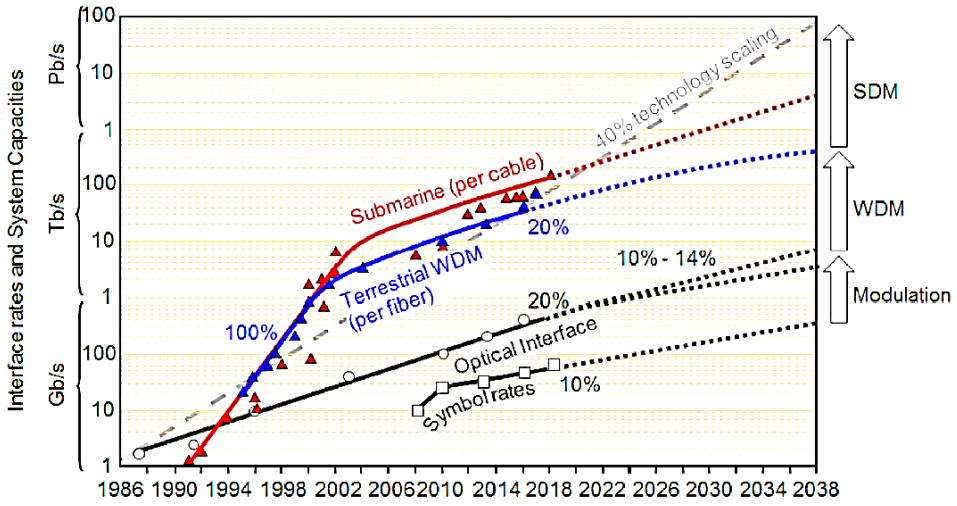

Figure (1.1). Evolution of commercial optical transmission systems [6]

The main obstacles to optical system capacity improvement are fiber link linear and nonlinear impairments [8]. Several nonlinearity compensation strategies have been developed in both the optical and digital domains to counteract dispersion and nonlinearities [9]. Digital compensation is flexible configuration and efficient for a simple system, while optical compensation is

stable, suitable for high transmission rates, and effective for a variety of division multiplexing impairments. As another option, algorithms based on Artificial Intelligence (AI) are utilized to distinguish and address optical problems. In addition to signal design, traffic control, and monitoring, AI has shown great promise for enhancing nonlinear compensation performance in optical communications by enabling statistically flexible analysis of complex systems without reliance on specified models [10, 11]. Therefore, this thesis employs a two-pronged strategy to investigate fiber dispersion and nonlinearity mitigation in optical fiber communication systems.

1.2 Fundamental Limits

The signal when propagating in fiber is attenuated due to a small loss of 0.2 dB/km. Optical amplifiers are used to compensate for the fiber loss [12]. Figure (1.2-a) illustrates how the received signal quality degrades at low signal levels due to the noise introduced by the amplifiers. When the signal strength of a constellation is low, the noise cloud surrounding those points has a Gaussian distribution with a circular symmetry. In a straight path (blue dashed lines), the signal quality increases as the signal strength increases. The Kerr nonlinearity reduces the signal quality at increasing signal power. In the nonlinear regime, the Kerr effect causes the constellation points to take on a banana form [13]. Recently, Nonlinear Compensation (NLC) has been extensively studied as a key strategy for enhancing optical transmission system capacity. Nonlinear impairments are the biggest challenges and capacity restrictions for optical transmission systems. The three primary focuses of current research and development efforts to enhance optical communications systems are depicted in figure (1.2-b). The main system

design challenge is to further increase the bit rate, which will be the main approach adopted in this thesis by mitigating fiber impairments.

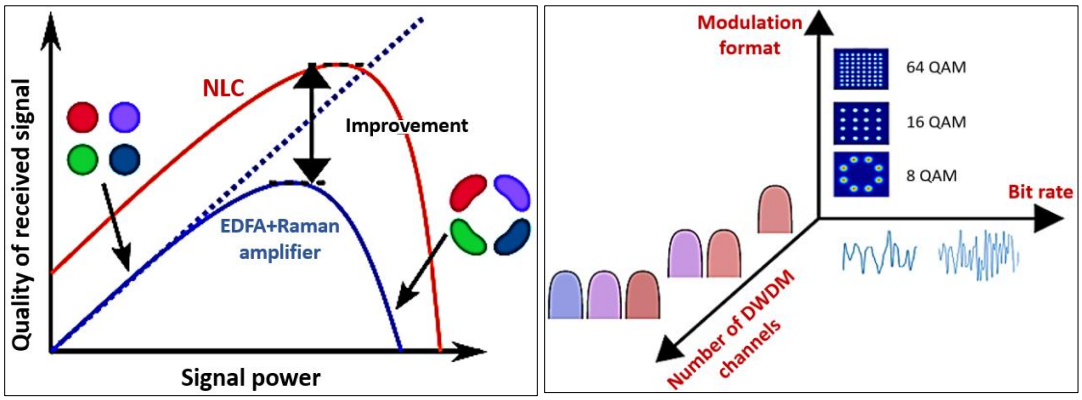

(a) **(b)**

Figure (1.2). (a) Quality of the received signal with constellation spots. (b) The central idea of this study is based on fiber mitigation in three areas: the number of DWDM channels, modulation type, and data rate.

1.3 Problem Statement

A significant impairment that limits the transmission performance of the long-haul optical communication system is fiber nonlinearity. The nonlinearity effects are due to an electro-optic effect, referred to as the Kerr effect, which arises from the dependence of the optical fiber refractive index on the transmit signal power. The detrimental effects of Kerr-induced signal nonlinear distortions grow at a faster rate than the signal to noise ratio capacity gain at higher launch powers. These conditions produce effects such as SPM (Self Phase Modulation), XPM (Cross Phase Modulation), and FWM (Four-wave Mixing). The achievable transmission rate decreases rapidly beyond the optimal power point as the launch power increases due to the corresponding increase in the Kerr induced signal nonlinear distortions. SPM is phase modulation of light caused by an instant change in the light intensity to

gradually broaden the signal spectrum. XPM occurs when the intensity of a beam influences the phase of another beam. FWM is the most prominent effect that occurs when sending multiple wavelengths on a single fiber, so on the receiver side a harmonic signal is generated with different frequencies.

The transmission performance of the single channel optical communication systems is mainly limited by the intra channel Kerr nonlinearity effect. In a Dense Wavelength Division Multiplexing (DWDM) super channel system, a significant portion of the nonlinear distortion comes from the nonlinear interaction between the channel under consideration and the co-propagating signals in adjacent channels referred to as inter channel nonlinearity effects. So, the detrimental effects of the inter channel Kerr nonlinearity limit optical communication systems' capacity.

1.4 Scope of Study

Studying the various facets of optical fiber communication systems is highly recommended. In order to present a comprehensive picture of the research scope with a simplified approach, figure (1.3) depicts the study's model. This block diagram provides a description of the relationship between the primary concerns in the field of fiber optic communication and the work of the researcher in this thesis. The items that are solid allude to the primary concerns on which this thesis has concentrated.

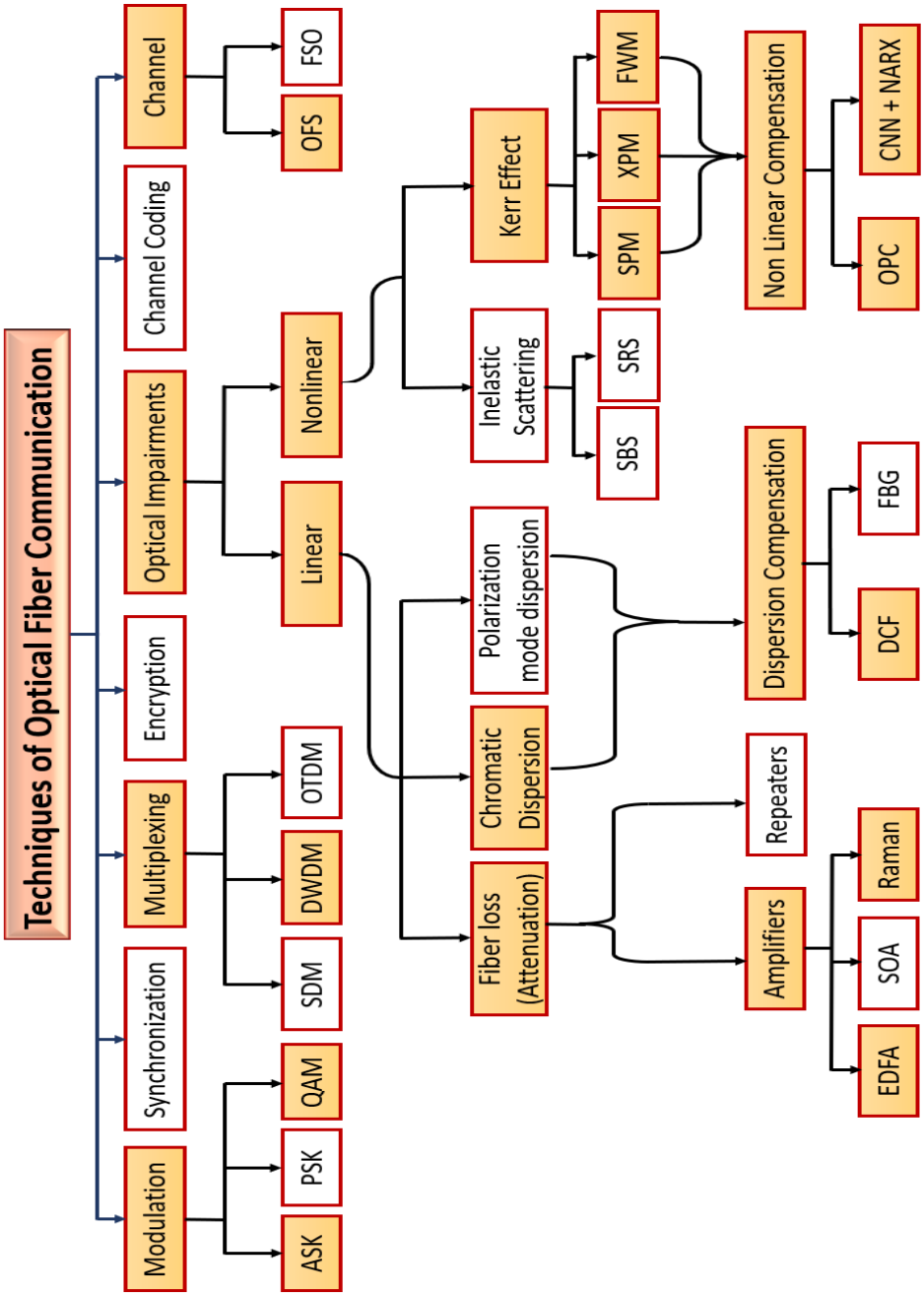

Figure (1.3). Block diagram the scope of study.

1.5 Literature Survey

This part provides a chronological overview of the relevant prior literature in the thesis's topic of study. The literature review is divided into two subsections:

1.5.1 Mitigation of Fiber Impairments Based Optical Methods

Kim, Inwoong, et al. (2018) [14], proposed enhanced pre-spectral inversion (E-PSI) to balance span dispersion to achieve virtually optimal link symmetry compared to (SI) and much improved nonlinearity compensation in non-uniform transmission networks. All optical repeaters received minimal dispersion adjustments to balance spans. Midspan E-PSI increased optical reach by 80% and compensated subcarrier inter and intra nonlinearity in 1Tb/s DP-16QAM super channel transmission via nonuniform networks.

Sabapathi, T., and R. Poovitha (2019) [15], proposed of eliminating FWM and SRS effects. In the first way, input power increases the FWM effect. Alternating transmitter circular polarizers before fiber link transit reduces FWM impact. Optimal input power allocation may reduce SRS. Allocating transmitted power randomly reduces SRS-induced power skew. Uniform-spaced multichannel networks were simulated and discovered the best power level allocation enhances system performance when the input power level between 0–4 dBm.

Ajmani, Manisha, et al. (2019) [16], improved FWM reduction and Q-factor over 180 km by combining DCF, FBG, and OPC. The results illustrated that hybrid DCF + OPC is more stable than FBG + OPC and DCF + FBG at different input power levels, according to the parametric analysis. Bitrate and channel variation had the same effect. Also, hybrid FBG + OPC works better when channel spacing is changed.

Huszanik et al. (2019) [17], proposed limiting FWM effect on optical signal transmission modulated 32 channels for DQPSK-modulated ultra-dense WDM system with 40 Gb/s per channel (1.28 Tb/s total). Results show that

adjusting CW launch power during launch reduces FWM. As well, DWDMs with spaced frequency of 50 and 100 GHz are less affected by FWM and better for long-distance transmission in fiber nonlinear environments.

Foo, Benjamin, et al. (2019) [18], conducted a detailed study of nonlinearity mitigation employing parametric amplifiers (PSAs) and a modified third-order Volterra nonlinear equalizer (VNLE) in the receiver. VNLE decreases residual distortions of nonlinear in networks using PSAs for modulation formats and multiple symbol rates, increasing transmission distance by up to 80%. This system can reduce residual distortions of nonlinear on a (10, 28, 50) Gbaud 16QAM signal across an 800 km link. The suggested method minimized dispersion pre-compensation reliance and increased maximum Q_{BER} by 0.4 dB using 10 Gbaud.

Kaminski, Pawel M., et al. (2020) [19], showed a module for pre-compensating all-optical nonlinearity in modern long-reach lasers. Raman amplified unrepeated links via OPC. FBG matches dispersion, DCF pre-distorts nonlinearly, and OPC reverses phase, are the three major components. The system's symmetry, compensation structure, and nonlinearity suppression were engineered. The compensator maximizes WDM transmission performance by maximizing propagation symmetry, improving SNR by 2.6 dB and 4.0 dB for 350 km and 250 km lines, respectively.

Amiri, I. S., et al. (2020) [20], examined and compared all hybrid fiber optic amplifiers in single/multi amplification stages. EDFA+ Raman, EDFA+ Raman+ EDFA, and Raman+ EDFA+ Raman combinations upgrade optical communication systems. Hybrid optical fiber amplifier structure improves optical system efficiency, according to the study. Results shows that Raman/EDFA/Raman setup improves performance 42%.

Wang, Jingjing, et al. (2021) [21], presented 640 Gbps 16-QAM CO-OFDM via 800 km fiber optic with mid link optical phase conjugation (OPC) utilizing extremely nonlinear fiber media called (HNLF). OPC characteristics like signal/pump power inputs and HNLF length are optimized first. Second, ASE noise, fiber dispersion, and nonlinearity affect long haul signal transmission and OPC compensation efficiency. Results demonstrate that mid link OPC improves BER by 6.1×10^{-4} and Q-factor by 3 dB compared to no OPC.

Venkatasubramani, Lakshmi Narayanan, et al. (2021) [22], showed SOA-based OPC dispersion and nonlinearity distortion compensation for coherent OFDM transmissions. Multi-carrier modulation requires different PAPR, digital signal processing, and phase noise than single carrier systems. It experimentally showed mid-span spectral inversion (MSSI)-aided CD compensation and fiber Kerr nonlinear distortion of 40 Gb/s QPSK CO-OFDM and 80 Gb/s 16QAM CO-OFDM signals. QPSK CO-OFDM signal released at 3 dBm strength can reach 1000 km, according to simulations. 16QAM CO-OFDM with SOA-based OPC has a 4.5 dB power margin.

Tan, Mingming, et al. (2022) [23], designed distributed Raman amplifiers (DRAs) to reduce signal power and improve link symmetry for transmission systems with mid link phase conjugators. Backward Raman pumping on a 50 km single span link only increases nonlinear product compensation by 12 dB compared to standard first-order DRA. This system shows a random fiber laser amplifier is the optimum choice for WDM systems with mid link OPC and span lengths between 60 km and 100 km, reducing Kerr product by 37.6 dB at 62 km.

Gordienko, Vladimir, et al. (2023) [24], Introduces Mach Zehnder interferometer (MZI) based interferometric fiber optic parametric amplifier

(FOPA) to suppress unwanted four wave mixing products. Eliminating wavelength specific combiners and filters for the pump and signals reduces noise figure, insertion loss, and pump wavelength tuneability in the suggested system topologies. The simulation findings indicated that practical pump phase shifters and couplers suppress idlers by >28 dB throughout at least 10 THz, allowing 16QAM signals to reuse idler frequencies with penalty <0.3 dB at BER of 10^{-3}.

Cao, Wenhua (2023) [25], studied the effects of mid-span OPC on EDFA-amplified dispersion managed quasilinear transmission networks with intrachannel nonlinearity compensation. To increase the performance of the DCF managed connection, nonlinearity mismatch across the spans can be counterbalanced by launching different powers into the spans before and after the OPC. Researchers found that the optimal energy ratio improved with input energy but was unaffected by link span size.

1.5.2 Mitigation of Fiber Impairments Based Machine Learning Methods

Närhi, Mikko, et al. (2018) [26], created a new method based on machine learning (ML) algorithms and demonstrated how ML might get over the limitations of utilizing spectrum intensity measurements alone to assess the time-domain aspects of the optical fiber modulation instability. In addition, unsupervised learning was used to partition the noisy modulation instability spectra into groups that accurately reflected their underlying temporal dynamic features.

Sidelnikov et al. (2018) [27], designed a neural network with delay taps to efficiently inverse nonlinear effects. This research compares linear compensation, digital back-propagation, and deep neural networks in long-

haul transmission systems. Results indicate a static neural networks equalizer outperform linear equalizers and cannot correct for nonlinear channel response. Furthermore, dynamic neural network architecture through 1000 km improved Q factor by 1.5 dB and 1.4 dB for single and multi-channel transmission, respectively.

Zhang, Shaoliang, et al. (2019) [28], used machine learning algorithms to determine DP-16QAM nonlinear impairment. After a 2800 km SSMF transmission link at 32 Gbaud signal data, researchers suggested a single-step, system-agnostic NLC technique based on NN that improved performance by (~0.6) dB Q-factor compared to the single-step filtered DBP approach. The input features used are Intra four wave mixing (IFWM) and cross phase modulation (IXPM).

Schaedler, Maximilian, et al. (2019) [29], proposed a DNN-NLE in a coherent DP-16QAM 88 Gbaud 600 Gbps optical system. Full kernel Volterra non-linear equalizers (FKVNEs) and memory polynomials (MPs) were compared to the suggested design. DNN-NLEs reflect systematic non-linearities better than 5^{th} MP and FKVNEs. It outperforms by 0.8 or 0.5 dB in back-to-back measurements that outperform Volterra systems.

Kotlyar, Oleksandr, et al. (2020) [30], proposed post-processing the nonlinear spectrum at the receiver with a neural network to optimize nonlinear Fourier transform (NFT) based optical transmission systems. Numerical modeling improves BER by one order of magnitude, compared to machine learning processing that classifies input signals. The recommended approach improves inverse NFT numerical precision, making it useful outside optical communications. This method improves BER by about sixfold at 74 Gbit/s for 1000 km at the ideal signal strength to attain BER=4.3×10^{-3}.

Melek, Marina, et al. (2020) [31], used IXPM and IFWM as inputs to simplify neural network architectures. This design optimizes the number of triplets, symbol window range, and activation function. Weight trimming and principal component analysis (PCA) were also introduced to simplify neural network structure by minimizing inputs. This system used double-polarization 16-QAM format. The results revealed a 0.85 dB Q-factor gain with 35% less inputs over 3200 km transmission link compared to earlier designs.

Sidelnikov, Oleg, et al. (2021) [32], used convolutional neural networks to correct signal distortions nonlinearity in 11x400 Gb/s for 3200 km optical fiber WDM PDM-16QAM formats. A filter trains a single layer convolutional neural network to establish layer weights. Layer wise training and combined optimization of all weights in the huge multi-layer network increased learning efficiency. This method outperforms the linear equalizer by 0.8 dB for single channels and 1.2 for multi-channels. Deep CNN beats DBP equalization by 0.45 dB in single channel compensation.

Hattori, Naoki, et al. (2021) [33], introduced a WDM based optical vector matrix multiplication (VMM) circuit for ultra-wideband inference processing. The original optical VMM circuit was designed for fully connected network designs, which demand high power laser light sources. This research proposes optical multi-layer perceptron. Thus, the laser source consumes less power without compromising inference speed. Optoelectronic circuits and an activation mechanism were designed to improve inference accuracy without affecting light speed. This circuit improves performance by enhancing inference accuracy and speed.

Li, Chao, et al. (2022) [34], proposed a convolutional neural network (CNN) based perturbative nonlinearity compensation. This approach reconstructs a

feature map and develops a nonlinear equalizer regressor and classifier using two channels and first-order perturbation theory. CNN equalizer uses coherent optical communication technologies with DP-64QAM and 375 km range at 120 Gbit/s. CNN equalization was evaluated on a WDM simulation system with 8 channels to determine how launching optical powers affected bit error rate. The BER performance exceeds HD-FEC at 3 dBm optical power, however at 0 dBm for CNN regressor and 1 dBm for CNN classifier, the optimum is 2×10^{-3} and 1.2×10^{-3}, respectively.

He, Pinjing, et al. (2022) [35], suggested a triplet-input neural network unsupervised learning TNN (TNN-UL) NLC scheme for 3200 km DP-16QAM with 256 Gb/s and 1800 km SP-16QAM with 80 Gb/s. In this approach, labels and parameters are iteratively updated for single and dual polarization 16-QAM. The suggested approach can obtain Q-factor 8.70 dB without pre-defined training data, similar to supervised learning (TNN-SL).

Li, Feiyu, et al. (2023) [36], used DNN-based DBP to mitigate fiber nonlinearity and monitor channel condition via Integrated Communication and Sensing (ICS). Instead of using empirical values, a DNN with adaptive updating determines the nonlinear compensation coefficients, improving system performance. Polarization Multiplexing 16QAM with 28 GBaud across 1200 km SSMF with DSP component constructed to examine ICS technique efficacy. When just the first DSP module has chromatic dispersion correction, zero dBm is the best launch power. When the launch optical power is 2 dBm and the DBP step size is 20 km, distance resolution improves and monitoring performance is good.

Costa, Camila, et al. (2023) [37], proposed clusters DP-16QAM signals in two polarizations to achieve 112 Gb/s single-channel data rates. A projection-

based initialization approach for 4D clustering of DP-16QAM constellations tackles the convergence problem caused by the large number of clusters. For a BER threshold of 10^{-3}, 4D clustering extends the system's maximum range from 138 km to 151.6 km, but 2D clustering only extends it to 146 km.

1.6 Thesis Objective

1. Enhancing DWDM transmission system performance through studying nonlinear mitigation strategies and cutting-edge fiber optic communication technologies.
2. Performance evaluation of optical nonlinear compensation model based on phase conjugation and advanced machine learning algorithms.
3. Maximize the exploitation capacity of a communication system by taking advantage of increasing the number of channels with different modulation formats.
4. Improving the system performance in terms of BER, Q-factor, received power, and link range, as well as comparing current findings results with recent works.

1.7 Thesis Contributions

1. Developing the work of the conventional phase conjugation technique by employing it with two hybrid methods to improve its ability against linear and nonlinear effects.
2. Taking advantage of the principle of image classification using the convolution neural network algorithms and employing it as a new work in the mitigation of impairments in fibers.

3. Applying a new approach to neural networks by employing the Nonlinear Auto Regressive with Exogenous algorithms as a novelty work in optical networks to solve problems in optical fibers.
4. Implementation of the optical system and the artificial intelligence algorithms using co-simulation programs to ensure the validity of the results obtained.

1.8 Thesis Organization

This dissertation is divided into five chapters, and the organization of the chapters is detailed as follows:

- **Chapter One:** Presents an introduction to optical impairments, limitations with a problem statement, related work, goal, and scope for this study.
- **Chapter Two:** describes a theory of light propagation in optical fiber with an illustration of the principle of compensation methods used.
- **Chapter Three:** Presented a simulation for the proposed designed system of compensation approach based on optical phase conjugation.
- **Chapter Four:** Introduced a simulation model of the compensation scheme based on machine learning.
- **Chapter Five:** The simulated results of the proposed system were illustrated in detail.
- **Chapter Six:** Offers the conclusion of the research results with suggestions and directions for future works that can improve the performance of the whole technique.

Chapter Two

Theoretical Background of Optical System

2.1 Introduction

The first part of this chapter introduced a model for the transmission of optical signals along a fiber. Relevant impairments for long-distance optical fiber communication systems will be discussed. These impairments can be divided into linear impairments like dispersion and attenuation, and nonlinear impairments due to the Kerr effect. In subsequent sections, an examination will be conducted at the many high-order modulation formats, multiplexing strategies, and optical amplifiers that make possible such high data rates across fiber optic networks. Finally, some cutting-edge techniques for compensating signal distortion in high-capacity optic communication systems, which can greatly enhance transmission performance will be covered.

2.2 Fiber Channel Modelling

The scalar nonlinear Schrödinger equation (NLSE) models the electric field propagation in an optical fiber without polarization [38].

$$\frac{\partial E(z,t)}{\partial z} = \underbrace{-j\frac{\beta_2}{2}\frac{\partial^2 E(z,t)}{\partial t^2} + \frac{\beta_3}{6}\frac{\partial^3 E(z,t)}{\partial t^3}}_{\text{dispersion}} + \underbrace{\frac{g(z)-\alpha(z)}{2}E(z,t)}_{\text{power evolution}} \underbrace{+j\gamma|E(z,t)|^2 E(z,t)}_{\text{Kerr effect}} \quad \textbf{(2.1)}$$

Where β_2 and β_3 are the second and third order dispersion parameter, α(z) is the attenuation, and γ is nonlinear coefficient. In a scenario where the electric field propagates in the z direction and t is a co-moving time frame, its envelope, $E(z, t)$, is expected to vary more slowly than the carrier wave. The strength of the applied field determines the relationship between the induced the applied field and dielectric polarization of the material. The response of the material is nonlinear when the field strength is high, but linear when the field strength is low. Therefore, only linear effects are present if the propagating field of optical is weak, but both linear and nonlinear effects are present at large powers [39]. The energy between different frequencies can be transferred or even new frequency components can be created due to nonlinear effects. Polarization-mode dispersion, chromatic dispersion, and fiber loss are all linear phenomena that have an impact on the propagating optical field. The Kerr effect and inelastic scattering effects are examples of nonlinear phenomena [38].

2.3 Linear Effects

This section delves deeply into the causes and consequences of the two primary kinds of linear impairments to the propagating optical signal field in optical fibers [38].

2.3.1 Optical Fibre Attenuation

Figure (2.1) shows that silica optical fibers are used for long-haul communications due to their low C-band losses (1530-1570 nm) [40]. Losses are caused by material absorption and Rayleigh scattering. Purifying fused silica reduces absorption. Beer-Lambert law controls fiber optical field power-law distribution [38].

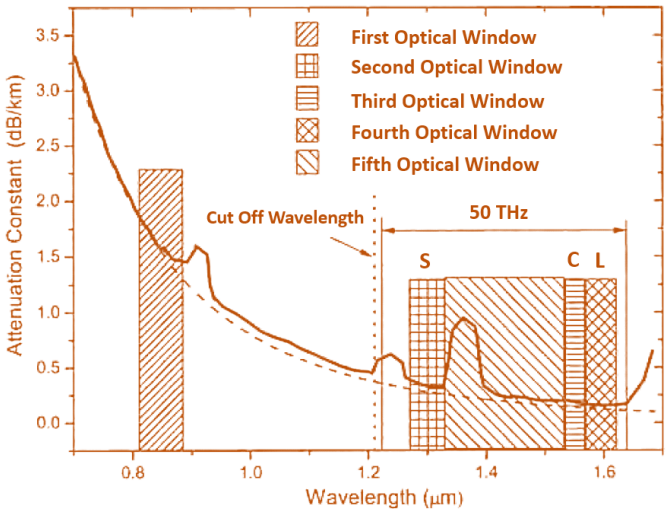

Figure (2.1). Relationship between optical wavelength and fiber attenuation [41]

$$P(z) = P(0)\exp(-\alpha z) \qquad (\mathbf{2.2})$$

where $P(z)$ is the transmitted power and $P(0)$ is the power launched at the input of fiber. Common SSMF loss parameters are 0.0461 km^{-1} or 0.2 dB/km at 1550 nm. Fiber loss varies with wavelength, reaching several dB/km at shorter wavelengths [42]. When loss is considered, the simplest equation for optical field E transmission across an optical fiber is [38].

$$\frac{\partial E}{\partial z} = -\frac{\alpha}{2}E \qquad (\mathbf{2.3})$$

2.3.2 Optical Fiber Dispersion

Chromatic dispersion is caused by the effective index of the optical fiber, which varies with frequency. Both the material qualities and the waveguide design contribute to dispersion. The dispersive nature of silica itself is responsible for the material characteristics contribution. Dispersion from waveguide design results from the employment of core and cladding for steering the optical field in the fiber. Optical field linear propagation, without considering losses, can be represented in the frequency domain as [38].

$$E(z,w) = E(0,w)\exp[j\beta(w)z] \quad (\mathbf{2.4})$$

where $\beta(w)$ is the propagation constant denoted by;

$$\beta(w) = \frac{n(w)w}{c} \quad (\mathbf{2.5})$$

Where $n(w)$ is the refractive index and c is the light velocity in vacuum. To account for the frequency dependence of the propagation constant, the propagation constant can be expanded using a Taylor series around the carrier frequency (w_0) as [38].

$$\beta(w) = \beta_0 + \beta_1(w - w_0) + \frac{\beta_2}{2}(w - w_0)^2 + \frac{\beta_3}{6}(w - w_0)^3 + \cdots \quad (\mathbf{2.6})$$

Where $\beta_i \equiv \frac{d^i\beta}{dw^i}\Big|_{w=w_0}$ is the Taylor expansion coefficients. The group velocity at the carrier frequency, (v_g), is proportional to β_1 as $v_g = \frac{1}{\beta_1}$, and $v_p = \frac{w_0}{\beta_0}$ corresponds to the phase velocity of the carrier wave β_0. The parameter β_2, denoted by the units [ps^2/km], is the group velocity dispersion (GVD) and characterizes the frequency dependence of the group velocity. During transmission, the GVD modifies the form of the pulse of optical. Third order Taylor expansion coefficient (β_3) gives the frequency dependence of the GVD [43]. However, the dispersion parameter (*D*) in [ps/(nm km)] and the dispersion slop (*S*) in [ps/(nm^2 km)] are more typically employed, and their values are related to the Taylor expansion coefficients as [38].

$$D = \frac{-2\pi c}{\lambda^2}\beta_2 \quad (\mathbf{2.7})$$

$$S = (\frac{2\pi c}{\lambda^2})^2\beta_3 \quad (\mathbf{2.8})$$

where λ is the wavelength of light.

2.4 Nonlinear Optic Effect

The connection between electric field and induced dielectric polarization determines the medium's nonlinear response. Total medium polarization ($\tilde{P}$) created by a high intensity electric field is [38, 44].

$$\tilde{P} = \epsilon_0\left(X^{(1)}.\tilde{E} + X^{(2)}:\tilde{E}\tilde{E} + X^{(3)}\vdots\tilde{E}\tilde{E}\tilde{E}\right) \qquad (\mathbf{2.9})$$

where $X^{(N)}$ is a tensor of rank $N+1$ and represents the N[th] order susceptibility, and ϵ_0 is the vacuum permittivity. The linear polarization is reflected in the susceptibility term of first order. First order susceptibility has a direct correlation with both dispersion and fiber loss. The second-order term $X^{(2)}$ disappears in centrosymmetric materials, while the third-order term gives rise to nonlinear interactions known as optical Kerr effects. Due to its amorphous nature, silica fiber displays inversion symmetry. After that, the nonlinear effects of the third order start to take over. The total polarization produced in the fiber optic can be expressed as where assuming the field of electric is linearly polarized and the third harmonic term is disregarded (attenuated in the fiber).

$$P = \epsilon_0\left(X^{(1)} + \frac{3\left|\tilde{E}\right|^2}{4}X^{(3)}\right)E = \epsilon_0 X_{eff}E \qquad (\mathbf{2.10})$$

where the effective susceptibility is denoted by X_{eff}. The effective susceptibility is proportional to the medium's refractive index as

$$n_2 = 1 + X_{eff} \qquad (\mathbf{2.11})$$

Nonlinear effects are then included into the refractive index, yielding [38].

$$n(w, I) = n(w) + n_2 I = n(w) + \tilde{n}_2|E|^2 \qquad (\mathbf{2.12})$$

where $n(w)$ represents the linear refractive index, n_2 and $\tilde{n}_2$ represents the nonlinear Kerr parameter and nonlinear index coefficient, respectively. The coefficient of nonlinear index is

$$\tilde{n}_2 = \frac{3}{8n} Re\left(X^{(3)}\right) \qquad (\mathbf{2.13})$$

Where $Re\left(X^{(3)}\right)$ is the real part of $X^{(3)}$. The coefficient of nonlinear index and Kerr parameter are related as

$$n_2 = \frac{2\tilde{n}_2}{\epsilon_0 nc} \qquad (\mathbf{2.14})$$

The refractive index is sensitive to both the wavelength and the instantaneous field strength. Kerr effect is the modification of the medium's refractive index as a result of the intensity of the propagating field [45]. The degree of the nonlinear effects when considering the transverse field distribution in the fiber optic is expressed by the nonlinear coefficient (γ).

$$\gamma = \frac{2\pi n_2}{\lambda A_{eff}} \qquad (\mathbf{2.15})$$

where A_{eff} is the effective mode area. Nonlinear coefficient (γ) for the SSMF is roughly 1.3 $(\text{W km})^{-1}$ [46]. The propagating signal experiences a nonlinear phase shift due to the Kerr effect. The total nonlinear phase shift experienced by an optical signal as it travels through an optical fiber can be found by using the formula [47].

$$\emptyset_{NL}(z) = \gamma \int_{z=0}^{z=L} P(\bar{z}).\, d\bar{z} \qquad (\mathbf{2.16})$$

where $P(\bar{z})$ is the power's change along the direction of propagation. The effective length (L_{eff}) can be used in place of the physical length (L) to determine the total nonlinear phase shift.

$$\emptyset_{NL}(L) = \gamma L_{eff} P(0) \qquad (\mathbf{2.17})$$

Where;

$$L_{eff} = \frac{1}{\alpha}[1 - \exp(-\alpha L)] \qquad (\mathbf{2.18})$$

Since the signal power drops off exponentially as it travels down a fiber due to attenuation, the impact of the Kerr effect is greatest near the beginning of the transmission line. In optical fibers, the first section is known as the high-power region. When = 0.2 dB/km is applied to a very long SSMF (100 km), the effective length is roughly 21.5 km. The signal power envelope versus transmission distance is shown in figure (2.2), where the high-power zone and the effective length is illustrated [48].

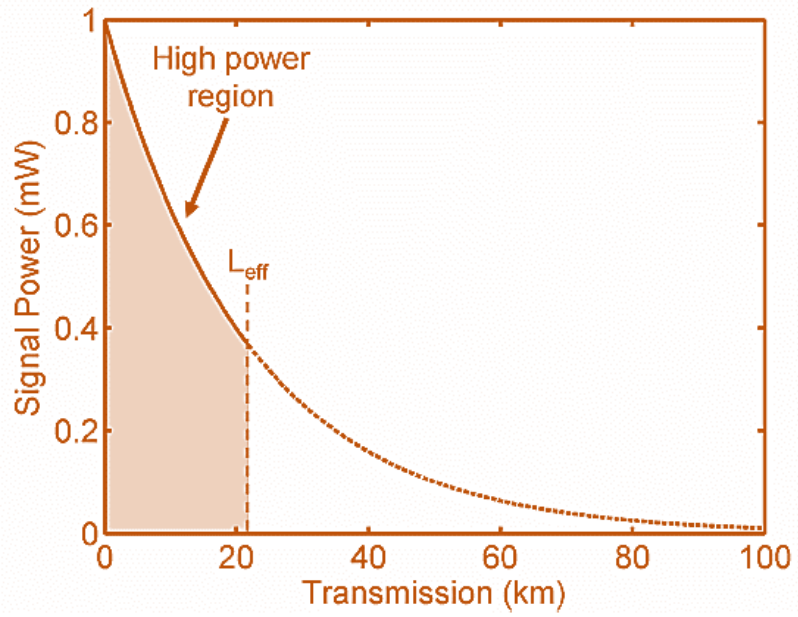

Figure (2.2).Signal power as a function of the transmission distance [38]

2.4.1 Self Phase Modulation (SPM)

SPM is the phase change in the optical pulse due to the intensity-induced refractive index change. Optical Kerr effect causes modest refractive index variation [49]. The

pulse's frequency spectrum changes due to refractive index-induced phase shift. Refractive index variation is described by

$$\Delta n = n_2 I \tag{2.19}$$

where I is the optical intensity and n_2 is the nonlinear coefficient. The nonlinear phase shift produced on the propagating field owing to SPM can be calculated by ignoring dispersion and taking into account the loss of fiber with the effective length:

$$\emptyset_{NL}^{SPM}(L) = \frac{2\pi}{\lambda}\tilde{n}_2|E|^2 L_{eff} = \gamma P L_{eff} \tag{2.20}$$

where P is the propagating wave's power.

2.4.2 Cross Phase Modulation (XPM)

XPM refers to the phenomenon in which the intensity of one beam affects the phase change of another beam. This phenomenon is able to be characterized by a change in the refractive index [50].

$$\Delta n(\lambda_2) = 2n_2 I(\lambda_1) \tag{2.21}$$

In WDM systems, fluctuations in power of optical in one channel are translated into phase changes in other copropagating channels [51]. Because the refractive index experienced by a given wavelength is influenced by both the optical power of the channel experiencing the XPM and the optical power of adjacent channels, SPM is always present when XPM happens. The SPM and XPM effect on channel one of an M-channel WDM system is written as an extension of the NLSE given by equation.

$$\frac{\partial E_1}{\partial z} = j\gamma[P_1(z,t) + 2\sum_{i=2}^{M} P_i(z,t)]E_1 \tag{2.22}$$

The XPM expression includes a multiplier of 2, indicating that the effect of XPM is two times that of SPM at the same power. The nonlinear phase shift in one wavelength field owing to XPM generated by N other wavelength fields which are co-polarized and co-propagating is illustrated as [39].

$$\emptyset_{NL,1}^{XPM}(L) = 2\gamma\left(P_2 L_{eff} + P_3 L_{eff} + \cdots + P_N L_{eff} + \cdots\right) \qquad (\mathbf{2.23})$$

where P_N is the power of N^{th} field. The corresponding spectral broadening is expressed by:

$$\Delta w_{XPM} = -\gamma L_{eff}[\frac{dP_1}{dt} + 2\sum_{i=2}^{M}\frac{dP_j}{dt}] \qquad (\mathbf{2.24})$$

2.4.3 Four Wave Mixing (FWM)

FWM happens when a fiber is used to transmit light at several frequencies (or wavelengths). If the parameters for phase matching are met, the power from the original frequencies can be converted into a new light frequency [52]. The refractive index varies as a result of the Kerr effect when two co-polarized fields, E_1 and E_2, propagate through an optical fiber at different frequencies, f_1 and f_2, with different propagation constants, β_1 and β_2. In this case assumed that the energy is conserved as illustrated in figure (2.3-a); two photons with frequencies of ω_2 and ω_3 are annihilated to producing two new photons with frequencies of ω_1 and ω_4, with no energy lost to non-radiative processes, making this a parametric process, so that the energy is conserved: $\omega_1 + \omega_4 = \omega_2 + \omega_3$. The spectrum of FWM is illustrated in figure (2.3-b), with the arrows indicating the energy transferring directions. The black dashed line in figure (2.3-b) represents the requirement that zero GVD frequency must be at the center of the four waves in order to satisfy the phase matching condition, which states that $k_1 + k_4 = k_2 + k_3$. This condition can be reduced to a single requirement by expanding the wavevectors k_j near the center of the four

frequencies. Non-degenerate FWM processes are those in which the optical fields oscillate at distinct frequencies, as opposed to degenerate processes in which the fields oscillate at the same frequency. Figure (2.4) depicts how three waves serve as the basis for the generation of additional fields at frequencies [53].

$$f_{jkl} = f_j + f_k - f_l \qquad (\mathbf{2.25})$$

There are three distinct new frequency fields generated by the none degenerate FWM processes, $j, k, l \in \{1,2,3\}, j \neq k, j \neq l, k \neq l$ and the degenerate FWM processes0$j, k, l \in \{1,2,3\}, j = k \neq l$. Both of the waves at frequencies $f_j \; and \; f_k$ are referred to as pump waves, while the wave at frequency f_l is the signal wave. f_{jkl} is the so-called idler wave. If the signal frequency f_l is equal to one of the pump frequencies (f_j, f_k), resulting in f_j or f_k respectively, $f_j + f_k - f_j = f_k$, will be the same as the other pump frequency. In fact, these cases give rise to either SPM $(n = l = j = k)$ or XPM $(n = j, k = l)$ [54]. Therefore, an additional condition for FWM process is $(l \neq j, k)$. Under this condition, the total number of FWM products in this scenario for N source channels is

$$M = \frac{1}{2}(N^3 - N^2) \qquad (\mathbf{2.26})$$

It is important to note that if the intensities of the newly formed FWM products are high enough, they can interact again with one other or with the channels, resulting in additional higher order mixing products.

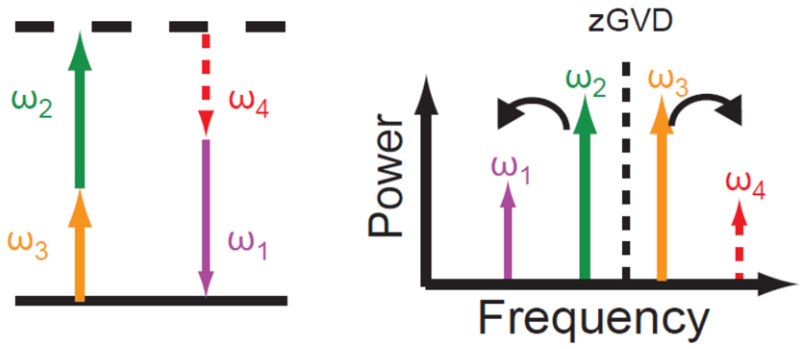

(a) (b)

Figure (2.3). (a) Schematic energy level diagrams and (b) spectra of FWM, the arrows show the energy transfer directions [55]

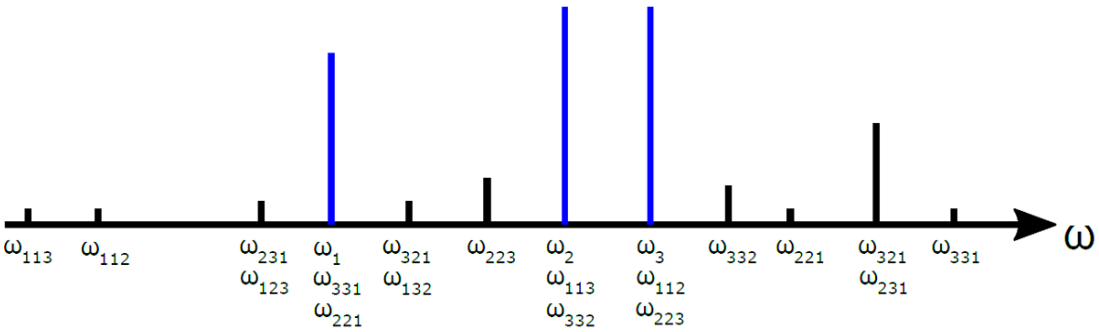

Figure (2.4). Degenerate and non-degenerate FWM components. Input fields are blue

2.5 Ultra High-Capacity Optical Transmission Techniques

Optical networks must expand their transmission capacity to keep up with the growing number of Internet users. This calls for enhanced fiber transmission capacity [1]. The capacity of a light wave flowing through a fiber transmission connection can be increased by fully using the six dimensions illustrated in figure (2.5).

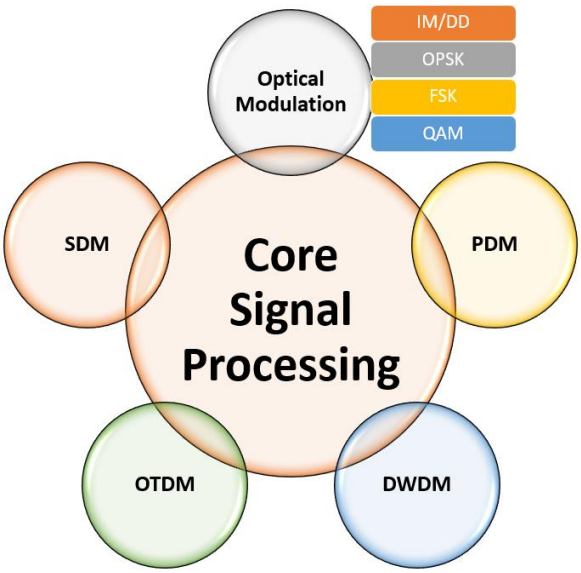

Figure (2.5). Optical transmission capacity enhancement in six dimensions

2.5.1 Overview of Optical Modulation Formats

A carrier is necessary for signal propagation in telecommunications; hence the signal must be transmitted above the baseband. In theory, the transporter can do double duty. As a result, the medium can be used for propagation, and the full bandwidth of the medium can be utilized by employing the multiplex technique. There are essentially two distinct methods for imbuing a carrier with information, known as "analog modulation" and "digital modulation" [56]. A symbol of length n bits can be constructed from a collection of bits from the transformed signal for use in digital modulation of the carrier. With the ability to send n bits at once, bandwidth utilization is maximized. One of $m = 2^n$ potential carrier signals must be used to send an n-bit symbol at the same time. This is why the related modulations are referred to as "m-ary." A monochromatic electromagnetic wave is what the equation (2.27) calls an optical carrier signal [57].

$$E(z,t) = \frac{1}{2}\left(\hat{E}e^{j(\hat{n}k_o z - wt)} + c.c.\right)e_i \qquad (\mathbf{2.27})$$

There are, in principle, just four distinct ways that the carrier signal can be modulated with the information. These are the signal's frequency, phase, amplitude, and polarization.

2.5.2 Channel Multiplexing Techniques

Multiplexing methods can be classified into four categories; polarization division multiplexing, dense wavelength division multiplexing, time division multiplexing, and space division multiplexing. Emphasis will be placed on the two most important techniques used in this study.

2.5.2.1 Polarization Division Multiplexing (PDM)

PDM is an efficient method that can effectively double the output. Both the x- and y-polarization modes are supported by a single mode fiber, with the electric field orientation determining which mode is used. Figure (2.6) depicts a PDM schematic, which a polarization splitter beam is employed at the transmitter to separate the laser's x and y polarizations. Using an optical modulator, Mod x (Mod y), electrical data of m_x (m_y) can be used to alter the laser's x (y)polarization component [58]. In a single mode fiber, these polarization components travel as two separate polarization modes.

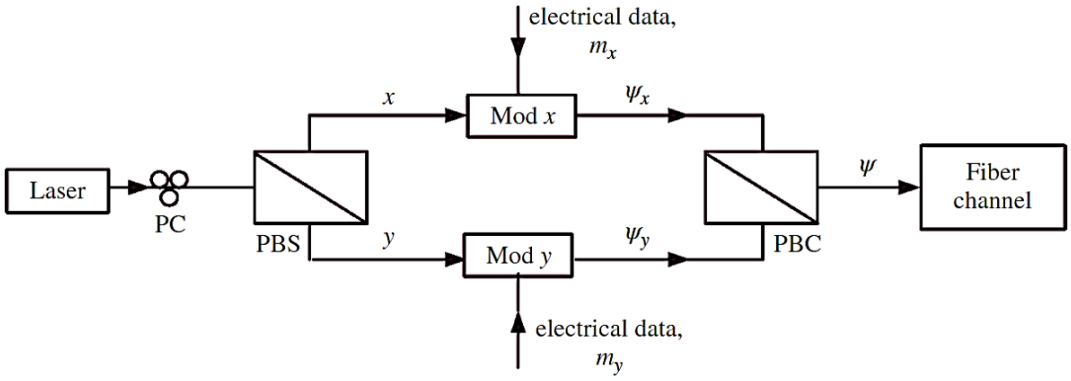

Figure (2.6). Polarization division multiplexing with polarization controller and optical modulator [58]

2.5.2.2 Dense Wavelength Division Multiplexing (DWDM)

In order to expand the data transfer capacity of current optical networks, dense wavelength division multiplexing (DWDM) is employed. As shown in figure (2.7), DWDM operates by simultaneously transmitting numerous signals of different wavelengths over a single optical fiber. By providing channel spacings of 50 GHz or less, several hundreds of wavelengths can be placed on a single fiber [59]. The capacity of fiber optic networks can be expanded with the help of this technology by creating several virtual optical fibers. A CW laser operating at λ_j, j = 1, 2, …, N is modulated by electrical data. The multiplexer combines the modulated signals before sending them across the optical connection. The channels are separated by a demultiplexer at the conclusion of the optical fiber connection. Modulating an optical carrier at wavelength λj with a data stream at rate B results in a total data rate of NB [60]. DWDM has many benefits over the traditional single channel technology, including increased network capacity, simplified expansion, and stable performance. When technology improves and wavelengths can be spaced closer together, system capacities increase. DWDM is expanding its role beyond simple transport to become the backbone of all optical networks, complete with wavelength provisioning and mesh-based security.

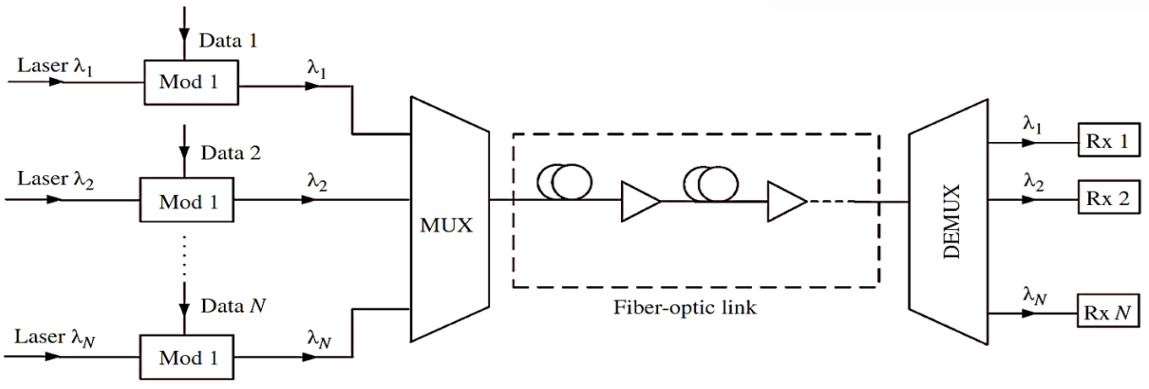

Figure (2.7). Block diagram for dense wavelength division multiplexing system [61]

2.6 Overcoming Linear Impairments

As a result of their linear nature, fiber loss, and dispersion are the primary factors limiting the capacity of optical fiber transmission systems. Even though 0.2 dB/km is a relatively small loss in the SSMF, the data signals suffer significant attenuation with increasing distance. The Transmission range is constrained by pulse broadening caused by dispersion. This section will be studied some of the ways that fiber loss and dispersion can be dealt with.

2.6.1 Optical Amplification

Attenuation of the signal during transmission and an increase in the number of wavelength division multiplexed (WDM) channels both add significant expense and complexity to fiber optic communication networks [62]. Erbium-doped fiber amplifiers (EDFAs), semiconductor optical amplifiers (SOAs), and Raman amplifiers were among the significant advances that helped to overcome these constraints. Figure (2.8) depicts the various configurations in which optical amplifiers can be used [63].

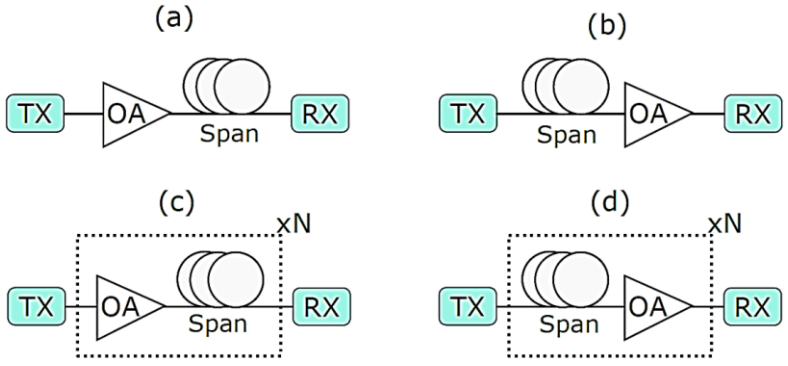

Figure (2.8). Fiber optic amplifier configurations (a)booster amplifiers, (b) pre-amplifiers, (c) in-line type A amplifiers, and (d) in-line type B amplifiers

2.6.1.1 Erbium Doped Fiber Amplifiers (EDFAs)

EDFAs have replaced repeaters in fiber optic networks since their introduction. Erbium doped optically pumped fiber is the gain medium. Either spontaneous or induced emission would return excited erbium ions to their ground state. EDFAs have large gains, saturation powers, and low noise [64]. Moreover, when a fully saturated, they are able to boost the signal without adding any nonlinear aberrations, thanks to the millisecond scale gain response time. Figure (2.8) illustrates the optimization of the design parameters that has allowed EDFAs to be employed in every conceivable arrangement as a preamplifier, booster, and inline amplifier.

2.6.1.2 Raman Amplifier

Stimulated Raman scattering is the foundation of Raman amplification; it occurs when an optical field excites the vibrational modes of the material, resulting in the emission of a second optical field of either lower or higher frequency. The silica fiber is simultaneously subjected to a powerful pump and a weak signal with less energy. Inelastic scattering of the pump photons produces photons with energies closer to those of the weak signal and optical phonons, led this strengthens feeble signal. The energy of the optical phonon is equal to the energy difference between the pump and signal photons. Once the pump power is over a critical value, the signal gain grows exponentially [65]. The maximal Raman gain in silica fiber occurs at a frequency 13 THz below the pump frequency, with a bandwidth of 40 THz [66]. Raman amplification is competitive for DWDM amplification outside of Cand L band because its large gain bandwidth can be controlled by simply adjusting the pump frequency. A Raman amplifier can function as a distributed or a lumped amplifier [67].

2.6.2 Dispersion Compensation Fiber (DCF)

Dispersion compensation basically means eliminating the compounded dispersion originating from length of the fiber [68]. DCF has a large negative dispersion parameter that can be inserted into the link at regular intervals. Conventional dispersion compensating fibers have a high negative dispersion (-70 to -90) ps/nm.km, therefore, used to compensate the positive value dispersion for the transmission fiber. There are three dispersion compensation schemes according to the relative position of SMF and DCF that is illustrated in figure (2.9) [69]. To compensate the losses, two optical amplifiers of gain G_1 and G_2 can be inserted and can be calculated as [70].

$$G = L.\alpha \qquad (\mathbf{2.28})$$

Where G the gain measured in dB, L is the length measured in km. If suppose the SMF and DCF be characterized by L_{SMF} and L_{DCF} respectively, the condition for perfect dispersion compensation is.

$$D_{SMF}.L_{SMF} + D_{DCF}.L_{DCF} = 0 \qquad (\mathbf{2.29})$$

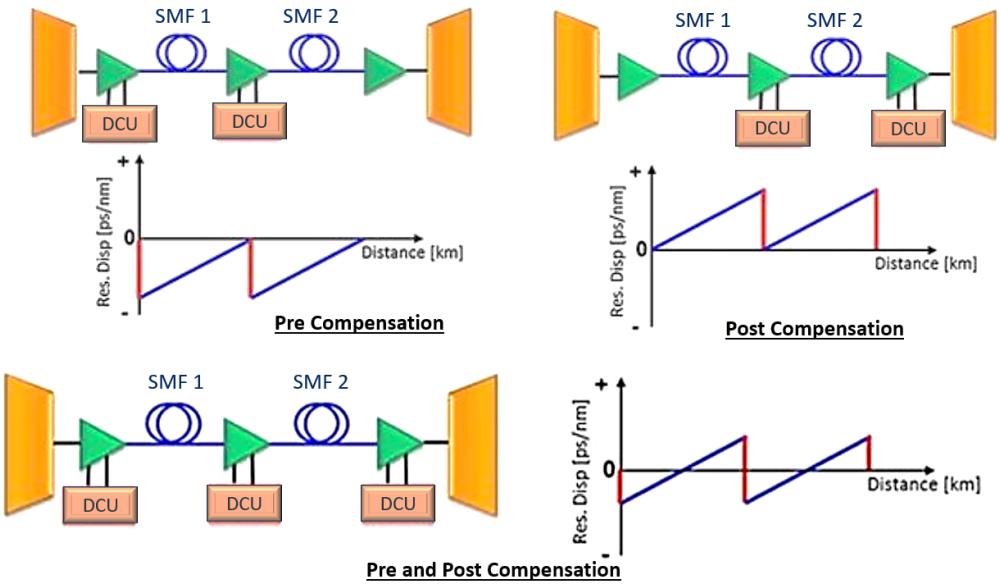

Figure (2.9). Three dispersion compensation techniques using DCF [69]

2.7 Overcoming Nonlinear Impairments

In optical fiber connections, the Kerr nonlinearity is a significant bottleneck [13, 71, 72]. These alterations may result from either intra- or inter-channel effects. Intracanal effects, such as signal-signal beating resulting to SPM, are caused by nonlinear beating within the frequencies of the same channel band. Single channel transmission systems have the intra-channel impact. Signal-signal beating results in XPM and FWM, which are the inter-channel effects generated by the interaction between the frequencies of neighboring channel bands and the channel band of interest. Interchannel effects caused by Kerr nonlinearity have a significant impact on DWDM transmission systems [73]. Digital and optical methods can be used to compensate for the nonlinear distortions. The use of a high bandwidth signal, in particular, increases the processing complexity and energy requirements of digital approaches. The fundamental benefit of optical methods is their simplicity in compensating nonlinearity with a large signal bandwidth. Two techniques were used to compensate the fiber impairments will be discussed in (2.8) and (2.9) sections.

2.8 Optical Phase Conjugation Technique

Optical Phase Conjugation (OPC) is an all-optical signal processing technique that performs spectral inversion (phase conjugation) which may compensate for the nonlinear interference accumulated along the transmission fibre. After optical phase conjugation, the transmission span's dispersion and nonlinearity are reversed in the second section, resulting in net zero compensation [74]. Complex conjugation of the signal is achieved using the phase conjugation process. The phase conjugation process can be represented using the equation below when the OPC is placed at location z_0 [74].

$$E(z_0 + \delta) = E^*(z_0 - \delta) \quad (\mathbf{2.30})$$

where δ is an infinitely small distance of transmission. Condition (2.30) can be used to characterize propagation through the transmission link equation. The NLSE in the second transmission link can be described to observe how phase conjugation affects dispersion and nonlinear impairments. This avoids the discontinuity in E introduced by equation (2.30). Equation 2.1 is rewritten after OPC by [75].

$$\frac{\partial E^*}{\partial z} = j\frac{\beta_2}{2}\frac{\partial^2 E^*}{\partial t^2} + \frac{\beta_3}{6}\frac{\partial^3 E^*}{\partial t^3} + \frac{g(z) - \alpha(z)}{2}E^* - j\gamma|E^*|^2 E^* \quad (\mathbf{2.31})$$

In this equation, E still stands for the signal evolution through the fiber in the second half of the transmission connection. Equation (2.31) shows that Kerr effect and the GVD terms switch signs while the attenuation and slope terms keep their original signs. Higher order dispersive effects due to β_3 and the effect of Raman and Brilluin scattering are not taken into account in equation (2.31). Propagation of the phase conjugated signal is defined as.

$$\frac{\partial E^*}{\partial z} = j\frac{\beta_2}{2}\frac{\partial^2 E^*}{\partial t^2} - \frac{\alpha(z)}{2}E^* - j\gamma|E^*|^2 E^* \quad (\mathbf{2.32})$$

OPC can be implemented by FWM based on third order nonlinearity in a nonlinear medium like semiconductor optical amplifiers (SOA) [76], zero dispersion single mode fiber [77], and highly nonlinear fiber (HNLF) [78].

2.8.1 Analytical Model for OPC

The analysis of OPC will be summarized based on nonlinear Schrödinger equation. In figure (2.10), the link is depicted as two fiber lengths connected by an OPC module, which is the basic notion of OPC based compensation. In this design, compensation has three stages:

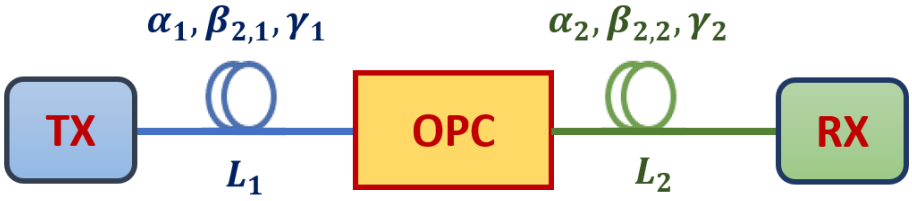

Figure (2.10). Two spans of transmission with (OPC); left is the original signal and right is conjugate (idler)

i. In the first part, nonlinearities accumulation.

ii. OPC inverted the sign of first span cumulative nonlinearities.

iii. In the second part, additional nonlinearities are applied.

Recall equation (2.1) to calculate optical fiber compensation requirements.

$$\frac{\partial E(z,t)}{\partial z} = -j\frac{\beta_2}{2}\frac{\partial^2 E(z,t)}{\partial t^2} + \frac{\beta_3}{6}\frac{\partial^3 E(z,t)}{\partial t^3} - \frac{g(z)-\alpha(z)}{2}E(z,t) + j\gamma|E(z,t)|^2 E(z,t) \quad (\mathbf{2.1})$$

Dispersive effects of higher orders, such as those caused by β_3 and Raman and Brillouin scattering, are not taken into account in equation (2.1). Consequently, the nonlinear Schrödinger equation (NLSE),

$$\frac{\partial E(z,t)}{\partial z} = -j\frac{\beta_2}{2}\frac{\partial^2 E(z,t)}{\partial t^2} - \frac{\alpha(z)}{2}E(z,t) + j\gamma|E(z,t)|^2 E(z,t) \quad (\mathbf{2.33})$$

By a few operators, it can transform this NLSE into a more manageable form:

$$\frac{\partial E(z,t)}{\partial z} = \left(j\hat{A}_{GVD} + \hat{A}_{loss} + j\hat{A}_{NL}\right)E(z,t) \quad (\mathbf{2.34})$$

Where:

$$\hat{A}_{GVD} = -\frac{\beta_2}{2}\frac{\partial^2}{\partial t^2} \quad (\mathbf{2.35})$$

$$\hat{A}_{loss} = -\frac{\alpha(z)}{2} \quad (\mathbf{2.36})$$

$$\hat{A}_{NL} = \gamma|E(z,t)|^2 \quad (\mathbf{2.37})$$

After transmission in the first span (left of OPC), the complex field amplitude E looks like this for a signal that travels from $z = 0$ to $z = L_1$:

$$E(L_1, t) = exp\left[\int_0^{L_1} \left(j\hat{A}_{GVD\,1} + j\hat{A}_{NL\,1} + \hat{A}_{loss\,1}\right)\partial z\right] E(0, t) \qquad (\mathbf{2.38})$$

As the field propagates through the first section, OPC is used to conjugate it, causing the phase distortions to flip. This leads to:

$$E^*(L_1, t) = exp\left[\int_0^{L_1} \left(-j\hat{A}_{GVD\,1} - j\hat{A}_{NL\,1} + \hat{A}_{loss\,1}\right)\partial z\right] E^*(0, t) \qquad (\mathbf{2.39})$$

When the OPC effect is taken, the signal propagates into a second fiber span of length L_2, where it suffers further impairments as a result of propagation:

$$E(L_1 + L_2, t) = exp\left[\int_{L_1}^{L_1+L_2} \left(j\hat{A}_{GVD\,2} + j\hat{A}_{NL\,2} + \hat{A}_{loss\,2}\right)\partial z\right] E^*(L_1, t) \qquad (\mathbf{2.40})$$

The relation between the output and input fields for this simple system is therefore:

$$E(L_1 + L_2, t) = exp\left[\int_{L_1}^{L_1+L_2} \left(j\hat{A}_{GVD\,2} + j\hat{A}_{NL\,2} + \hat{A}_{loss\,2}\right)\partial z\right] exp\left[\int_0^{L_1} \left(-j\hat{A}_{GVD\,1} - j\hat{A}_{NL\,1} + \hat{A}_{loss\,1}\right)\partial z\right] E^*(0, t) \qquad (\mathbf{2.41})$$

The operators $\hat{A}_{GVD}$ and $\hat{A}_{loss}$ are functionally distinct from one another, although they are inherently related to the operator A_{NL}. It doesn't care about this coupling, so make the following assumption:

$$\int^{L} \left(j\hat{A}_{GVD} + j\hat{A}_{NL} + \hat{A}_{loss}\right)\partial z \approx \int^{L} j\hat{A}_{GVD}\partial z + \int^{L} j\hat{A}_{NL}\partial z + \int^{L} \hat{A}_{loss}\partial z \qquad (\mathbf{2.42})$$

The impact of OPC can be better understood by grouping the integrals from Eq. (2.41) according to the underlying physical effects:

$$E(L_1+L_2,t) \approx exp\left[\left(\int_0^{L_1} \hat{A}_{loss\,1}\partial z + \int_{L_1}^{L_1+L_2} \hat{A}_{loss\,2}\,\partial z\right)\right.$$
$$+ j\left(\int_0^{L_1} -\hat{A}_{GVD\,1}\partial z + \int_{L_1}^{L_1+L_2} \hat{A}_{GVD\,2}\partial z\right)$$
$$\left.+ j\left(\int_0^{L_1} -\hat{A}_{NL\,1}\partial z + \int_{L_1}^{L_1+L_2} \hat{A}_{NL\,2}\partial z\right)\right] E^*(0,t) \qquad (\mathbf{2.43})$$

Therefore, if the corresponding transmission impairments between the two spans cancel out, the complex field amplitude at the end of the system can be an exact reproduction of the input, as shown by Eq. (2.43). What I mean is:

$$E(L_1+L_2,t) = E^*(L_0,t) \qquad (\mathbf{2.44})$$

If the following conditions are met:

$$\int_0^{L_1} \hat{A}_{loss\,1}\ \partial z = -\int_{L_1}^{L_1+L_2} \hat{A}_{loss\,2}\partial z \qquad (\mathbf{2.45})$$

$$\int_0^{L_1} \hat{A}_{GVD\,1}\ \partial z = \int_{L_1}^{L_1+L_2} \hat{A}_{GVD\,2}\partial z \qquad (\mathbf{2.46})$$

$$\int_0^{L_1} \hat{A}_{NL\,1}\ \partial z = \int_{L_1}^{L_1+L_2} \hat{A}_{NL\,2}\partial z \qquad (\mathbf{2.47})$$

Finally, these requirements can be described in terms of each span's fiber characteristics, as follows:

$$\int_0^{L_1} \alpha_1\ \partial z = -\int_{L_1}^{L_1+L_2} \alpha_2\partial z \qquad (\mathbf{2.48})$$

$$\int_0^{L_1} \beta_{2,1}\ \partial z = \int_{L_1}^{L_1+L_2} \beta_{2,2}\partial z \qquad (\mathbf{2.49})$$

$$\int_0^{L_1} \gamma_1|E(z,t)|^2\ \partial z = \int_{L_1}^{L_1+L_2} \gamma_2|E(z,t)|^2\partial z \qquad (\mathbf{2.50})$$

The OPC requirements are decomposed into subsets for the various physical effects, as in Eqs. (2.48) through (2.50). Because conjugation does not affect

fiber loss, the loss (α) in the first span must be offset by ($-\alpha$) in the second span, as in Eq. (2.48). GVD and nonlinearity, however, have a chance of being balanced out if they are similar in both spans, as demonstrated in Eqs. (2.49) and (2.50), because OPC alters the sign of the phase impairments. Finally, in this work, only care about satisfying Eq. (2.50) to compensate for the Kerr effects, and want to do for a variety of proposed systems [79].

2.8.2 Four Wave Mixing in High Nonlinear Fiber (HNLF)

The use of HNLF is promising for its simplicity and low cost; moreover, having an all-fiber based OPC allows low coupling losses. The HNLF doesn't stray too far from the standard optical fiber layout. So, the same method used to create standard silica-based single mode fibers can also be used to create HNLFs. Core refractive index of the typical HNLF is high and nearly flat. The fibre dispersion and effective area, which cause fibre non-linearity, can be closely controlled using this fibre. In comparison, the typical HNLF has a Kerr coefficient (n_2) median value of about 3.1×10^{-20} m^2/W, yielding a nonlinear coefficient of about 10.8 W^{-1} km^{-1} at 1550 nm. An important advantage of FWM based optical phase conjugation is that it makes it possible to generate phase-conjugated copies of e.g., DWDM signals with large total bandwidth. This was done using a fiber optic parametric amplifier (FOPA) [80]. In HNLF, the FWM approach uses the FOPA concept as its foundation for wavelength conversion.

2.8.3 Fiber Optical Parametric Amplifier (FOPA)

In FOPA, energy is transferred from one or two powerful pump fields to relatively weak signal fields by using the nonlinear phenomenon of FWMs. A vital role in the FOPA system is the gain characteristic. In addition to being a

promising choice for FWM in optical fibers, the immediate nonlinear electronic response of silica makes FOPA a promising candidate for ultrafast, all-optical data processing. The Kerr nonlinearity effect causes FOPA to arise when a string pump and a weak signal propagate together in an optical fiber and then interact with one another. By transferring energy from the pump to the signal, a new wavelength component is created, allowing the process to function as a wavelength converter [81]. One or two pumps are needed to achieve FOPA. Therefore, FOPA is divided into two types; single pumped represent degenerate FWM and dual pumped represent non-degenerate FWM.

2.8.3.1 Single Pumped Fiber Optical Parametric Amplifier

Figure (2.11) illustrates the injection of one strong pumping photon at frequency f_P and one weak signal photon at frequency f_s into a high nonlinear fiber (HNLF), produces an idler wave at frequency f_i, as demonstrated in equation below [80],

$$f_{idler} = 2f_P - f_s \qquad (\mathbf{2.51})$$

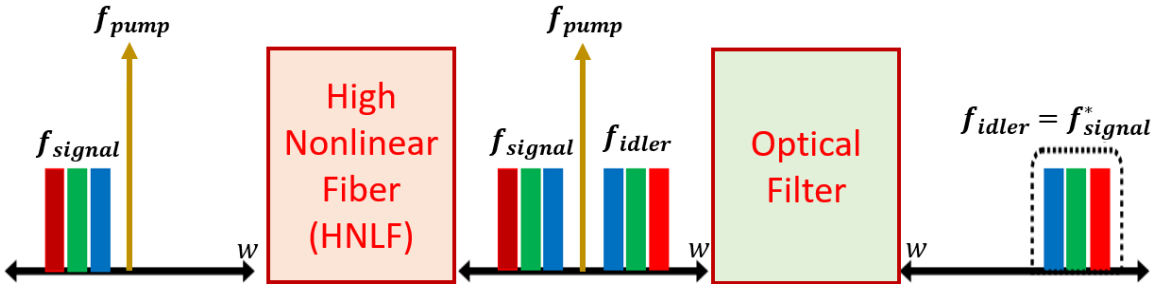

Figure (2.11). Concept of OPC with single pumped FOPA [80]

The wavelength of the pump has a significant bearing on the gain parameters of a single pump design. Gain is greatest when the signal is far from the pump because of the nonlinear phase matching's contribution to the overall phase mismatch. Since the gain increases exponentially with the fiber length, the

pump power, or the nonlinear coefficient, it is extremely difficult to obtain a flat gain spectrum with a single pump.

2.8.3.2 Dual Pumped Fiber Optical Parametric Amplifier

This configuration has important advantage represented by which can supply comparatively flat-gain on a much large bandwidth than what is possible with the single pumped. This technique uses a pair of pumps placed in a symmetrical arrangement with regard to the zero-dispersion wavelength. This allows a fixed gain to be attained while using only half the power on each pump. As demonstrated by equation (2.52), an idler wave at frequency f_i is produced when two pumping photons with frequencies f_{P1} and f_{P2} ($f_{P1} \neq f_{P2}$) co-propagate with the signal at frequency f_s in the (HNLF) [80].

$$f_{idler} = f_{P1} + f_{P2} - f_s \qquad (\mathbf{2.52})$$

Figure (2.12) illustrate a simple block diagram of dual pumped FOPA. OPCs filter the conjugated signals at the output of the HNLF to drop the remains of the higher power pump(s) and the original optical input signals. The idler wave that produced contains the same information as the signal launched at the input end. The only difference between them is at a various wavelength, therefore, this reason makes FOPAs-can act as a wavelength converter.

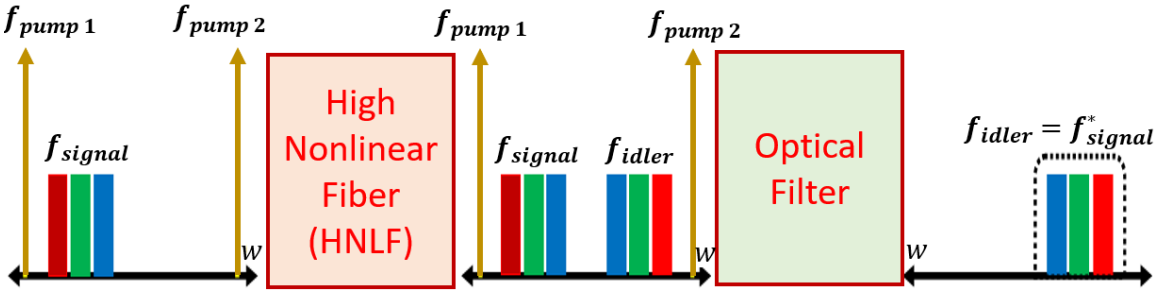

Figure (2.12). Concept of OPC with dual pumped FOPA [82]

2.8.4 Implementation of Optical Phase Conjugation

There are two ways in which OPCs can be employed to mitigate the negative effects of the Kerr on the efficiency of a high-capacity communication system. To do this, it can either utilize a single OPC unit at the midpoint of the optical link or a many units OPCs, known as inline OPCs.

2.8.4.1 Symmetric OPC Placement

This technique, also known as mid span spectral inversion (MSSI), requires the exact same quantity of transmission fiber both before and after conjugation [25, 78, 83]. In this system, after a certain length (N spans) of optical fiber link, the entire signal is phase conjugated and then transmits through another link with similar properties of fiber. In order to maintain the same transmission characteristics along the whole link, the OPC is typically needs to be located in the middle of the link (N/2 spans), as shown in figure (2.13), which flips the constellation around the imaginary axis. The characteristic of this system gives the transmission systems many advantages like wide dynamic ranges, and nonlinearity compensation for simultaneous multichannel.

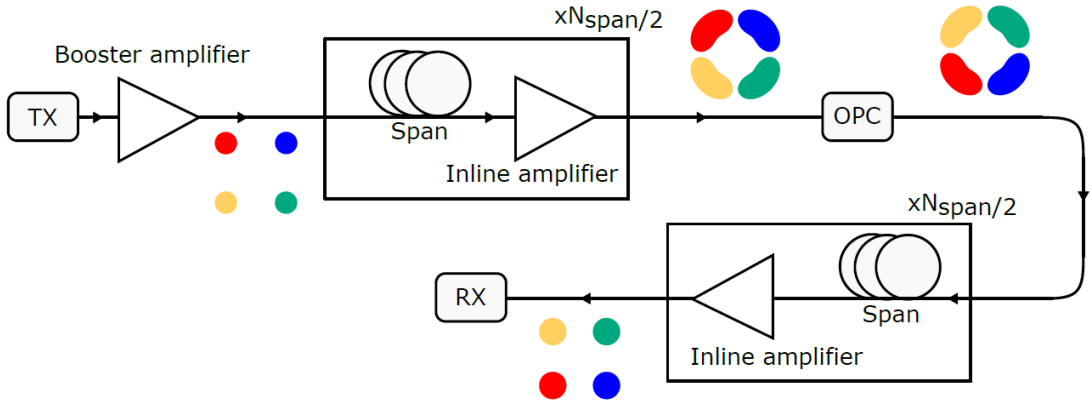

Figure (2.13). Schematic representation of mid-span spectral inversion (MSSI) optical phase conjugation

2.8.4.2 In Line Optical Phase Conjugation

In line OPCs can be placed in the fiber optic link to conjugate the phase of the signal after every certain transmission fiber length and repeat the phase conjugation after another same length of transmission fiber as shown in figure (2.14). This led to mitigate the fiber nonlinearity along the transmission link, which lets the signals to be routed dynamically [22, 84, 85]. Multiple OPCs are preferable to mid span OPCs because they allow the signal wavelength to be maintained while reducing receiver complexity and extending the transmission range. More importantly, multiple OPCs has been shown that have performance is betterer for mitigation of fiber nonlinearity than mid span OPC. In addition to that, the bulk dispersion during the transmission link can as well be compensated by using multiple OPCs.

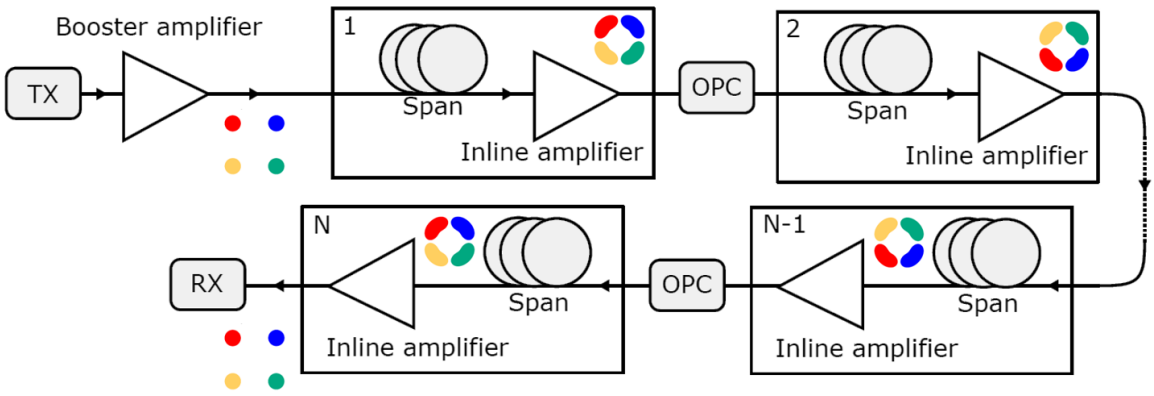

Figure (2.14). Schematic representation of in line optical phase conjugation

2.9 Fiber Impairments Compensation Using Machine Learning Techniques

Because of the challenges when using the nonlinearity of equalizations and techniques of compensations, and because of the impressive results achieved when using artificial intelligence (AI), the applications of AI-based techniques

to improve the performance of optical systems communication have recently received increased concern and become a hots area under researcher extensive in the past years. In addition to its use in traffic control, monitoring, and signal design, AI shows great promise for increasing nonlinearity compensation performance in optical communication by enabling flexible statistical analysis of complex systems without reliance on specific models [26, 86]. Figure (2.15) provides a high-level, systematic overview of the various AI approaches used in a variety of optical transmission system applications, the most prominent of which are statistics, analysis, and compensation for nonlinearity disabilities to enhance the performance of system.

ML is an area of artificial intelligence that use computational algorithms to transform empirical data into actionable models. Furthermore, the point of ML is to make the machine more capable of automatically learning from experience as opposed to being explicitly programmed. The ML algorithms are particularly useful in situations when it would be impossible or difficult to deploy explicitly written algorithms, such as in high-performance, real-time systems. Reinforcement learning, unsupervised learning, and supervised learning are the three primary categories into which ML systems fall according to how the system learns [87]. To dynamically train the model in an interactive setting, reinforcement learning employs a trial-and-error feedback method. With no prior knowledge of labels, unsupervised ML models attempt to discover hidden relationships within training data. In the end, supervised ML models learn from the labels on their training data to recognize their own unique complicated patterns, which they then use to make inferences or predictions about previously unknown data. The basic structures of the three learning paradigms are illustrated in figure (2.16).

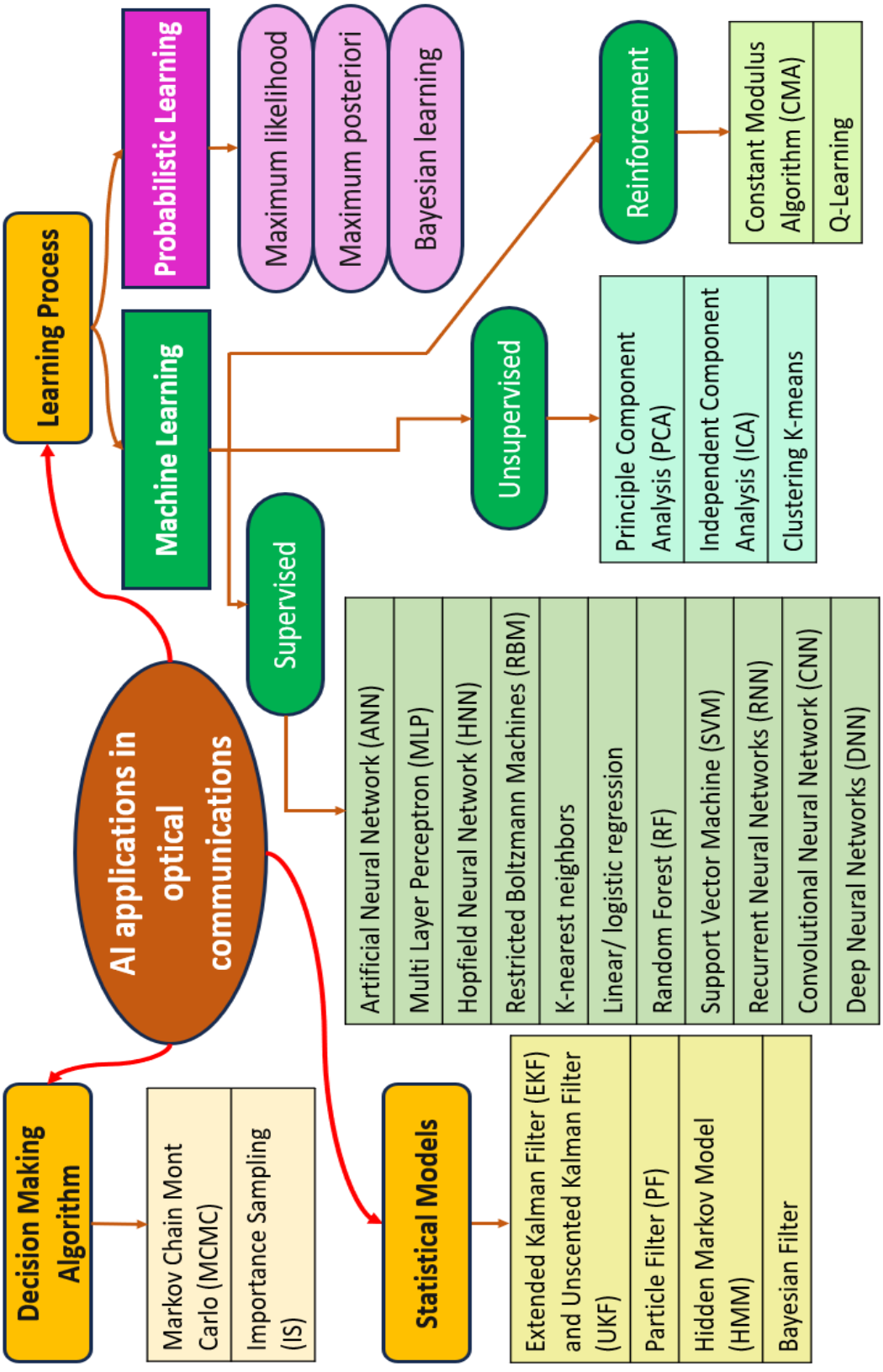

Figure (2.15). Fiber optic communications systems using AI techniques [86]

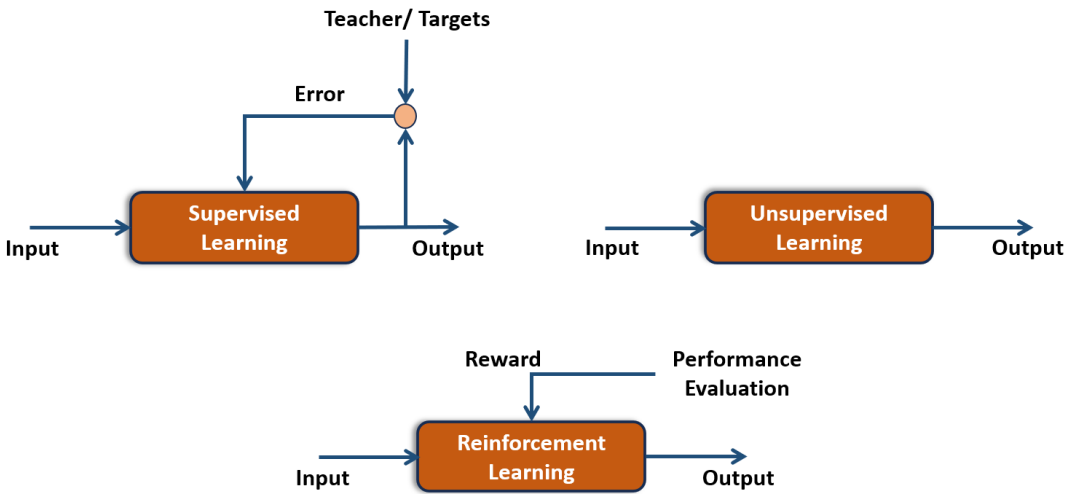

Figure (2.16). Structures of supervised learning, unsupervised learning, and reinforcement learning [88]

2.9.1 Learning Algorithms

ML is a branch of computer science which uses statistical approaches for enabling computers to learn from pieces of information or interactions with a virtual or real environment. It's usually divided to three sub-fields [87].

2.9.1.1 Supervised Machine Learning

Supervised ML technique uses training data attributes to model an outcome variable. ML algorithm target function is a mathematical transformation of input features to output variable. ML models usually optimize a parameter that influences the goal function. Supervised learning solves regression and classification problems [87].

2.9.1.2 Unsupervised Machine Learning

The purpose of unsupervised ML is to investigate a dataset and identify patterns or relationships. Unsupervised ML algorithms are trained on unlabeled data. Clustering and dimensionality reduction are the two basic components of unsupervised ML [89].

2.9.1.3 Reinforcement Machine Learning

A computer agent learns a task by interacting with its dynamic environment and experimenting. With this technique of learning, the agent may do the work without human assistance or instructions [90].

2.9.2 Neural Network (NN)

In order for a neural network to function properly, the basic unit that is responsible for the processing of information is called a neuron [91]. An output is produced by the individual processing unit after it has received input from other sources or signals generated by the output of other units. A neuron scheme's block diagram is shown in figure (2.17). There are essentially three parts:

• A set of connections, or synapses, where each node has its own unique strength. Multiplying the input signal x_m by the unit m to the weight w_{km} by the unit k produces the output signal.

• An adder that adds up the individual signal components at each synapses input, multiplying by the weight of that synapses input. Linear combining is represented by the steps outlined here.

• The activation function which allows the total of the input weights to pass through. By reducing the amplitude of the adder output, the neuron output is created.

Figure (2.17) shows a neuron scheme with an externally applied bias or threshold represented by b_k. Whether the bias b_k is positive or negative, the net input to the activation function goes up or down accordingly. The following two equations describe the neuron mathematically [92].

$$u_k = \sum_{j=1}^{m} w_{kj} x_j \qquad (\mathbf{2.53})(\boldsymbol{a})$$

$$y_k = \sigma(u_k + b_k) \qquad (\mathbf{2.53})(\boldsymbol{b})$$

where m the number of inputs and $x_1, x_2, \ldots\ldots, x_m$ are the input signals, $w_1, w_2, \ldots\ldots, w_m$ are the synaptic weights of the neuron, u_k is the output of the linear combiner caused by the input signals, $\sigma(.)$ represents the nonlinear activation function, and y_k is the signal output.

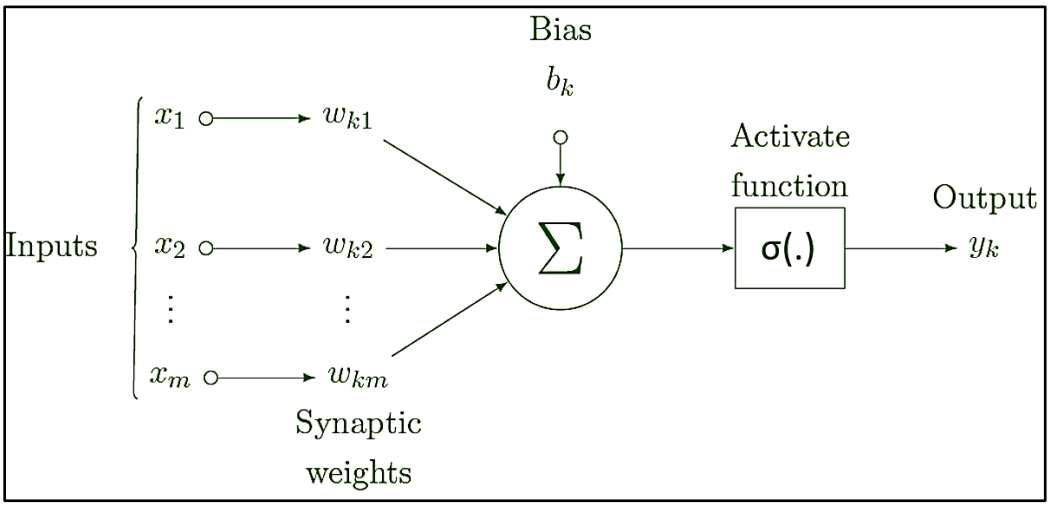

Figure (2.17). Basic neural network structure [93]

2.9.2.1 Activation Function

This function allows the NNs to learn nonlinear relationships between the input and output in the dataset though adding nonlinearity functions. There are many activation functions, but the most commonly used are illustrated in figure (2.18). One popular activation function used in NNs is the rectified linear unit (ReLu) [94], which retains positive values and converts negative ones to zero, i.e., $y = \sigma_{ReLU}(u)$ with

$$y = \max(0, u) \qquad (\mathbf{2.54})$$

The sigmoid function is another common source of activation for the artificial neurons $y = \sigma_{sigmoid}(u)$ where

$$y = \frac{1}{1 + \exp(-u)} \tag{2.55}$$

The input is translated into the (0,1) interval at the output of the sigmoid. The hyperbolic tangent function is widely used with negative output that is also frequently employed in practice, expressed as $y = \sigma_{tanh}(u)$ with

$$y = \frac{\exp(u) - \exp(-u)}{\exp(u) + \exp(-u)} \tag{2.56}$$

The output of a neuron can take on any value between -1 and 1 thanks to the hyperbolic tangent function. The SoftMax function is another crucial activation function since it standardizes the entire neuron layer to produce probability outputs. Element by element it is applied, and its definition as $y = softmax(u)$ with [95].

$$y_i = \frac{\exp(u_i)}{\sum_j \exp(u_j)} \tag{2.57}$$

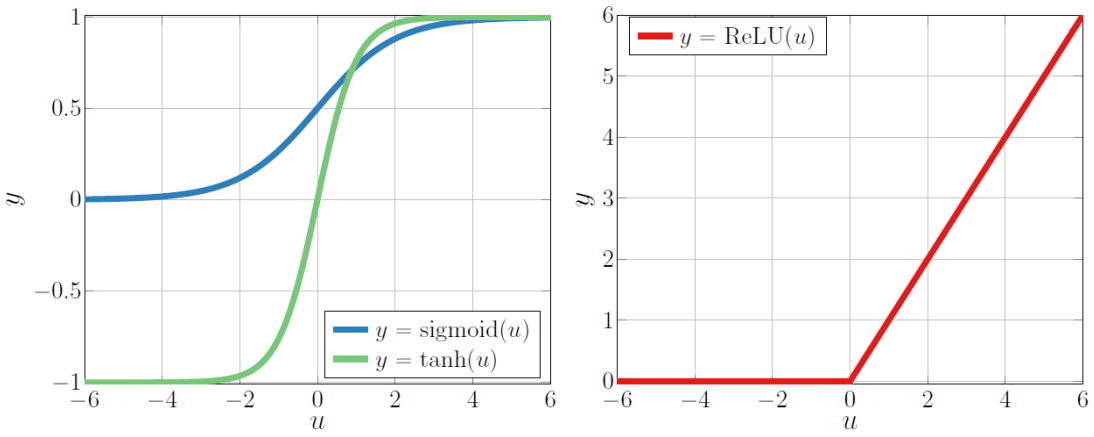

(a) (b)

Figure (2.18). (a) tanh and sigmoid functions (b) ReLu function

2.10 Structure of Neural Network

The topology of a neural network is the structure of its connections between neurons. The choice of neuronal structure is crucial to the network's performance and learning behavior [96], as is the specification of the network's architecture and the selection of appropriate parameter estimation or learning laws. Feedforward networks and feedback networks are the two primary categories of artificial neural networks. The former has a unidirectional flow of data, where the output is determined solely by the input's true values, and no loops or cycles exist in the system [97]. The latter are models with at least one feedback loop, as opposed to feedforward networks where the data flow is bi-directional [98]. Despite their computational benefits for modeling and storing temporal information, recurrent networks are best suited for tasks that need associative memory. For functional mapping challenges where insight into how inputs shape outcomes is of interest, feedforward networks are ideally suitable.

2.10.1 Convolution Neural Network (CNN)

In the past few decades, deep learning has proved to be a very powerful tool because of its ability to handle large amounts of data. The interest to use hidden layers has surpassed traditional techniques, especially in pattern recognition [99]. One of the most popular deep neural networks is Convolutional Neural Networks (CNN) in deep learning. A convolutional neural network is a series of convolutional and pooling layers which allow extracting the main features from the images responding the best to the final objective [100]. One significant benefit of this method is that CNNs can learn complex nonlinear correlations in the data and generalize effectively to unseen measures [101]. The CNN architecture consists of several layers, including an

input layer, one or more convolutional layers, one or more pooling layers, and an output layer. In general, a convolutional neural network is a series of all the operations described in figure (2.19). CNNs are composed of multiple layers of neurons, each of which performs a specific function. The purpose of the CNN is to model nonlinear distortions by learning a mapping from input to output. The mathematical model of a CNN is based on the concept of convolution, which is a mathematical operation that combines two functions to produce a third function.

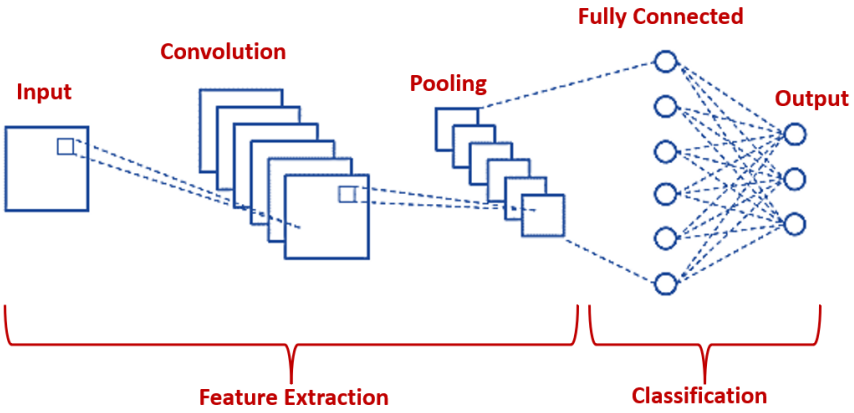

Figure (2.19). Architecture of CNN neural network [102]

A CNN is topically composed by four types of layers; convolution, activation function, pooling, and fully connected. The convolution operation is applied to the input signal or image to extract features from it. These features are then passed through multiple layers of neurons, each of which performs a nonlinear operation on the features to extract higher level features. Convolution can be mathematically described for a discrete domain of one variable [103].

$$y[n] = x[n] * h[n] = \sum x[k] * h[n-k]k \qquad (\mathbf{2.58})$$

Where $k \in [-\infty, +\infty]$. For a discrete domain of two variables:

$$(f * g)(x, y) = \sum_u \sum_v f(u, v).\, g(x-u, y-v) \qquad (\mathbf{2.59})$$

The second layer is activation functions which are desirable for multi-layer networks to detect nonlinear features and an essential part of CNNs as they allow it possible for the network to model complex nonlinear relationships between inputs and outputs. Different activation functions have different properties and can be more or less suitable for different tasks and architectures. Some of the most commonly used activation functions was discussed in section (2.9.2.1). The task at hand, the nature of the data, and the network's architecture all play a role in determining the optimal activation function to use [94, 95].

A pooling layer is a type of third layer commonly used in CNNs [104]. Its goal is to compress the feature maps produced by the convolutional layers without losing any relevant details. This is known as down-sampling or subsampling, and it helps to reduce the computational cost of the network and prevent overfitting. There are different types of pooling layers, such as max pooling, average pooling, and sum pooling.

Fully connected layers represented the fourth layer which are a powerful tool for building neural networks, allowing the network to learn complex and non-linear relationships between inputs and outputs [105]. They are typically used as the final layer in a CNN to make predictions based on the features extracted by the previous layers and can also be used to reduce the number of features in the final output. In a fully connected layer, each neuron receives input from every neuron in the previous layer, and in turn sends output to every neuron in the next layer. This allows the network to learn a more complex and non-linear relationship between the inputs and outputs. Each neuron in a fully connected layer applies a linear combination of the inputs, and an activation function, before passing the output to the next layer.

2.10.1.1 Solver Algorithms

Training a neural network requires an algorithm called a solver, which adjusts the network's parameters in response to differences between the predicted and actual outputs. There are several different types of solvers available, such as stochastic gradient descent (SGD), Adam, and root mean squared propagation (RMSprop). There are a variety of different solvers available, and selecting one relies on the nature of the problem at hand and the details of the data being solved [106].

Stochastic gradient descent (SGD) is a widely used optimization algorithm for neural networks. It updates the weights of the network by taking the gradient of the error function with respect to the weights and moving in the opposite direction. The main disadvantage of SGD is that it is sensitive to the learning rate [107].

Adam is an optimization algorithm that combines the advantages of SGD and RMSprop. It uses the gradient of the error function with respect to the weights and also estimates the second order moments of the gradients to adjust the learning rate adaptively. This allows Adam to converge faster and be more robust to the choice of the learning rate [108].

RMSprop is an optimization algorithm that uses the gradient of the error function with respect to the weights and also estimates the second order moments of the gradients to adjust the learning rate adaptively. It is similar to Adam but it uses a different form of the moving average of the second-order moments [107].

2.10.2 Recurrent Neural Network (RNN)

Recurrent Neural Network (RNN) is an advanced Artificial Neural Network (ANN) architecture that can be useful in such situations [109]. The fundamental idea of a recurrent neural network is depicted in figure (2.20-a). As can be seen in the illustration, an RNN has the shape of a loop, which incorporates the results of past processing steps into the current one. This is illustrated further in figure (2.20-b), which shows a temporal loop diagram for an RNN. The sequence (…; x_{t-1}; x_t; x_{t+1}; …) is fed into the recurrent structure as input. An updated output h_t is generated at time *t* by the recurrent cell using the input vector x_t and the prior output h_{t-1}. The recurrent cell output can be represented by the formula

$$h_t = \sigma(W(x_t^T \quad h_{t-1}^T)^T + b) \tag{2.60}$$

where RNN input at time *t* is denoted by $x_t \in R^l$, RNN output at time *t-1* by $h_{t-1} \in R^n$, $W \in R^{n\times(n+1)}$ is the weight matrix, $b \in R^n$ is the bias vector, ^{T} signifies the matrix transpose, and σ denotes the activation function. Since RNN are more effective in jobs requiring associative memory, such as time series analysis, they offer substantial computational advantages for modeling and storing temporal information [110]. There are a variety of neural network architectures that can be used for time-series prediction, including Nonlinear Autoregressive with exogenous inputs (NARX) networks, Nonlinear Autoregressive (NAR) networks, and Nonlinear Input-Output (NIO) networks. Each of these architectures have their own unique advantages and can be applied to different scenarios depending on the specific requirements of the application. In the context of the proposed system design, the NARX network was chosen due to its ability to model nonlinear systems with

feedback, which is essential for compensating for the nonlinearity introduced by the optical components in the communication system.

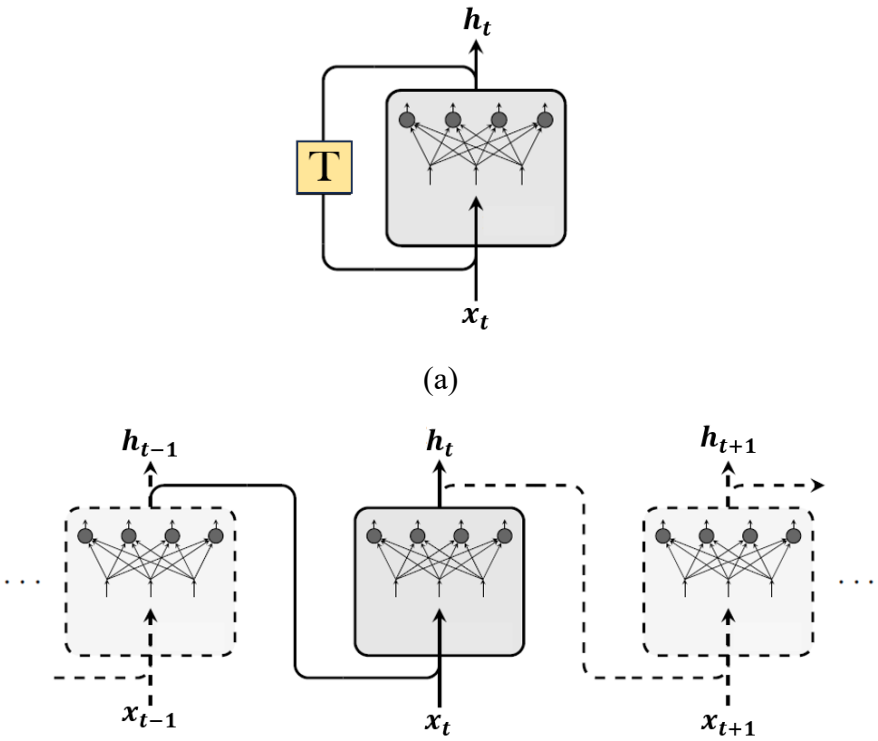

Figure (2.20). A graphical illustration of (a) artificial recurrent neural network (b)RNN 'unfolded' in time

2.10.2.1 NARX Architecture

Based on the nonlinear autoregressive model, the NARX is a specific kind of feedback neural network. The NARX network architecture typically consists of an input layer, one or more hidden layers, and an output layer as shown in figure (2.21) [111]. The input to the network is the current state of the system, and the output is the predicted future state of the system. The feedback connections in the network allow the network to take into account the dynamic nature of the system, making it well-suited for modeling and compensating for nonlinear effects in optical fibers. The nonlinear function is implemented

using a neural network, which can have one or more hidden layers. The NARX model is trained by adjusting the weights and biases of the neural network to discover the system's nonlinear relationship between input and output.

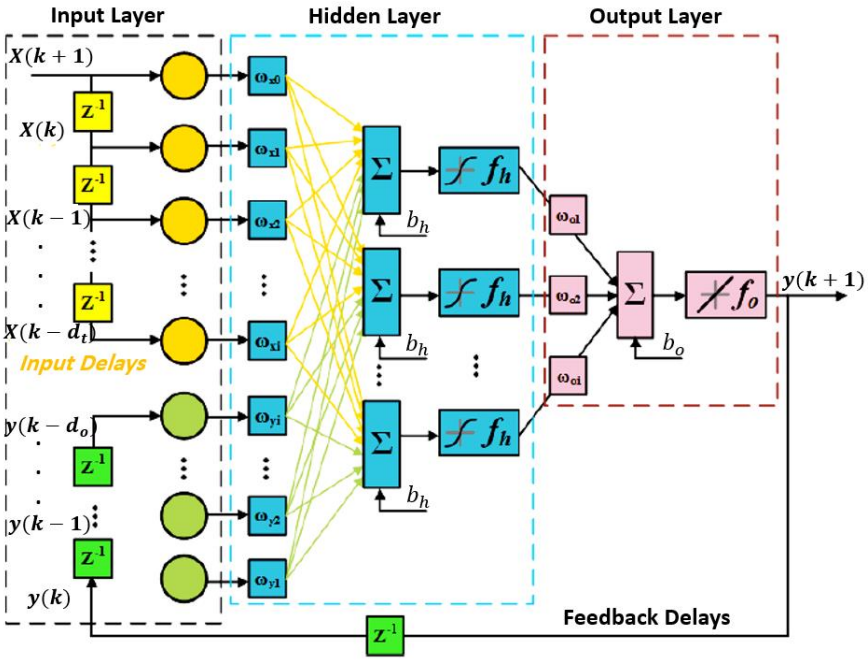

Figure (2.21). NARX neural network architecture [112]

There are several techniques that can be used to optimize the network's performance, each technique has its own strengths and weaknesses, and the choice of which to use depends on the specific requirements of the application. The most popular techniques used in NARX training are:

- ✓ **Backpropagation:** This is a commonly used technique for training neural networks, including NARX networks. The basic idea behind backpropagation is to compute the gradient of the loss function with respect to the network's weights, and then update the weights in the direction of the negative gradient [113].

- ✓ **Levenberg-Marquardt:** This is a specific optimization algorithm that can be used to train NARX networks as an alternative to backpropagation. This algorithm is based on a trust region approach, where the step size is adaptively adjusted depending on the local curvature of the loss function. This can help the algorithm converge more quickly and avoid getting stuck in local minima [114].
- ✓ **Gradient descent:** is another popular training function that works by minimizing the error between the predicted output and the actual output, by moving the weights in the direction of the negative gradient of the error function [115].

Regarding training functions, there are various type of functions can be used to train NARX each with their own unique set of advantages and disadvantages [113]. One such function is 'trainlm', which uses the Levenberg-Marquardt algorithm to train the NARX. This function is known to be efficient, especially when dealing with large datasets, and can converge quickly.

Another training function that can be used is 'trainbr', which utilizes the Bayesian Regularization algorithm to train the NARX. This function is known to be robust and can handle noise effectively, and it is also less sensitive to the initial weights. However, it may require more computational resources and can take longer to converge compared to 'trainlm' [116].

A third training function that can be used is 'trainscg', which uses the scaled conjugate gradient algorithm to train the NARX. This function is efficient and can handle large datasets effectively. It is also less sensitive to the initial weights compared to 'trainlm' [116]. However, it may not be as robust to noise as 'trainbr'.

Chapter Three

The Proposed Compensation System Based on Phase Conjugation

3.1 Introduction

This chapter presents the main stages used to construct the proposed compensation system in detail based on the information presented in the previous two chapters that will be used as a foundation for the proposed design of a nonlinear mitigation technique. The chapter describes the optical compensation technique based on phase conjugation. The use of Optical Phase Conjugation (OPC) in this thesis is divided into two ways, mid span OPC and multi OPC. The effect of each method was studied with three different scenarios; a conventional approach, a hybrid OPC approach using dispersion compensation fiber (DCF), and a hybrid OPC approach using a Raman amplifier. The proposed compensation technique is implemented with different types of optical communication systems, such as dual polarization NRZ-OOK, single polarization 8 QAM, and dual polarization 16 QAM. This system was constructed using the DWDM technique with a channel spacing of 50 GHz, which allows for a total of sixteen channels at varying data rates. The design of the system should be chosen properly to the exact selection of the different components in the system. A brief description of the main simulation tools and software that were used in this work is described in Appendix A.

3.2 OPC System Design

The OPC system design is shown in figure (3.1). The architecture of the proposed system is divided into three parts; transmitter part, fiber optic channel with OPC, and receiver part.

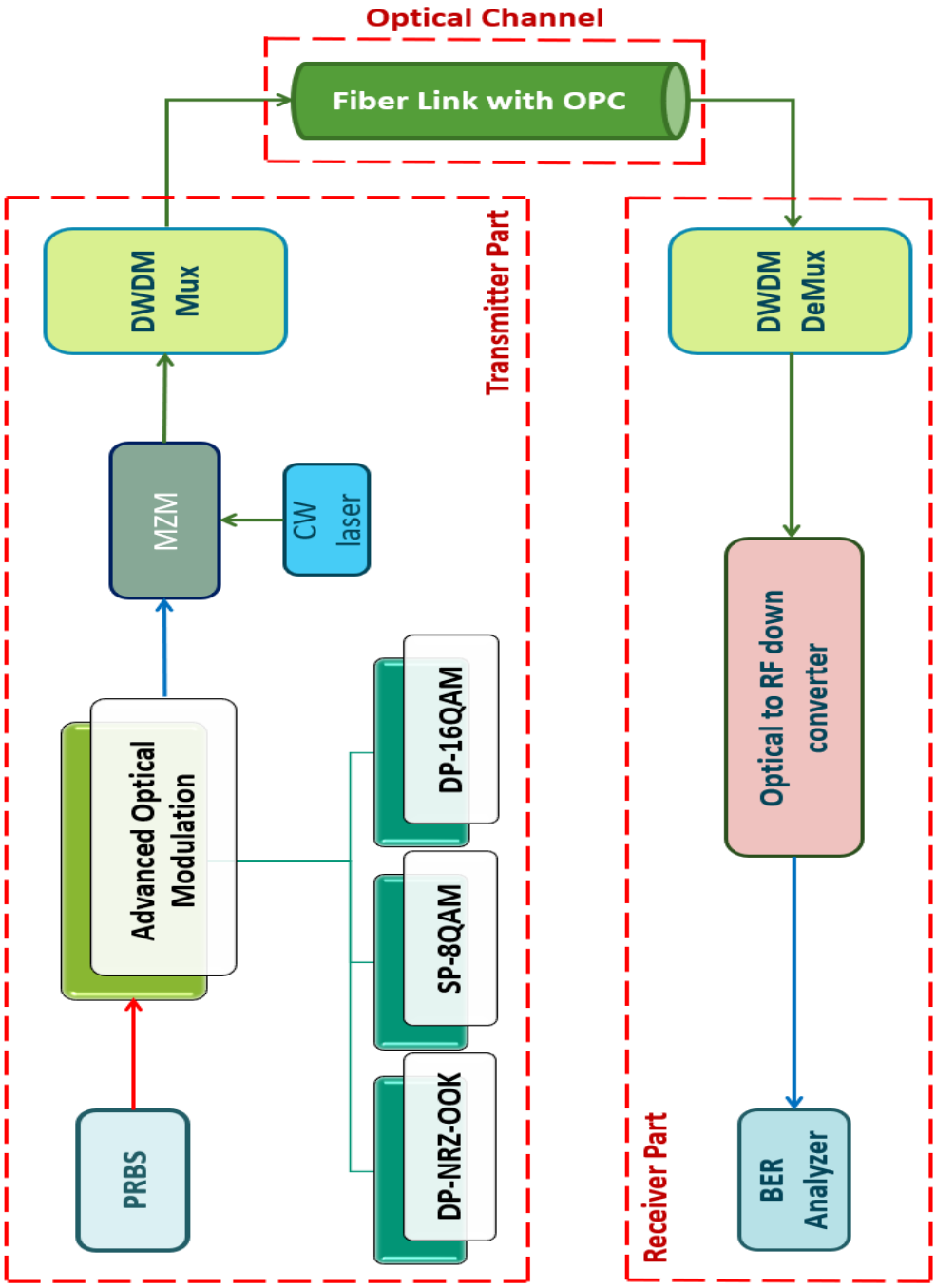

Figure (3.1). The proposed system based OPC

3.2.1 Transmitter Part

In the transmitter part, Pseudo Random Binary Sequence (PRBS) generates a bit sequence with the length of input data sequence equal to 2^{16} fed into the advanced modulation system, which is three types used in this system; DP-NRZ-OOK, SP-8QAM, and DP-16QAM. The brief details with a block diagram of each optical modulation are illustrated below.

3.2.1.1 DP-NRZ-OOK

In the DP-NRZ-OOK format, a CW laser is used to produce a continuous wave optical signal with different frequencies with 0.1 MHz line width. CW is divided into two branches using a polarization splitter device as shown in figure (3.2). Each branch starts with the Bit-Sequence Generator (BSG) that produces the binary information for transmission. Each bit is subsequently converted into an NRZ pulse by the NRZ pulse generator. Next, to complete the transformation from electrical to optical, a Mach-Zehnder Modulator (MZM) is used to modulate the pulses with an optical CW carrier. The polarization components of the signal are then combined through a polarization combiner (PC) to send to the multiplexer.

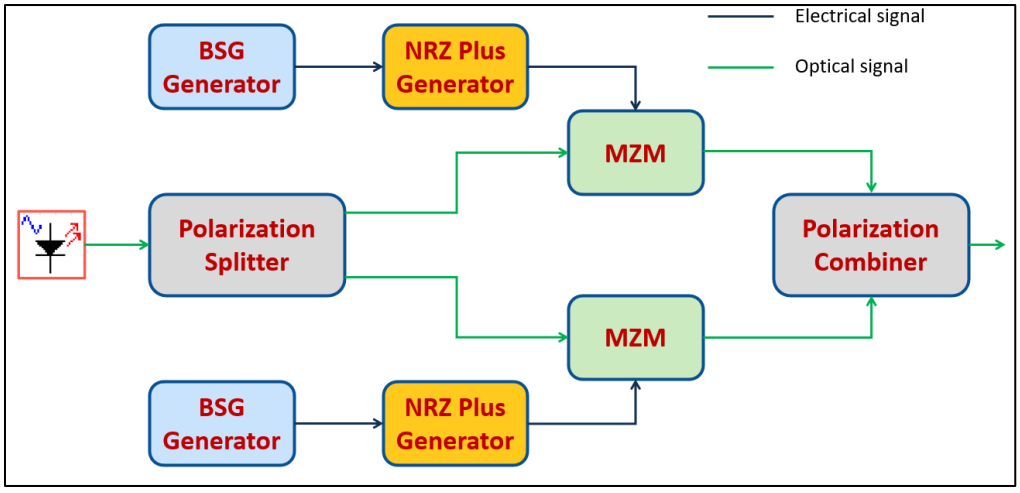

Figure (3.2). Block diagram of the transmitter part for DP-OOK

3.2.1.2 SP-mQAM

The input data sequence is built by using PRBS to generate a bit sequence and then fed to the QAM sequence generator encoder in order to generate two parallel M-ary symbol sequences as in-phase (I) and quadrature (Q) components from input binary signals. The output resulting signal from the M-ary encoder (in-phase (I)/ quadrature (Q)) is fed to the Radio to Optical (RTO) unit. RTO unit consists of x-coupler and two dual drive lithium Niubate Mach Zehnder modulators (MZM) as shown in figure (3.3). Each baseband (I/Q) signal component is split into two parts by using a fork device (1×2) to copy the electrical input signal into two output electrical signals which will be fed to electrical input ports of the MZM, in addition, the optical input port of the MZM will connect on CW Leaser. Finally, the optical output signals of both MZMs are combined by another x-coupler device that has a 90° phase shift to combine the two (I/Q) MZM optical signals into the complex optical signal with amplified it to prepare for transmission.

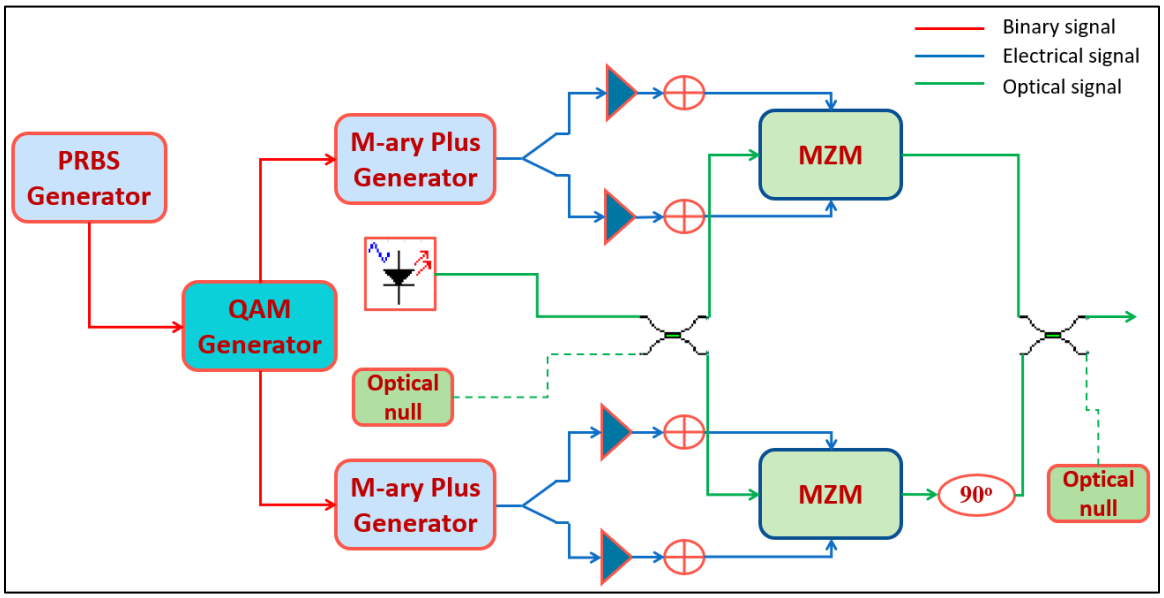

Figure (3.3). Block diagram of the transmitter part for SP-mQAM system

3.2.1.3 DP-mQAM

The proposed dual polarization coherent detection optical system block diagram is shown in figure (3.4). It's essentially constituted of two transmitter parts that operate in a parallel process, every one of them generating a base band signal (one for each one of the polarizations). The first transmitter here has been referred to as the x-polarization and the second transmitter as Y-polarization.

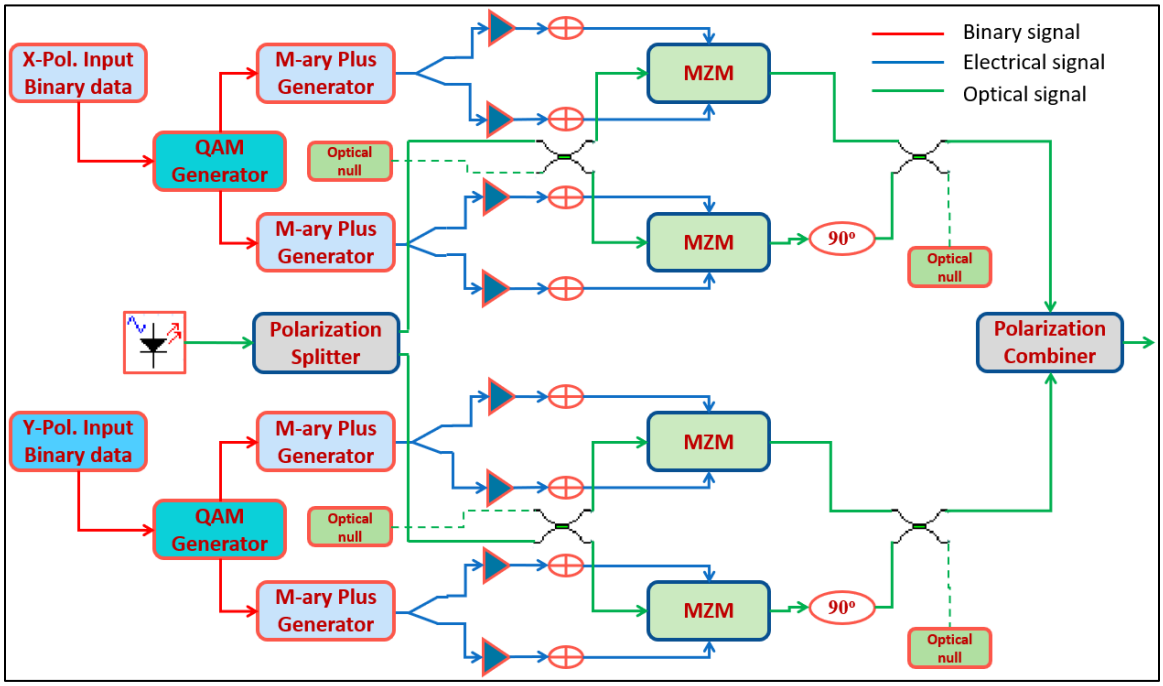

Figure (3.4). Block diagram of the transmitter part for DP-mQAM system

The architecture of the transmitter part is described in the previous SP-mQAM section in brief detail. The two electrical baseband signals from both (X/Y) polarization of the transmitter part are fed directly to the RTO unit as the first input, while the second input of the RTO unit is fed from the output of the polarization splitter (1×2) which divides the beam of the CW laser source into two beams with 90° degree orthogonal polarization. The output signal from each one of the RTO units represents one polarization, after that the two

generated polarizations X and Y have been combined with the polarization combiner (2×1) device for the purpose of forming a dual polarization optical signal and then it is amplified and sent through the optical fiber.

3.2.2 DWDM System

The baseband signal will be fed to the electrical input ports of the MZM, in addition, the optical input port of the MZM will connect to CW Leaser. The output optical signal from MZMs is fed to the dense WDM system with different frequency lasers. DWDM is used with all of the proposed optical communication systems as one technique that supports increasing the data rate of the system. This multiplexer device is added at the transmitter part to combine all the optical sub-channels so that they can be transmitted over the optic fibers. These signals are combined in one signal and propagated in the optical fiber. The DWDM multiplexer simulation parameters are shown in Table (3.1).

Table (3.1). DWDM system optical multiplexer and demultiplexer simulation parameters

Parameter	Value	Units
channel spacing	50	GHz
Bandwidth	10	GHz
Depth	100	dB
Noise threshold	-100	dB
Number of channels	8, 16	
Filter type	Bessel	
Filter order	2	

3.2.3 Fiber Optic Channel Link

In a multichannel system, the output of the DWDM is propagated through the fiber optic transmission media. The output channel consists of single mode fiber (SMF) and an optical amplifier (OA) with gain depending on the length of the fiber to compensate for the losses. The main parameter value of the optical channel is listed in Table (3.2). Signals propagated through SMF over long distances will suffer from distortion and nonlinear problems. At this point, an optical phase conjugation method will be used to solve the problems that optical fibers suffer from. The brief details of the concept of OPC and its working mechanism are illustrated in section (3.3).

Tabel (3.2). Parameters of fiber optic link

Parameter	Value	Units
Reference wavelength	1550	nm
Length	variable	km
Attenuation	0.2	dB/km
Dispersion	16.75	ps/nm/km
PMD coefficient	0.05	ps/sqrt(km)
Differential group delay	0.2	ps/km
Effective area	80.0	μm^2
Nonlinear index	2.6×10^{-20}	m^2/w

3.2.4 DeMux DWDM System

A demultiplexer device should be added at the receiver part which will be providing the separation of optical subchannels in a frequency domain and it may be easier to analyze them separately. The simulating parameters of the DWDM demultiplexer system are listed in the table (3.1).

3.2.5 Receiver Part

The received optical signal is detected by the Optical to Radio (OTR) unit with balanced noise detectors. The work of the OTR unit will be different based on the advanced modulation technique used. The brief details with the block diagram of each optical modulation are illustrated below as in the transmitter part.

3.2.5.1 DP-NRZ-OOK

The optical signal from DWDM DeMUX is passed through a polarization splitter device to be divided into X and Y polarization to receive the signal as it was transmitted in the transmitter part as shown in figure (3.5). Each branch generated RF signal by the PIN Photodetector passed through a low pass filter to filter the signal with cut off frequency (0.5×bit rate) to separate the modulated data from the frequency carrier and to reduce the noise generated in the detection and amplification process.

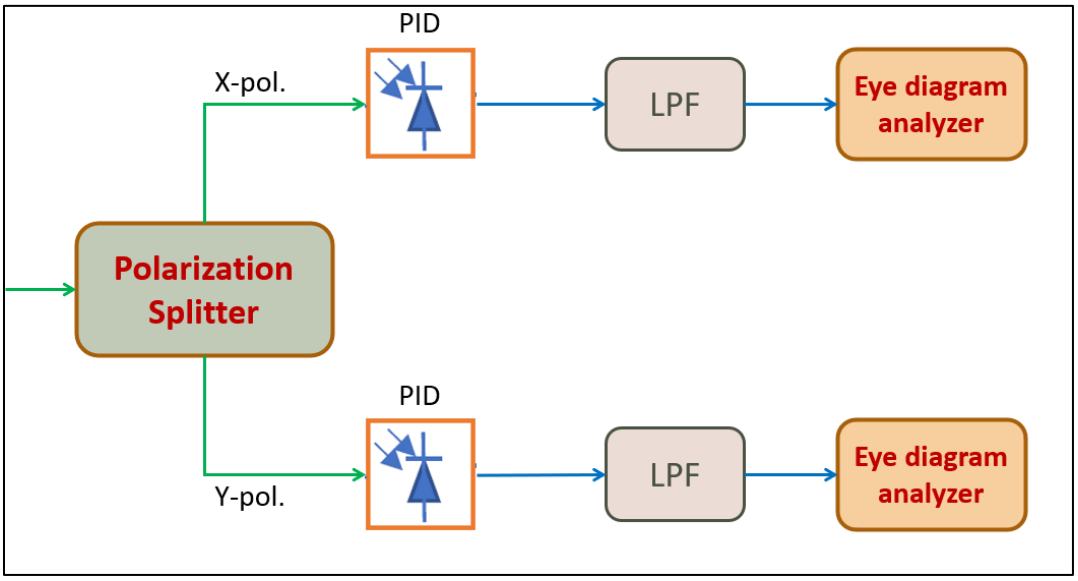

Figure (3.5). Block diagram of the receiver part for DP-OOK

Finally, the electrical signal is received using eye diagram analyzer to calculate and display the signal which can calculate different metrics from the eye diagram, such as Q factor, eye opening, eye closure, extinction ratio, eye height, and BER.

3.2.5.2 SP-mQAM

Figure (3.6) represents the block diagram of the SP-mQAM OTR down converter. This component is installed using four X-couplers, phase shift, four photodetectors, two electrical subtractors, and two electrical amplifiers. For the purpose of extracting components (I) and (Q) separately, the first X-coupler divides the incoming optical signal of DWDM DeMux into two parts, while the second X-coupler is utilized to divide the local oscillator signal into two parts that have 90^{o} phase shift to merge with the output of the first X-coupler signals in I and Q branches by using two pair X-coupler (3rd / 4th). The output signal for the third and fourth X-coupler fed to PIDs to generate the I and Q components of every signal (X and Y polarization) after subtracting the output of photocurrents from the two PDs. Finally, the I and Q component that represents the electrical signals received are amplified with two electrical amplifiers with 20 dB gain. After coherent detection, the signals are sent to a digital signal processor (DSP) for each individual channel, where they aid in the restoration of the original broadcast. After receiving the electrical signals from the DSP stage, the decision component processes them, normalizes the electrical amplitudes of both polarization channels to the appropriate m-QAM grid, and makes a judgment on each symbol received based on settings of thresholds. Lastly, QAM decoders are then utilized to convert the binary output signals from the two parallel m-QAM M-ary symbol sequences.

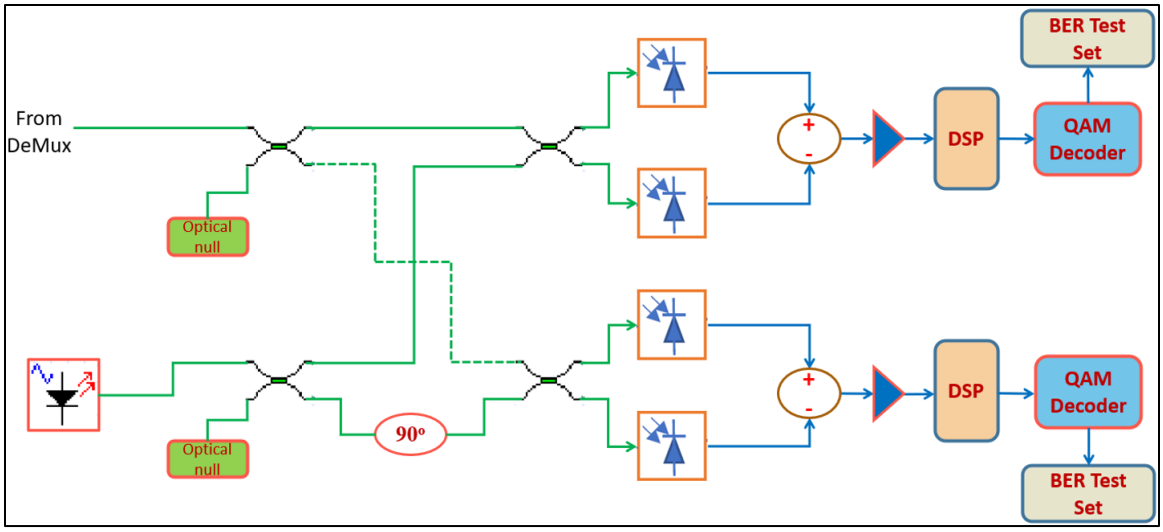

Figure (3.6). Block diagram of the receiver part for SP-mQAM system

3.2.5.3 DP-mQAM

The proposed Dual Polarization (DP) coherent detection optical system block diagram is shown in figure (3.7). The architecture of the receiver part is described as in the previous SP-mQAM section in brief detail.

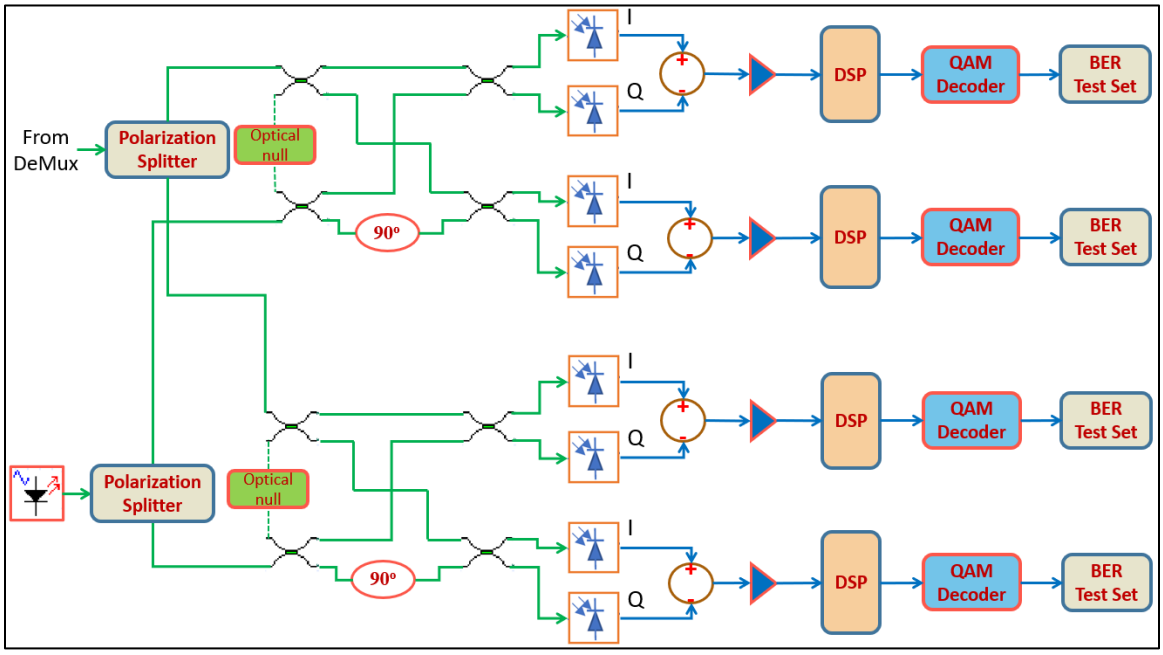

Figure (3.7). Block diagram of the receiver part for DP-mQAM system

OTR in DP is essentially constituted of two receiver parts that operate in a parallel process, every one of them extracting components (I) and (Q) separately (one for each one of the polarizations). The first receiver (from the polarization splitter) has been referred to as the X-polarization and the second receiver is Y-polarization.

3.3 Optical Compensation Method Using FOPA Based HNLF

Optical phase conjugation can be implemented by Four Wave Mixing (FWM) based on third order nonlinearity in a nonlinear medium called Highly Nonlinear Fiber (HNLF) based on Fiber Optic Parametric Amplifier (FOPA). The schematic configuration of the FOPA process in the HNLF medium is shown in figure (3.8). To achieve zero dispersion at 1550 nm, using two orthogonally polarized continuous wave (CW) pumps at 1502.6 nm and 1600.6 nm, the DWDM input signal with random polarization was launched into a HNLF of equal length (L) and nonlinear coefficient (n) (depending on a proposed modulation technique will be used). The linewidth of the CW pumps is less than 100 kHz. The idler receives the phases from the pumps and the signal in the form of $\Phi_{Idler} = \Phi_{Pump1} + \Phi_{Pump2} - \Phi_{Signal}$. After that, a 3 dB coupler was used to merge the signal from the two pumps into a single one with input powers of (P) dBm into the HNLF. Finally, an optical filter was placed at the HNLF's output to eliminate the two pumps and produce a filtered phase conjugated idler wave. Table (3.3) shows the simulated parameter of the FOPA based HNLF medium with the proposed system.

The use of OPC in this thesis is divided into two ways, mid span OPC and multi OPC, and study the effect of both methods in the proposed system. There are three different scenarios in this proposed system was used OPC in conjunction with DWDM with a channel spacing of 50 GHz: a conventional

approach, a hybrid OPC approach using dispersion compensation fiber (DCF), and a hybrid OPC approach using a Raman amplifier.

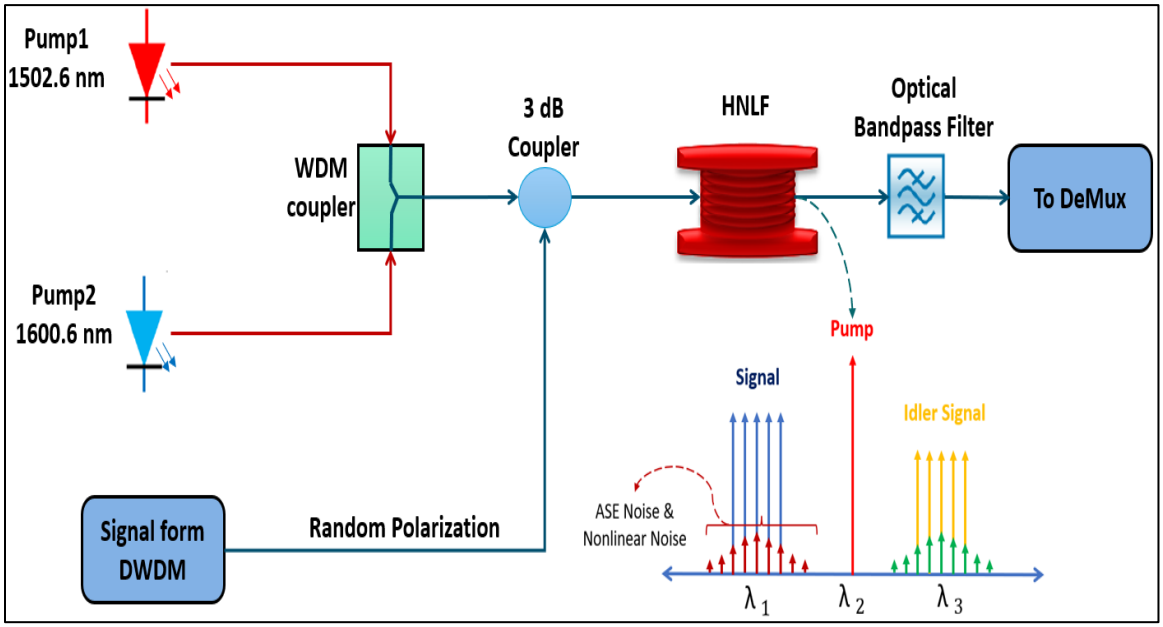

Figure (3.8). Polarization fiber optic parametric amplifier configuration with two pumps and HNLF

Table (3.3). Simulated parameter of OPC with the proposed system

Parameter		NRZ-OOK	8-QAM	16-QAM	Units
Pump1 and Pump2	Laser wavelength of pump1	1502.6	1502.6	1502.6	nm
	Laser wavelength of pump2	1600.6	1600.6	1600.6	
	Power	23	23	25	dBm
	Line width	0.1	0.1	0.1	MHz
Filter	Type	Gaussian			
	Bandwidth	6×Bit rate	14×Bit rate	4×Bit rate	Hz

Parameter		NRZ-OOK	8-QAM	16-QAM	Units
HNLF	Length	0.35	0.6	0.2	km
	Attenuations	0.35	0.6	0.2	dB/km
	Dispersions	16.75	16.75	16.75	ps/nm/km
	Dispersion slope	0.075	0.075	0.075	$ps/nm^2/km$
	Nonlinear coefficient	10.2	10.1	10	1/W.km
	Nonlinear refractive index	31×10^{-21}	26×10^{-21}	26×10^{-21}	m^2/w

3.4 Mid Span OPC with Proposed System

The first way to use OPC is known as mid span OPC. In this configuration, the DWDM modulated signal in this setup passes via a fiber optic with a length (0.5×L). This work used three scenarios that will compare the performance between them to solve the problem of nonlinear in multichannel as shown in figure (3.9); a conventional approach, a hybrid OPC approach using dispersion compensation fiber (DCF), and a hybrid OPC approach using a Raman amplifier.

In the conventional OPC approach shown in figure (3.9-a), the transmission link was a recirculating loop with two uncompensated dispersions. To compensate for the loss introduced by the transmitter, this modulated signal is amplified using an optical amplifier with a gain equal (L×0.2). Amplified Spontaneous Emission (ASE) is removed by sending the optical signal's output through the optical filter. The output of the optical signal is passed through OPC that was performed using a FOPA, as shown in figure (3.8).

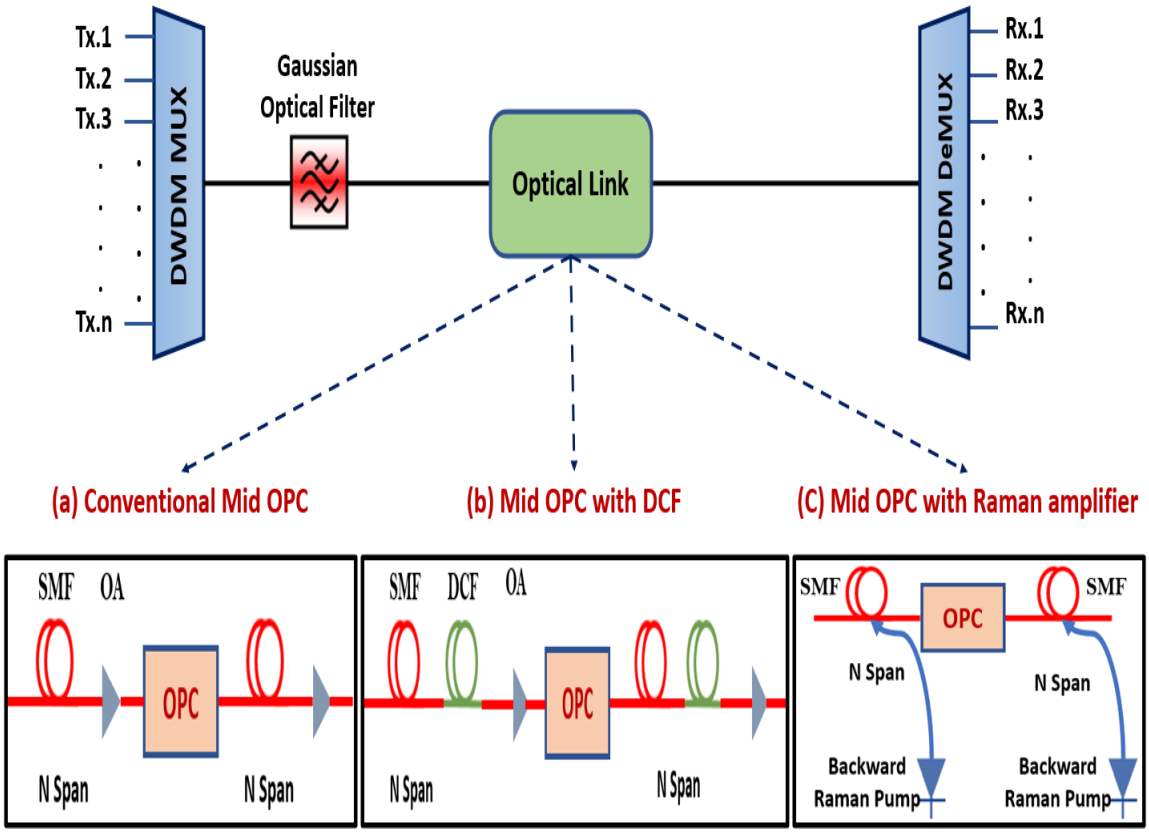

Figure (3.9). Proposed system model of Mid OPC with three scenarios

To improve installed links of standard single mode fiber, the use of dispersion compensation fiber (DCF) is an efficient method. Conventional DCFs have a high negative dispersion (-70 to -90) ps/nm.km, therefore, used to compensate for the positive value dispersion for the transmission fiber. Figure (3.9-b) shows a hybrid OPC approach with DCF to enhance the performance of the system by eliminating the compound dispersion originating from the fiber. Thirdly, in figure (3.9-c), counter propagating Raman pumps were used to make up for the span loss utilizing OPC. A Raman amplified link consists of a single mode fiber followed by a Raman backward bumping source. To achieve optimal Raman amplification, a continuous wave non-polarized fiber laser is used as the Raman pump; specifically, one that operates at 1452 nm. When it comes to efficient OPC based fiber nonlinearity mitigation,

distributed Raman amplification better satisfies the power symmetry criteria than discrete amplifiers.

In all three cases depicted in figure (3.9), an Idler wave is created after the signal travels through the nonlinear medium. The idler wave has a different wavelength than the input signal, but it contains the same information. A band pass filter with a frequency of the same frequency as the idler is applied to these signals to isolate the idler wave and eliminate the pump component. Following, this idle wave passes through an optical fiber whose length is identical to that of the transmitter. Since the signal from the transmitter is conjugated, any chromatic dispersion or FWM in the second section of the fiber will be nullified. The idler wave is amplified and filtered using an optical amplifier and optical filter. Finally, after going via a demultiplexer, the idler wave reaches the receiver, where it may be picked up.

3.5 Multiple Span OPC with Proposed System

The second configuration of OPC is in line OPC which is known as multiple OPC. The multiple OPC is investigated as mid OPC with three scenarios as illustrated in figure (3.10). The difference between multiple OPC and mid OPC can be seen when an optical fiber with twice the length of the transmitter and receiver is put in between two OPC modules. The DWDM system's optical signal output travels through the first optical fiber and the optical amplifier, as described in the mid OPC method. Following the optical filter, this signal is transmitted to the first OPC sharing the same parameter. When an idler waveforms in the first OPC, it is transmitted to the receiver via a second optical fiber whose length is twice that of the first. In this section, the idler wave carries the same data as the signal that travels through the optical amplifier and optical filter at the same frequency. In the following stage, after

going through HNLF, the idler wave travels through a second OPC with the same parameters as the first OPC, unless the signal representing the idler wave is itself a new signal that combines with the two pumps of the second OPC to generate a new idler wave. The second OPC's two optical filters have a frequency that is identical to that of the input signal (before passing through the first OPC). Finally, the signal is sent through a demultiplexer after going through an optical filter and an optical fiber of the same length as the transmission segment.

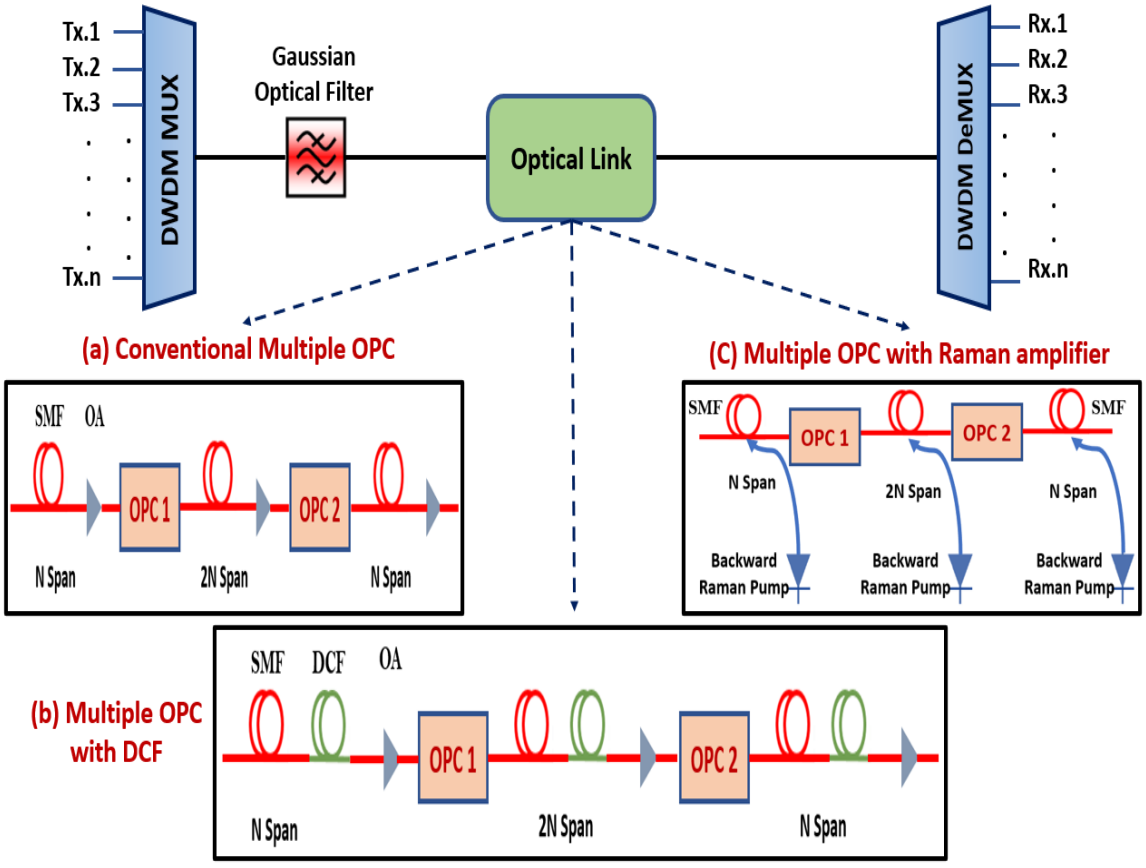

Figure (3.10). Proposed system model of Multiple OPC with three scenarios

Chapter Four

The Proposed Compensation System Based on Machine Learning

4.1 Introduction

The second proposed method to mitigate nonlinear effects in this work was used in the received part based on advanced machine learning. This chapter describes and illustrates the use of machine learning based neural networks for compensating nonlinearity in fiber optic systems. Specifically, it discusses two types of neural network architecture; Convolutional Neural Networks (CNNs) and Nonlinear Autoregressive with Exogenous inputs (NARX) time series networks. The proposed compensation technique is implemented with two different types of modulation formats; single polarization 16 QAM and single polarization 64 QAM with sixteen channels, taking advantage of the DWDM approach. The framework for implementing this work includes several stages: data collection, selecting machine learning algorithms and neural network architecture, training the network, and evaluating the performance of the optical system with the trained neural network for different power levels that will achieve improved performance and greater efficiency in compensating for nonlinear distortions in optical communication systems.

4.2 Machine Learning System Model

The proposed system model is a comprehensive design that incorporates several key components to mitigate nonlinear impairments in optical communications. The architecture of the proposed system shown in figure (4.1) is divided into three parts, which will be explained below.

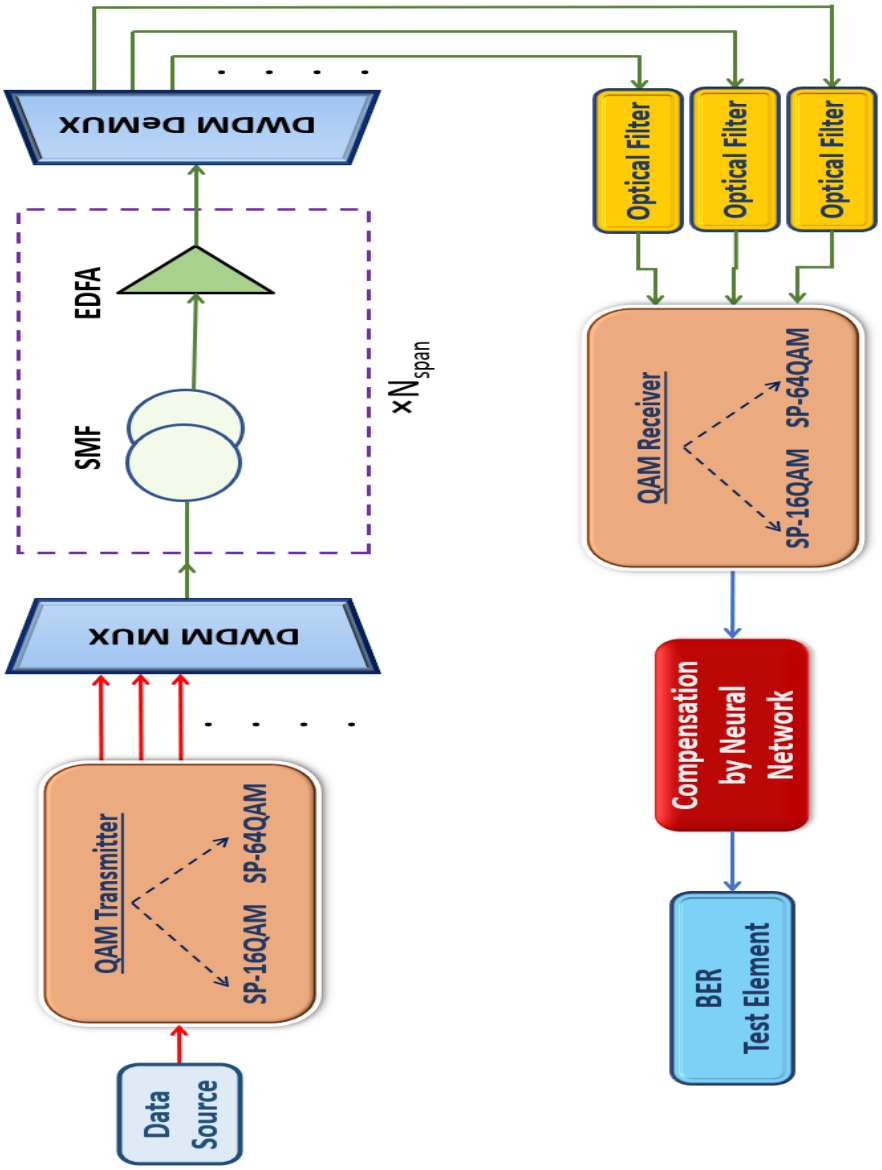

Figure (4.1). The proposed compensation system based neural network

4.2.1 Transmitter Part

The components of the subsystem are illustrated in figure (4.2) with the main parameters settings of the m-QAM system shown in table (4.1). This subsystem is composed of several key components that work together to modulate the data onto the optical carrier signal, creating the QAM signal that is transmitted over the optical fiber. The key components of the subsystem include:

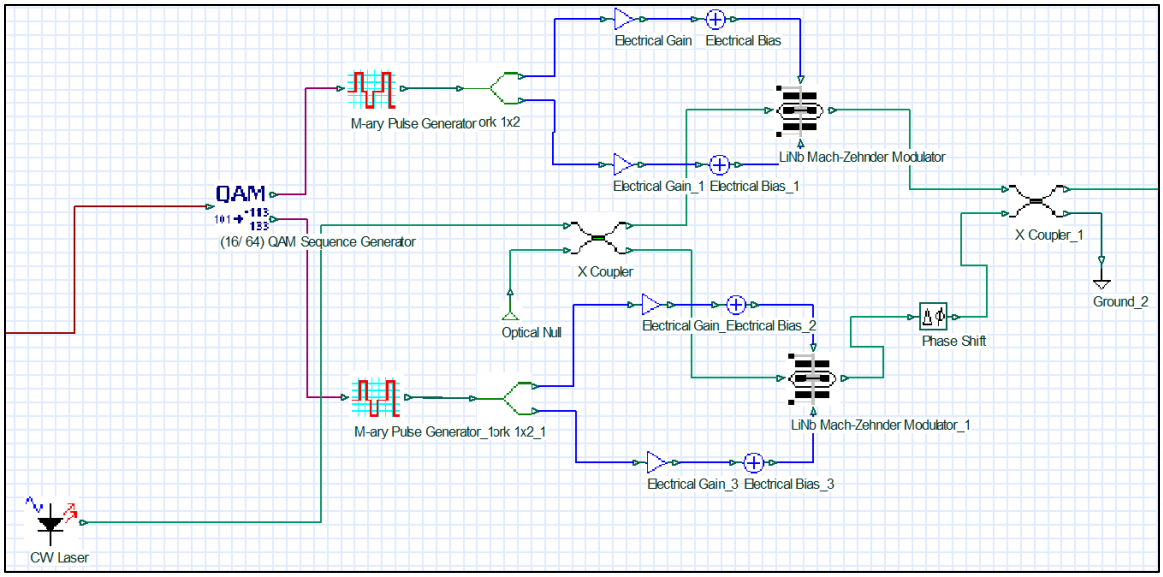

Figure (4.2). QAM transmitter signal

i. A 16/64 QAM sequence generator, generates a digital sequence of symbols for modulating the amplitude and phase of the optical carrier signal. The generator generates the In-phase and Quadrature phase independently, which allows for more precise signal modulation.

ii. An M array pulse generator generates electrical pulses with precise timing and duration to drive the modulator in the QAM transmitter. These pulses provide the electrical signal required for modulating the optical carrier signal, allowing for the generation of the QAM signal.

iii. A CW laser is an optical source that generates the optical carrier signal.

iv. Electrical gain is the ratio of the output signal to the input signal, which can be adjusted to optimize the transmitter's performance. This component ensures optical fiber signal is strong and high quality.

v. Electrical bias is the DC voltage applied to the modulator to control its operating point. This component is used to fine-tune the modulator's performance and ensure that it is operating at the optimal level.

vi. The Mach-Zehnder modulator (MZM) is a commonly used in optical QAM systems as it can provide both amplitude and phase modulation. This component is used to modulate the data onto the optical carrier signal, creating the QAM signal transmitted over the optical fiber.

Table (4.1). M-QAM main parameter of NN proposed system

Parameter	Value	Units
Bit rate	120	Gb/s
Symbol rate	Bit rate/ bit per symbol	symbols/s
Mapper	(16, 64) QAM	
Sequence length	65536	Bits
Bits per symbol	4, 6	Bits
Electrical gain	0.021	
Electrical bias	1.5	

4.2.2 Channels Multiplexing/ DE Multiplexing and Fiber links

The proposed design incorporates a variety of key components and highlights the link between the transmitter and receiver sides. One of the key technologies employed in this design is Dense Wavelength Division Multiplexing (DWDM) which allows for the simultaneous transmission of multiple channels of data, each operating at distinct wavelengths, onto a single optical fiber as shown in figure (4.3). This not only increases the capacity of the optical communication system but also enhances its efficiency. The proposed model implements DWDM with 16 channels, and an overall bandwidth of 10 GHz with a channel spacing of 50 GHz. Furthermore, in order to ensure optimal performance, the CW laser in each transmitter is set to correspond to the values of these channels. This composite signal is then

sent over a single mode fiber that is equipped with an Erbium Doped Fiber Amplifier (EDFA). The EDFA serves to amplify the signal as it travels through the fiber, allowing for longer transmission distances and ensuring that the signal remains robust throughout the transmission process. To control the length of the communication link, the system model includes ×N spans, which are implemented in the simulation model. These spans can be adjusted to simulate different scenarios and study the impact of transmission distance on system performance. Later, a DWDM Demultiplexer is employed to separate the transmitted signals, after which each channel enters a QAM receiver that is operating on the same channel frequency. This allows for the recovery of the original data transmitted on each channel and ensures that the data is accurately received.

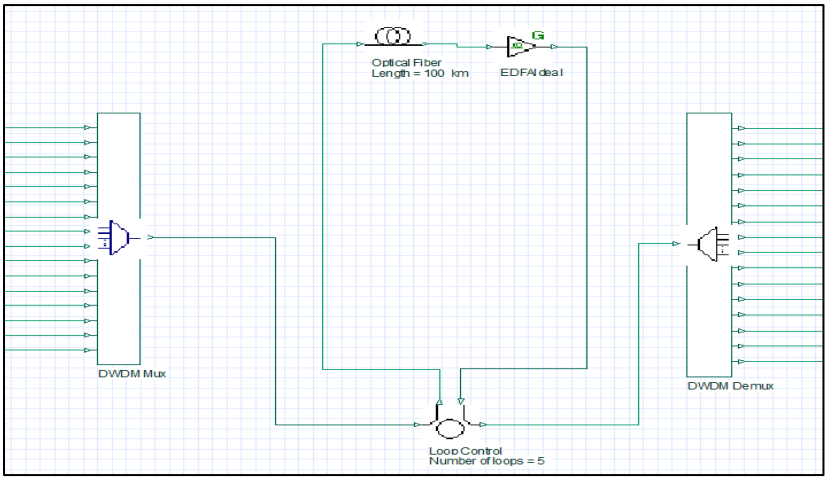

Figure (4.3). Multiplexer and De multiplexer with fiber links

4.2.3 Filtering and Receivers Side

Optical Gaussian filters are an important component in the proposed system design, as they are employed to selectively isolate specific wavelengths of light, thus enabling the separation of multiple channels that are transmitted on the same optical fiber. This is crucial in the context of DWDM which allows

for the simultaneous transmission of multiple channels of data, each operating at distinct wavelengths, onto a single optical fiber. As shown in figure (4.4), a 90-degree optical hybrid is used to extract electrical signals from the optical signals. This component typically comprises several key elements, including optical splitters that divide the incoming optical signal into two separate paths, with one path being delayed by a quarter of a wavelength; phase shifters that shift the phase of one of the optical signals by 90 degrees, creating a phase difference necessary for the interference process; a combiner that combines the two optical signals and creates interference patterns at the output ports; detectors that convert the optical signals into electrical signals; and electronics that process and analyze the electrical signals, extracting the original information. These components work together to extract the electrical signal from the optical signal by creating the interference pattern and converting the optical signal to an electrical signal.

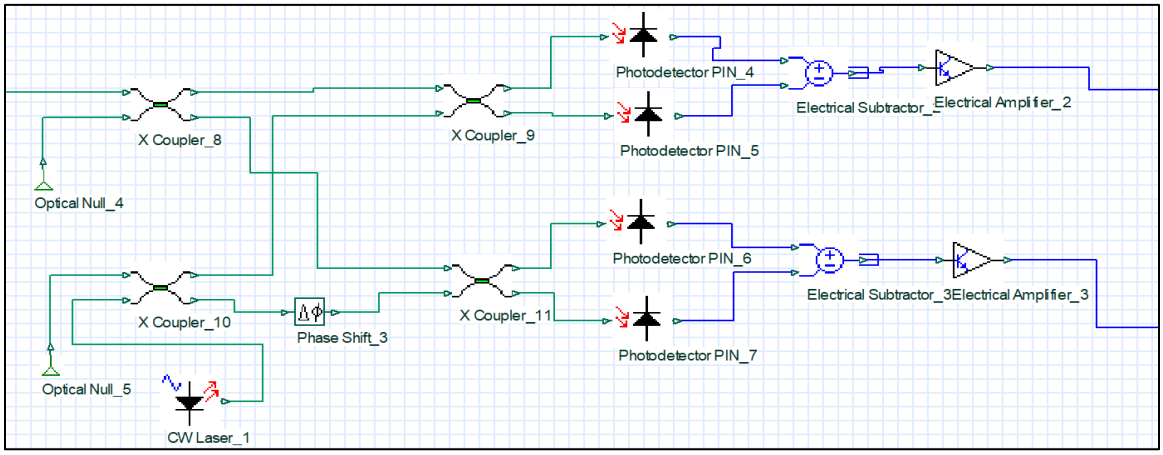

Figure (4.4). QAM receiver signal

Following the receiver, there is a subsystem that includes a MATLAB component which receives the electrical I and Q components of the signal as shown in figure (4.5). These components are then processed through a MATLAB code that includes a neural network-based equalizer. This equalizer

is trained to analyze the received signal and make adjustments to mitigate linear and nonlinear effects that may have occurred during transmission. The output of the MATLAB component is an electrical in-phase and quadrature-phase signal which is then inputted into the M-array threshold component to generate the QAM symbol. The output of this component is then fed into the QAM sequence decoder to generate the received bits.

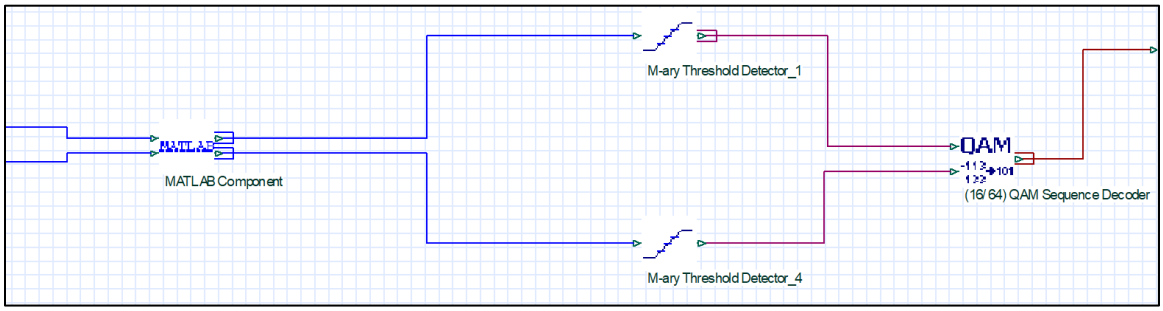

Figure (4.5). Subsystem with MATLAB component and received bits producing

4.3 Machine Learning Based Convolutional Neural Network

The first model of neural network used to mitigate the effects of nonlinear is Convolutional Neural Networks (CNNs). The proposed CNN model is a supervised learning algorithm that deals with classification problems, therefore the proposed optical NLC will be treated as a supervised nonlinear classification problem in machine learning terms for identifying the symbols of the received signal that have been encoded by the transmitter. To accomplish this, reshaped the frames of data obtained from the optical channel receiver to generate separate inputs for the I and Q components of the signal. Then utilized Optisys to generate frames for different distances, ranging from 100 to 5000 km, with different power for each channel from -15 dBm to 15 dBm. To ensure that the CNN input is in the form of an image in this work, it was carefully designed the frame length to match the length of the symbols. Specifically, it used a length of 128 for 16 QAM and 192 for 64 QAM, with a

number of samples of 2097152, a total sequence length of 65655 samples, a symbol rate of 20 e+9 for both modulation types, and sixteen channels with a data rate of 120 Gb/s for each channel. All of the data was stored in a class frame store and was created in separate frame stores for both training and validation, with 80% of the data used for training, and the remaining 20% used for validation and testing. This approach allows the network to make each decision based on single frames rather than on multiple consecutive frames. This allows the CNN to focus on specific symbols, thereby improving the accuracy of the classification.

4.3.1 Proposed M-QAM IQ Maps and Targets

With the QAM sequence generator, the bit sequence has been split into two parallel sub sequences, every one of which may be transmitted in two quadrature carriers in the case of building a QAM modulator. This has been accomplished with the use of serial to parallel converter. In the square QAM maps, can vary signal amplitude based on source symbols in the case of information transmission. The proposed reference target and classes of (16-64) QAM is shown in figures (4.6) and (4.7), respectively.

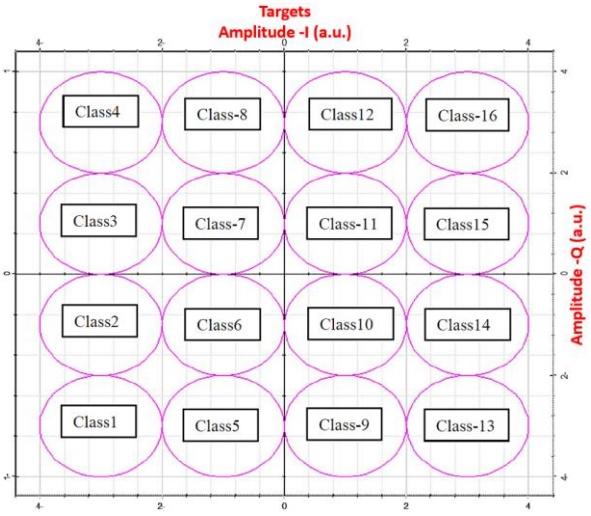

Figure (4.6). 16QAM reference target and classes

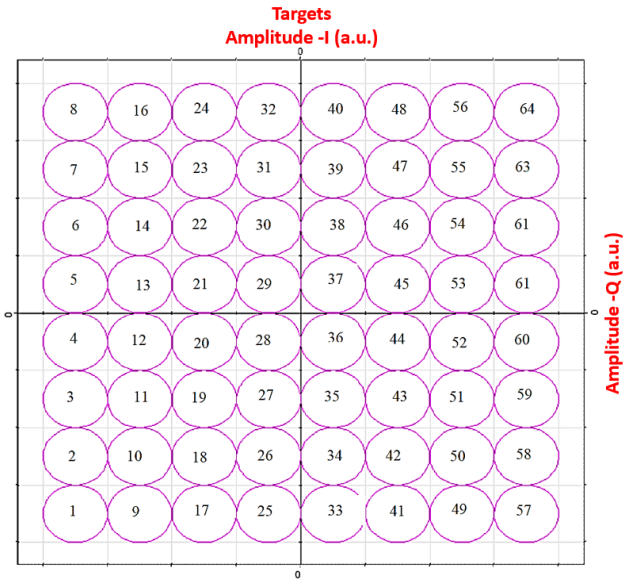

Figure (4.7). 64 QAM reference target and classes

4.3.2 CNN-ML System Design

The proposed CNN-ML based optical NLC is shown in Figure (4.8). The architecture of the network is designed to be able to compensate for the nonlinear effects of fiber optic communication systems. The convolutional layers of the network can learn complex features from the input data, which can help to compensate for the nonlinear distortions caused by the fiber optic channel. The proposed CNNs network is composed of several layers, each with a specific function:

a. **Image Input Layer:** This is the first layer of the network, and it is used to create an input layer for the network. The input layer has a size of 2×spf×1, and the normalization is set to 'none'. This layer is used to take the input data and reshape it to a format that the network can process.
b. **Convolution 2d Layer:** These layers are used to perform the convolution operation, which is the core operation of CNNs. These layers are used to learn features from the input data. The number of filters

used in each layer is determined by the net width parameter, and the filter size is defined by the filter size variable.

c. **Batch Normalization Layer:** These layers normalize the output from the previous convolutional layer. This can help to improve the training stability and speed.
d. **ReLu Layer:** These layers apply the rectified linear unit (ReLu) activation function to the output from the previous layer. It's a simple and computationally efficient activation function that helps to reduce the risk of vanishing gradient problems and improve the network's training speed and performance.
e. **maxPooling2dLayer:** These layers perform max pooling on the output from the previous layer. Pooling is used to down sample the data, which helps to reduce the computational complexity of the network and reduce the spatial dimensionality of the data.
f. **AveragePooling2dLayer:** These layers perform average pooling on the output from the previous layer. This can be used instead of max pooling to down sample data and regularize the network, reducing computational complexity.
g. **Fully Connected Layer:** This layer connects all the neurons of the previous layers and creates a fully connected layer. This layer is used to map the features learned by the convolutional layers to the output layer.
h. **SoftMax Layer:** This layer applies the SoftMax activation function to the output from the previous layer. This function is often used in the output layer of a classification network because it produces a probability distribution over the classes.
i. **Classification Layer:** The final input data classification is produced by this layer, which is an output layer.

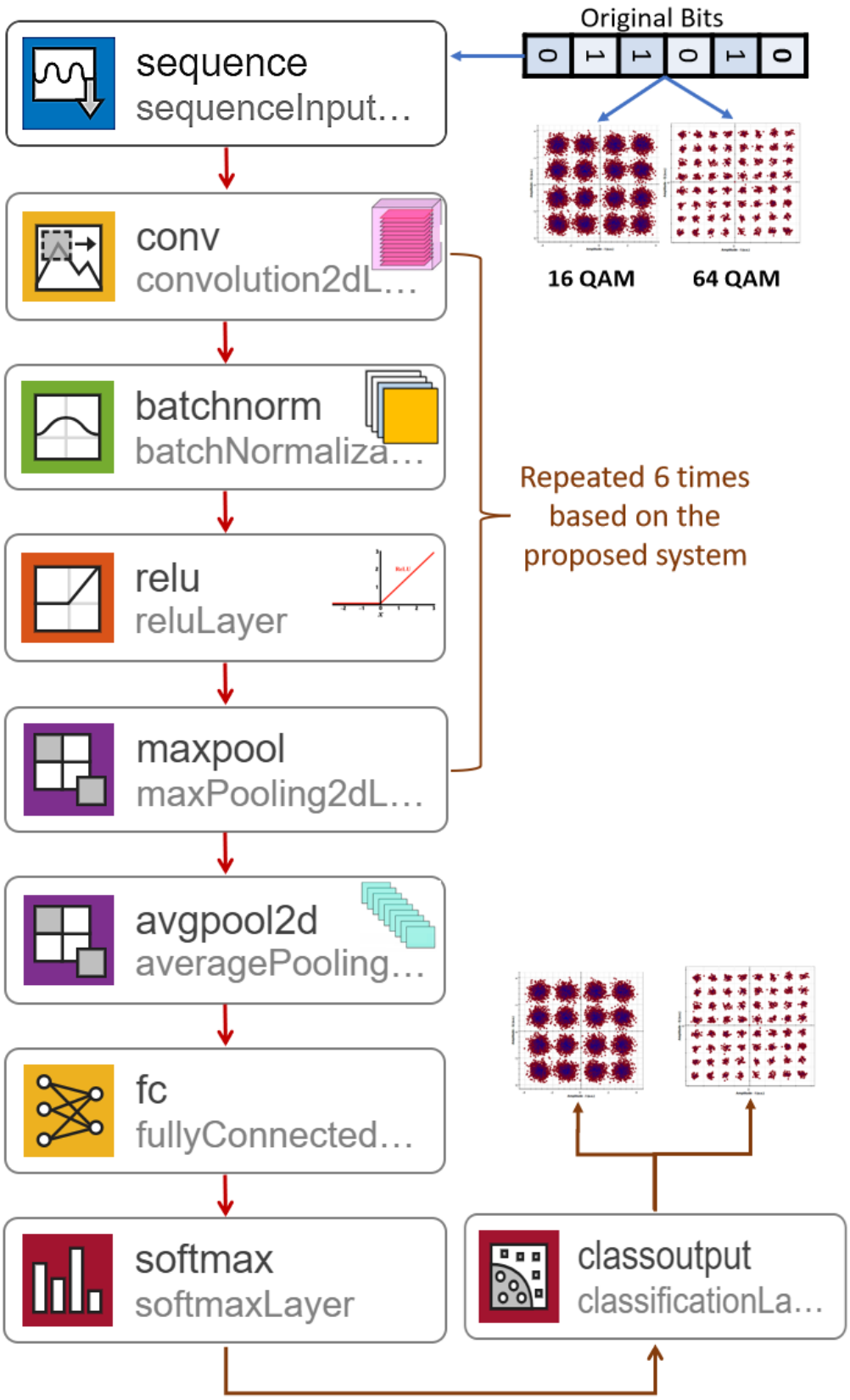

Figure (4.8). The proposed CNN layers architecture

The use of a deep architecture with 28 layers allows the network to learn more complex features from the input data, which can help to compensate for the nonlinear distortions caused by the fiber optic channel but also increases the computational complexity and the risk of overfitting. It's worth noting that the network uses 'same' padding in all the convolutional layers. This means that the spatial dimensions of the input and output will be the same, and it helps to preserve the spatial dimensions of the input data. Also, the pooling size is set to [1 2], which means that it takes the maximum value of a 2×1 area in the feature maps. Another thing to notice is that the number of filters increases as the network goes deeper, this allows the network to learn more complex features as it progresses through the layers. The last convolutional layer has 96 filters which is the highest among all layers, this allows the network to extract the most complex features from the input data. Overall, the architecture of the network is designed to extract features from the input data, reduce the spatial dimensionality of the data, and map the features to the output layer.

4.3.3 Training of Network

The training process likely used a specific set of hyperparameters, including a maximum number of training epochs, a mini-batch size, an optimization algorithm (Adam), an initial learning rate, a shuffling method, and validation data. The CNN is trained by iteratively processing small batches of the input data, and adjusting the weights and biases of the network based on the error between the predicted output and the true output. The work of these hyperparameters can be illustrated and explained below:

i. Max Epochs: This variable sets the maximum number of training iterations or "epochs" that the network will run for. An epoch is a

complete pass through the entire training data set. The purpose of this parameter is to set the limit of the number of iterations the network will go through. This work used max Epochs =750 and 1100 for our model.

ii. Mini Batch Size: This option controls training gradient update samples. Mini batch gradient descent updates network weights using a small set of training instances. This speeds training and prevents model overfitting.

iii. Adam: This approach updates model parameters using loss function gradient. It's a popular, computationally efficient way to optimize weights and biases for deep neural networks to reduce error.

iv. Initial Learn Rate: This option determines the optimizer's initial learning rate, which controls weight update step size. Lower learning rates result in smaller step sizes and slower convergence, while higher rates result in bigger step sizes and faster convergence.

v. Shuffle: The network shuffles training data every epoch. This can assist the network avoid local minima and see different examples each iteration.

vi. Validation Data: This option sets the validation data set and labels to evaluate the network's training performance. The validation data is used to assess network performance during training and detect overfitting.

After the training process is complete, the CNN can compensate for the fiber optic system's nonlinearity by processing input data and creating an output after training. Hyperparameter tuning occurs to identify the ideal settings for a dataset and job because these hyperparameters can significantly affect model performance. Additionally, it is also important to monitor the performance of the model using the validation data during the training process and make adjustments as necessary. The goal of the training is to make the network generalize well to unseen data, to perform well on new inputs.

4.4 Machine Learning Based NARX Time Series Network

The second model of neural network used to mitigate the effects of nonlinear is Nonlinear Auto regressive with Exogenous inputs (NARX). The NARX feedback neural network is a type of mathematical model that is based on the nonlinear autoregressive model. This model is designed to capture the nonlinear relationships between inputs and outputs in dynamic systems, making it a powerful tool for analyzing and predicting the behavior of such systems. The NARX neural network is utilized to forecast future values in time series data by effectively integrating past information. The external input and subsequent outputs of the time series data are what decide the NARX neural network's nonlinear model's prediction of the next value. In the proposed system, the NARX neural network has been employed effectively in modeling and compensating for nonlinearity in optical fibers by training on a dataset of nonlinearity measurements taken from an optical fiber and was able to accurately predict the nonlinearity of the fiber to mitigate the effects of it. NARX NNs are able to learn the complex nonlinear relationships in the data and generalize well to unseen measurements.

4.4.1 Data Preparation

To prepare data for a NARX time series network, as illustrated in the CNN model, the power level is set to different values ranging from -15 dBm to 15 dBm and the distance varies between 100 and 5000 km. Additionally, using the same symbol length for both 64 QAM and 16 QAM, which are 192 and 128, respectively. The total sequence length is 2097024 samples, with a rate of 20e+9 for both modulation types, and sixteen channels with channel spacing of 50 GHz using the DWDM technique. To generate the data for the NARX network, it was created individual frames for each symbol and stored

them in unique variables. These frames were then sequentially added together to create a dynamic representation of the channel, which simulates the behavior of a fiber optic link. This results in two vectors, representing the input and output of the dynamic channel, that can be used to train the NARX network to accurately predict the nonlinearity of the optical fiber. The procedure for a NARX model identification is shown in figure (4.9). The data preparation process for NARX models involves the following steps:

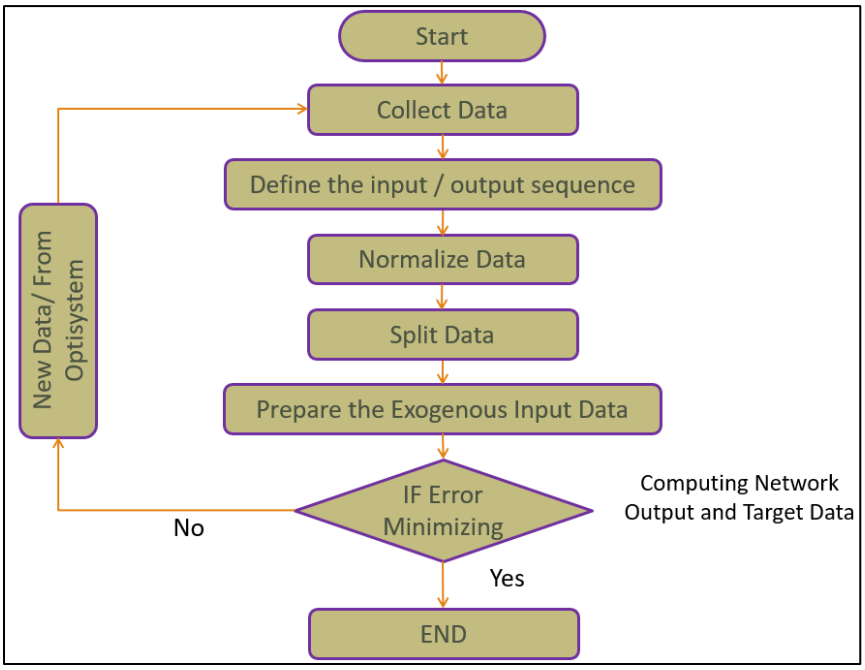

Figure (4.9). Flow chart of NARX model

a. The first step is to collect and preprocess the data. This includes identifying the variables that will be used as inputs and outputs, cleaning the data, and dealing with any missing values or outliers.
b. Define the input and output sequences: In a NARX model, the input sequence includes previous output values and exogenous inputs, while the output sequence includes future output values. The amount of past time steps needed to make predictions determines the input sequence

length, whereas the output sequence length depends on how far into the future the model must predict.

c. Normalize the data: It is important to normalize the data to ensure that all variables are on the same scale. This can be done using techniques such as min-max scaling.
d. Split the data into training and testing sets: The data is often divided into training and testing sets so that the effectiveness of the model can be assessed.
e. Preparing the exogenous input data: Exogenous inputs are any additional variables that are not part of the output sequence. These variables must be included in the input sequence and prepared in the same way as the output sequence.
f. Error Minimizing: During each epoch of training, the NARX network calculates the prediction errors between its output and the corresponding reference output from the dataset. The weights and biases of the network are adjusted using optimization algorithms, such as backpropagation or variants of gradient descent, to minimize these prediction errors. The optimization process continues iteratively, with the network updating its parameters to improve its ability to predict the undistorted signals accurately.

4.4.2 Network Architecture

A NARX time series prediction model in MATLAB is a type of feedback neural network that is used to predict future values of a time series based on its past values and exogenous variables. As can be seen in figure (4.10), the architecture of the NARX model consists of an input layer, a set of hidden layers, and an output layer with a feedback path.

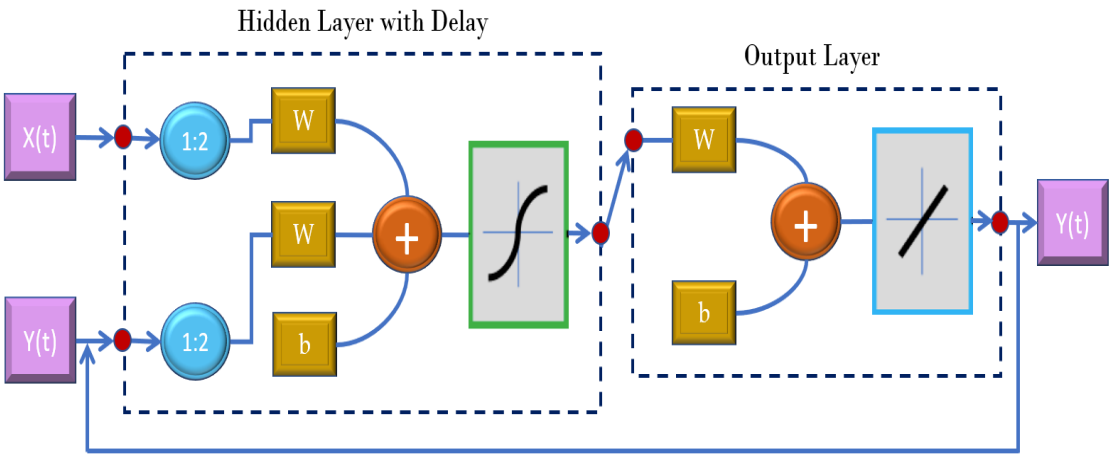

Figure (4.10). Training structure of the NARX model

The input layer receives the past values of the time series, as well as any exogenous variables that are used to predict future values. To improve prediction results, the NARX model takes into account the true condition of the passive target as one input variable. Levenberg Marquardt (LM) algorithms were used to train each model, with the epoch-based training function being propagated backward in time via the Back-propagation algorithm; a delay parameter ranging from 1 to 2 was assumed at the input to ensure accurate predictions and prevent overfitting.

In the hidden layer, the activation function of neurons is based on a hyperbolic tangent function that maps the input to a value between -1 and 1. This activation function is used to achieve high accuracy and minimize error. For more accurate results in state estimation, NARX structure simulations in this work use a hidden layer composed of 10 and 25 hidden neurons to analyze input and produce a nonlinear relationship between input and output. The neural networks were evaluated and validated using real and imaginary results (Grid reveal I-component and Grid reveal Q-component). The network predicts the value of the performance parameters at time t + 1 from the values of the inputs at prior times, making the prediction one step forward in time.

The last layer is the output layer which is a single layer and contains a linear type activation function, to generate a continuous output and provide a wider field in the sense that the output is not completely identical to the input.

4.4.3 Training Network

To train the NARX model, the data for each neural network was split into 70% training data, 15% validation data, and 15% test data. The dataset was trained on the training set, validated on the validation set to rule out overfitting, and then tested on the testing set to determine how well it performed. The dataset used for training the NARX network is collected over multiple values of power, encompassing a range of power levels. This dataset includes input-output pairs, where the inputs represent the distorted signals with varying power levels, and the outputs represent the corresponding undistorted or reference signals. The first step of training by the NARX network is initialized with random weights and biases. The training process consists of multiple iterations or epochs, where each epoch involves presenting the training data to the network and adjusting its weights and biases to minimize the prediction errors and accurately model the nonlinear behavior of the channel. The network's recurrent structure and feedback connections enable it to learn and adapt to various power levels, allowing it to compensate for nonlinearity and predict undistorted signals across a range of power and frequency variations in optical communication systems. The training of the NARX network involves two stages as shown in Figure (4.11); open loop and closed loop training. These stages offer distinct advantages and contribute to the network's ability to compensate for nonlinearity and predict undistorted signals in the presence of changes in power, phase, and frequency.

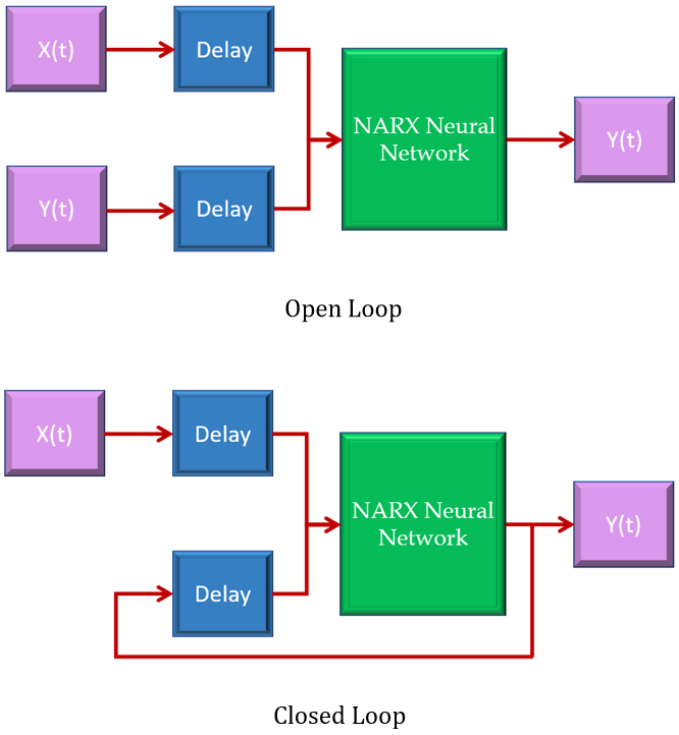

Figure (4.11). NARX neural network configuration

In the open loop configuration, the NARX network is trained by feeding back the estimated output to the input of the feedforward neural network. During open loop training, the network learns to approximate the nonlinear function by minimizing the prediction errors between its output and the reference output. This configuration allows for the modeling of the dynamic system and captures the temporal dependencies and nonlinear behavior of the channel. Open loop training provides flexibility in the network's architecture, enabling the use of feedback connections to enhance its learning capabilities. After completing the open loop training, the NARX network can be transformed into the closed loop configuration, also known as the series-parallel architecture. In this configuration, the NARX network is reorganized to enable multi-step ahead prediction and evaluation of its performance over extended time periods. The closed loop training allows for more rigorous testing and

validation of the network's ability to compensate for nonlinearity and predict accurately over consecutive time steps. By converting the network to the closed loop, the predicted output is replaced with the true output during training, improving the accuracy of the input to the feedforward network. The resulting network has a purely feedforward architecture, making it compatible with static backpropagation, a widely used training algorithm.

To evaluate the performance of the trained NARX model, it will use various evaluation metrics. The accuracy was calculated as the Mean Square Error (MSE) between the predicted and actual output values. As well as it will be monitoring the number of epochs required for the algorithm to converge to a satisfactory solution. It also recorded the elapsed time, which is the time taken by the NARX model to complete the training process. This is an important metric as it helps in determining the practicality of the model for real-time applications. Additionally, it will be monitored the gradient, which is the slope of the loss function with respect to the weights and biases. This metric helps in identifying the direction and magnitude of the updates required to minimize the error. Furthermore, it also will be used the learning rate parameter (mu) to control the rate at which the weights and biases are updated during training.

Chapter Five

Simulation Results and Discussion

5.1 Introduction

The results of a simulation of an optical fiber communication system using two compensation approaches that are illustrated in previous chapters three and four with different high order modulation formats are presented in this chapter. The data was collected from sixteen channels using dense wavelength division multiplexing with 50 GHz channel spacing, which is considered the most prominent technique that was used in this thesis to increase the transmission capacity. However, the nonlinear effects increase due to channel spacing causing signal deterioration. So, to reach the desired goal of reducing the nonlinear optical impairments, nonlinear compensation methods based on optical phase conjugation and advanced machine learning based neural networks will be investigated.

This chapter is divided into several key sections to provide a comprehensive overview of the results obtained as shown in figure (5.1). The first section shows the outcomes of simulations of mid span OPC in fiber optic communication systems. The second section contains the results obtained from multiple OPCs. The mid and multiple OPC were implemented with three advanced modulation formats; DP-NRZ-OOK, SP-8QAM, and DP-16QAM modulation formats. The results of phase conjugation were investigated and implemented with three scenarios; (conventional, hybrid with DCF, and hybrid with backward Raman amplifier). The third section discusses the results obtained from the communication system when Convolutional Neural

Networks (CNN) were used as an artificial intelligence technique. This will be followed by a similar analysis of the results obtained when NARX time series neural networks were employed in section four. Both of the two algorithms of machine learning sections were implemented using SP-16 QAM and SP-64 QAM modulation format. Finally, at the end of each investigation of the compensation method, a comparison is made to clarify the compensation method used in the previous studies and to indicate the most important contributions that were added to this work and their difference from previous works.

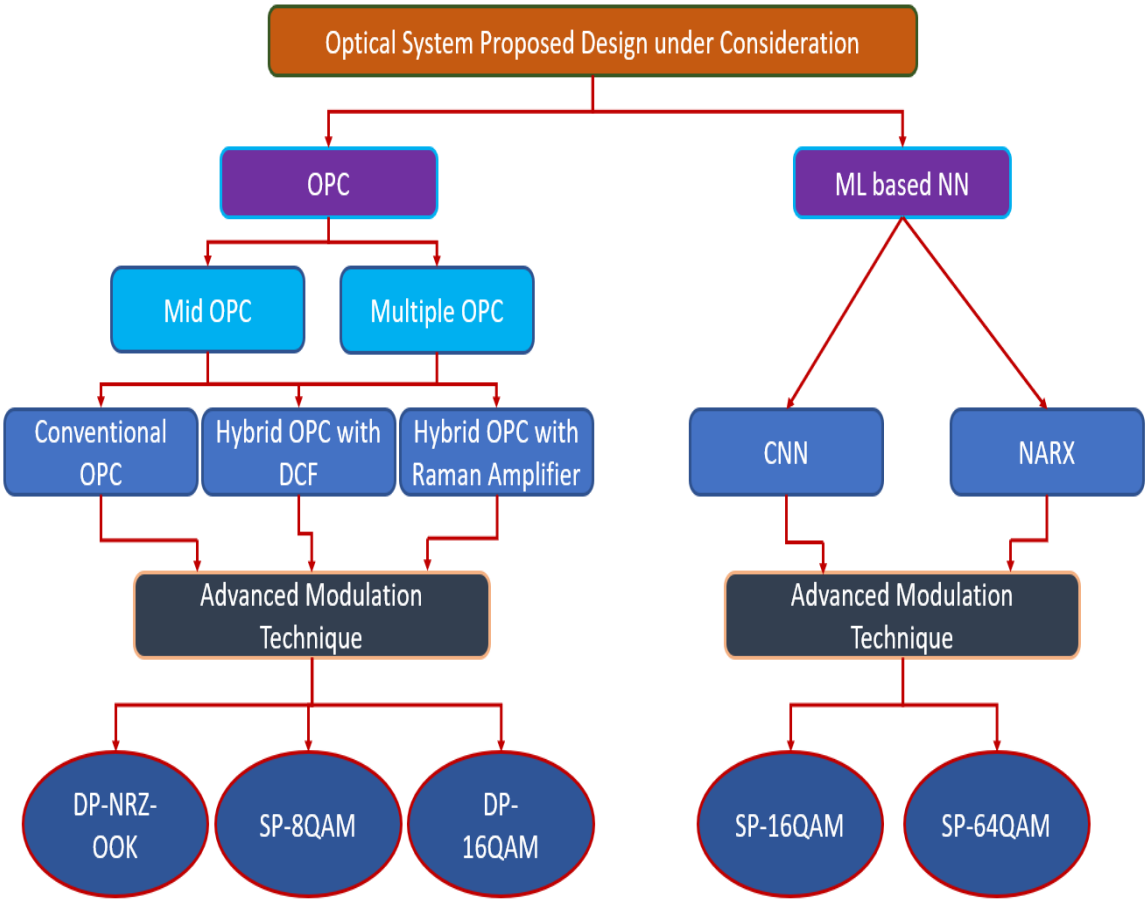

Figure (5.1). Optical system under study

The simulation was carried out using Optisys program and the artificial intelligence algorithms were implemented and simulated using MATLAB. The two programs were linked using co-simulations to ensure the validity of the results obtained. The simulation is performed, analyzed, and evaluating in terms of several metrics such as Bit Error Rate (BER), constellation diagram, Q-factor, and Error Vector Magnitude (EVM) with different launched power and transmission links.

5.2 Nonlinearity Compensation of 800 Gb/s DP-NRZ-OOK

The performance of compensation of fiber impairment is investigated using an advanced modulation format called Dual Polarization-Non Return to Zero-On Off Keying (DP-NRZ-OOK) with multichannel systems over an 800 km transmission link. A simulation model of the long haul DWDM transmission system is discussed with the mid and multiple OPC technique to mitigate signal nonlinearity of 16 channels with 25 Gb/s data rate for each channel. Initially, the mid and multiple OPC compensation scheme is investigated in the first, eighth, and sixteenth channels operating at 192.95, 193.3, and 193.7 THz, which correspond to the wavelength (1553.73, 1550.92, 1547.72) nm for the three channels. These frequencies are currently in use and were taken from the DWDM multiplexer in the Etisalat and Postal building of Karbala in Iraq. The transmission length consists of four spans before and after OPC (in the state of mid OPC), while (in the state of multiple OPC) two spans before OPC1 and after OPC2 and in the central part of the link are four spans, where each span length is 100 km. The results will be compared with three cases of implementation; conventional OPC; hybrid with DCF, and hybrid with Raman amplifier. After showing the results of mid and multiple OPC, the last section displays the comparison between them.

5.2.1 Mitigation of Fiber Impairments Using Mid OPC

Figure (3.9) depicts a 16-channel DWDM transmission system with mid-span OPC, as was discussed in chapter three. Some of the simulation's parameter settings are chosen to match those that were utilized in [38]. Figure (5.2) shows the optical spectra of the center channel signal at 193.30 THz (λ= 1550.92 nm) before and after Gaussian Optical Filter (GOF) and Optical Amplifier (OA). The optical signal is collected by a multiplexer and transferred through optical fiber. The DWDM multiplexer output optical spectrum analyzer is shown in Figure (5.3).

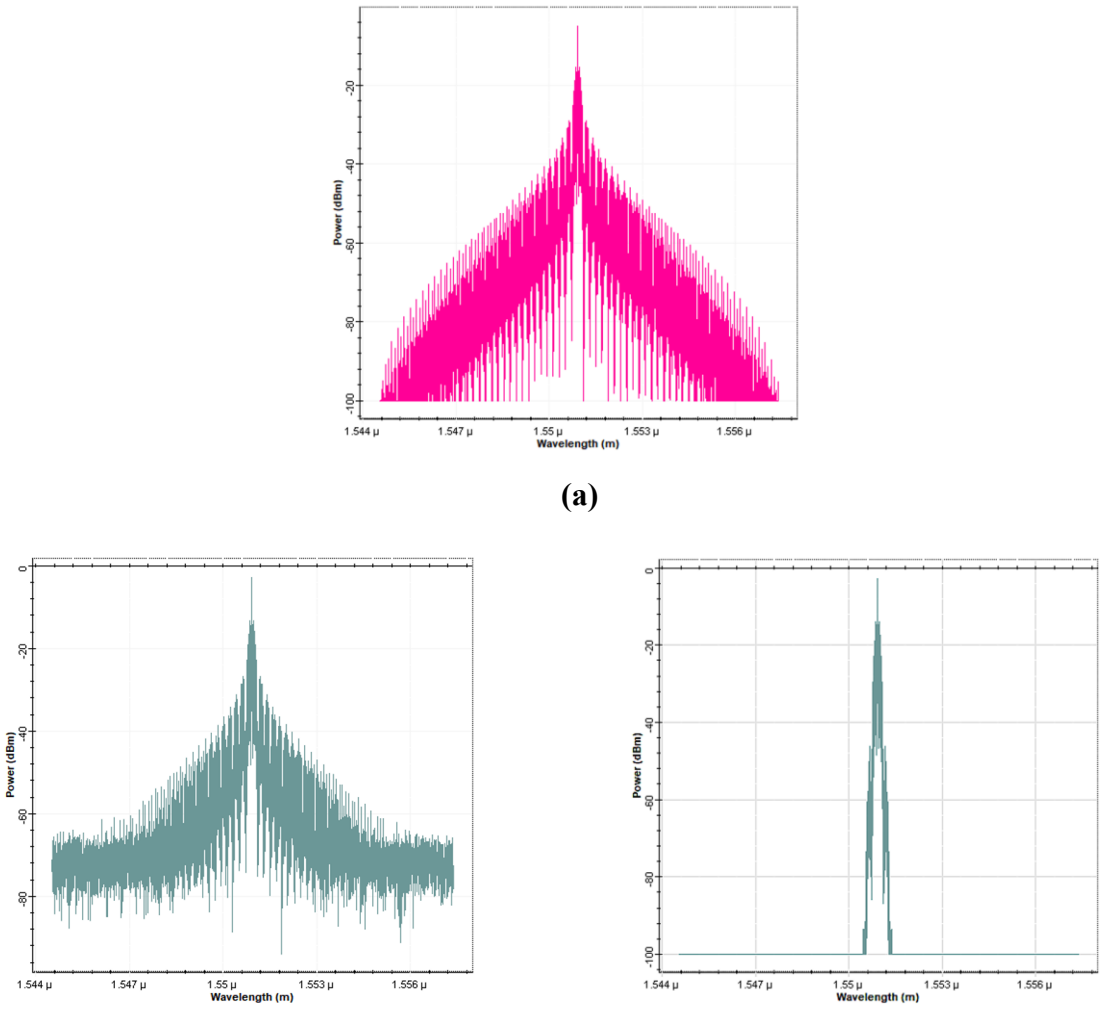

(a)

(b) **(c)**

Figure (5.2). Optical spectrum analyzer (a) before OA (b) before GOF (c) after GOF

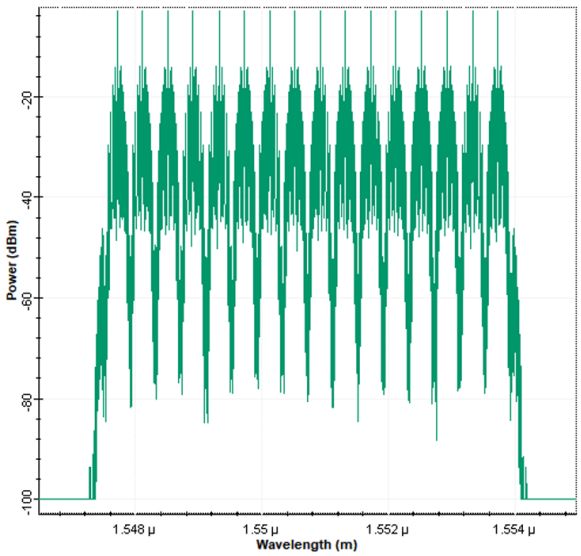

Figure (5.3). Optical spectrum output for 16 channels

After the output of the DWDM multiplexer signal passes through the optical link, this signal suffers from degradation due to linear and nonlinear effects as shown in figure (5.4). At this point, these signals are being processed by the OPC link. The spectra of pumps 1 and 2 are displayed in figure (5.5), with pump 1 operating at a frequency of 199.5 THz (λ= 1502.6 nm) and pump 2 operating at a frequency of 187.3 THz (λ= 1600.6 nm).

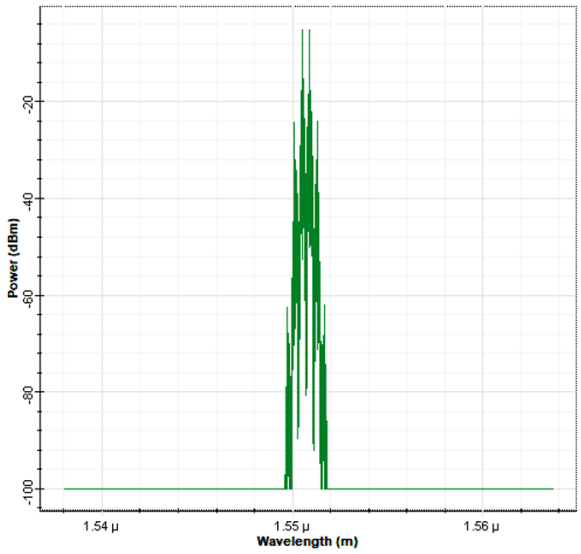

Figure (5.4). Optical spectrum analyzer of the output signal from SMF

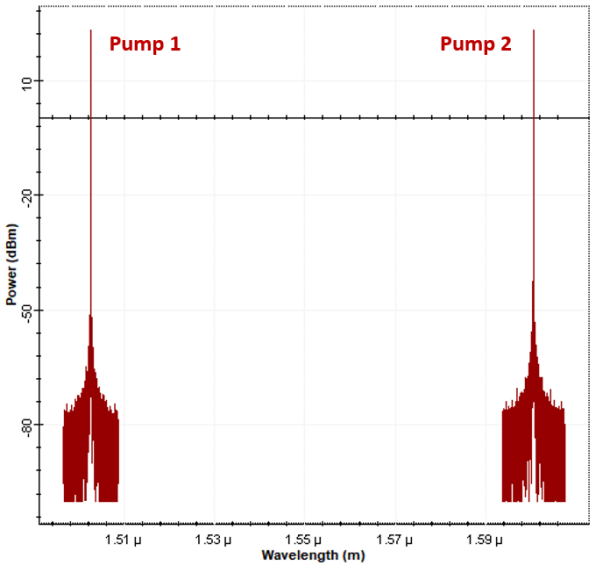

Figure (5.5). Optical spectrum analyzer of pump1 and pump 2

The wave spectra at the HNLF input (figure 5.6-a) and the HNLF output (figure 5.6-b) are depicted. Using the FWM equation ($f_i = f_{p1} + f_{p2} - f_s$), Figure (5.6-b) depicts the formation of the conjugated idler at the HNLF output as a result of the FWM process at frequency 193.49 THz (1549.39 nm).

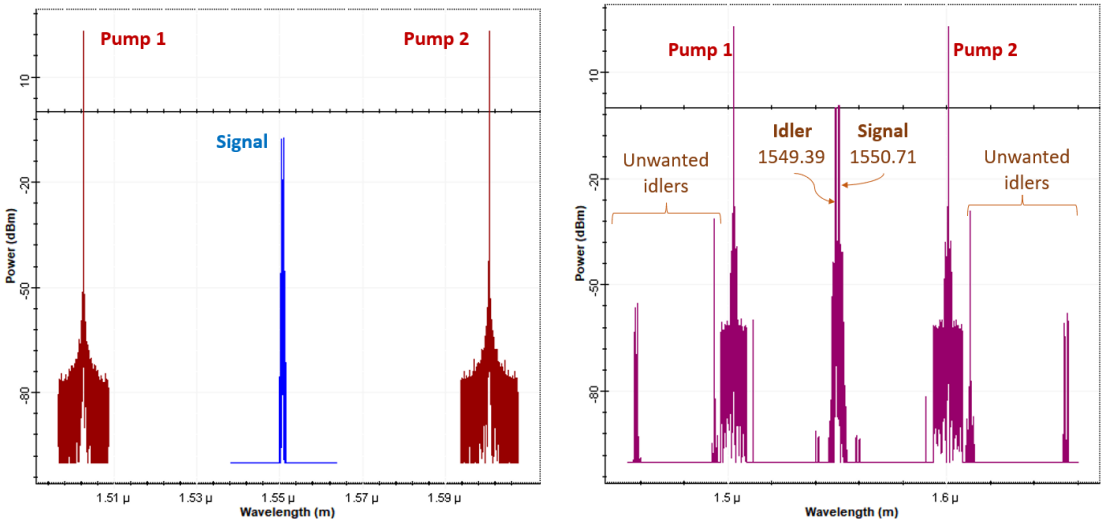

(a) **(b)**

Figure (5.6). Optical spectrum analyzer (a) input of HNLF (b) output of HNLF

All of the above is based on the premise that the HNLF is produced entirely by the nondegenerate FWM process. The problem is somewhat more complicated than it appears at first glance due to the simultaneous occurrence of the degenerate FWM process associated with each pump. As demonstrated in figure (5.6-b), many more unnecessary idlers can be generated when degenerate and nondegenerate FWM processes are combined. Figure (5.7) illustrates the output for the idler conjugated spectrum generated after the OPC device and passing by two optical filters.

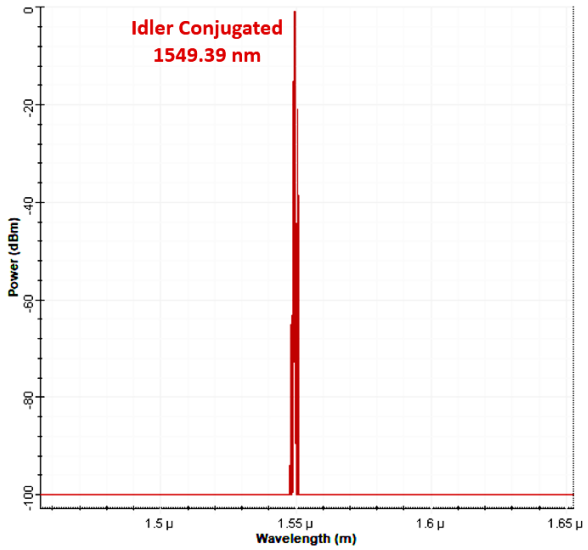

Figure (5.7). The optical spectrum analyzer of the idler conjugated the OPC's output

Firstly, it was investigated the performance of the mid span OPC as a conventional method. The values of BER for the first, middle, and last channel with different launch power from -10 dBm to 10 dBm was illustrated in Appendix B (Table B.1). Figure (5.8) shows the Q factor with an eye diagram for the channel 1, 8, and 16 at -2 dBm launch power due to it is the best value.

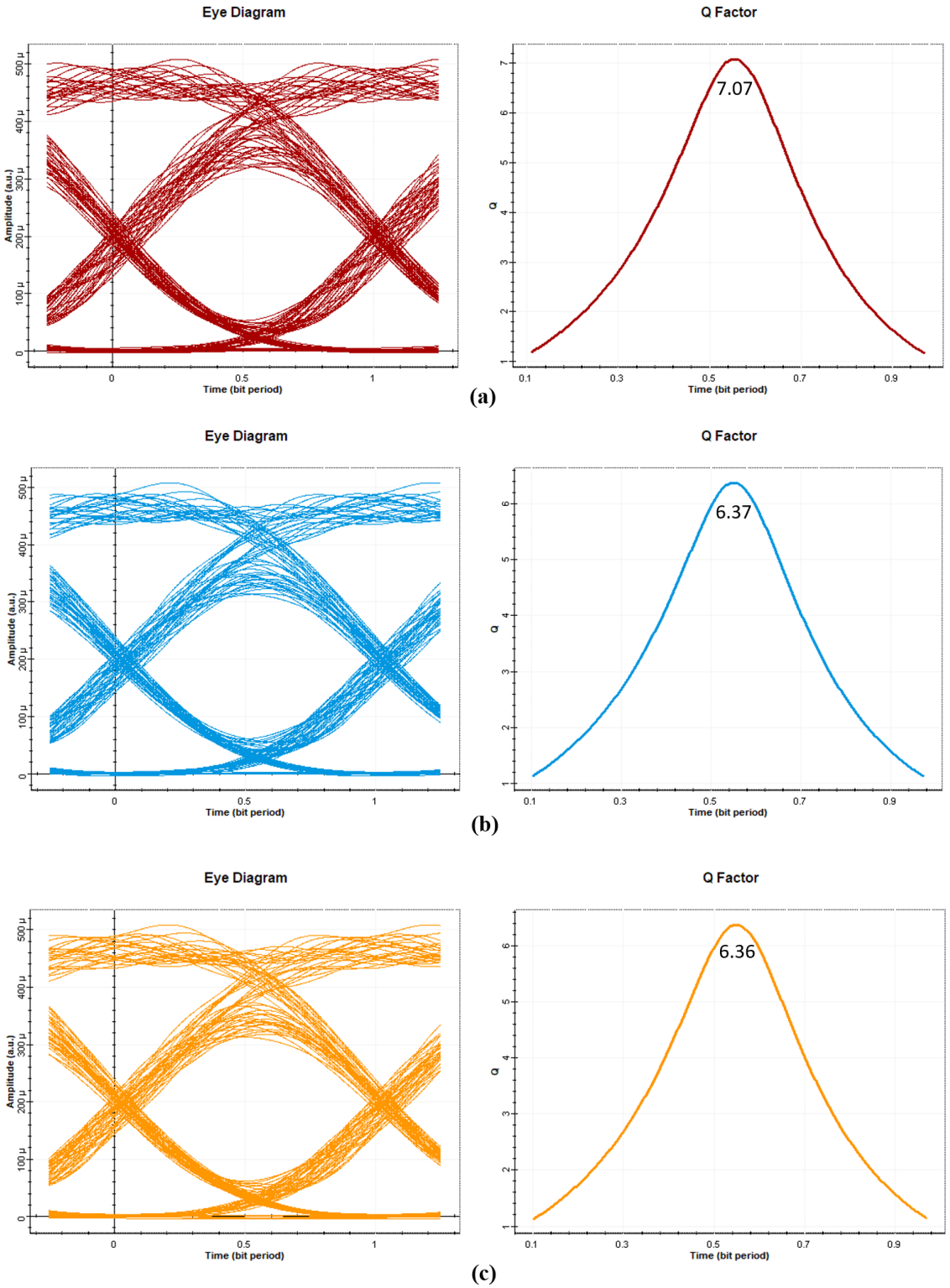

Figure (5.8). Eye diagram and Q-factor for conventional OPC (a) Ch.1 (b) Ch.8 (c) Ch.16

Secondly, the performance of hybrid OPC with the DCF technique was analyzed and tested. The values of BER for various launch powers are illustrated in Appendix B (Table B.2). The Q factor together with the eye diagram is displayed in figure (5.9) for channels 1, 8, and 16 at 2 dBm launch power because it is the optimal value.

Finally, the performance of hybrid OPC was evaluated and investigated using the backward Raman amplifier approach. Table (B.3) in Appendix B displays the values of BER for a variety of launch powers. Since 1 dBm is the optimum launch power in this method, the Q factor together with an eye diagram is displayed in figure (5.10) for channels 1, 8, and 16.

At the end of mid OPC method, it can be concluded that this method was effective in treating nonlinear effects for the three scenarios that were presented. The best results were obtained when using hybrid OPC with a backward Raman amplifier for all sixteen channels because of its unique features that contributed to improving the quality of the received signal compared to the other two methods. The best values of BER for the first, middle, and last channels are 1.11×10^{-29}, 1.07×10^{-29}, and 2.94×10^{-29}, while the value of Q-factor for these three channels equal 11.07 dB, 11.2 dB, and 11.1 dB, respectively.

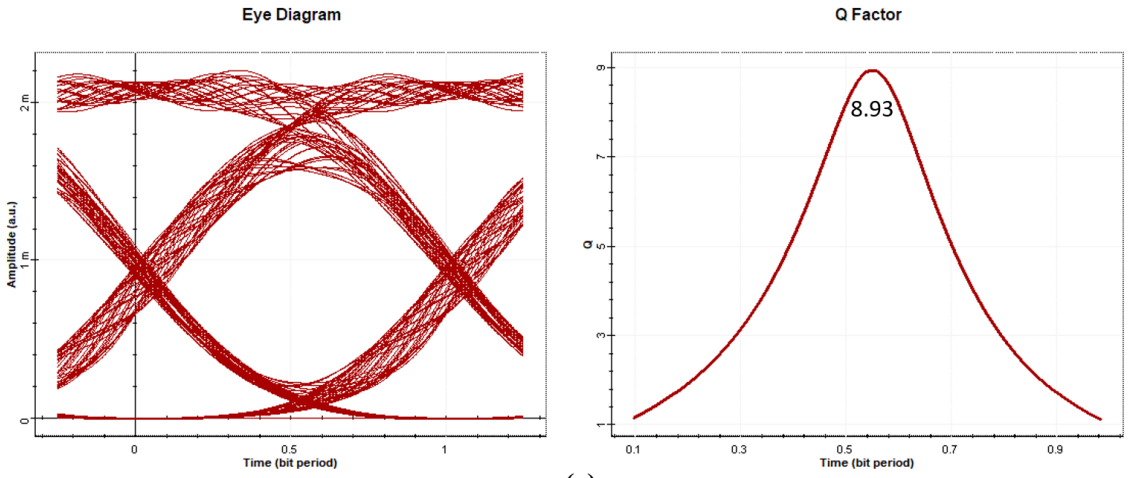

(a)

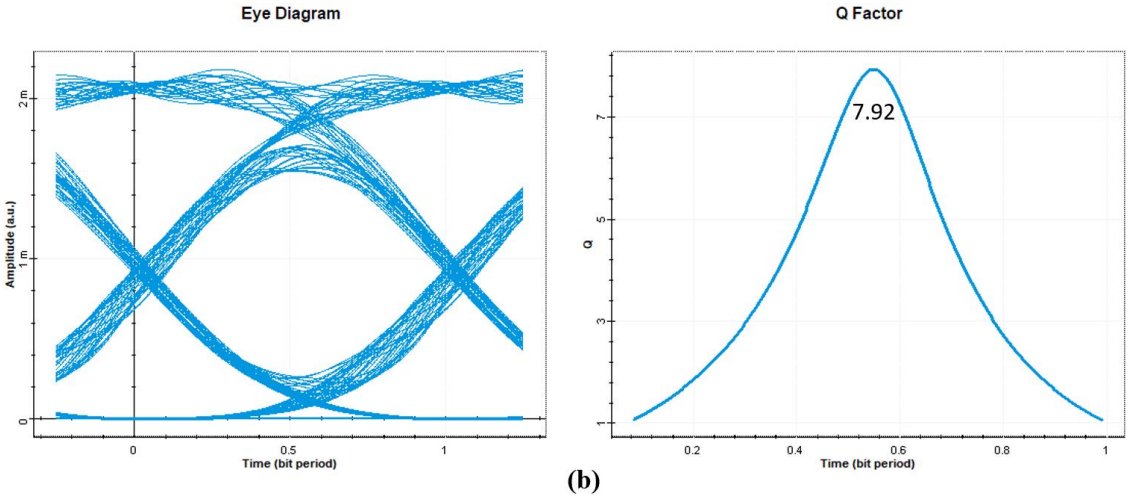

(b)

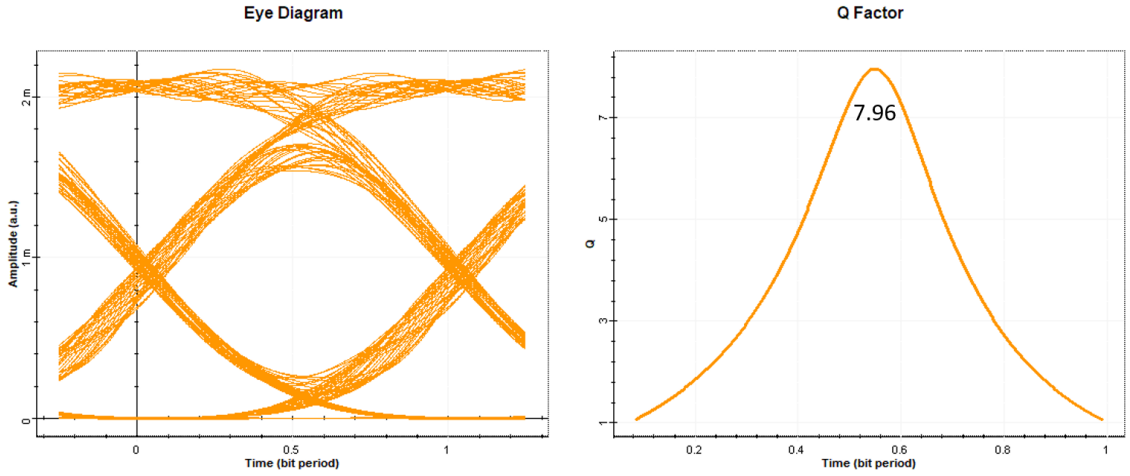

(c)

Figure (5.9). Eye diagram and Q-factor for hybrid (OPC + DCF) (a) Ch.1 (b) Ch.8 (c) Ch.16

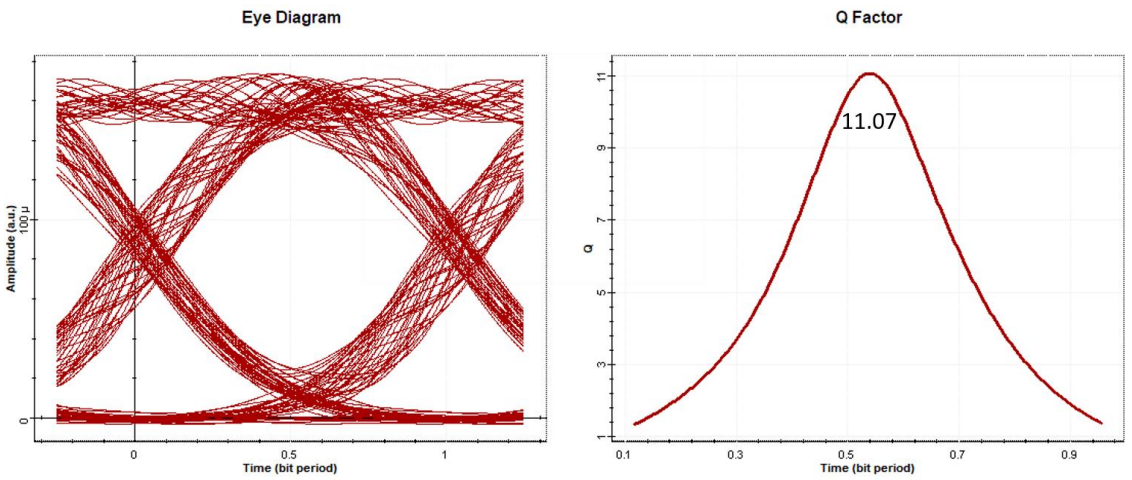

(a)

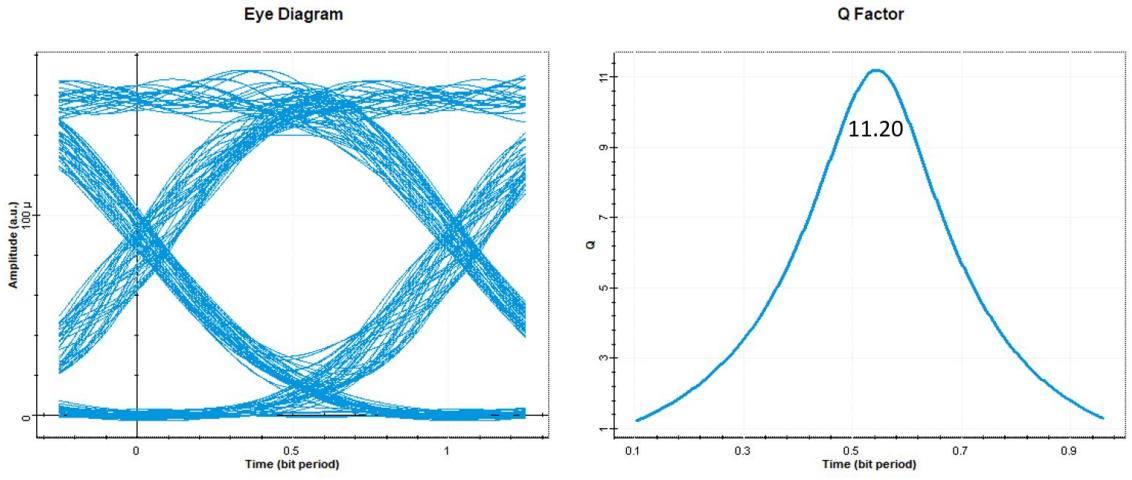

(b)

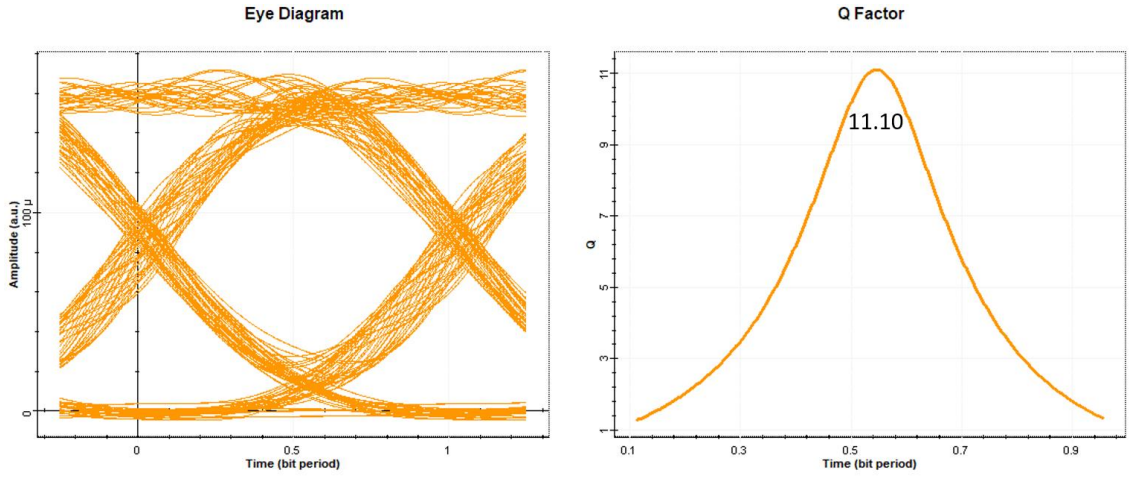

(c)

Figure (5.10). Eye diagram and Q-factor for hybrid (OPC + Raman amplifier) (a) Ch.1 (b) Ch.8 (c) Ch.16

5.2.2 Fiber Nonlinearity Compensation Based Multiple OPC

In this section, the mitigation of nonlinear effects that discussed in the previous section will be re-analyzed and investigated depending on the multiple OPC method as explained in figure (3.10) in Chapter Three. Due to the difficulty in determining the middle distance which is one of the problems with the previous method, using multiple OPC methods will help to overcome this problem, as well as improve the signal quality along the transmission distance.

The output conjugated idler of the first OPC, shown in figure (5.7), is supplied into the second OPC module. A second OPC will then undergo the same OPC procedure described in the first way. The wave optical spectra are shown in figure (5.11) at the HNLF's input and output, respectively, at the second OPC device. At the HNLF's output, as shown in figure (5.11-b), the FWM process creates a new conjugated idler with a frequency of 193.325 THz (1550.71 nm), identical to that of the transmitted signal.

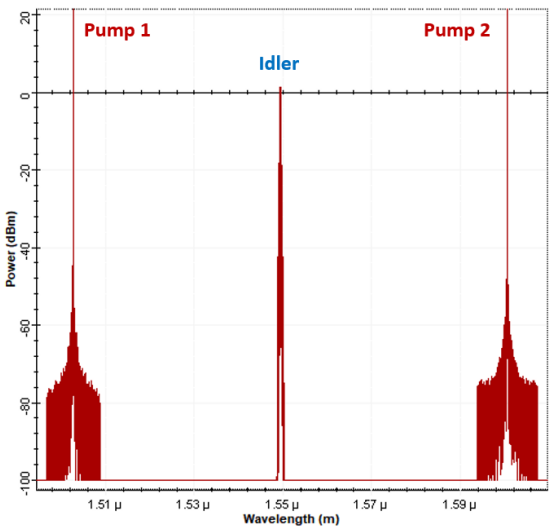

(a)

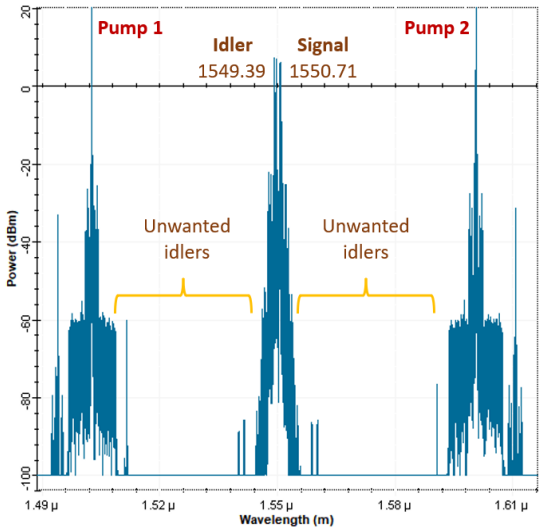

(b)

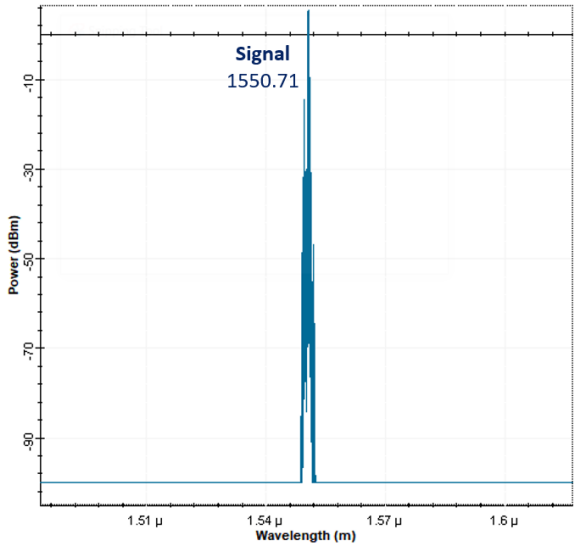

(c)

Figure (5.11). Optical spectrum analyzer of second OPC (a) before HNLF (b) after HNLF (c) received optical signal

This compensation method will be investigated with three scenarios as in the previous section. In the first step, the performance of the conventional multiple span OPC was analyzed and studied. The values of BER are illustrated in Appendix B (Table B.4) for 1, 8, and 16 channel configurations with varying amounts of launch power from 10 dBm to -10 dBm. The Q factor and eye diagram are depicted in figure (5.12) for the first, middle, and final channel at 0 dBm launch power because this value represents the optimal value in this case as illustrated in (Table B.4).

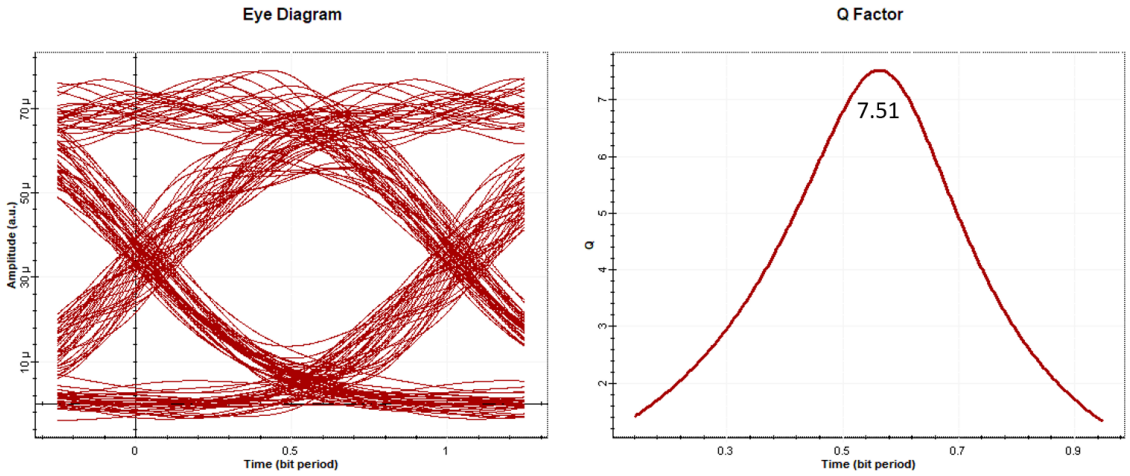

(a)

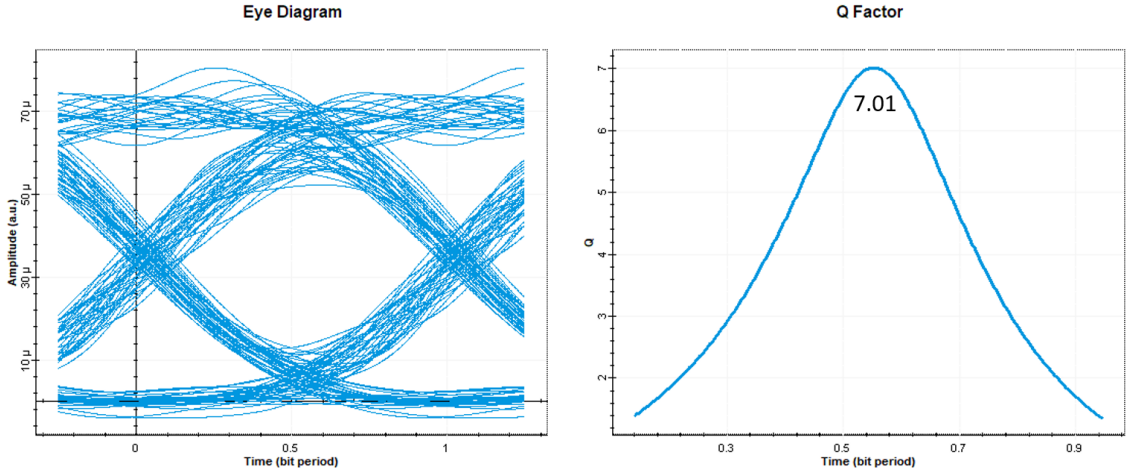

(b)

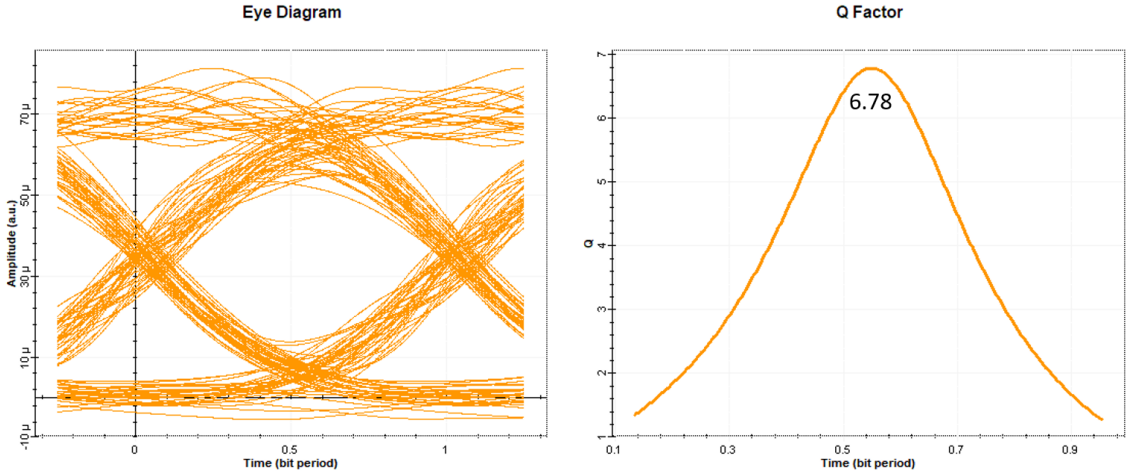

(c)

Figure (5.12). Eye diagram and Q-factor for conventional multiple OPC (a) Ch.1 (b) Ch.8 (c) Ch.16

Second, an investigation and evaluation of the performance of hybrid multiple OPC with the DCF approach was carried out. Table (B.5) in Appendix B provides an illustration of the values of BER for a number of different launch powers. The eye diagram as well as the Q factor are presented in figure (5.13) for the three channels when the power launching is set to 2 dBm because this value represents the best results in this case compared with other values.

In the last step, the performance of hybrid multiple OPC was analyzed and evaluated utilizing the approach of a backward Raman amplifier. The results of the BER calculation for a number of different launch powers are presented in table (B.6) in Appendix B. Figure (5.14) depicts the eye diagram together with the Q factor for channels 1, 8, and 16 when the power launching is 1 dBm because this is the value that yields the greatest results in this scenario.

At the epilogue of the multiple OPC method, it is possible to draw the conclusion that this technique was successful in effectively handling nonlinear effects for all three of the scenarios that were provided. When compared to the conventional and hybrid DCF approaches, the hybrid OPC with backward Raman amplifier produced the highest quality received signal for all 16 channels, which resulted in the best outcomes. The values of BER for the first, eighth, and sixteenth channels for OPC with Raman are 8.61×10^{-35}, 6.60×10^{-35}, and 5.40×10^{-35}, while Q factor equal 12.34 dB, 12.36 dB, and 12.35 dB for the three channels, respectively.

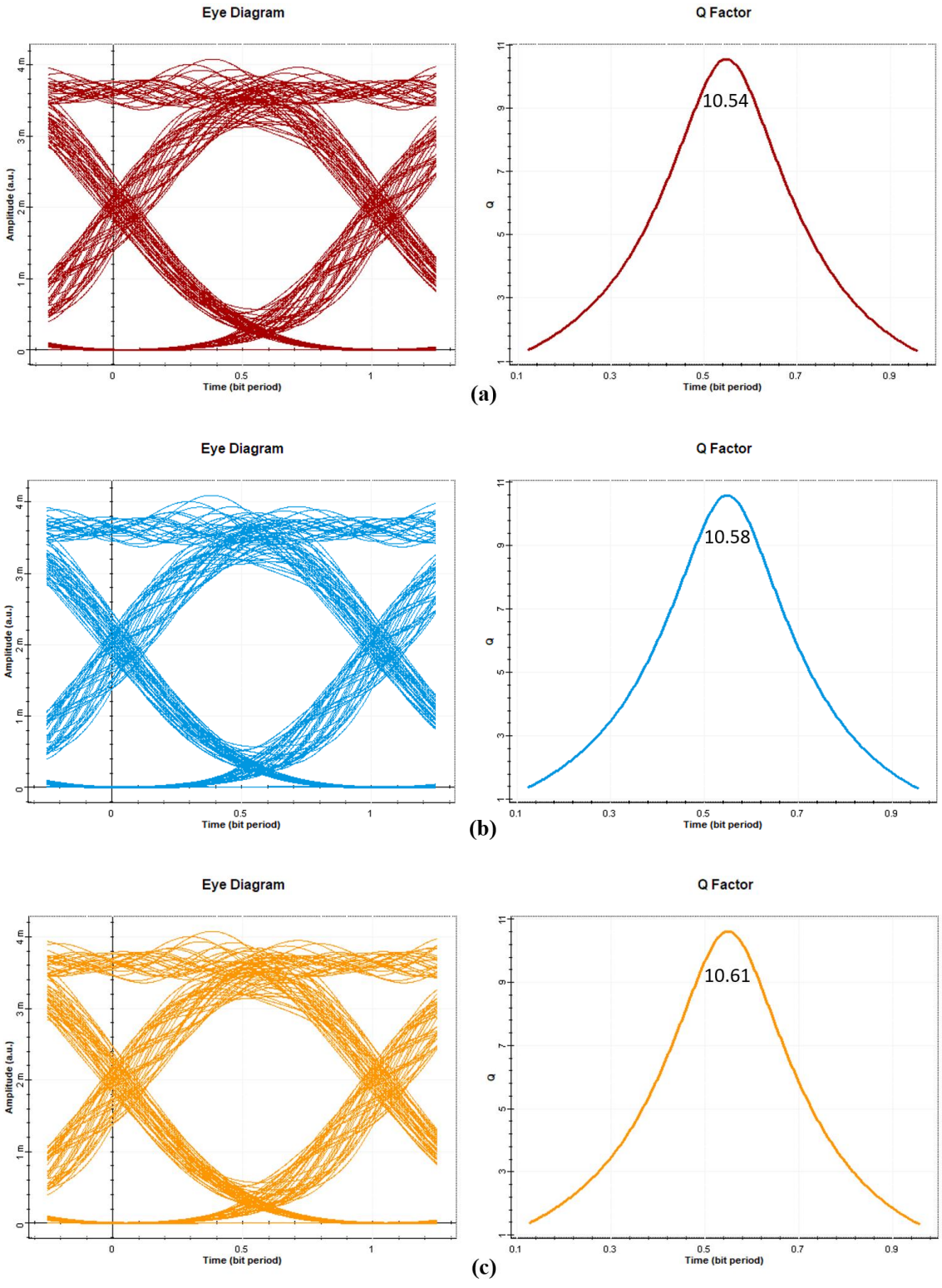

Figure (5.13). Eye diagram and Q-factor for hybrid multiple OPC with DCF (a) Ch.1 (b) Ch.8 (c) Ch.16

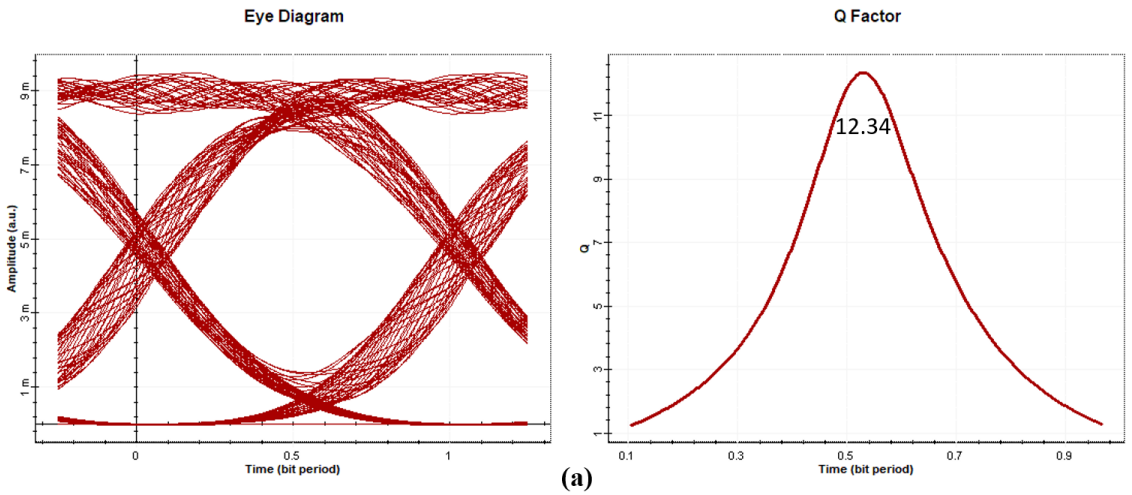

(a)

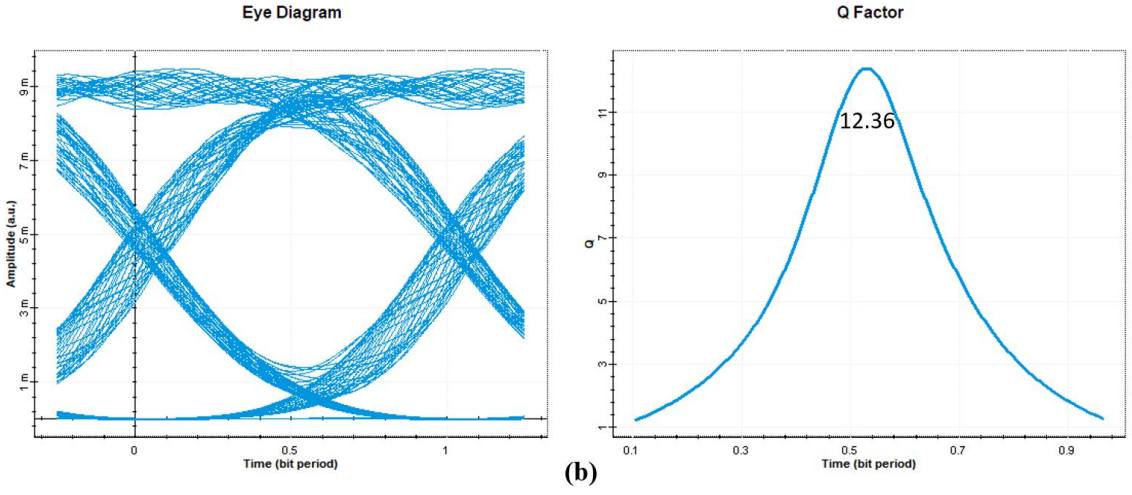

(b)

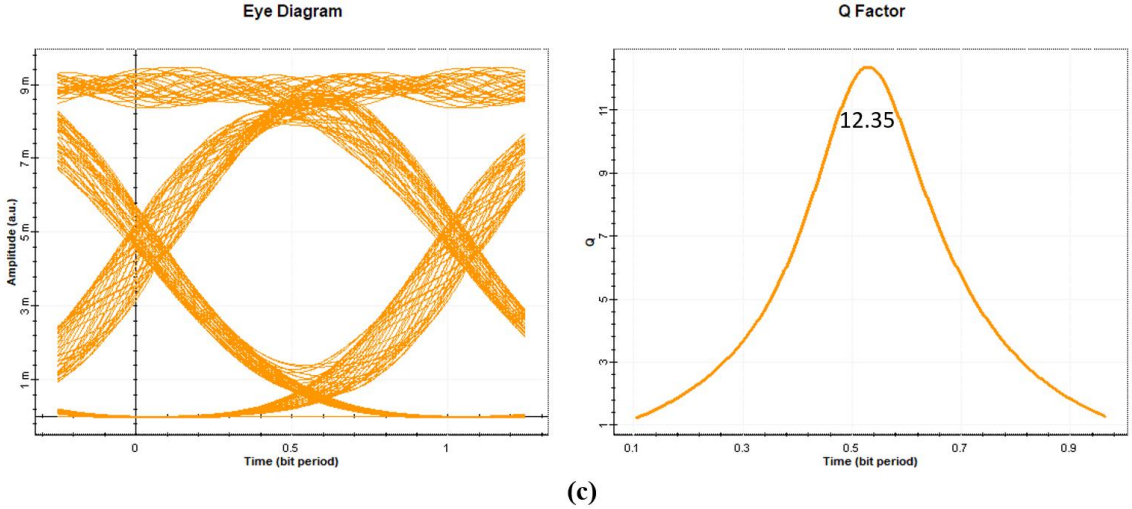

(c)

Figure (5.14). Eye diagram and Q-factor for hybrid multiple OPC with Raman amplifier (a) Ch.1 (b) Ch.8 (c) Ch.16

5.2.3 Performance Evaluation Between Mid and Multiple Approach

This section compares the performance of mid and multiple OPC compensation methods on the proposed system in terms of BER, Q-factor, and EVM for the middle channel (channel 8).

The optimum launching power for conventional mid OPC is close to -2 dBm per channel, with a bit error rate of (7.10×10^{-11}), while the EVM is 0.15. Because of the OSNR reduction of optical noise in the unoccupied band at the input of FOPA, the optimum launched power is improved by roughly 2 dBm, and the Q factor is increased by 1.55 dB with improvement of EVM about 0.029 in the case of 'hybrid OPC with DCF' compared to conventional OPC.

Figure (5.15) shows the Q-factor for 'conventional mid OPC' and 'hybrid mid OPC with DCF' with different signal powers and the number of system improvements after using DCF with OPC to compensate for transmission fiber positive value dispersion.

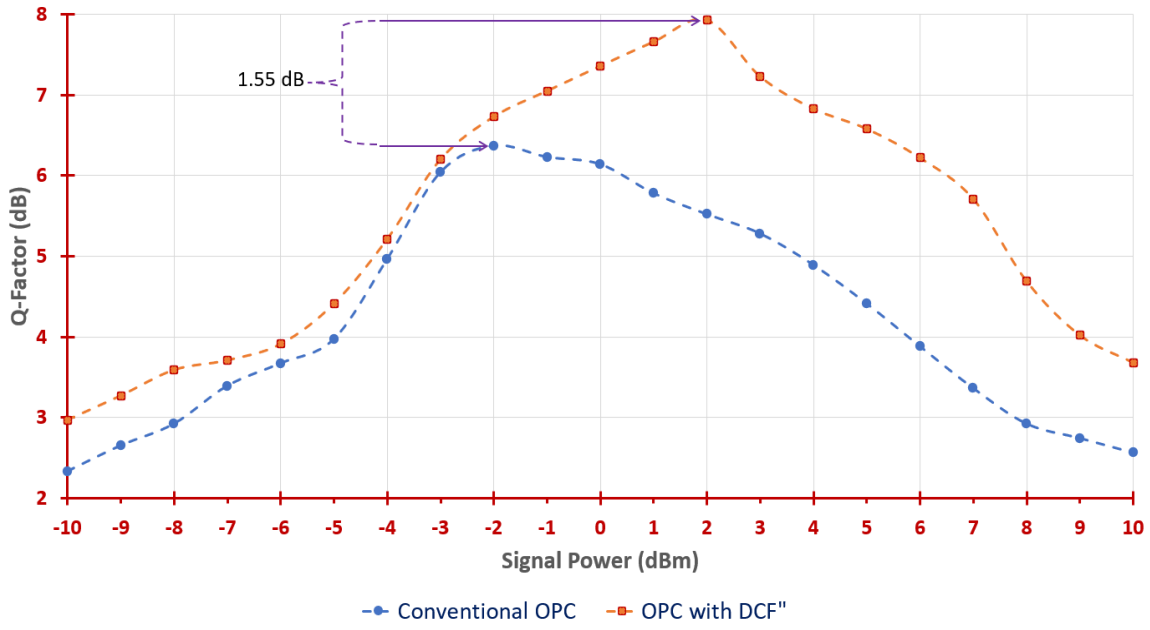

Figure (5.15). Q-factor versus signal input power for conventional mid OPC and mid OPC with DCF

Incorporating backward Raman amplification into a conventional OPC setup alleviates the trade-off between the output OSNR and the nonlinear penalty. Raman amplification provides a broadband gain to the interacting light waves, which allows for a lower input signal power, hence enhancing the effectiveness of the FWM process in the HNLF. The Raman pump is set to 30 dBm to make up for the loss of power from the output idler. So, at the same idler power level, the Q factors of the idlers in the OPC with Raman amplifier and the conventional OPC are compared. As shown in figure (5.16), hybrid OPC with a Raman amplifier raises the best amount of input power by 3 dB and the Q factor by 4.83 dB as compared to conventional OPC, while the amount of improvement in the value of EVM by 0.067. Also, compared to OPC with DCF, OPC with Raman enhancement improves the Q-factor by 3.28 dB with an increase of EVM by 0.038. Figure (5.17) shows the comparison of improvements for the Q-factor in the proposed system after using a Raman pump as compared with DCF.

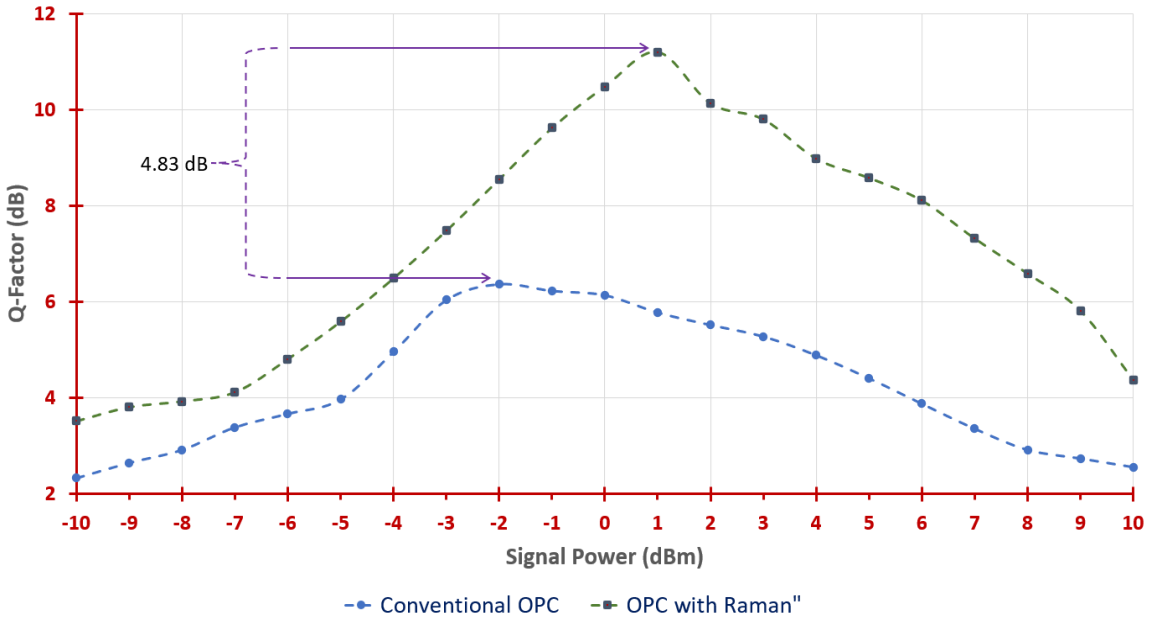

Figure (5.16). Q-factor versus signal input power for conventional mid OPC and mid OPC with Raman amplifier

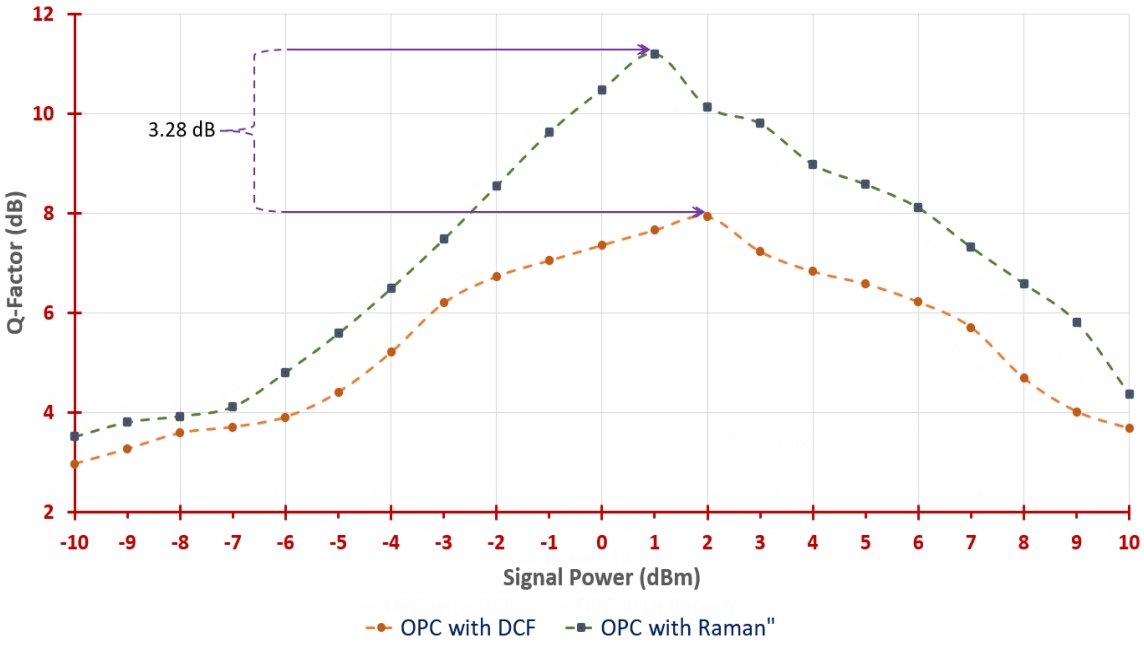

Figure (5.17). Q-factor versus signal input power for hybrid mid OPC+DCF and Raman amplifier

To further mitigate inter-channel nonlinear impairments, it was investigated using multiple OPC with three scenarios as illustrated in section 5.2.2. Analyses are performed on the effects of nonlinearity in fibers subjected to varying levels of input signal strength. The transmission performance of the conventional multiple OPC module is compared first. The measurement results show the peak Q-factor is 7.51 dB at 0 dBm signal power with BER 5.60×10^{-14} and EVM 0.014. Results show that conventional multiple OPC produces less distortion than conventional mid OPC with the improvement of Q-factor by 1.14 dB, as illustrated in figure (5.18).

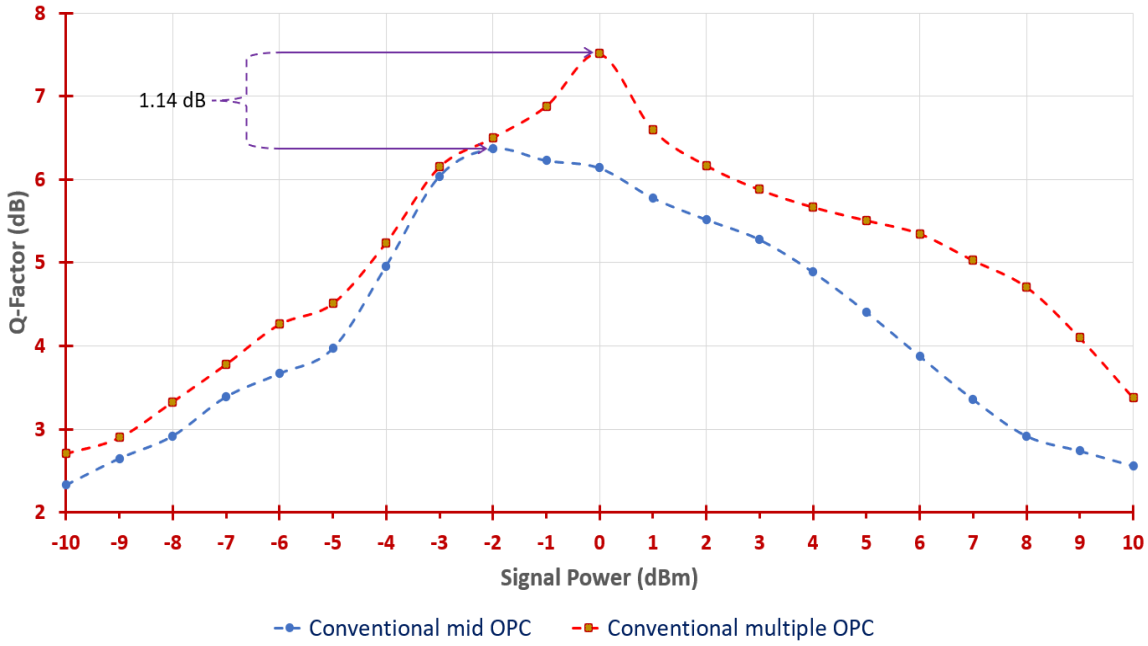

Figure (5.18). Q-factor versus signal input power for conventional mid and multiple OPC

To improve the efficiency of the system in terms of increasing the transmission distance and bit rate, a DCF will be introduced, which is responsible for addressing the attenuation that occurs in the fiber. Specifically, the optimal launching power for "multiple OPC with DCF" is roughly 2 dBm per channel, which is an improvement of about 2 dB compared to conventional multiple OPC. The improvement of the Q factor is increased by about 3.57 dB, while EVM is enhanced by 0.048 when using DCF as compared to conventional multiple OPC. On the other hand, multiple OPC with DCF improves the system performance compared with mid OPC with DCF. Q-factor can be increased by 2.66 dB as shown in figure (5.19) with an EVM value of 0.032.

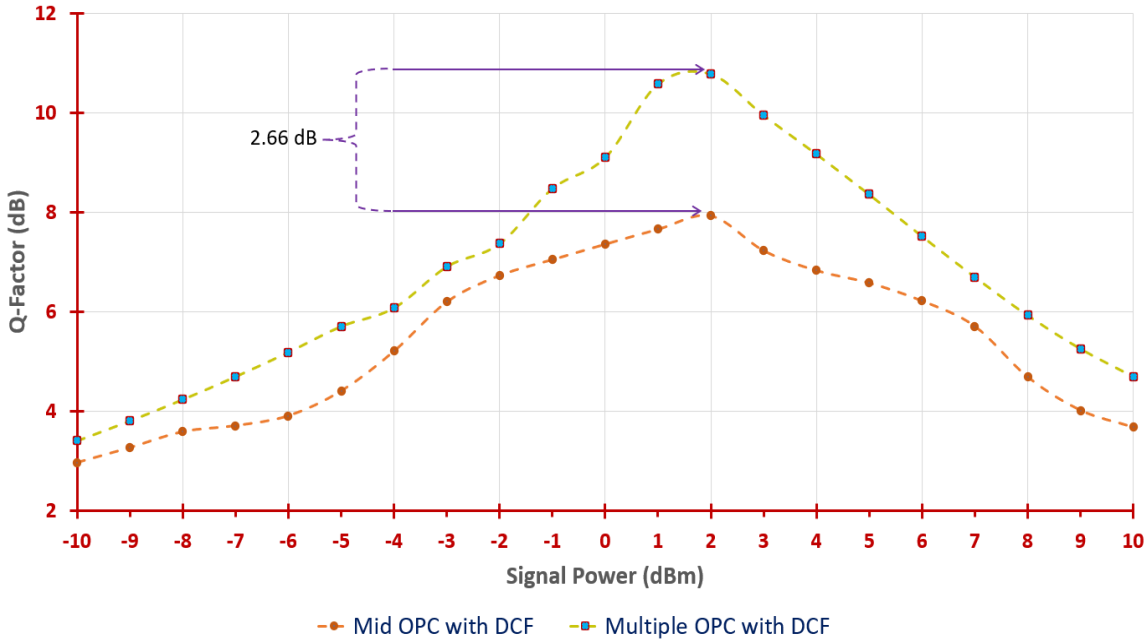

Figure (5.19). Q-factor versus signal input power for hybrid mid OPC and multiple OPC with DCF

Finally, the use of backward Raman amplification is implemented in the multiple OPC to reduce the amount of nonlinear distortion present in the system. The optimal launching power in this case equals 1 dBm. The improvement of the Q factor is increased to 12.36 dB with EVM amounting to 0.081. If this value is compared with the mid OPC method, the amount of improvement in the value of the Q-factor will be 1.16 dB. Figure (5.20) analyses the results of a transmission performance comparison between the mid and multiple OPC with the Raman amplifier.

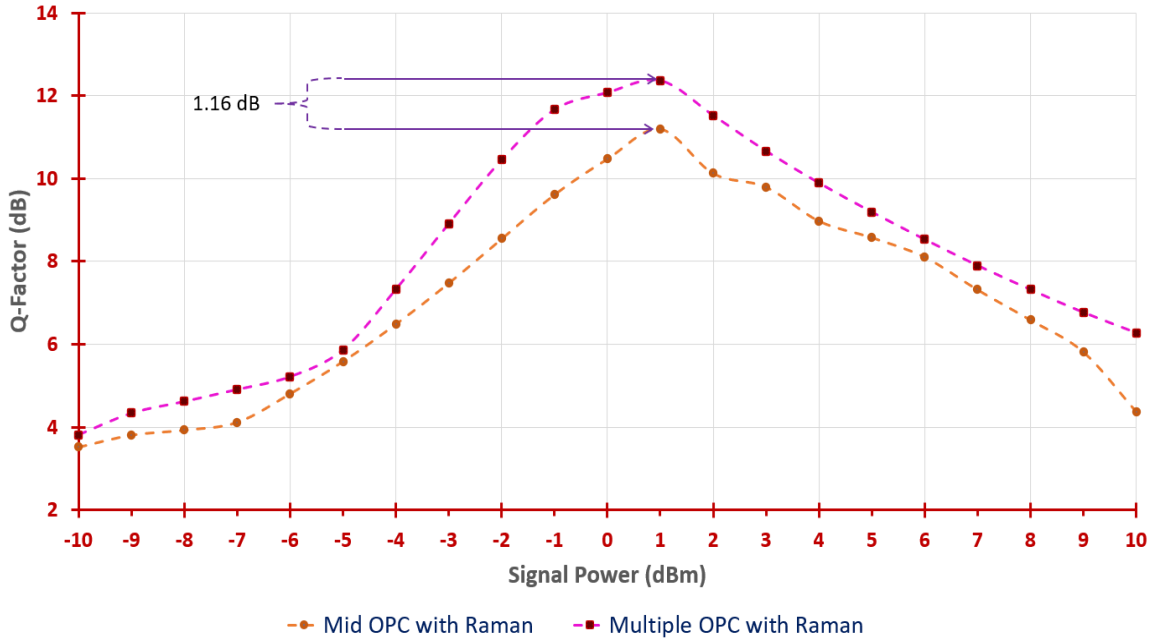

Figure (5.20). Q-factor versus signal input power for hybrid mid OPC and multiple OPC with Raman amplifier

Overall, it has been concluded that multiple OPC works better than mid OPC in terms of the BER, EVM, and peak Q factor with the same transmission length and optimal signal launched power. In addition, the use of a backward Raman amplifier with OPC gave advanced results over the other two methods, which represents an important addition to this work. Figures (5.21) and (5.22) show the summary between the three scenarios for mid and multiple techniques.

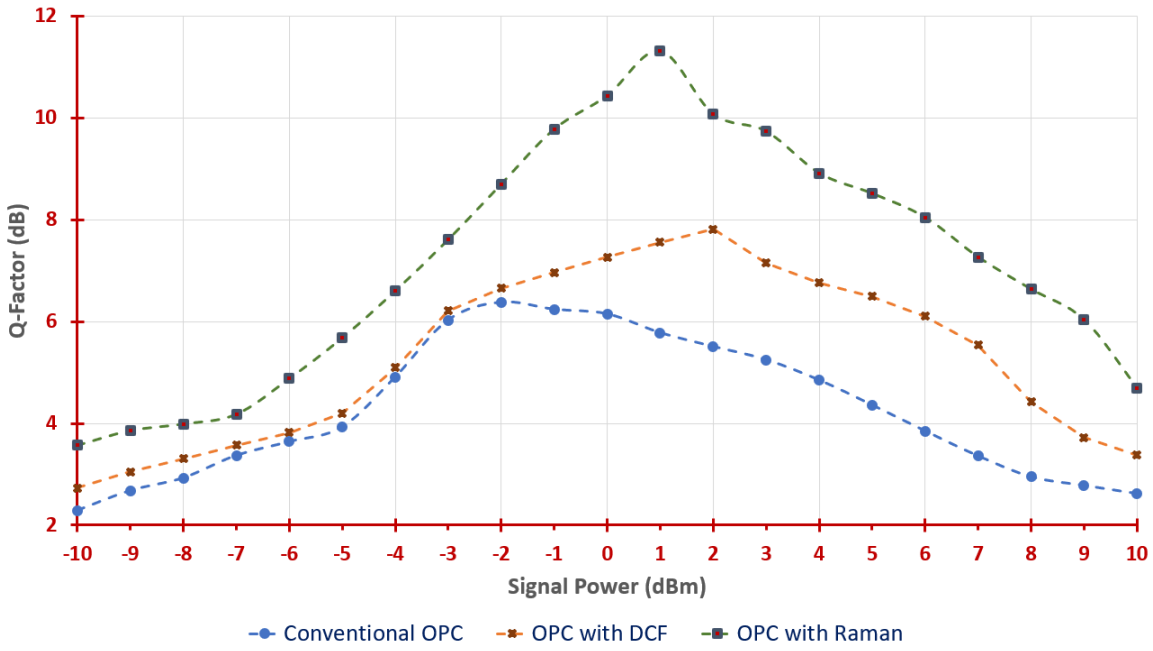

Figure (5.21). Q-factor versus signal input power for mid OPC with three cases (conventional, DCF, and Raman amplifier)

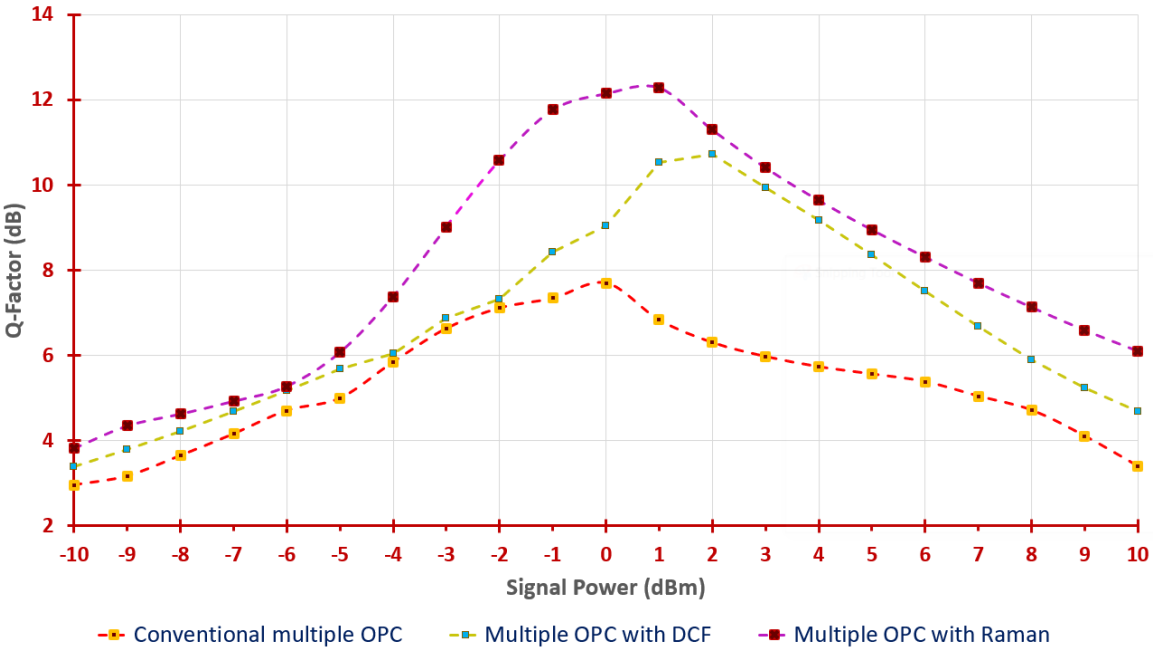

Figure (5.22). Q-factor versus signal input power for multiple OPC with three cases (conventional, DCF, and Raman amplifier)

5.3 Improvement and Mitigation of Kerr Effects on SP-8QAM Communication Systems

This section studies the fiber nonlinearities mitigation especially Kerr effects in high-capacity optical communication systems for 1.728 Tbps Single Polarization Eight Quadrature Amplitude Modulation (SP-8QAM) signaling. This work presents backward Raman amplification employed in conjunction with OPC to improve the performance of an optical link of dense wavelength division multiplexing (DWDM) transmission systems with a 16 ×108 Gbps data rate. The mid and multiple OPC compensation technique is tested in the first, middle, and last channels running at 194.04, 194.39, and 194.79 THz. The results will be compared with two cases of implementation; conventional OPC; and hybrid with Raman amplifier for various power levels launched into the fiber from -15 dBm to 15 dBm.

To illustrate the effect of OPC on the performance of SP-8QAM, firstly show the performance of the system that operates back-to-back. Figure (5.23) illustrates the constellation diagram for 8-QAM for the first, eighth, and sixteen channels.

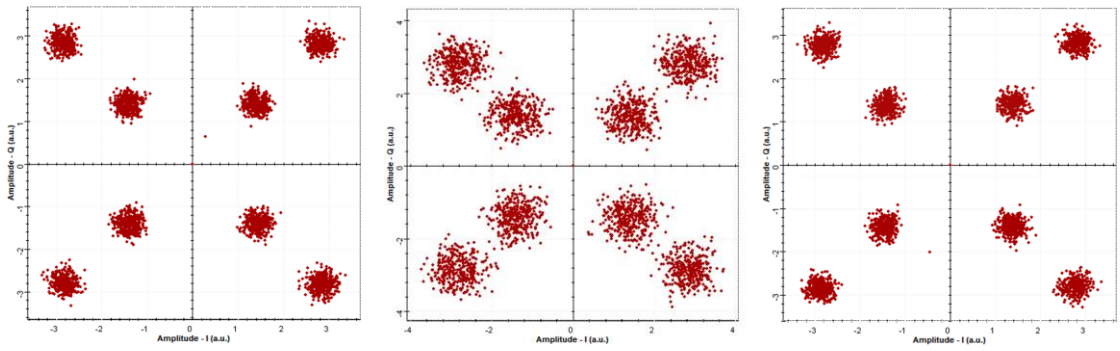

(a) **(b)** **(c)**

Figure (5.23). Constellation diagram of the received 8QAM signal transmission back-to-back for (a) Ch.1 (b) Ch.8 (c) Ch.16

As shown in figure (5.23), the constellation diagram is very clear and BER for the three channels is equal to zero with Q factor 12.56, 12.03, and 12.21 for channels 1, 8, and 16, respectively. Also, the Error Vector Magnitude (EVM) for these three channels is 0.079, 0.083, and 0.081. At this point insert optical fiber with a length of 800 km between DWDM multiplexer and demultiplexer. The constellation diagram is illustrated in figure (5.24).

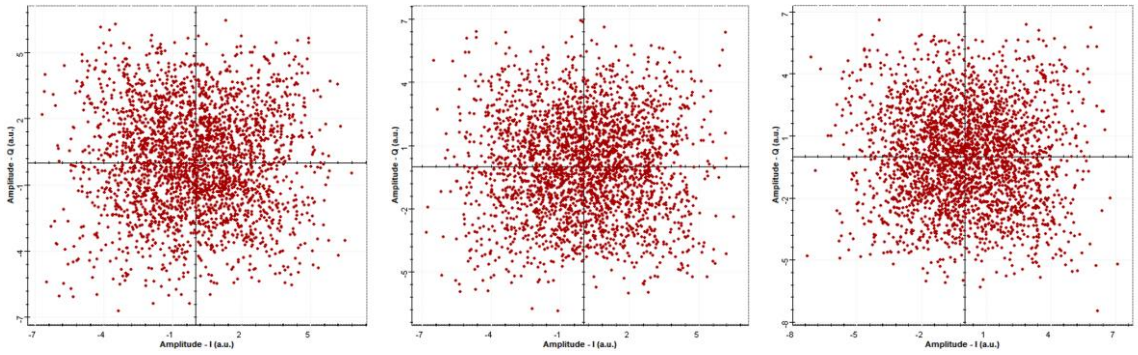

(a) **(b)** **(c)**

Figure (5.24). Constellation diagram of the received 8QAM signal over 800 km SMF (a) Ch.1 (b) Ch.8 (c) Ch.16

As shown in figure (5.24), the constellation diagram is bad due to the effect of nonlinearity with a high bit rate equal to 0.494, 0.495, and 0.496 with 1.73, 1.72, and 1.75 for Q-factor and 0.574, 0.581, and 0.571 for error vector magnitude for channel 1, 8, and 16, respectively. The degradation of the received signal back to Kerr effects. At this point, using an OPC device enhances the performance of the system against nonlinear effects.

5.3.1 Mid Way OPC with and without Raman Amplifier

In this method, insert OPC in the middle of a transmission link with a two-part optical fiber link before and after OPC. In the OPC, the idler wave is formed after passing through the nonlinear medium. Figure (5.25) shows the spectrum of the signal before and after a pass through HNLF.

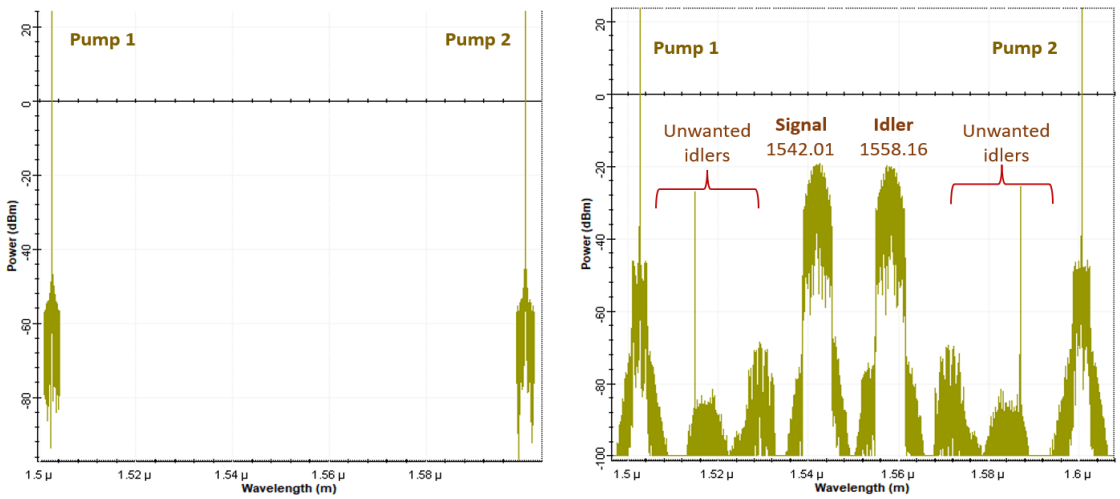

(a) **(b)**

Figure (5.25). Optical spectrum analyzer (a) input of HNLF (b) output of HNLF

The idler signal is distributed to the sixteen channels by taking advantage of the De DWDM technique. The performance was tested at different power levels with and without a Raman amplifier. Firstly, the optimal transmit power per channel for the conventional mid OPC is around 2 dBm, with a BER of 7.42×10^{-2}, 7.55×10^{-2}, and 7.63×10^{-2} for channels (1, 8, and 16), respectively. The values of the Q-factor are 3.19 dB, 3.13 dB, and 3.08 dB while EVM values are 0.313, 0.319, and 0.324. In Appendix B, Table (B.7) shows BER, Q-factor, and EVM for the three channels with various launch power. The constellation diagram is shown in figure (5.26).

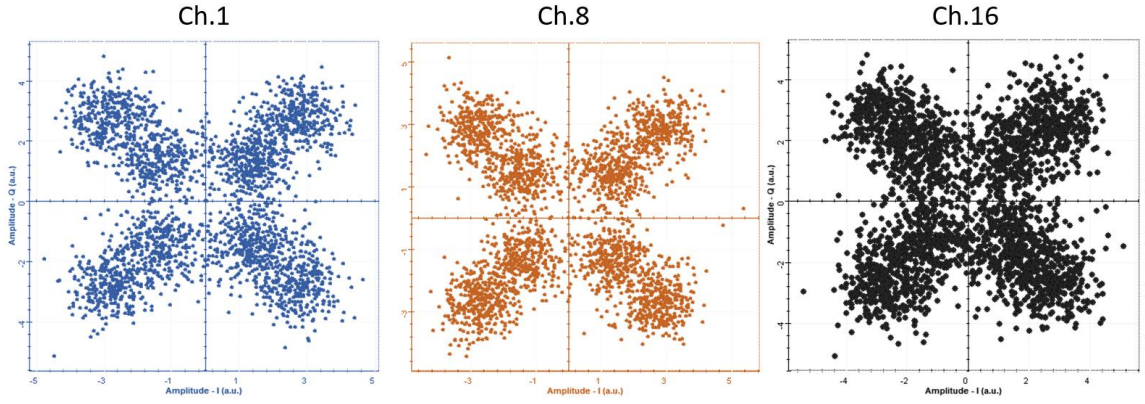

Figure (5.26). Constellation diagram for channels (1, 8, and 16)

Secondly, when Raman amplification is added to a conventional OPC module, the output OSNR will improve while the nonlinear penalty is decreased. It is necessary to adjust the Raman pump to 31 dBm to compensate for the power loss caused by the output idler. Hence, the Q-factors of the OPC with Raman amplifier and the conventional OPC are compared at a constant idler power level. The BER of the three channels is 1.53×10^{-2}, 1.86×10^{-2}, and 1.91×10^{-2} for the first, eighth, and sixteenth, respectively. As can be shown in figure (5.27), when OPC is combined with a Raman amplifier, the best possible value of input power is increased by 1 dB to be about 3 dBm, while the Q factor is increased by 3.50 dB, 3.24 dB, and 3.23 dB for the three channels, respectively, with enlarged by 14.9%, 15.6%, and 15.8% as compared when the conventional method is used. In Appendix B, Table (B.8) illustrates BER, Q-factor, and EVM for the first, middle, and last channels.

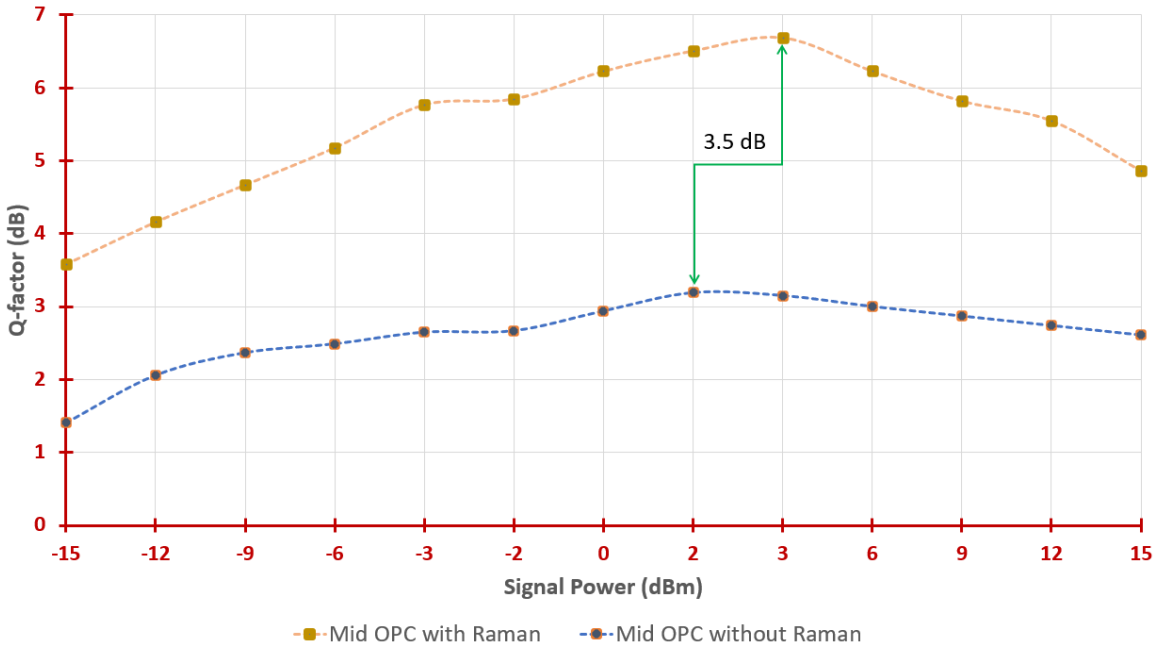

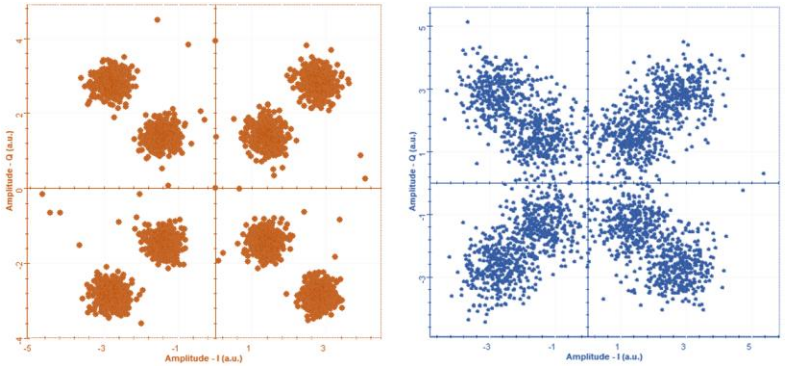
Amplitude - Q (a.u.)
Amplitude - I (a.u.)
Amplitude - Q (a.u.)
Amplitude - I (a.u.)

(a)

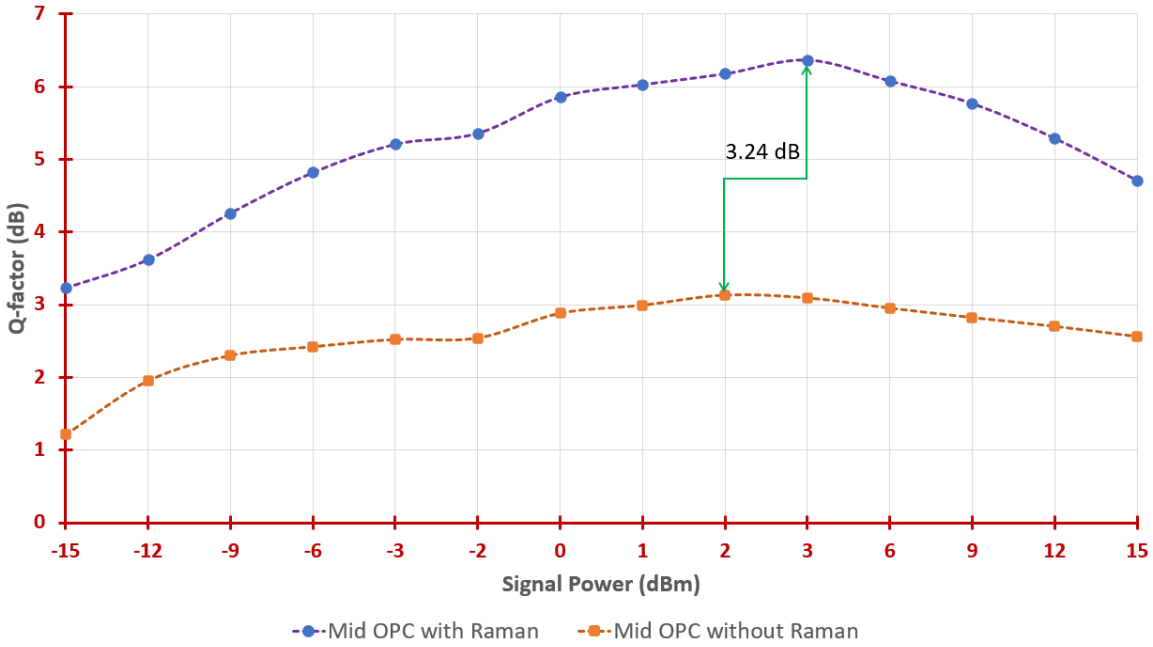
Q-factor (dB)
Signal Power (dBm)
3.24 dB
Mid OPC with Raman
Mid OPC without Raman

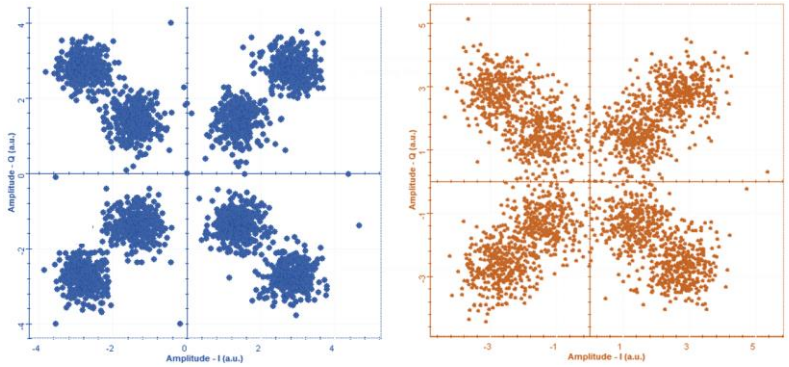
Amplitude - Q (a.u.)
Amplitude - I (a.u.)
Amplitude - Q (a.u.)
Amplitude - I (a.u.)

(b)

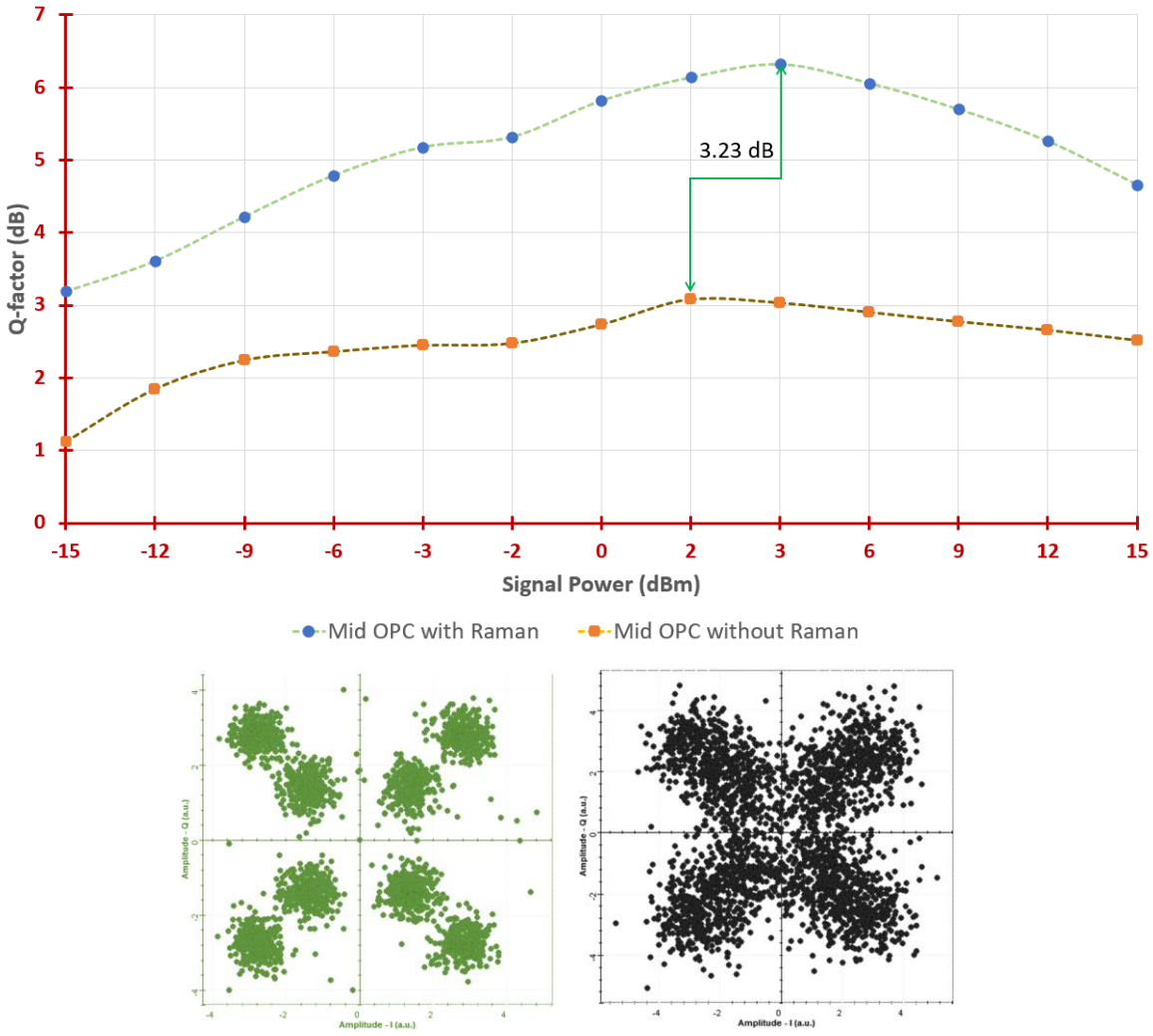

(c)

Figure (5.27). Q-factor and constellation diagram for mid OPC with and without Raman amplifier for (a) Ch.1 (b) Ch.8 (c) Ch.16

As shown in figure 5.27, the constellation diagram for the three channels before and after using the Raman amplifier is somewhat obvious as compared to without using it, with increasing BER and Q-factor. However, the signal quality is still below the required level, which will be further improved in the next section.

5.3.2 Multiple OPC with and without Raman Amplifier

The simulation implementation in the previous method is repeated here but using multiple OPCs. It will be clarified also the use of multiple OPC with two different cases, to reduce the impact of interchannel nonlinear impairments. Analyses are done on the nonlinearity effects in fibers that are exposed to different levels of input signal power. First, it will evaluate the transmission performance of the multiple OPC modules without a Raman amplifier. According to the data obtained, the max Q factor for the first, middle, and last channels are 5.53 dB, 5.49 dB, and 5.36 dB at 4 dBm signal power (which is the best value) and BER 2.92×10^{-2}, 3.01×10^{-2},and 3.18×10^{-2}. As can be seen in figure (5.28), comparing conventional multiple OPC to conventional mid OPC, the results reveal that this method causes less distortion with an improved Q-factor by 2.34 dB, 2.36 dB, and 2.28 dB with an enlarge by 42% for the first and middle channel, while 43% for the last channel to conventional mid OPC for the three channels. In Appendix B, Table (B.9) shows BER, Q-factor, and EVM for the first, middle, and last channels.

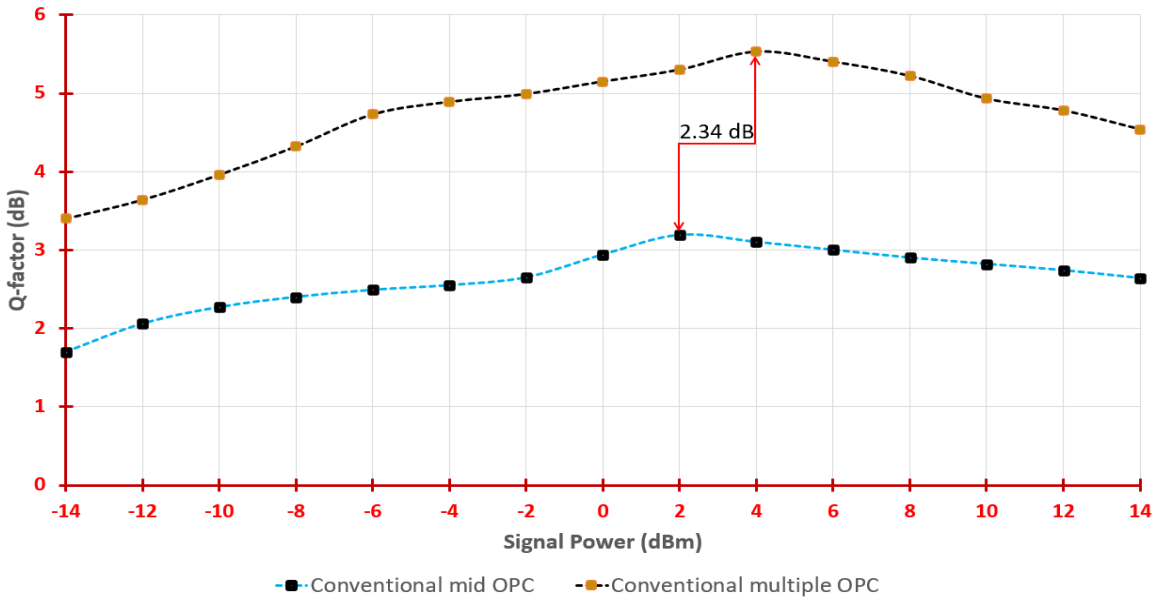

(a)

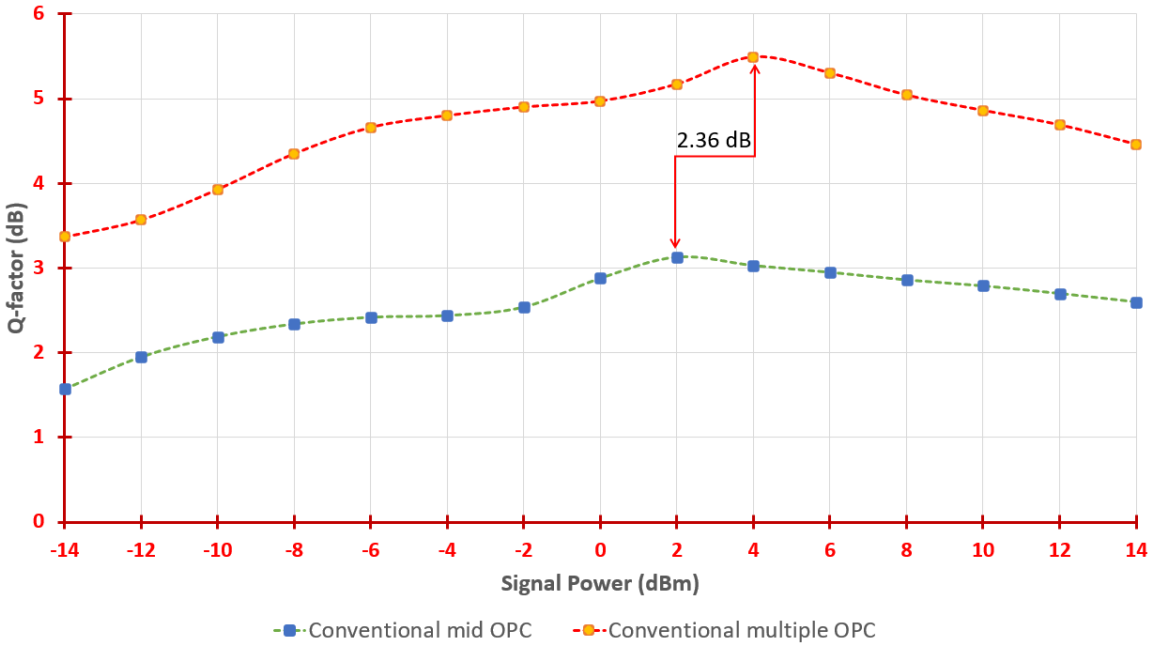

(b)

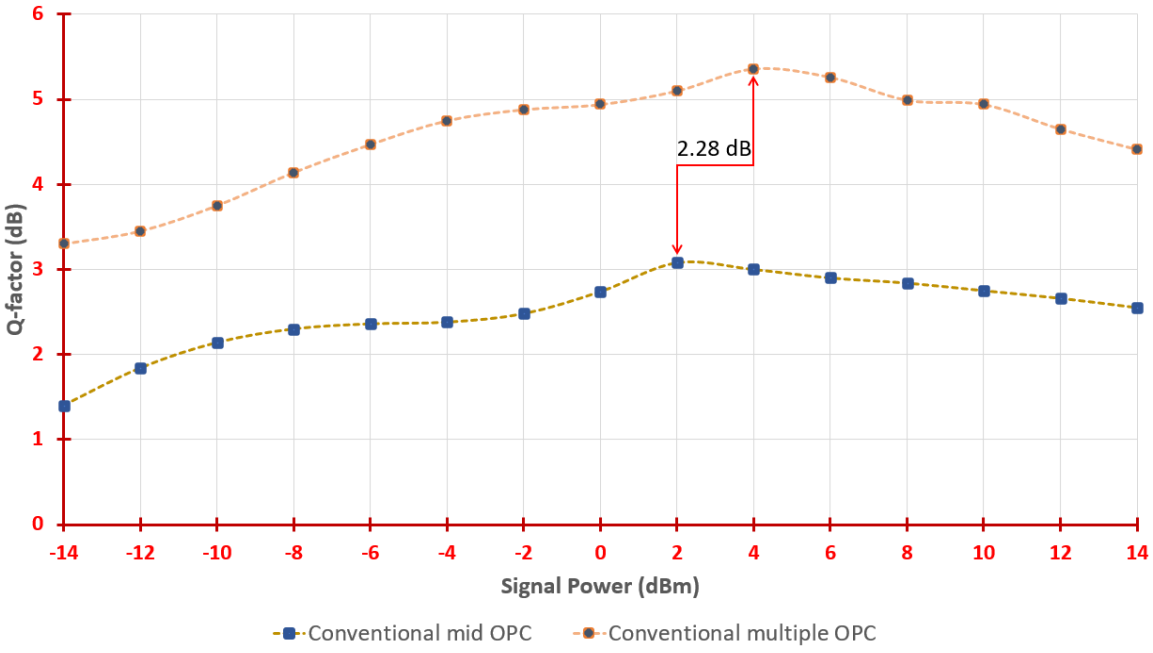

(c)

Figure (5.28). Q-factor for conventional mid and multiple OPC for (a) Ch.1 (b) Ch.8 (c) Ch.16

Then, the distortion of nonlinear in the system is reduced by the OPC's use of Raman amplification. The performance of transmission of multiple OPC modules with and without a Raman amplifier is illustrated in figure (5.29). It has been demonstrated that, as compared to conventional OPC, multiple OPCs outfitted with a Raman pump provide superior performance in terms of both peak Q factor and optimal launched signal power. The improvement of the Q factor is increased from (5.35, 5.49, and 5.36) dB at 4 dBm in conventional multiple OPC to (9.63, 9.57, and 9.50) dB at 5 dBm with a backward Raman amplifier that enhanced about (4.28, 4.08, and 4.14) dB for the channel (1, 8, and 16) respectively, with enlarged by 10.3%, 10.4%, and 10.5% for these channels. In Appendix B, Table (B.10) illustrates the three parameters (BER, Q-factor, and EVM) for this system.

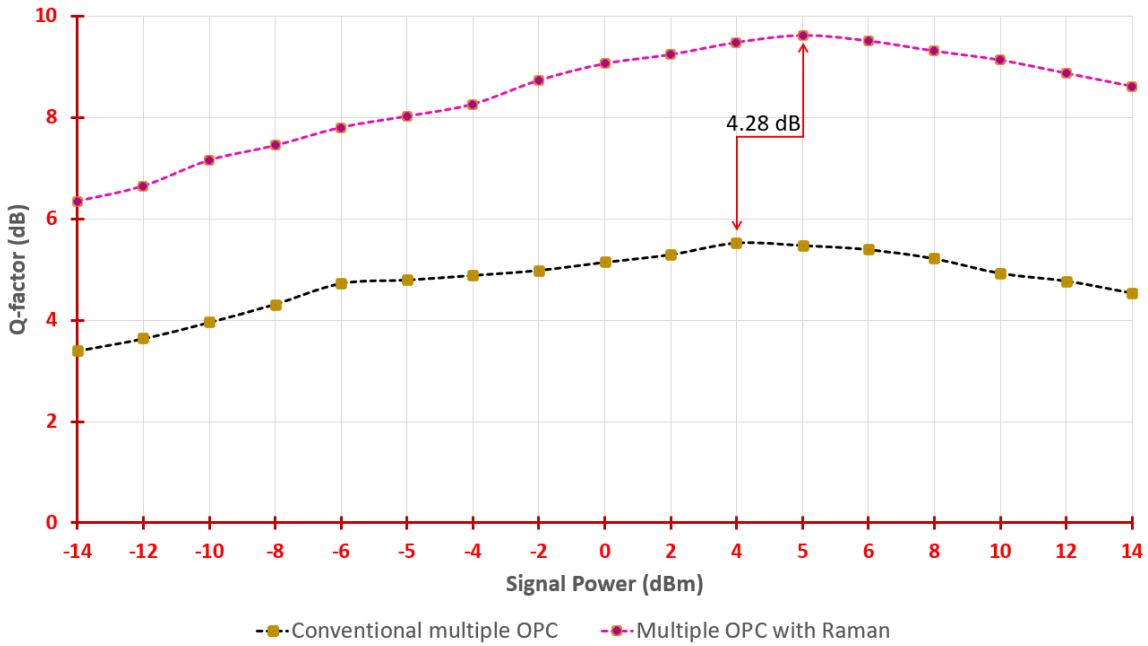

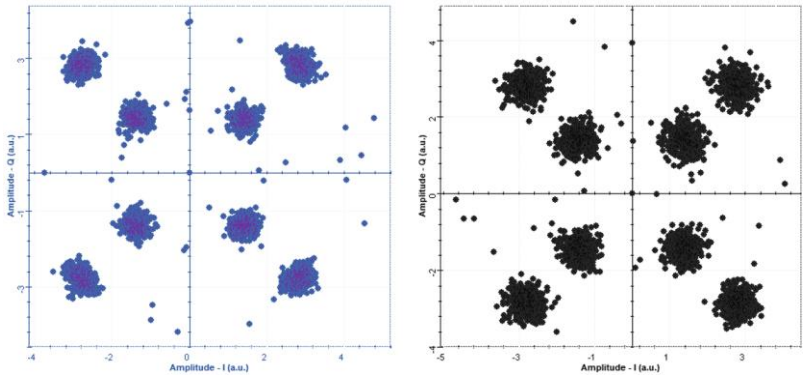
Amplitude - Q (a.u.)
Amplitude - I (a.u.)
Amplitude - Q (a.u.)
Amplitude - I (a.u.)

(a)

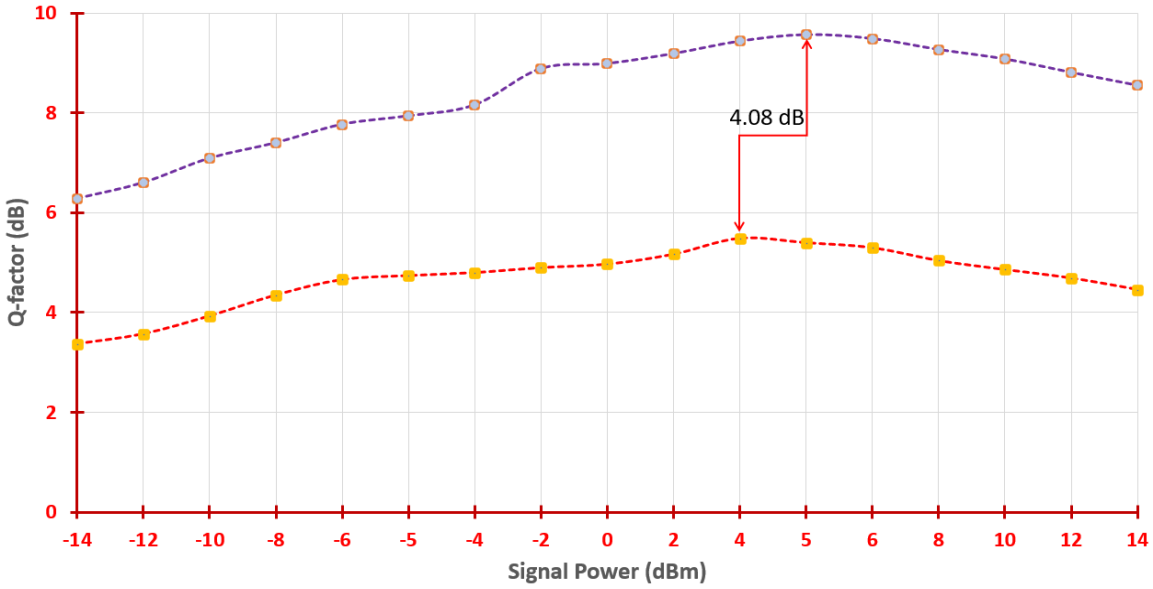
10
8
6
4
2
0
Q-factor (dB)
4.08 dB
-14
-12
-10
-8
-6
-5
-4
-2
0
2
4
5
6
8
10
12
14
Signal Power (dBm)
Conventional Multiple OPC
Multiple OPC with Raman

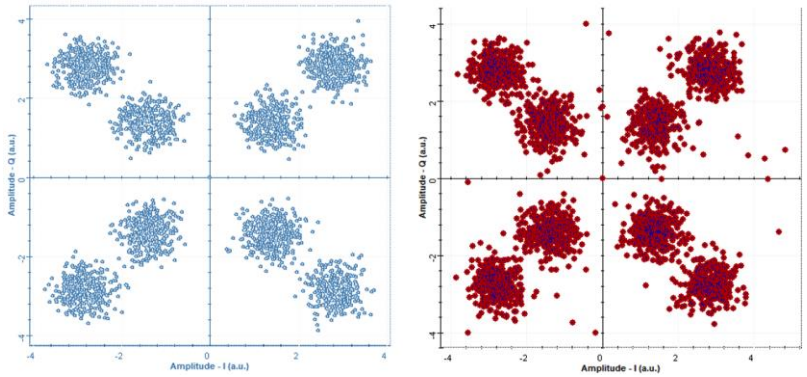
Amplitude - Q (a.u.)
Amplitude - I (a.u.)
Amplitude - Q (a.u.)
Amplitude - I (a.u.)

(b)

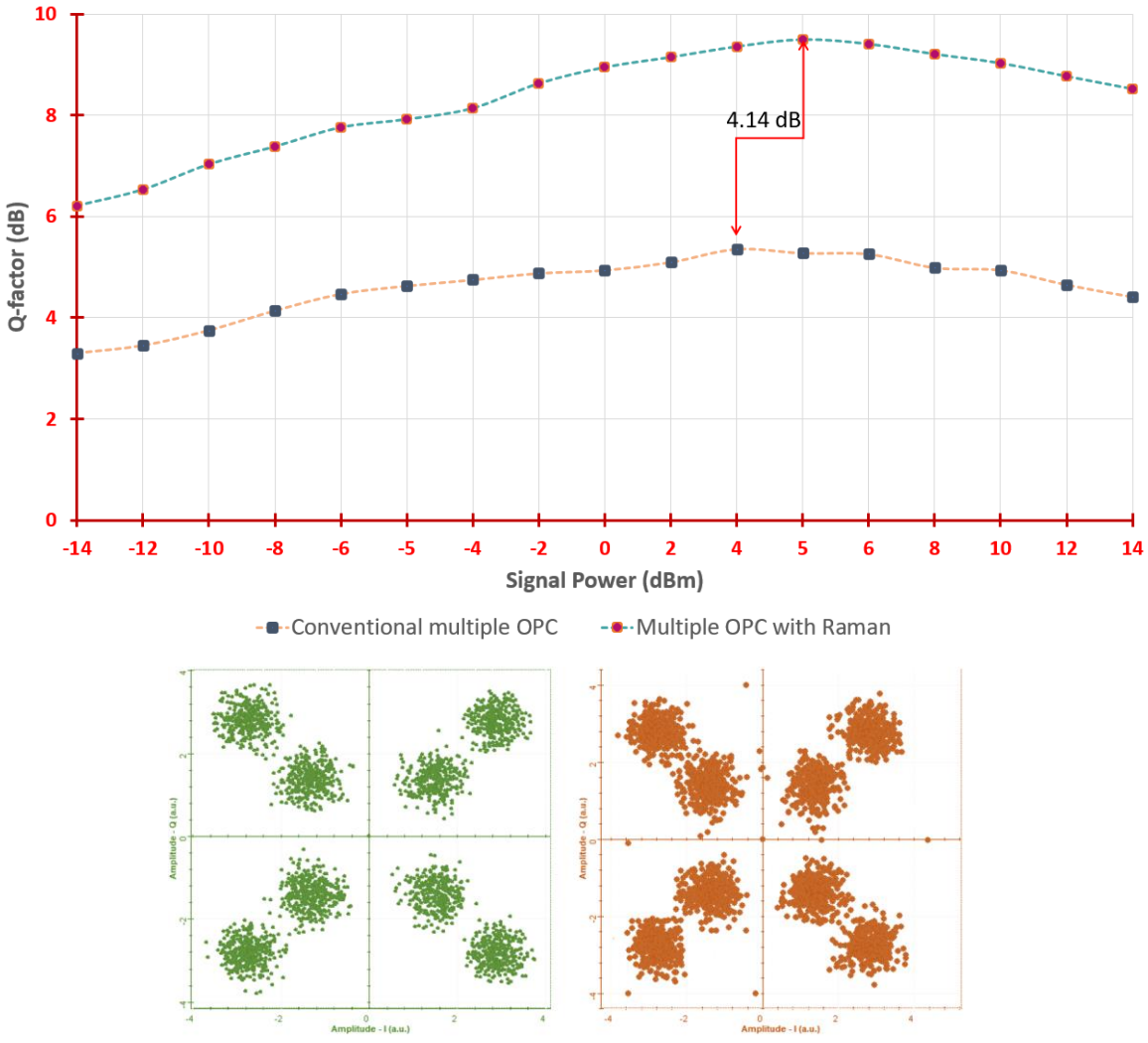

(c)

Figure (5.29). Q-factor and constellation diagram for multiple OPC with and without Raman amplifier for (a) Ch.1 (b) Ch.8 (c) Ch.16

Finally, a comparison of the mid OPC and the multiple OPC transmission performance using a Raman amplifier is analyzed in figure (5.30). The best value of input power is increased by 2 dBm when using an OPC with a Raman amplifier, and the Q factor is increased by (2.94, 3.20, and 3.18) dB, with enlarged by 34.2%, %, and 31.2%, and 31.4% for the first, middle, and last channel.

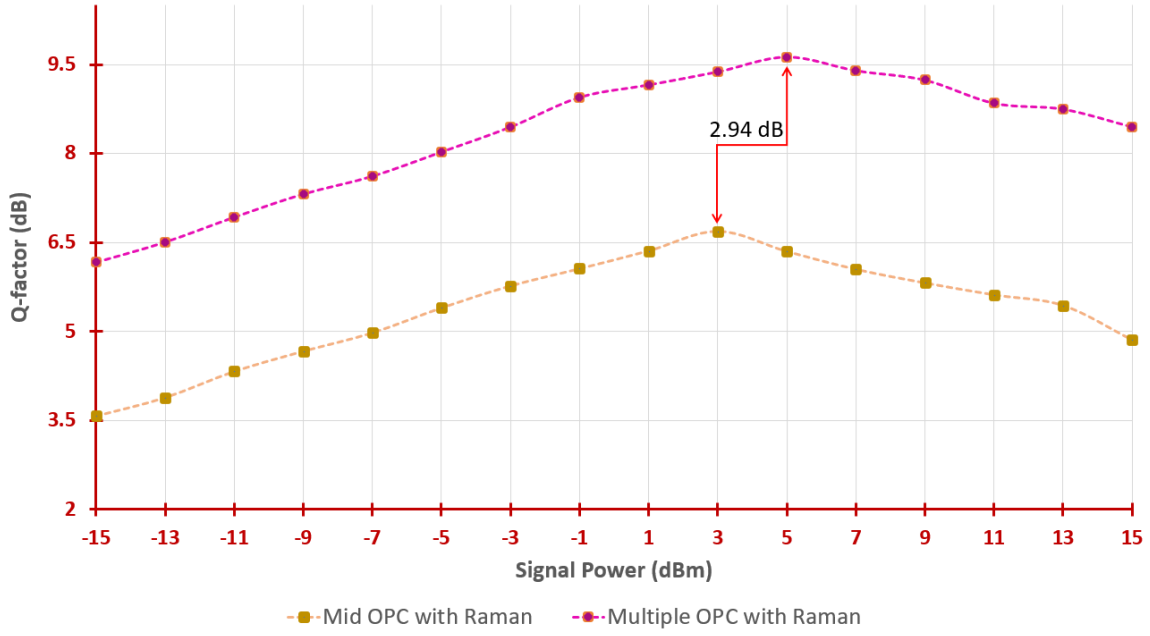
9.5
8
6.5
5
3.5
2
Q-factor (dB)
2.94 dB
-15 -13 -11 -9 -7 -5 -3 -1 1 3 5 7 9 11 13 15
Signal Power (dBm)
Mid OPC with Raman
Multiple OPC with Raman

(a)

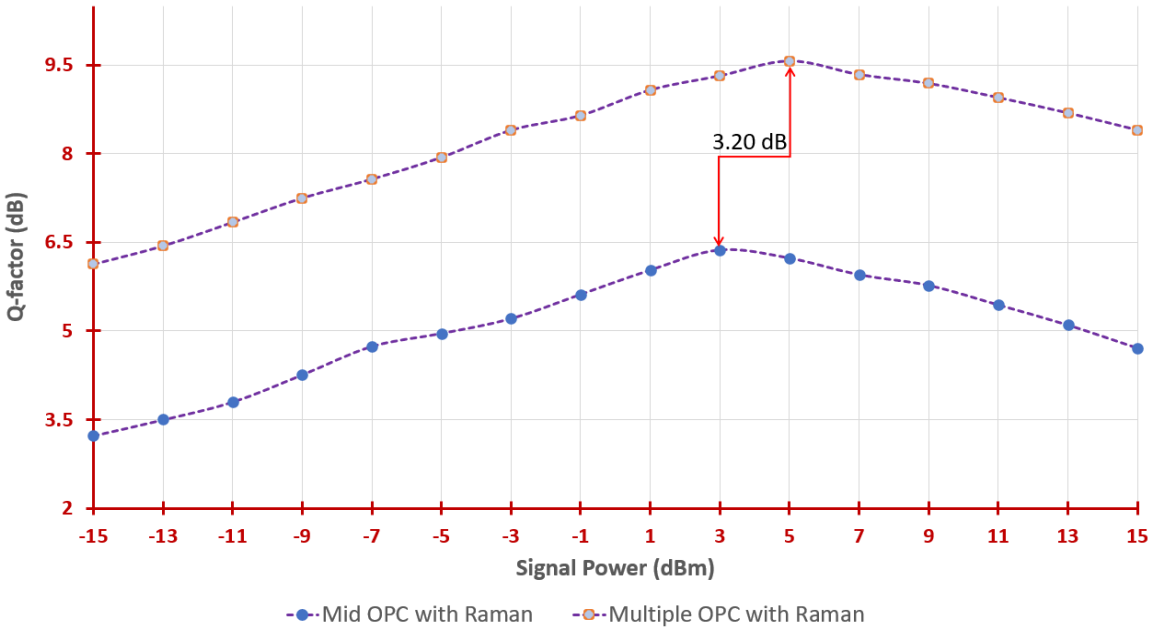
9.5
8
6.5
5
3.5
2
Q-factor (dB)
3.20 dB
-15 -13 -11 -9 -7 -5 -3 -1 1 3 5 7 9 11 13 15
Signal Power (dBm)
Mid OPC with Raman
Multiple OPC with Raman

(b)

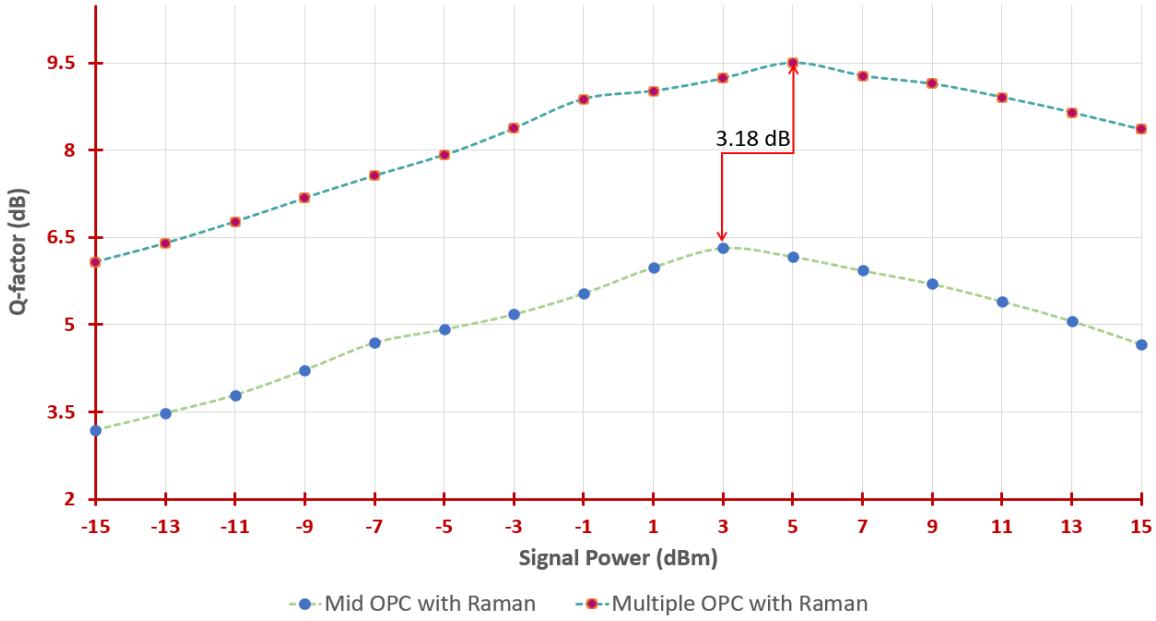

(c)

Figure (5.30). Q-factor for mid OPC and multiple OPC with Raman amplifier for (a) Ch.1 (b) Ch.8 (c) Ch.16

5.4 Enhanced Mitigation of Nonlinearity Signal Distortion of 3.58 Tb/s for DP-16QAM Communication System

In this section, it will be investigated and tested the optical compensation method using a communications system that supports a higher data transfer rate and is more susceptible to linear and nonlinear effects. This section studied and discussed fiber nonlinearities mitigation for 3.584 Tbps dual polarization sixteen quadrature amplitude modulation (DP-16QAM), 50 GHz channel spacing of DWDM transmission systems with 16 ×224 Gbps. In this section, the OPC compensation will take place with three scenarios; conventional, hybrid with DCF, and hybrid with backward Raman amplifier with a mid and multiple methods. The compensation scheme is investigated also in the first, middle, and last channels operating at 193.1, 193.45, and 193.85 THz, which correspond to the wavelength (1552.52, 1549.72,

1546.52) nm for the first, eighth, and sixteenth channels. To demonstrate the impact of OPC on the performance of a 16QAM system, it will first display the results obtained from a system operating in a back-to-back configuration, where the constellation diagram and BER are calculated without the interference of linear or nonlinear effects. In Figure (5.31) can see the 16QAM constellation diagram in x and y polarization.

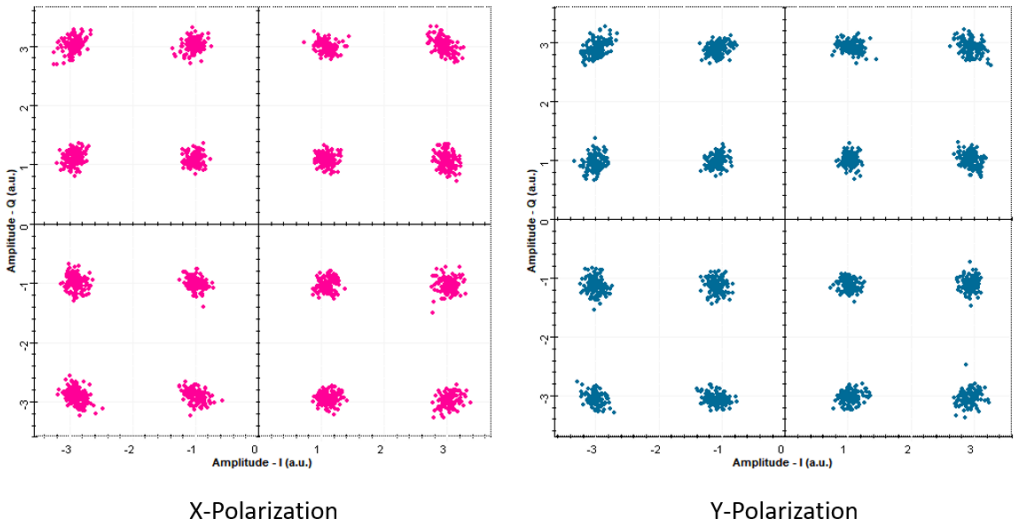

Figure (5.31). Constellation diagram of the received 16QAM signal transmission back-to-back for the middle channel

The constellation diagram is quite clear, and the BER is equal to zero for both polarizations. At this point, an optical fiber will be inserted to determine the extent to which the signal will be altered while the data is being transmitted. Figure (5.32) provides a visual representation of the constellation diagram. As can be seen in figure (5.32), the constellation diagram is poor because of the nonlinearity effect, which results in a high bit rate of (0.5), with an error vector magnitude of (2). When a signal is received and then degraded, the consequences can be linear or nonlinear. In order to mitigate these effects and improve the system's overall performance, an OPC technique is being used.

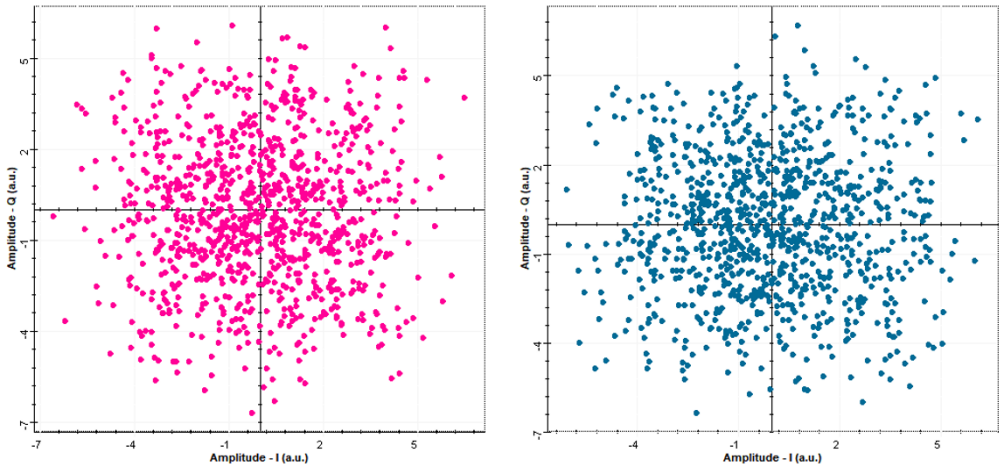

Figure (5.32). Constellation diagram of the received 16QAM signal over 800 km SMF for the middle channel

5.4.1 Compensation of Fiber Impairments Using Mid OPC

Firstly, the best transmit power per channel is 2 dBm for the conventional method, with a BER of 5.30×10^{-2}, 5.4×10^{-2}, and 5.48×10^{-2} for channels 1, 8, and 16, respectively. In Appendix B, Table (B.11) shows the values of BER, Q-factor, and EVM for three channels with different launch power.

Second, the effectiveness of hybrid OPC was evaluated using the DCF method. Table (B.12) in Appendix B displays the BER, Q-factor, and EVM values for a range of launch powers. When compared to conventional OPC, hybrid OPC with DCF improves and raises the Q-factor by 1.56 dB, 1.57 dB, and 1.60 dB for channels 1, 8, and 16, respectively, with 2 dBm optimum launched power. In contrast, the values of EVM are 0.174 for channel 1 and 0.176 for channels 8 and 16, due to the optical signal noise ratio reduction of optical noise in the unoccupied band at the input of the fiber optic parametric amplifier. Figure (5.33) shows the Q-factor for the conventional and hybrid with DCF cases with different signal power with improvements that have been added to the system to compensate for the positive value dispersion of fiber.

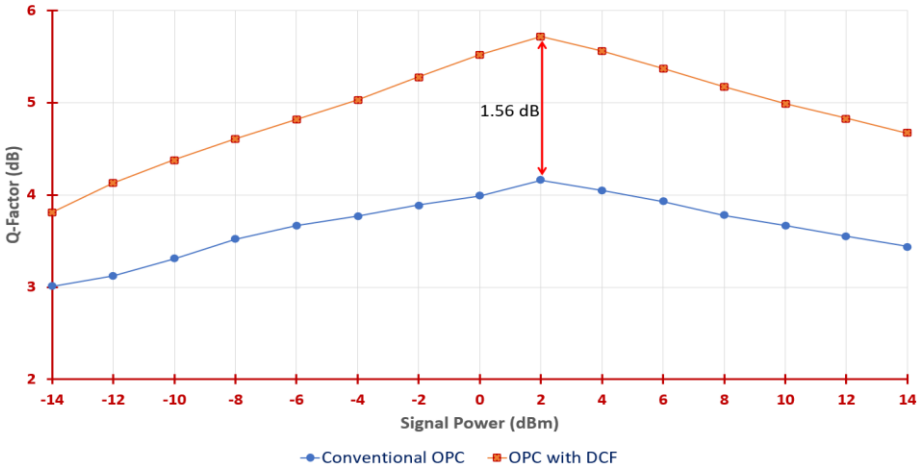

(a)

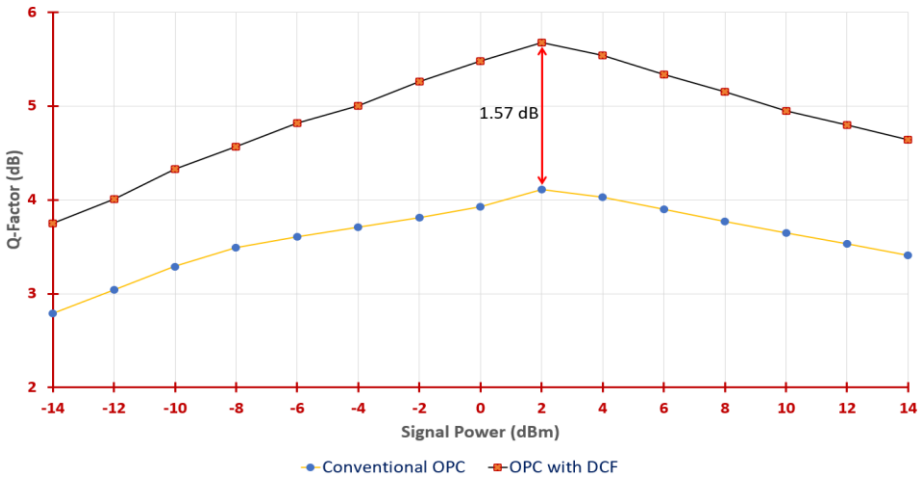

(b)

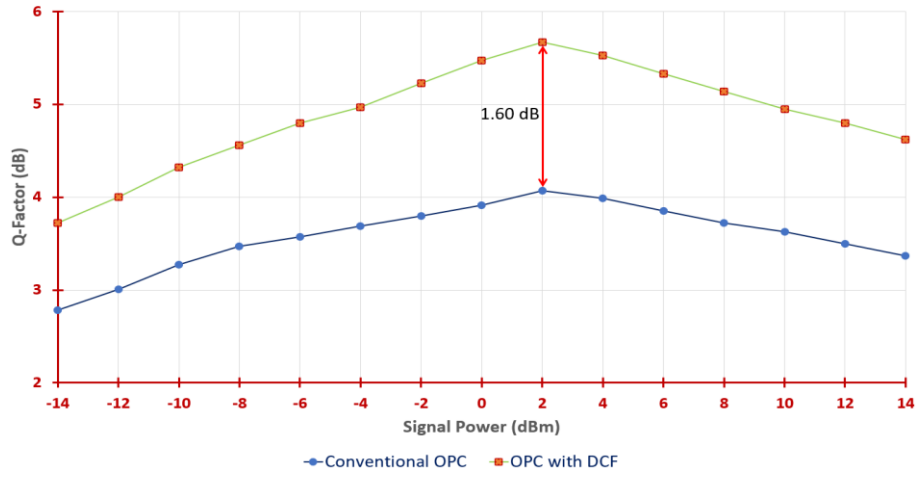

(c)

Figure (5.33). Q-factor versus signal input power for mid OPC with and without DCF (a) Ch.1 (b) Ch.8 (c) Ch.16

Thirdly, the backward Raman amplifier method was used to analyze and assess the efficiency of hybrid OPC. The values of BER, Q-factor, and EVM for several different launch powers are shown in Table (B.13) in Appendix B. As previously explained, incorporating backward Raman amplification into a conventional OPC setup alleviates the trade-off between the output optical signal noise ratio and the nonlinear penalty. The Raman pump is set to 1.5 W to make up for the loss of power from the output idler. As shown in figure (5.34), hybrid OPC with a Raman amplifier raises the best amount of input power by 1 dB to be about 3 dBm and the Q factor by 3.08 dB, 2.99 dB, and 3 dB for channels 1, 8, and 16, respectively, as compared to conventional OPC, with enlarged by 10.22%, 10.25%, and 10.43% for the three channels. Also, compared to OPC with DCF, Raman enhancement improves the Q-factor by 1.52 dB, 1.42 dB, and 1.40 dB as shown in figure (5.34) for the channel 1, 8, and 16, respectively, with enlarged by 3.67%, 3.52% and 3.49%.

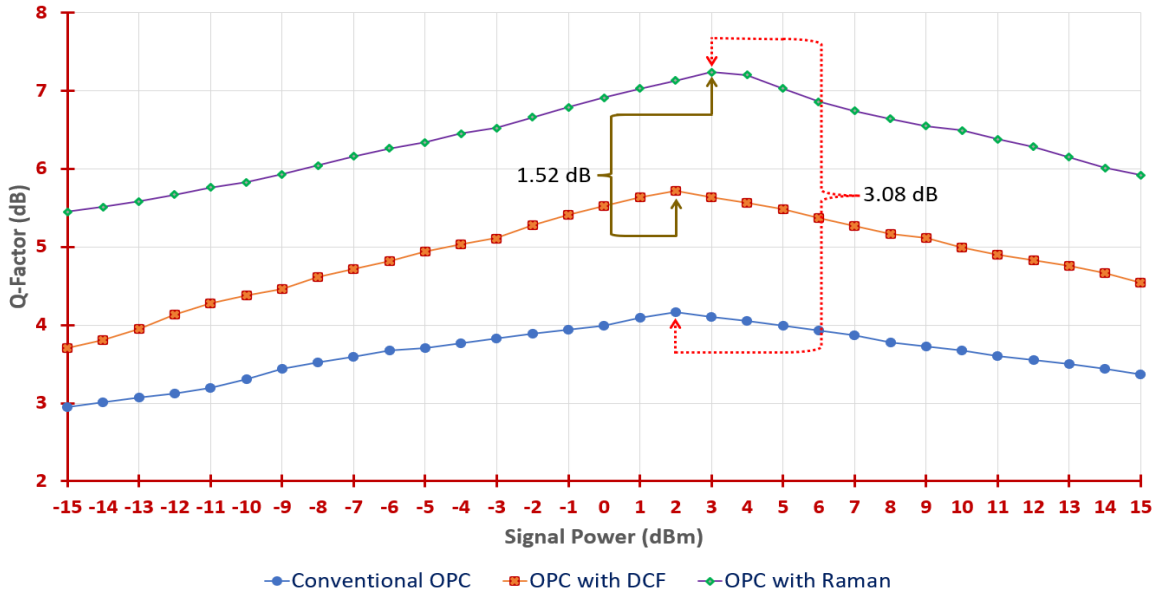

(a)

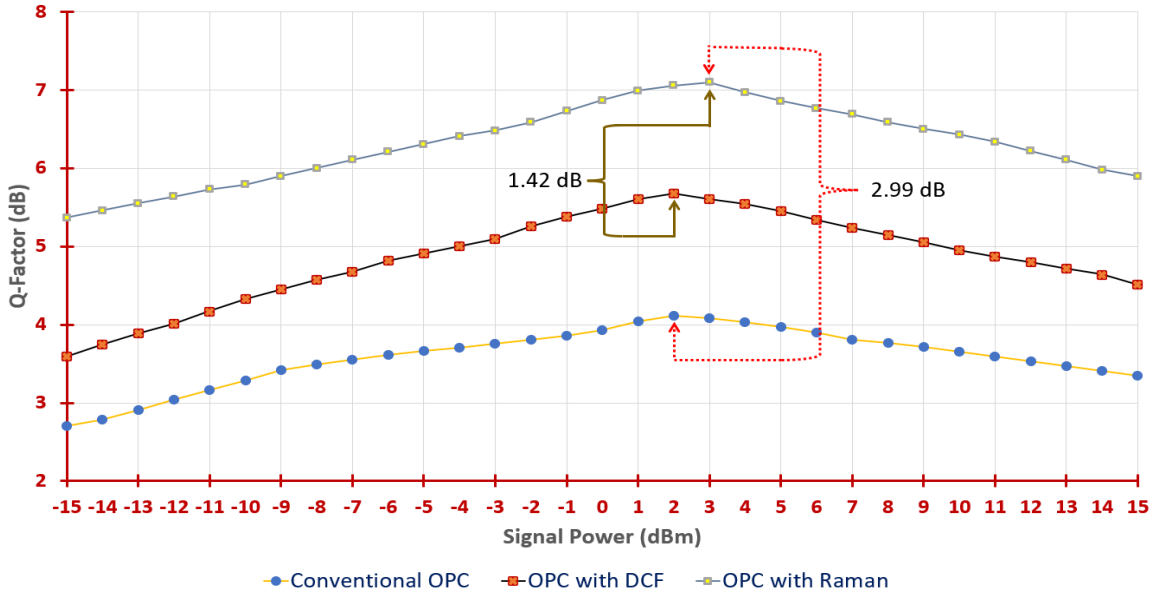

(b)

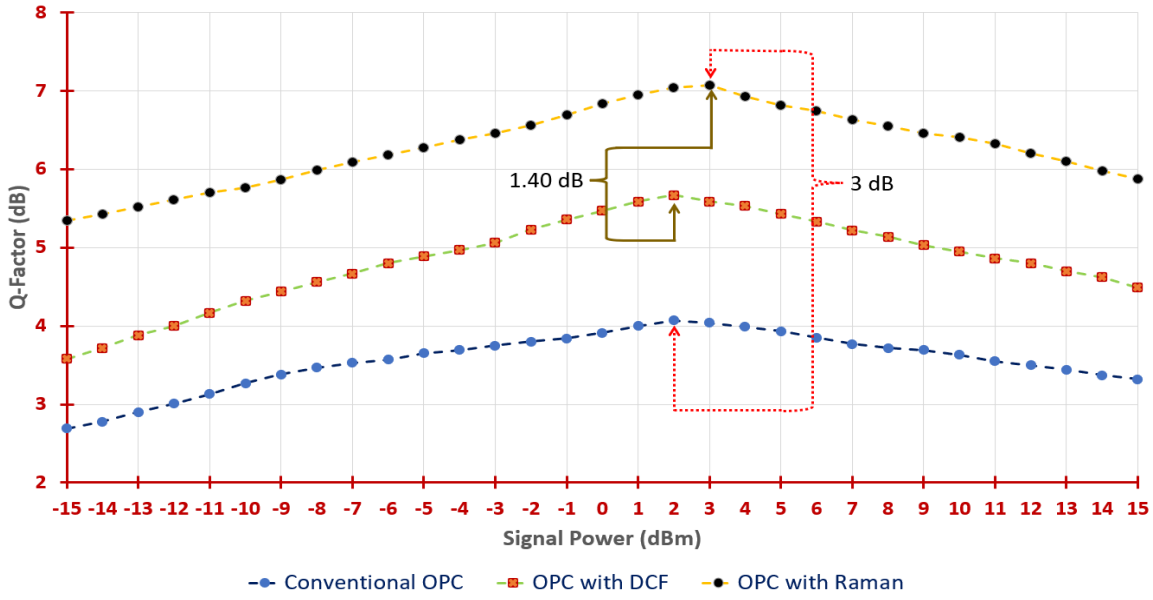

(c)

Figure (5.34). Q-factor versus signal input power for mid OPC with three cases (conventional, DCF, and Raman amplifier) (a) Ch.1 (b) Ch.8 (c) Ch.16

It can show that all parameters used to calculate the efficiency of the proposed system are the best in the state of using hybrid OPC with Raman amplifier as compared to conventional and DCF but it is less than HD-FEC limit, which can be improved by using multiple OPC method.

5.4.2 Compensation of Fiber Impairments Using Multiple OPC

In this section, the reduction of nonlinear impacts, which will be reanalyzed and studied depending on the multiple OPC approach, will be discussed. Firstly, Conventional multiple OPC will be studied. In Appendix B, table (B.14) shows the results of BER, Q-factor, and EVM for different signal power. According to the data, the max Q-factor for the three channels when the signal power is at 3 dBm. If comparing this result with the result obtained in mid OPC, the improvement on the Q-factor is about 5.64 dB, 5.62 dB, and 5.64 dB for the first, middle, and last channel, respectively, with the clearest constellation diagram as shown in figure (5.35). This is mainly due to the reduction of the distortion rate, which indicates the effectiveness of the multiple methods used.

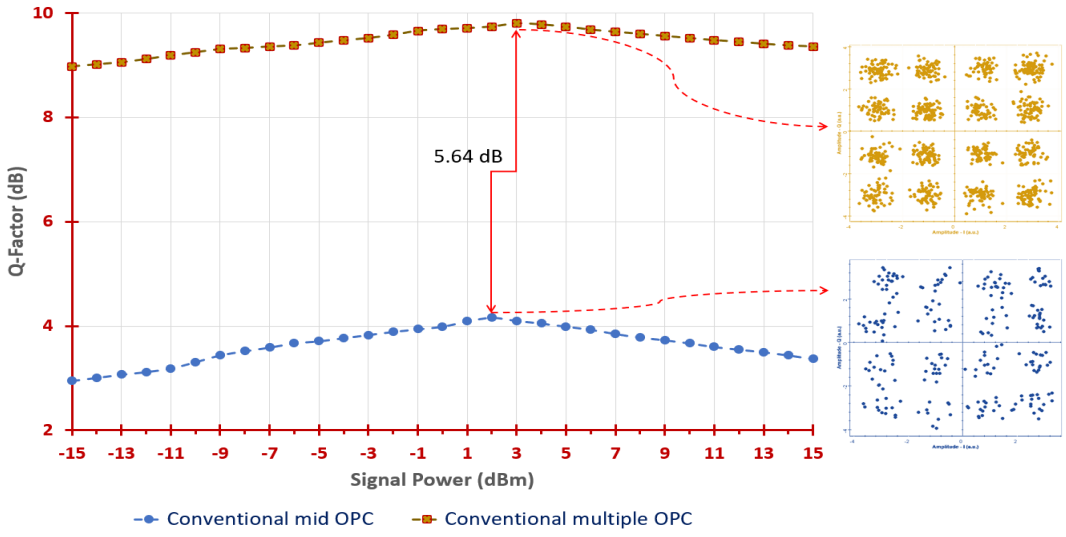

(a)

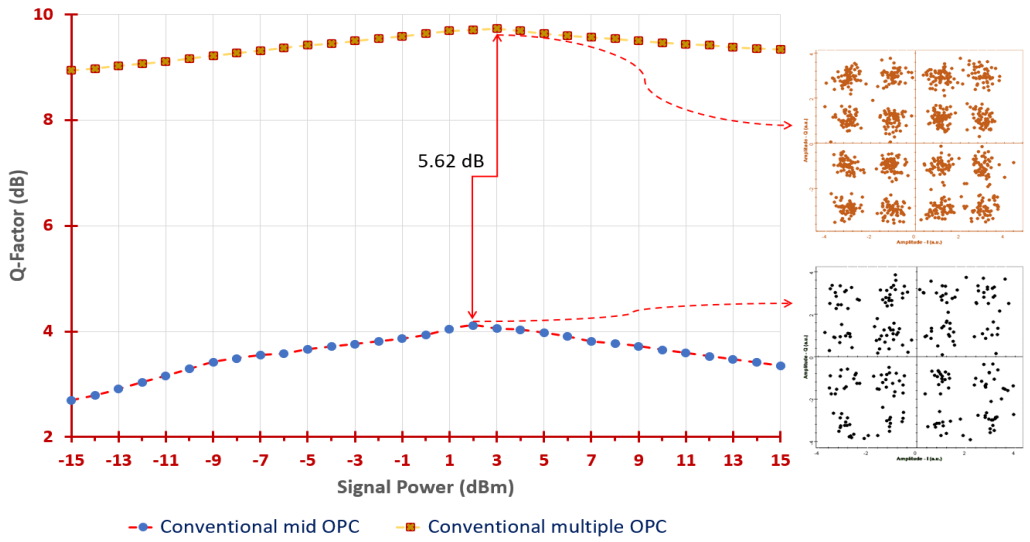

(b)

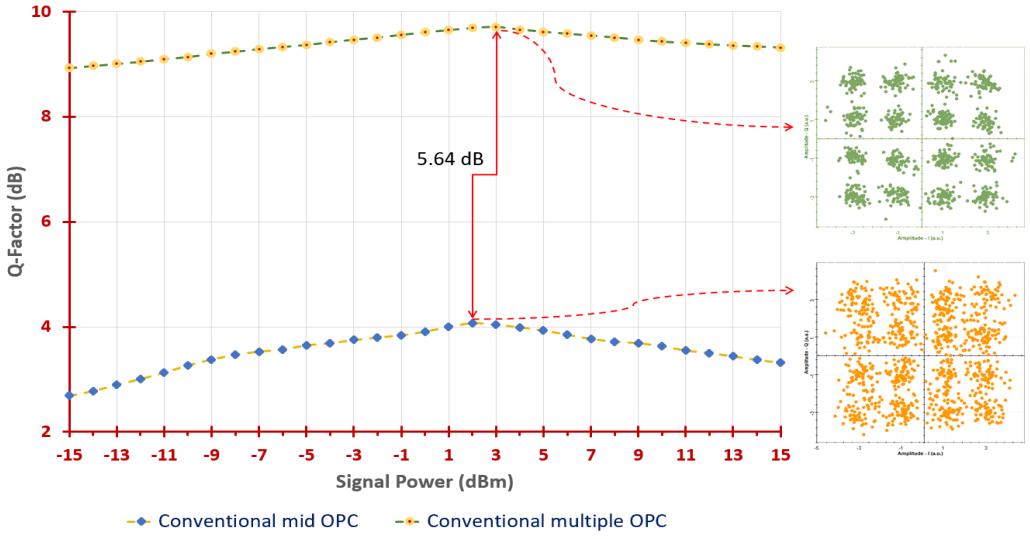

(c)

Figure (5.35). Q-factor and constellation diagram for conventional mid and multiple OPC for (a) Ch.1 (b) Ch.8 (c) Ch.16

Next, when using hybrid compensation with DCF, it was getting the results that found in table (B.15) in Appendix B. When comparing this method with the mid method, concluded the improvement of Q-factor, BER, and EVM as well as the signal power by 2 dB to be 4 dBm, which improvement of 19.3% for the first and middle channel while 19.4% for the last channels. Figure

(5.36) illustrates the comparison of hybrid OPC with DCF for mid and multiple method.

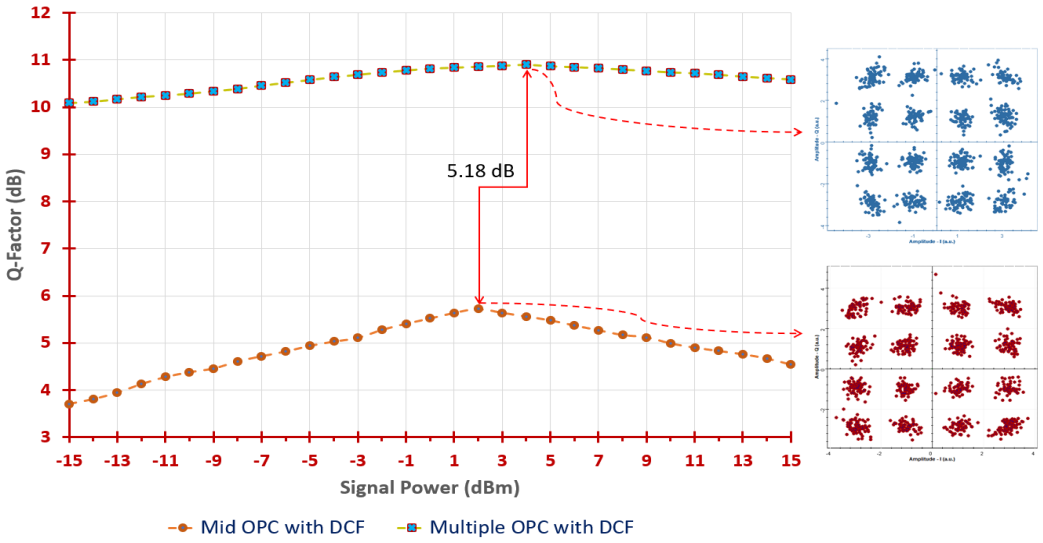

(a)

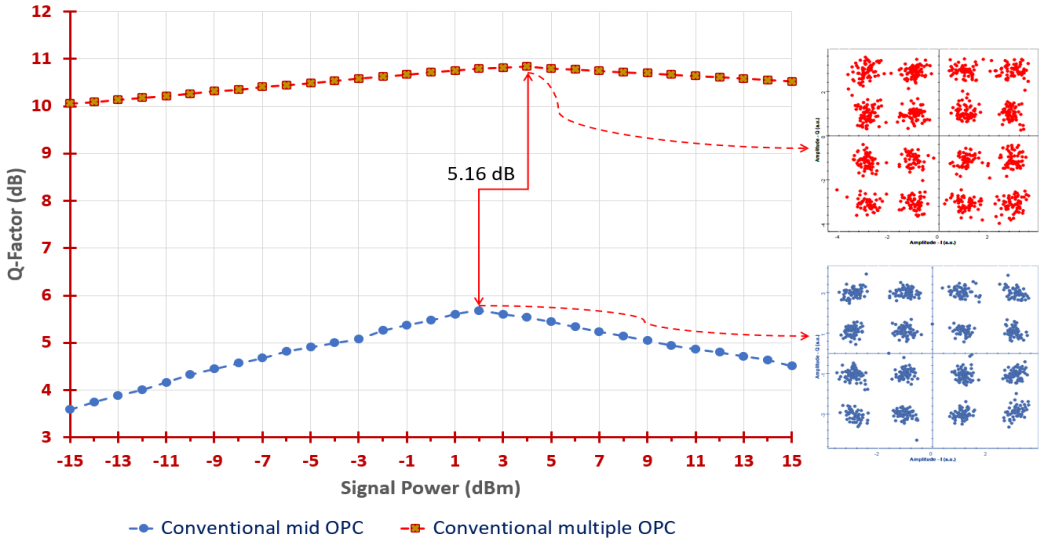

(b)

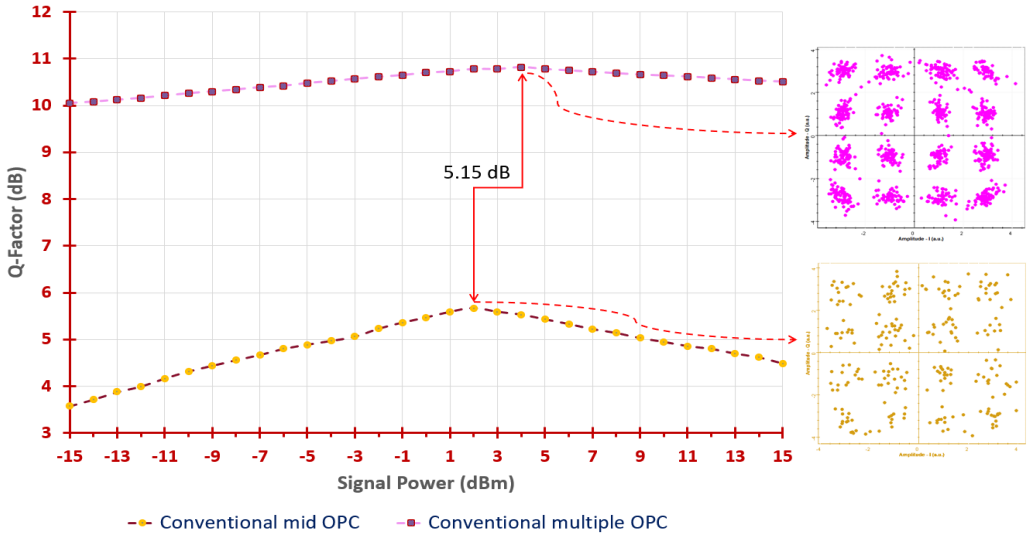

(c)

Figure (5.36). Q-factor and constellation diagram for hybrid OPC with DCF for mid and multiple methods for (a) Ch.1 (b) Ch.8 (c) Ch.16

The final findings obtained utilizing the hybrid compensation technique with the Raman amplifier are shown in table (B.16) in Appendix B. The broadband gain provided by Raman amplification of the interacting light waves with a lower input signal strength is employed to improve the FWM process in the HNLF, and this method has proven to be of high quality in giving the best and most accurate results when compared to the two previous techniques. Figure (5.37) illustrates the Q-factor with a constellation diagram for the mid and multiple OPC with Raman amplifier. As shown in figure (5.37), the amelioration of multiple method over mid method using backward Raman amplifier proves it effective against nonlinear effect by increasing the values of all parameters (BER, Q-factor, EVM) with 5 dBm optimal launch power that improves by 2 dB compared to mid method with enlarged by 17.03%, 16.67%, and 16.63% for the first, middle, and last channels. This proves that this method is the most effective compared to the previous two scenarios with

a clear and significant improvement in the quality of the signal received and the transmission exceeding the value of the HD-FEC limit (BER=3.8×10^{-3}).

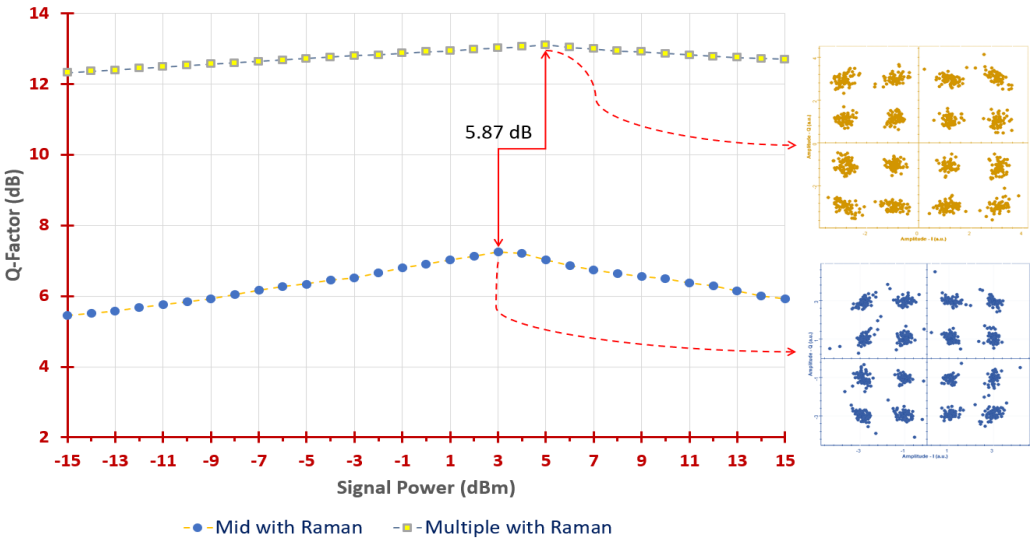

(a)

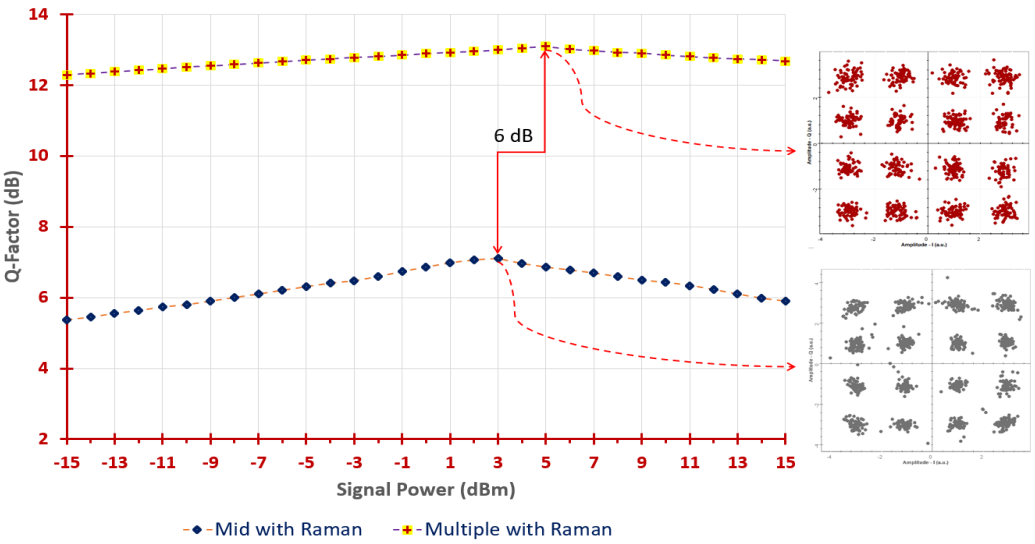

(b)

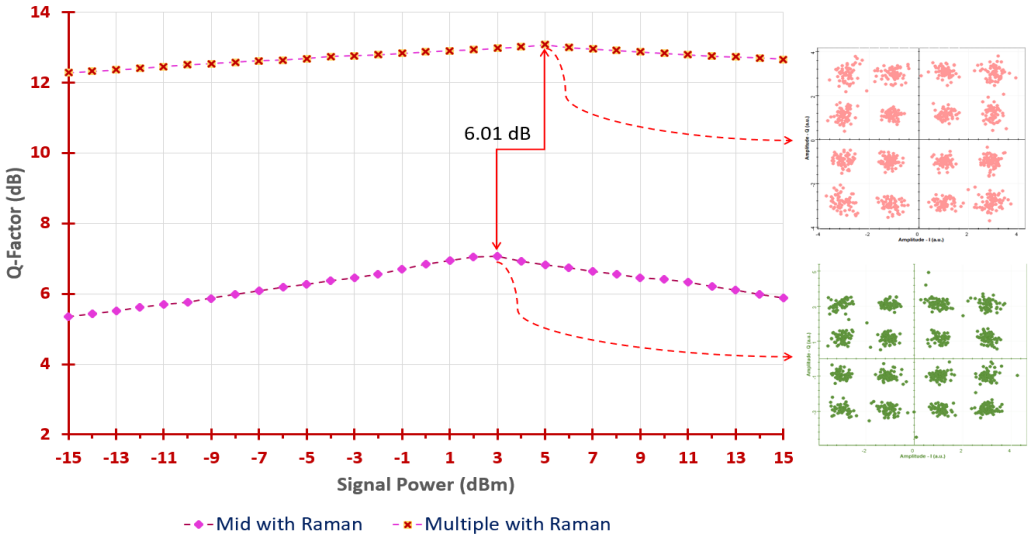

(c)

Figure (5.37). Q-factor and constellation diagram for hybrid OPC with Raman amplifier for mid and multiple method for (a) Ch.1 (b) Ch.8 (c) Ch.16

5.5 Summarization and Contributions of OPC Technique

Finally, after investigating the optical compensation method-based phase conjugation, Table (5.1) provides a comparison of the current study with previously published works of different nonlinear compensation methods with the most prominent contributions that have been employed in this work. The proposed method with the three cases (conventional, DCF, and Raman) has proven effective for both linear and nonlinear effects, especially in multichannel systems using the DWDM technique. The data rate reaches 3.58 Tb/s in 16 QAM state, while the BER to 10^{-35}, 1.33×10^{-3}, and 3.5×10^{-6} in NRZ-OOK, 8QAM, and 16QAM, respectively. The data rate, BER, and transmission distance achieved advanced and acceptable values compared to previous studies.

Table (5.1). Comparison of proposed work with previously published work

Parameters	Ref. [117]	Ref. [16]	Ref. [118]	Ref. [21]	Ref. [22]	Ref. [23]	Ref. [25]	Ref. [119]	Proposed work
Type of compensation	XPM	FWM	FWM	FWM	Kerr nonlinear	Kerr nonlinear	FWM	FWM	Linear and nonlinear effect
Method of compensation	DBP	Hybrid OPC with DCF & FBG	Mid OPC	Mid OPC	Mid OPC	Mid OPC with Raman	Mid OPC	Mid OPC	Mid & Multiple OPC with three methods (Conventional, hybrid with DCF & Raman)
Multiplexing type	WDM	WDM	WDM	WDM	AWG	——	WDM	——	DWDM
Input power	Variable	-10 to 10	-20 to 20	10	-4 to 12	-6 to 12	Variable	-25 to 10	-15 to 15
Modulation format	QAM & QPSK	ASK	16 QAM	16QAM CO-OFDM	QPSK & 16QAM CO-OFDM	16QAM	——	QPSK	DP-OOK SP-8QAM DP-16QAM
No. of channel	5	8	7	2	2	Single	Multi	Single	16
Data rate per channel (Gb/s)	——	2.5	——	320	40 & 80	200	80	20	25, 108, and 112
Transmission distance (km)	800	185	350	800	200	Variable	160	——	800
Channel spacing (GHz)	32	100	100	80	20	——	100	——	50
BER	——	10^{-3}	——	6.1×10^{-4}	7.5×10^{-3}	7×10^{-5}	10^{-3}	——	10^{-35} 1.33×10^{-3} 3.5×10^{-6}

5.6 Mitigation and Compensation of Linear and Nonlinear Effects Based Convolutional Neural Network

In this section, advanced coherent optical systems are simulated, investigated, and analyzed with the most important improvements made to reach the desired goal of reducing fiber impairments using machine learning based on a Convolutional Neural Network (CNN). The simulation of optical implementation was carried out using the Optisystem program and the artificial intelligence algorithms were implemented and simulated using MATLAB. The two programs were linked using co-simulations to ensure the validity of the results obtained in real-time. In this work, implemented multichannel (16 channels) with a data rate of 120 Gb/s for each channel to reach a total rate of 1.92 Tb/s using DWDM multiplexing technique with 50 GHz channel spacing to collect these all channels and sent over standard single mode fiber (SMF) towards coherent receiver side to demonstrate improvement after different distances, reach to 5000 km (100 km per span).

5.6.1 CNN-NLC for Single Polarization 16QAM

One of the modern methods that have been employed in this proposed work to give strength and originality in dealing with the effects that optical fibers suffer from is the use of the machine learning method based on CNN. These algorithms excel at recognizing and analyzing complex and nonlinear patterns in data, providing advanced solutions for the nonlinearity and interference issues in optical communication systems. Figure (5.38) illustrates the optical spectrum of 16QAM-DWDM multiplexer. The frequencies of these channels began at (193.1 THz) for the first channel which corresponded to (1552.52 nm) wavelength, while the frequency of the last channel (193.85 THz) corresponded (1546.52 nm).

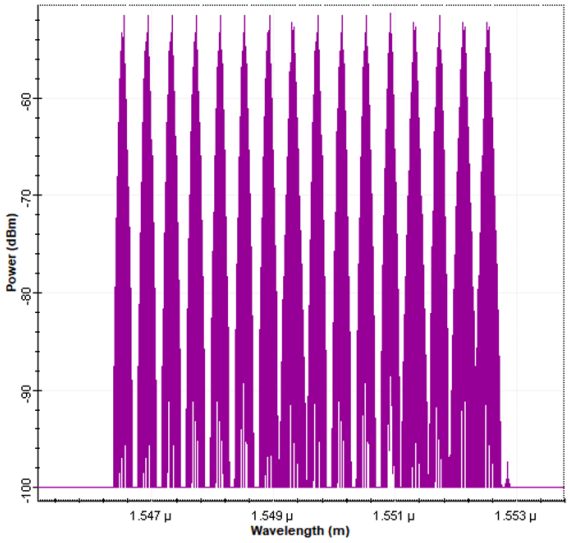

Figure (5.38). 16QAM-DWDM optical spectrum output for 16 channels

Optical fiber follows next Erbium Doped Fiber Amplifiers (EDFA) with a noise figure is 4 dB and is used to compensate span loss with all ASE noise added completely before the receiver side. EDFA is especially suited for performing the prompt analysis of the performance of the amplifiers in the long-haul system. Also, used a third order optical filter with a Gaussian frequency transfer function at the receiver side only with 100 dB Depth (maximum attenuation value for the filter). In addition, at the receiver, the incoming optical signal is coherently detected and the symbols are fed to a linear equalization (LE) for compensating chromatic dispersion (CD) and channel distortions (linear dispersion). As a result of fiber non-linearity, residual distortions after LE will limit achievable rates of information. Figure (5.39) illustrates the constellation visualizer for the received optical signal after 1000 km with 10 dBm launch power. This figure shows the performance degradation of the optical communication system due to nonlinearity and interference. The system's performance is negatively affected as the power levels and distance increase. This means that with higher signal power and

long transmission distance in the system, the impact of nonlinearity and interference becomes more pronounced, resulting in a deterioration of the communication quality.

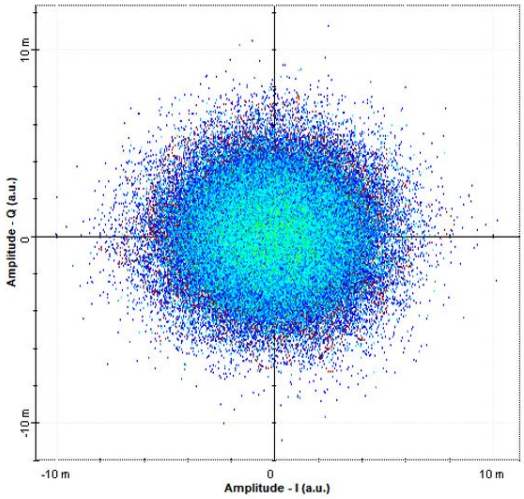

Figure (5.39). Constellation diagram of the received 16QAM signal over 1000 km SMF for the middle channel

For the purpose of compensating for the residual linear and nonlinear distortion, the CNN-based NLC will be applied. The CNNs-NLC ability was evaluated based on BER and the correct constellation mapper decoder. Firstly, there are 4 bits per symbol (m=4) in SP-16QAM, leading to (2^4 = 16) classes to identify per symbol. The single Nonbinary SoftMax Classification Algorithm can be used but does not perform well for higher-order mapper constellations because it needed to unrealistically hugely datasets for training. So, will be used multi-label classification, which is more scalable for high-dimensional and high-order modulation. The carrier data after LE and dispersion compensation are including inter symbol interference (ISI) with propagation distance. In addition, the optical nonlinear effects are deterministic ISI in this system. The received data after LE and dispersion

compensation are fid to the CNNs which utilize multiple techniques to compensate for nonlinearity in the NLSE, including the use of nonlinear activation functions, convolutional layers, batch normalization layers, max pooling layers, and a fully connected layer. These techniques allow the network to model complex, nonlinear relationships between the input data and the target class, resulting in improved performance in compensating for nonlinearity in the NLSE.

To tune CNN parameters, it will evaluate the performance of the network in terms of accuracy and loss. Specifically, it compares two different models: the first model consists of 5 CNN layers with learning rates of 1e-3 and 1e-4, while the second model consists of 6 CNN layers also with the same learning rate trained for 1100 epochs with varying minibatch sizes for the two models. The goal of the training is to make the network generalize well to unseen data, in order to perform well on new inputs. Accuracy and loss results after training a CNN can provide insight into how well the network has learned to perform its task. Accuracy is a measure of how well the network is able to correctly classify or predict the input data. It is usually expressed as a percentage, with a value of 100% indicating that the network has correctly classified or predicted all of the input data, and a value of 0% indicating that the network has not correctly classified or predicted any of the input data. Loss, on the other hand, is a measure of how well the network's predictions match the true labels or values of the input data. It is typically expressed as a scalar value, with a lower value indicating that the network's predictions are closer to the true labels or values, and a higher value indicating that the network's predictions are further away from the true labels or values.

5.6.1.1 Five CNN Layers:

The aim of the training is to obtain a sufficient estimation weight vector. The NN has been trained by using an Adam optimizer with a mini-batch size varying from 64 to 512, which corresponds to 1100 epochs of the algorithm of optimization. The presence of the performance of the 5 CNN model is shown in Tables (5.2) and (5.3).

Table (5.2). Performance of 16QAM for 5 CNN layers @learning rate 1e-4

Batch size	Training		Testing	
	Accuracy %	Loss	Accuracy %	Loss
64	53.12	1.33	69	1.02
128	76	1.01	74	1.01
256	84	0.78	80	0.85
512	85	0.8	83.3	0.82

Table (5.3). Performance of 16QAM for 5 CNN layers @learning rate 1e-3

Batch size	Training		Testing	
	Accuracy %	Loss	Accuracy %	Loss
64	85	0.8	85.8	0.8
128	88	0.65	86	0.7
256	88.41	0.52	89	0.45
512	90	0.4	89.9	0.45

As can be seen in the previous two tables, the best value of training and testing in terms of accuracy and loss is when the learning rate is equal to 1e-3 with mini batch size 512, while the performance of training is worse when the lower value of these two parameters decreases. Figure (5.40) shows accuracy and loss after the end of training. However, it is still possible to improve accuracy and reduce error by increasing the number of layers, but at the expense of training time.

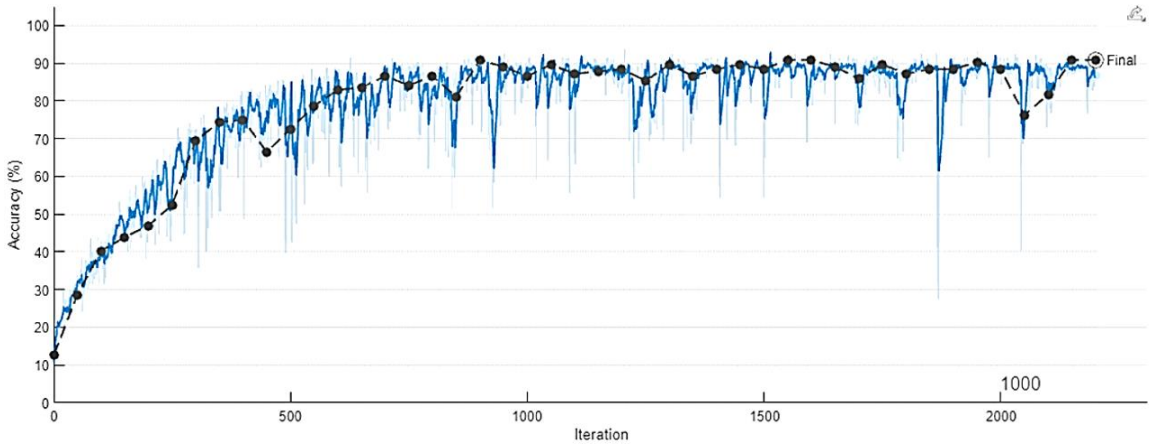

(a)

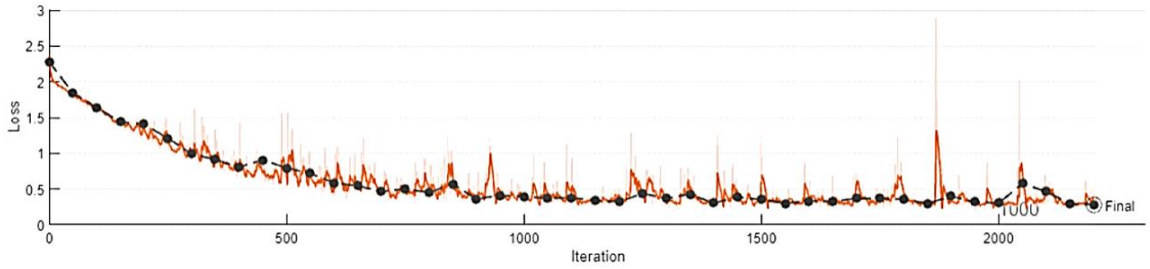

(b)

Figure (5.40). Final training progress of 5 CNN @1e-3 (a) accuracy (b) loss

5.6.1.2 Six CNN Layers:

The empirical results reveal that augmenting the batch size of the model enhances its performance but simultaneously increases its computational complexity. Despite setting the batch size to 512 with a learning rate of 1e-3, the targeted performance was not achieved. Notably, the experimental evaluation of the CNN network with a batch size of 512 at a learning rate of 1e-3 unveiled that the peak performance was only 90%. Consequently, a shift was made towards testing the second CNN model that consisted of six CNN layers as the results presented in Tables (5.4) and (5.5).

Table (5.4). Performance of 16QAM for 6 CNN layers @learning rate 1e-4

Batch size	Training		Testing	
	Accuracy %	Loss	Accuracy %	Loss
64	87.8	0.52	88	0.5
128	90.24	0.4	89	0.48
256	89	0.5	90	0.48
512	90.1	0.4	90	0.4

Table (5.5). Performance of 16QAM for 6 CNN layers @learning rate 1e-3

Batch size	Training		Testing	
	Accuracy %	Loss	Accuracy %	Loss
64	89.2	0.5	89.02	0.53
128	90	0.45	89.84	0.48
256	94.92	0.16	90.89	0.26
512	98.24	0.08	98.17	0.09

It was observed that the performance target was not met for the 6 CNN layers with a learning rate of 1e-4. However, upon testing the model with a learning rate of 1e-3 and a batch size of 512, the performance target was achieved, with the accuracy reaching up to 98% for the training and testing data as illustrated in figure (5.41).

The hyperparameters utilized for training the proposed CNN model are as follows: the CNN Layers were set to 6, the activation function utilized was ReLu, the learning rate was 0.001, and the optimization approach was Adam. The mini-batch size was set to 512, and 1100 epochs were used (equivalent to 14 iterations per epoch).

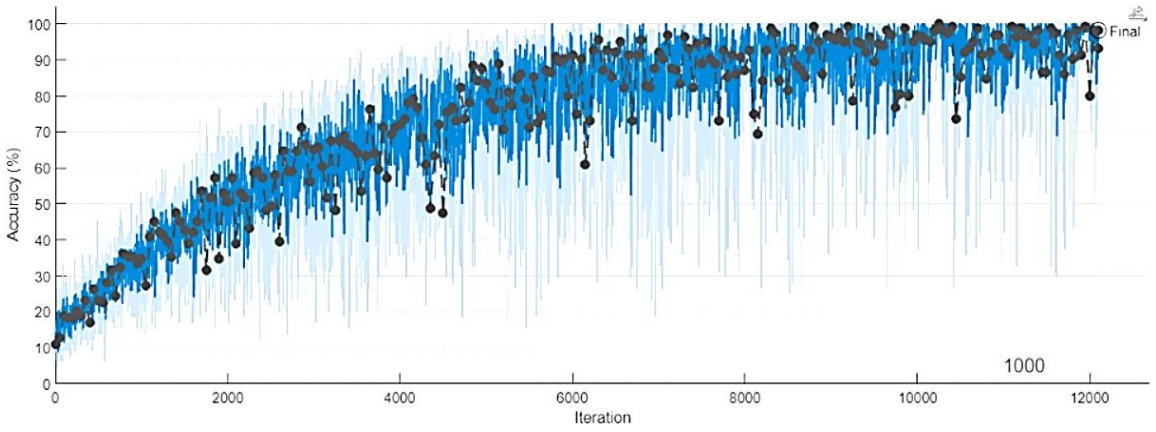

(a)

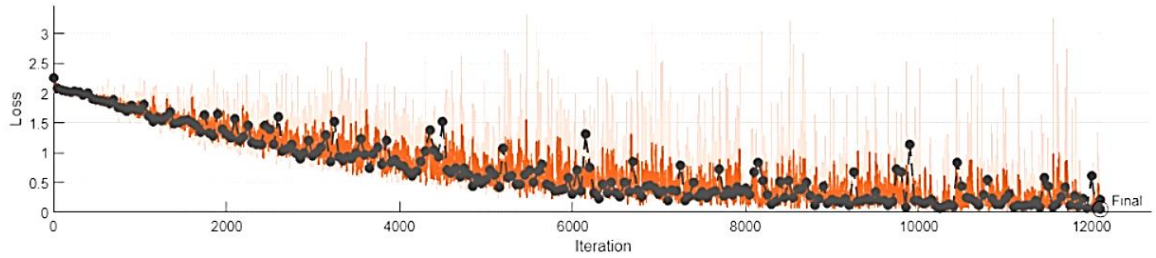

(b)

Figure (5.41). Final training progress of 6 CNN @1e-3 (a) accuracy (b) loss

The analyzed results of the proposed model are obtained with the training accuracy and loss being 98.2% and 0.08, respectively, while the testing accuracy and loss were 98.1% and 0.09, respectively. The CNNs have 28 layers with (16-96) hidden nodes. The size of the dataset was determined to be (sps × 16384) where sps is the sample per frame and equal to 128 from 16QAM. The number 128 indicates that: the optical transmission system will be repeated 128 times for the same sequence input for the purpose of properly training the neural network and reaching the perfect estimates of neuron weights (W), where 80-85% of the dataset utilized for training and 15-20% for the testing and validation. The data set will be separated into imaginary and real parts prior to being fed to the CNN. The dataset used in this study

was collected from Optisystem software covering a range of launched power levels from -15 to +15 dBm.

5.6.2 Results of Implementation CNN-16QAM

The results obtained from applying the CNN algorithm to a 16-QAM modulation scheme have been presented in this section. CNN has emerged as a powerful technique for handling complex data patterns and has shown promising potential in various domains, including optical communication systems. By analyzing the performance metrics of BER, Q-factor, and EVM, it will be gaining insights into the effectiveness of the CNN algorithm in compensating for linear and nonlinear effects and optimizing signal transmission within the 16-QAM modulation scheme.

Firstly, it will be finding the optimum launched power that gives the best received signal against the fiber impairments. In Appendix B, Table (B.17) illustrates the BER with Q-factor and EVM at 500 km at first, middle, and last channels at different signal power. From table (B.17), it can be observed the best value in terms of the quality of the received signal at 5 dBm. At this point, the effect of the CNN algorithm was present and able to process the fiber impairments at all the channels and obtain the same quality of the signal received by taking advantage of the classification process on which the training process was built based on the I and Q sites. So, at this signal power, it will be investigated and tested the performance of the proposed system at different fiber lengths by changing the number of spans to find out the effectiveness of the CNN compensation method. Figure (5.42) illustrates BER at different span links (each iteration is 500 km) for three channels.

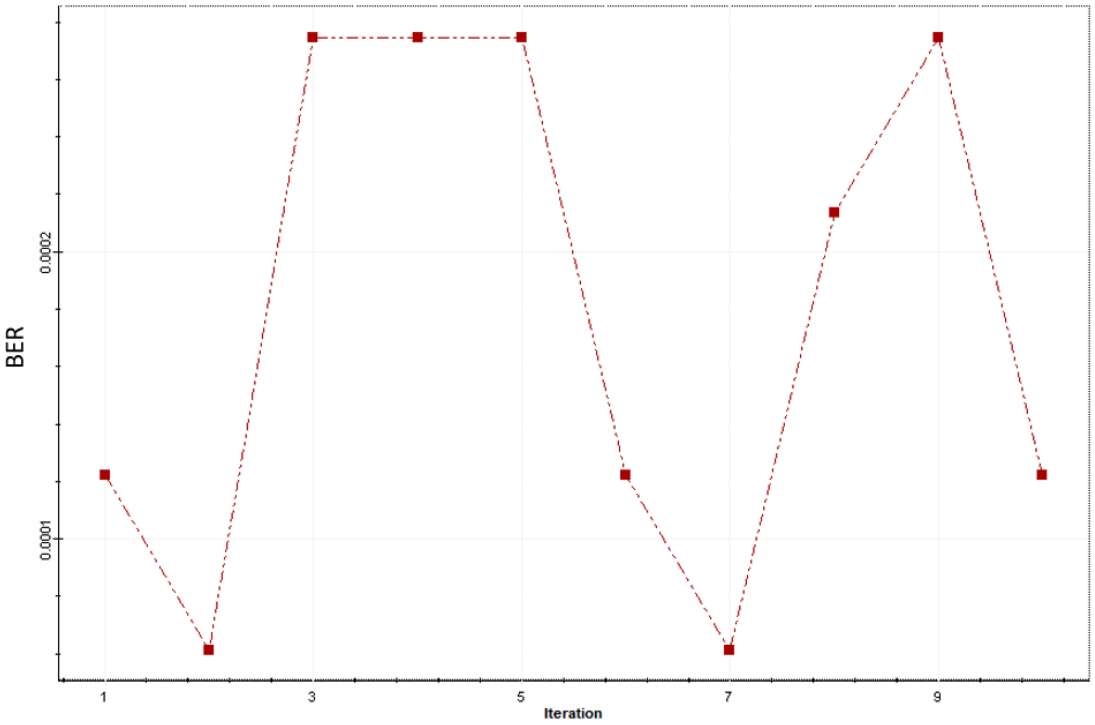
BER
0.0002
0.0001
1
3
5
7
9
Iteration

(a)

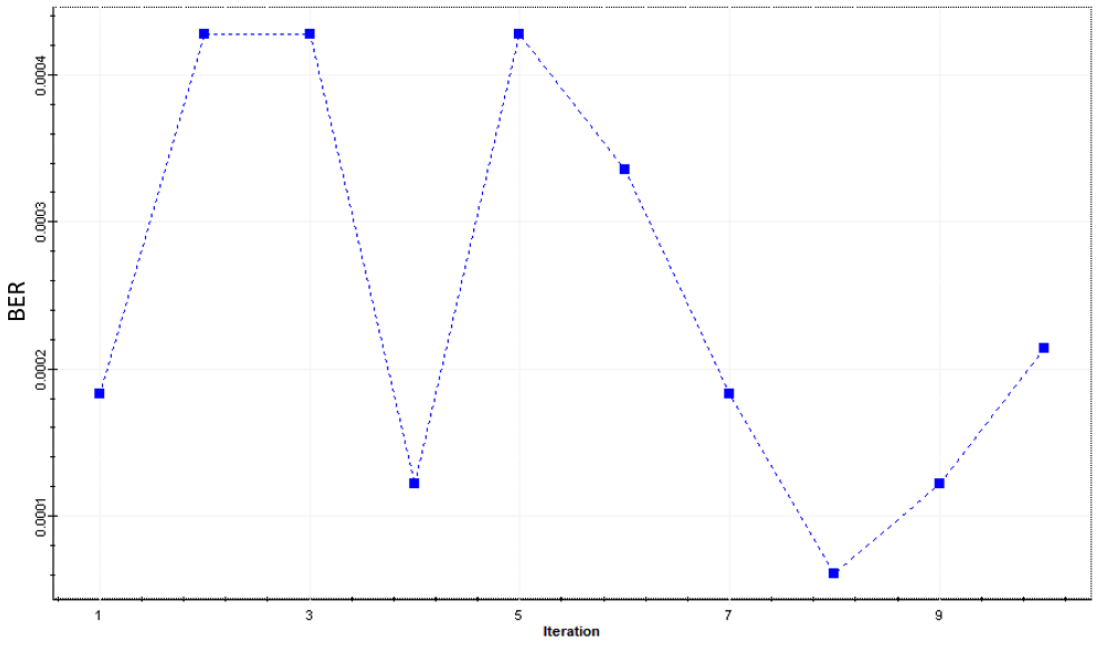
BER
0.0004
0.0003
0.0002
0.0001
1
3
5
7
9
Iteration

(b)

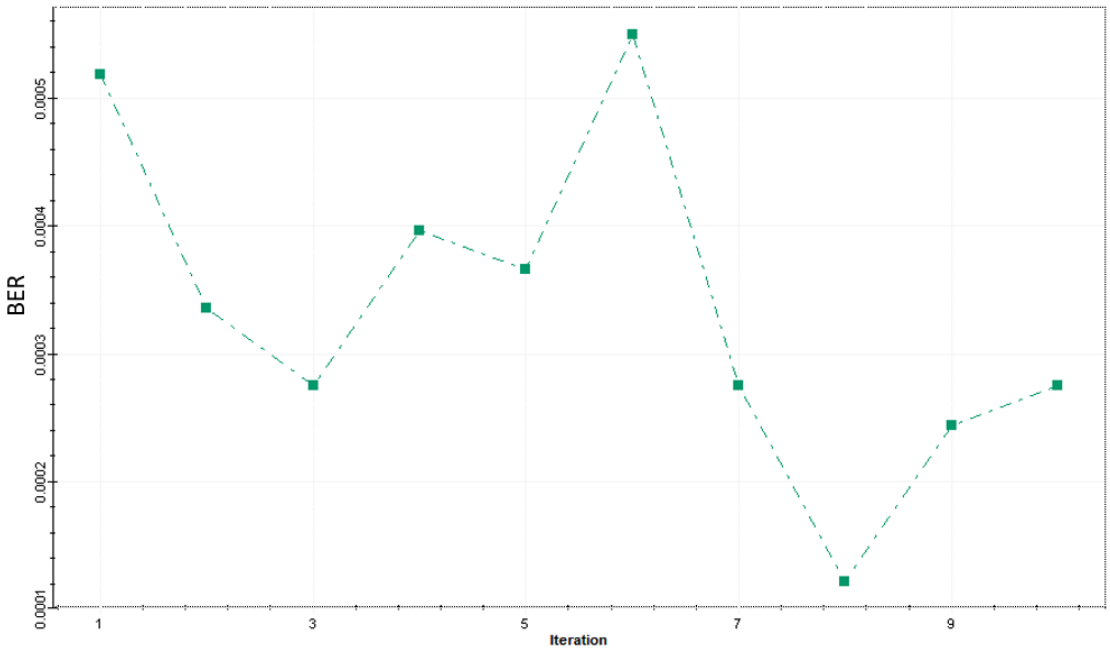

(c)

Figure (5.42). BER patterns in 16QAM-CNN for (a) Ch.1 (b) Ch.8 (c) Ch.16

Based on the figure (5.42), it can be concluded that the received signal based on the value of BER has been greatly improved compared to when the CNN-NLC was not used. As well, it can also be noted that by increasing the transmission distance, the received signal is not affected and its quality is preserved due to the individual characteristics of neural networks that can guess and treat problems that occur in the channel. Figures (5.43), (5.44), and (5.45) show the Q-factor, EVM, and constellation diagram for the channels (1, 8, and 16), respectively. The results of the Q-factor for the three channels indicate that transmission exceeds the value of the HD-FEC limit (Q-factor=8.52), which gives a good impression of this method of compensation.

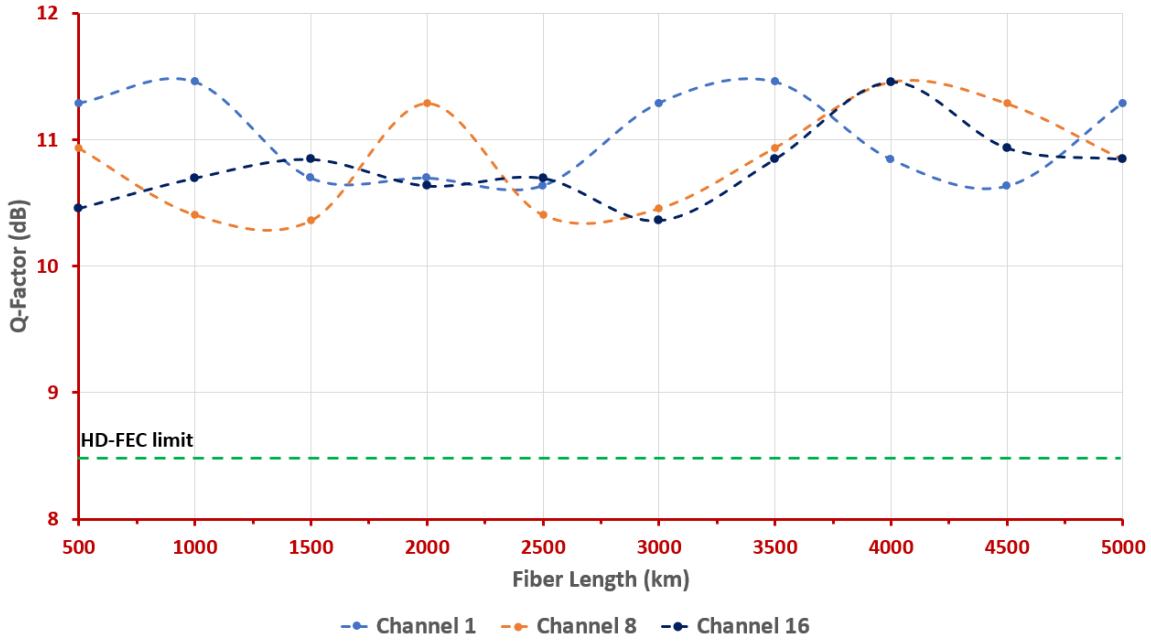

Figure (5.43). Q-factor in 16QAM-CNN for three channels

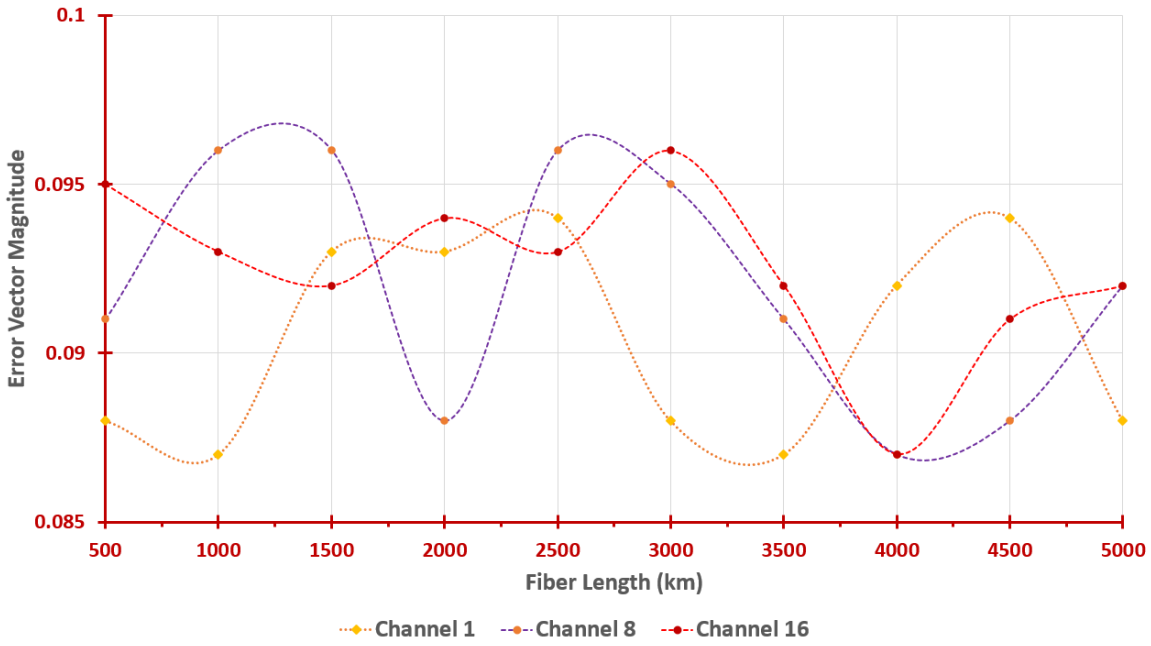

Figure (5.44). Error vector magnitude (EVM) in 16QAM-CNN for three channels

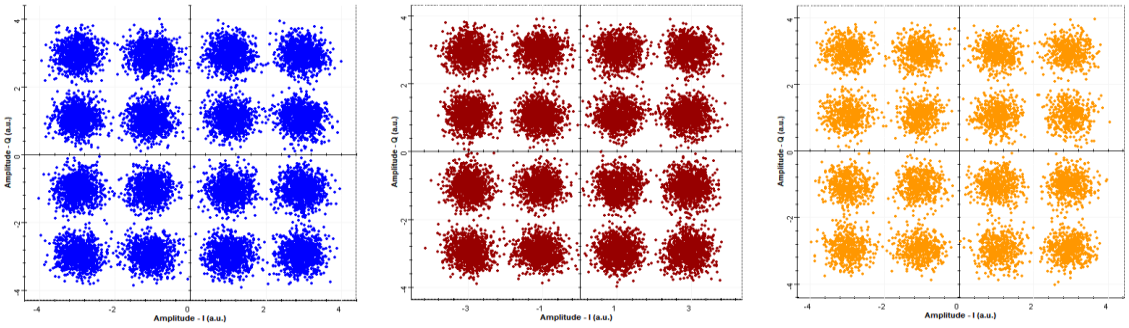

(a) (b) (c)

Figure (5.45). Constellation diagram in 16QAM-CNN for (a) Ch.1 (b) Ch.8 (c) Ch.16

The obtained results provide valuable information regarding the CNN algorithm's ability to detect and mitigate impairments caused by noise, interference, and other factors in the optical communication channel. Through the analysis of BER patterns, it can assess the quality of the signal received and evaluate the system's performance in terms of error rates. Furthermore, the examination of the Q-factor, constellation diagram, and EVM values offers insights into the level of distortion or interference present in the transmission and reception process. This enables to gauge the effectiveness of the CNN algorithm in minimizing the impact of such disturbances and maintaining received signal integrity.

5.6.3 CNN-NLC for Single Polarization 64QAM

In this section, it will be delved into the results obtained from applying the CNN algorithm to another advanced modulation format that is 64-QAM modulation scheme in which the carrier can exist in one of sixty-four different states. The advantage of higher order modulation is the possibility to transmit more bits compared to the previous modulation technique investigated. On the other hand, the disadvantage is that the data becomes more susceptible to noise and interference since the receiver must accurately detect more discrete phases and amplitudes of a signal. After receiving the signal through the

demultiplexer, it will be distributed to the sixteen channels, at each channel it will be noted that the received signal is distorted by virtue of the linear and nonlinear effects. Figure (5.46) illustrates the constellation visualizer for the middle channel for the received optical signal after 5000 km with 10 dBm launch power.

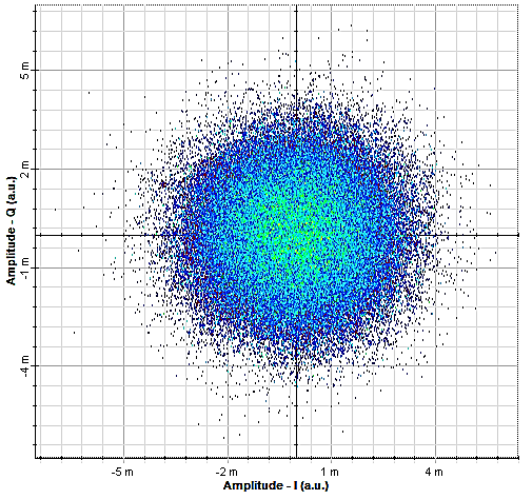

Figure (5.46). Constellation diagram of the received 64QAM signal over 5000 km SMF for the middle channel

Because of the long fiber span, the high launch power, and the close distance between the channels, they are the main factors in the deterioration of the received signal shown in figure (5.46), and the impact of nonlinearity and interference becomes more pronounced. The unique properties of 64-QAM, such as the increased number of symbol constellations and tighter signal spacing, pose additional challenges in accurately estimating and compensating for nonlinearity induced impairments. At this point, the CNN-based nonlinear compensator (NLC) is going to be used so that can mitigate the linear and nonlinear effects that are still present. In SP-64QAM, there are 6 bits used to represent each symbol (m=6), which results in a total of 64 different classes that can be used to identify each symbol. Additionally, multi-label classification, which is an approach that is better suited to high-

dimensional and high order modulation, will be utilized. The data that have been received are then sent to the CNNs, which use a variety of methods to correct for the nonlinearity that is present in the channel. These methods include the utilization of nonlinear activation functions, convolutional layers, batch normalization layers, max pooling layers, and a fully connected layer. These strategies make it possible for the network to simulate intricate, nonlinear relationships between the input data and the target class.

To fine tune the CNN parameters, it will first conduct an evaluation of the performance of the network in terms of accuracy and loss. The training will be based on six CNN and contrast two different learning rates trained for 750 epochs (106 per iteration) with variable minibatch sizes. This decision was made in light of the prior findings about the modulation format. The presence of the performance of 6 CNN model is shown in Tables (5.6) and (5.7).

Table (5.6). Performance of 64QAM for 6 CNN layers @learning rate 1e-4

Batch size	Training		Testing	
	Accuracy %	Loss	Accuracy %	Loss
64	67.4	0.85	77.9	0.64
128	82.5	0.53	77.4	0.66
256	87.7	0.43	79.5	0.61
512	89.3	0.39	84.9	0.49

Table (5.7). Performance of 64QAM for 6 CNN layers @learning rate 1e-3

Batch size	Training		Testing	
	Accuracy %	Loss	Accuracy %	Loss
64	88.2	0.42	81.8	0.56
128	91.7	0.34	87.16	0.42
256	95.12	0.17	94.06	0.19
512	99.02	0.06	97.43	0.10

Results from the two tables show that the performance of training is negatively impacted when the lower value of the two parameters is decreased, however, the results of testing have the best value in terms of accuracy and loss when the learning rate is equal to 1e-3 with a mini batch size of 512. Accuracy and subsequent loss are depicted in figure (5.47) upon completion of training.

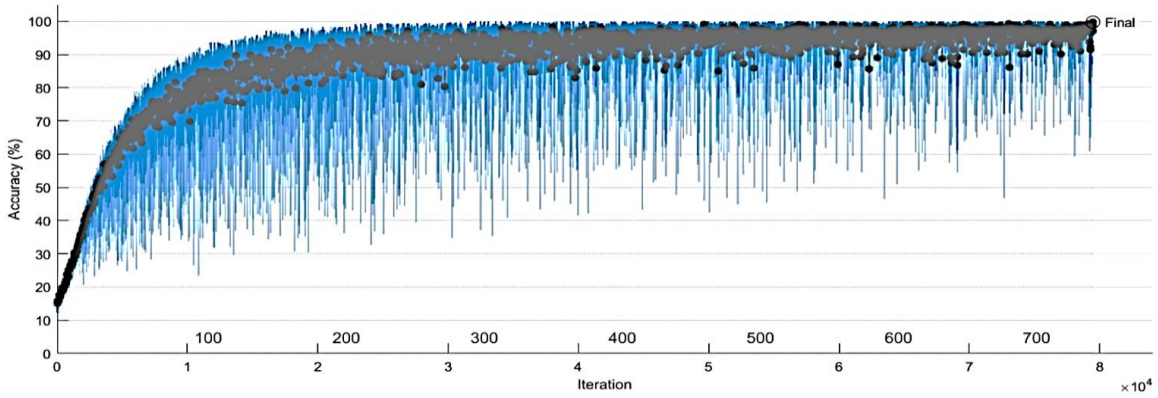

(a)

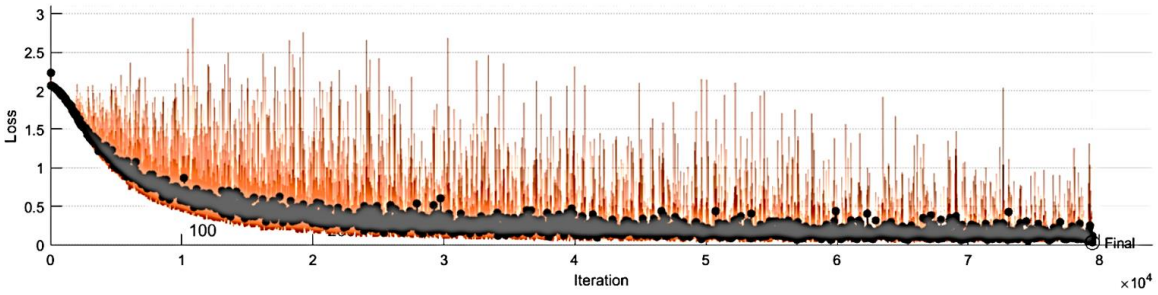

(b)

Figure (5.47). Final training progress of six CNN at 1e-3 learning rate for 64QAM (a) accuracy (b) loss

Finally, the following is a list of the hyperparameters that were utilized for training the proposed CNN model: CNN Layers were adjusted to a value of 6, the ReLu activation function was used, the learning rate was set to 0.001, and the Adam optimization strategy was used. The mini-batch size was changed to 512, and 750 epochs were utilized (which resulted in 106 iterations for each epoch). The obtained results for the training accuracy and loss came

in at 99.02% and 0.06, respectively, while the testing accuracy and loss came in at 97.43% and 0.10, respectively. The size of the dataset was calculated to be (sps× 10922), where sps refers to the number of samples that are taken during each frame and is equal to 192 when using 64QAM. Before the data set is input into the CNN, it will first be broken down into its real and imagined components. The Optisystem program was utilized to collect the dataset that was used in this investigation. The launch power levels ranged from -15 to +15 dBm and were accounted for in the dataset.

5.6.4 Results of Implementation CNN-64QAM

Due to the near signal spacing, this section will delve into the findings produced by applying the CNN algorithm to the 64-QAM modulation scheme, which is a more difficult modulation scheme than 16-QAM. The findings that were collected shed light on the performance of the CNN algorithm in terms of its ability to handle the complexity that is related to 64QAM modulation. By analyzing the BER patterns, Q-factor, and EVM, it will be able to determine the error rates and evaluate the network's capacity to reliably decode signals, which enables it to transmit data in a trustworthy manner. In addition, an analysis of these metrics' values reveals vital information regarding the degree of distortion or interference present in the communication channel. This makes it possible to evaluate how well the CNN algorithm can cope with these kinds of disturbances and keep the signals' integrity intact.

Finding the optimal launching power that gives the best received signal despite the limitations caused by the fiber will be the first step in this process. In Appendix B, Table (B.18) provided an illustration of the BER together with the Q-factor and EVM at a distance of 500 km for the first, middle, and last

channels with varying levels of signal power. It is possible to deduce from the data presented in table (B.18) that the quality of the signal that was received was highest at a value of 10 dBm. The reason for this is that the modulation pattern determines the amount of power that is required, and the higher the pattern, the more power is required; however, this comes at the cost of more distortion. At this point, the influence of the CNN algorithm was already evident, and it was able to process the fiber impairments at all of the channels and achieve the same quality of the received signal. This was accomplished by taking advantage of the classification process on which the training process was constructed, which was based on the I and Q sites. Therefore, the performance of the suggested system will be researched and evaluated at 10 dBm signal power at various fiber lengths (from 500 km to 5000 km) by varying the number of spans in order to determine how successful the CNN compensation approach is. The BER was presented for various span connections for three channels shown in figure (5.48).

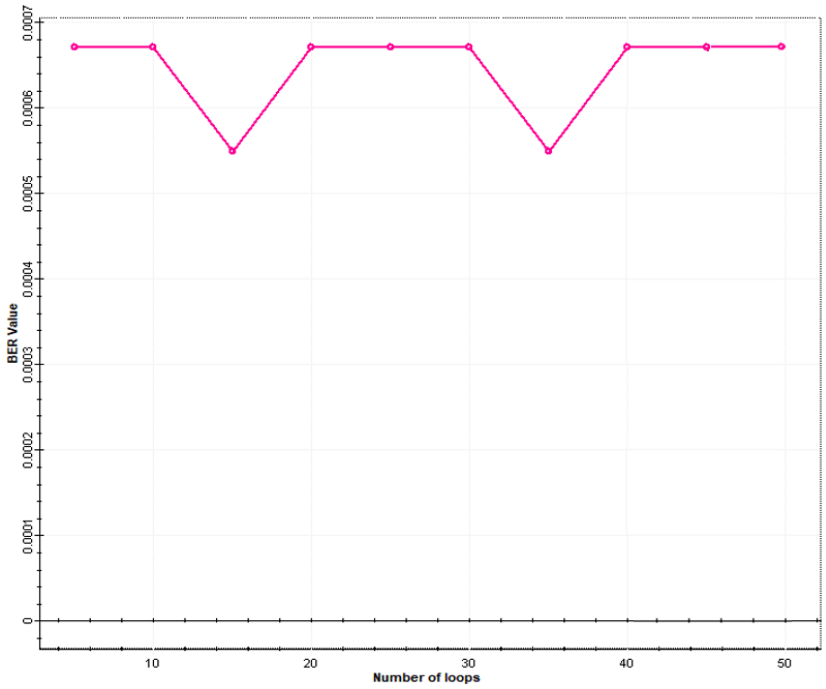

(a)

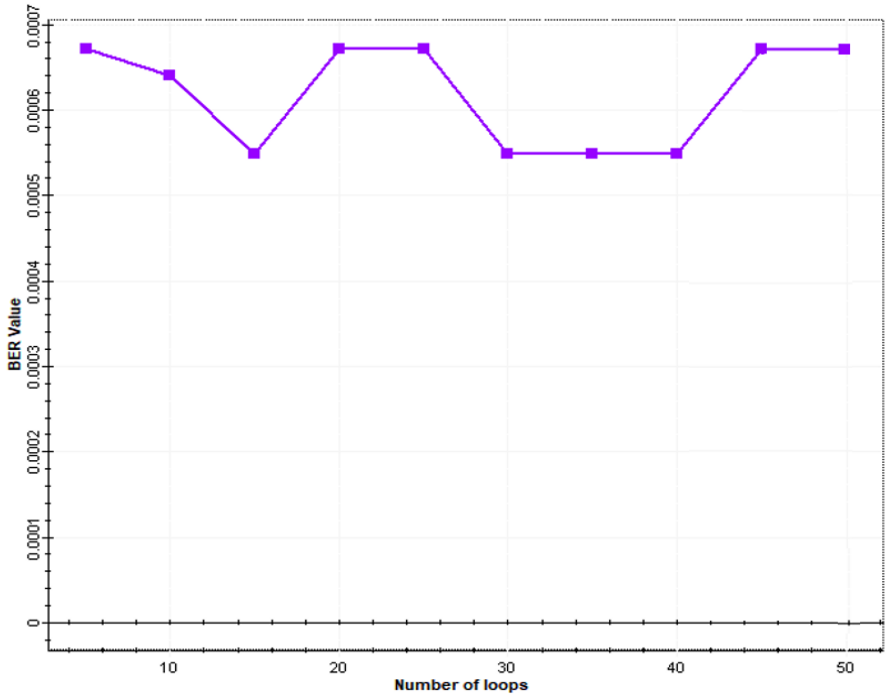

(b)

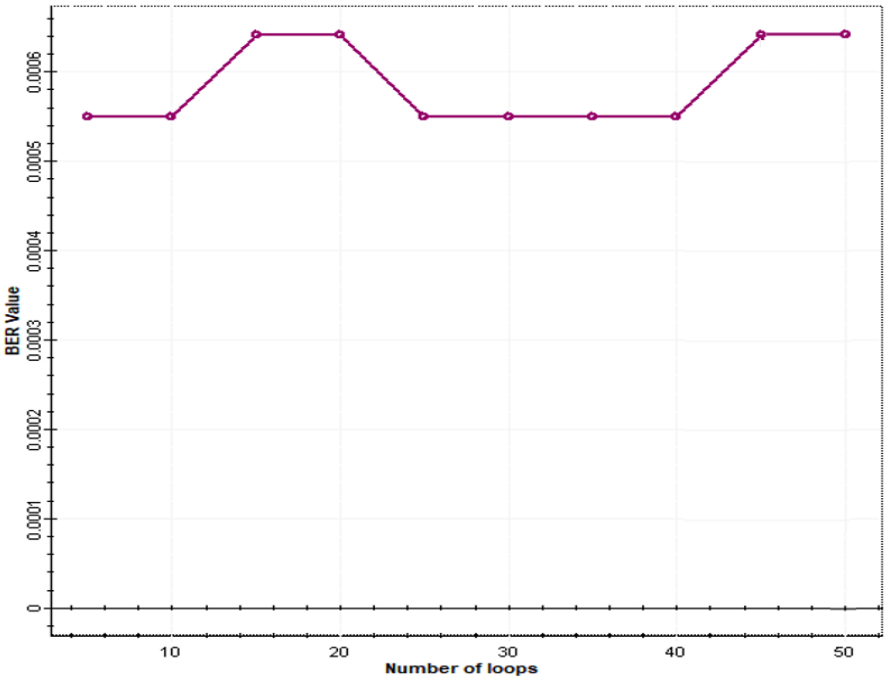

(c)

Figure (5.48). BER patterns in 64QAM-CNN for (a) Ch.1 (b) Ch.8 (c) Ch.16

Based on the figure (5.48), the signal quality, as assessed by BER, greatly improved when the CNN-NLC was used. Increasing the transmission distance with high launch power does not affect the received signal quality. Neural networks can guess and fix channel issues due to their unique properties. The Q-factor, EVM, and constellation diagram for the first, middle, and last channels are depicted in Figures (5.49), (5.50), and (5.51), respectively. The fact that the transmission achieved a value that was higher than the HD-FEC limit as shown by the results of the Q-factor for all three channels, provides a favorable impression regarding this method of compensation. In addition to this, looking at the values of the EVM and the constellation diagram can provide some insight into the amount of distortion or interference that is present in the process of transmission and reception. Because of this, it is possible to evaluate how good the CNN algorithm is in reducing the negative effects of such disturbances and preserving the integrity of the signal.

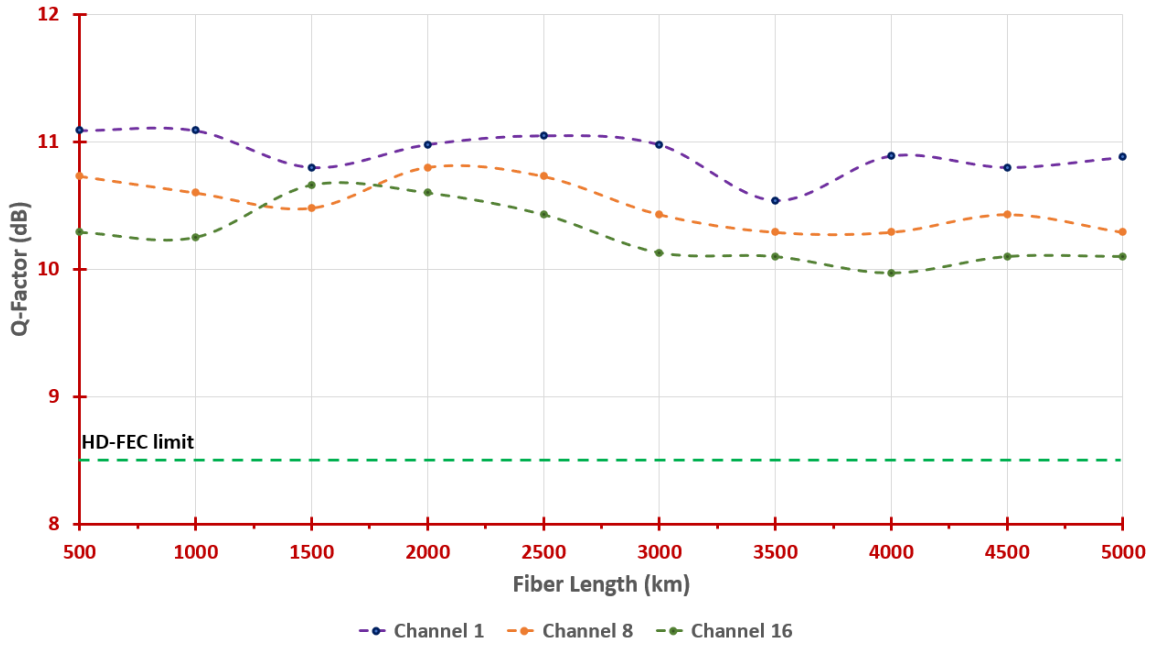

Figure (5.49). Q-factor in 64QAM-CNN for channels 1, 8, and 16

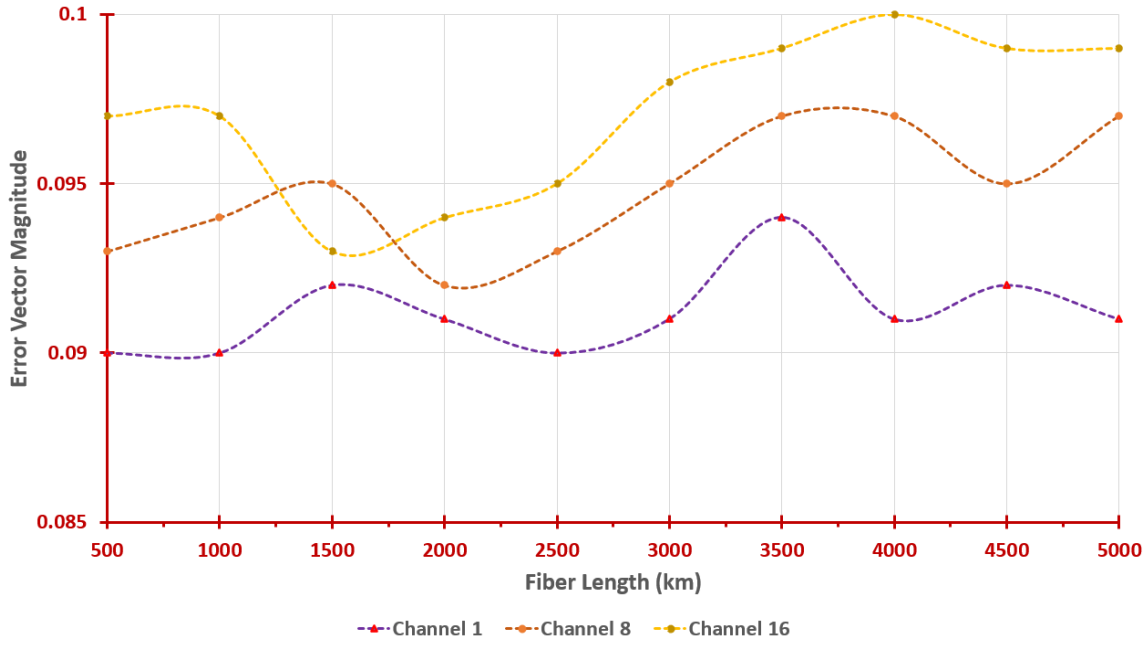

Figure (5.50). Error vector magnitude (EVM) in 64QAM-CNN for channels 1, 8, and 16

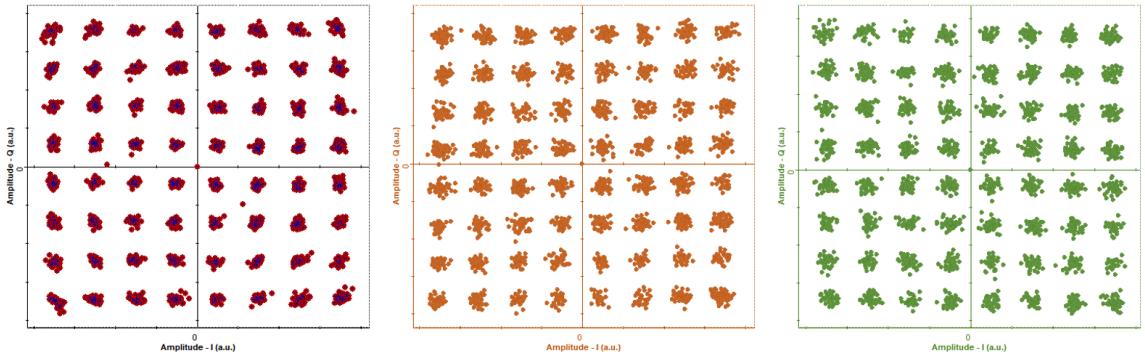

(a) **(b)** **(c)**

Figure (5.51). Constellation diagram in 64QAM-CNN for (a) Ch.1 (b) Ch.8 (c) Ch.16

The results show that the CNN algorithm can identify and mitigate noise, interference, linear, and nonlinear effects in the optical communication channel, especially with multi-channel DWDM systems. As training samples expand, convolution neural network training can be computationally expensive and need a large investment of computer resources over a long time.

5.7 Fiber Impairment Compensation Using NARX Time Series Network

This section introduces the results of another sophisticated machine learning technique for compensating nonlinearities in optical fiber communications called Nonlinear Auto Regressive with Exogenous (NARX) inputs algorithms. The method of NARX time series neural networks has been employed as an essential part of fiber optic networks, to be a novel method of this work presented in addressing the effects of optical fiber impairments. The MATLAB program was used to implement and simulate the artificial intelligence algorithms, and the Optisystem program was used to run the simulation of those algorithms optically. Co-simulations were used to link the two programs, which were done in order to ensure the validity of the results that were acquired. The effectiveness of this proposed compensation method will be verified by testing and investigating with two types of modulation formats; SP-16QAM and SP-64QAM. For both modulations, it will compare the performance of the communication system before and after using the NARX method. This will provide insights into the impact of the modulation technique on the performance of the communication system and the efficacy of the advanced machine learning technique in compensating for linear and nonlinear effects. The dataset that was utilized in this method was obtained from Optisystem, and it was designed to span a range of launching power levels ranging from -15 to +15 dBm.

5.7.1 Mitigation Fiber Impairment for Single Polarization-16QAM

NARX is a type of time series neural network that utilizes feedback and exogenous input, making them well suited for modeling dynamic systems such as optical fibers. A NARX network was trained on a dataset of

nonlinearity measurements acquired from an optical fiber, and the network was able to accurately predict the nonlinearity of the fiber after being fed the information. The NARX network is able to learn the complicated nonlinear correlations in the data and generalize effectively to unseen measurements, which provides advanced solutions for the problems of nonlinearity and interference in optical communication systems. The results in this work are based on choosing the same parameters that were used in the CNN approach so that can conduct a comparison of the results acquired in this method to demonstrate how successful it is in resolving issues that arise in fiber. It is going to be implemented 16 channels of SP-16QAM with a data rate of 120 Gb/s for each channel to reach a total rate of 1.92 Tb/s with 50 GHz channel spacing using DWDM multiplexing to collect the 16 channels and send them over standard single mode fiber towards coherent receiver side to demonstrate improvement after different distances ranging reaching to 5000 km.

The three main factors that effect on the quality of the signal received are the launched power of the CW laser, channel spacing between the channels, and the transmission distance of the fiber, which are considered the main factors of linear and nonlinear effects. At this point, the purpose of compensate for the residual linear and nonlinear distortion by using the NARX algorithm. The performance evaluation is based on the analysis of BER, Q-factor, and EVM. The received data after De DWDM are fed to the NARX module which utilizes multiple techniques to compensate for nonlinearity in the NLSE, including the use of nonlinear activation functions, training algorithm, and hidden layer size. The NARX feedback neural network is a type of mathematical model that is based on the nonlinear autoregressive model. This model is designed to capture the nonlinear relationships between inputs and

outputs in dynamic systems, making it a powerful tool for analyzing and predicting the behavior of such systems.

The first step of training the module by choosing the best value of hidden neurons, and in this work the choice was made by experimentation, experience, and prior knowledge of the problem with the aim of keeping the networks rather small and therefore, the efforts of the training controllable. The NARX module has 25 hidden neurons, which is the best value. The training function is “trainlm”, which is the fastest and uses less memory. The size of the dataset was determined to be (sps × 16512) where sps is the sample per frame and is equal to 128 from 16QAM, where 70% of the dataset is utilized for training, and 30% for the testing and validation, equally. The result of the NARX machine learning model is shown in figure (5.52). The figure reveals that network coverage as a result of reaching minimum gradients needs 6 and 8 epochs for real and imaginary parts, respectively, leading to increasing the overall performance (MSE). At this point, the gradient value was equal to 9.56 E-8 and 2.67e-8 and the value of mu reached 1e-9 and 1e-10 for real and imaginary sections, respectively. The optimal performance is equal to 2.4229E-8 at epoch 6 and 2.0049E-8 at epoch 8 for the real and imaginary parts as indicated in figure (5.53). This suggests that the network was able to converge and reach a stable solution at this point in the training process. In Figure (5.54), It can be seen the error histogram with 20 bins for the proposed model. The results show that the majority of data points have an error of 2.4 E-5, with the minimum error being -0.00041 and the maximum error being 0.000997 for the real part. On the other hand, for the imaginary part, the majority of data points have an error of 3.5E-5 with -0.00014 and 0.000165 for the minimum and maximum error, respectively.

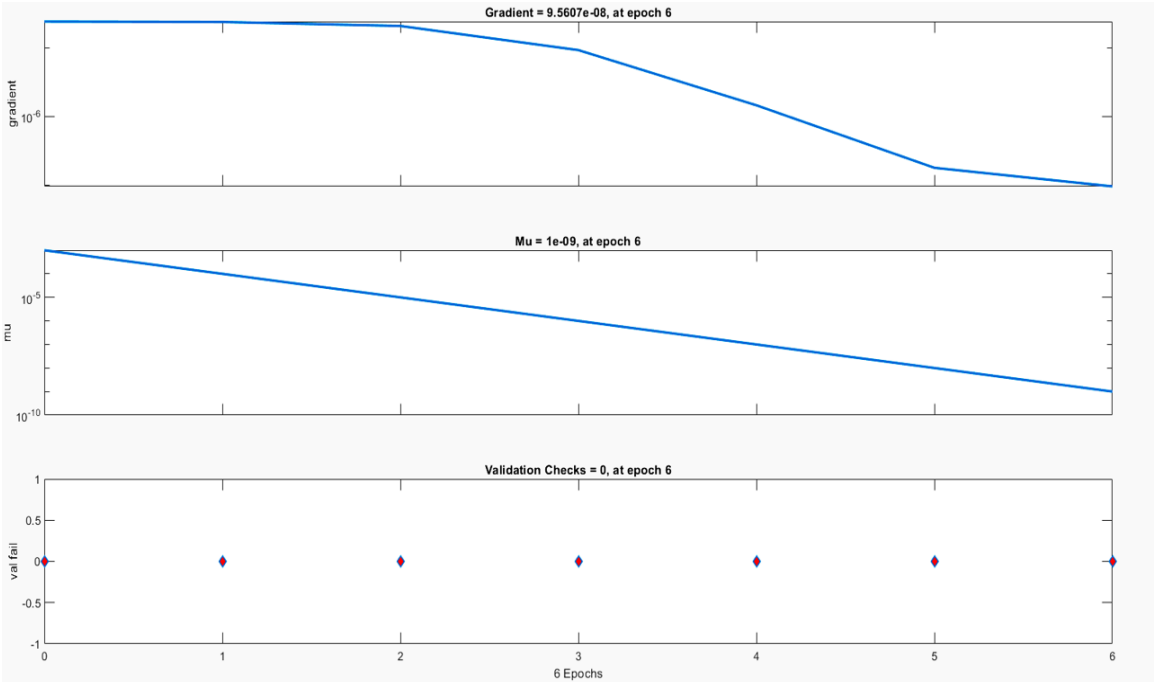

(a)

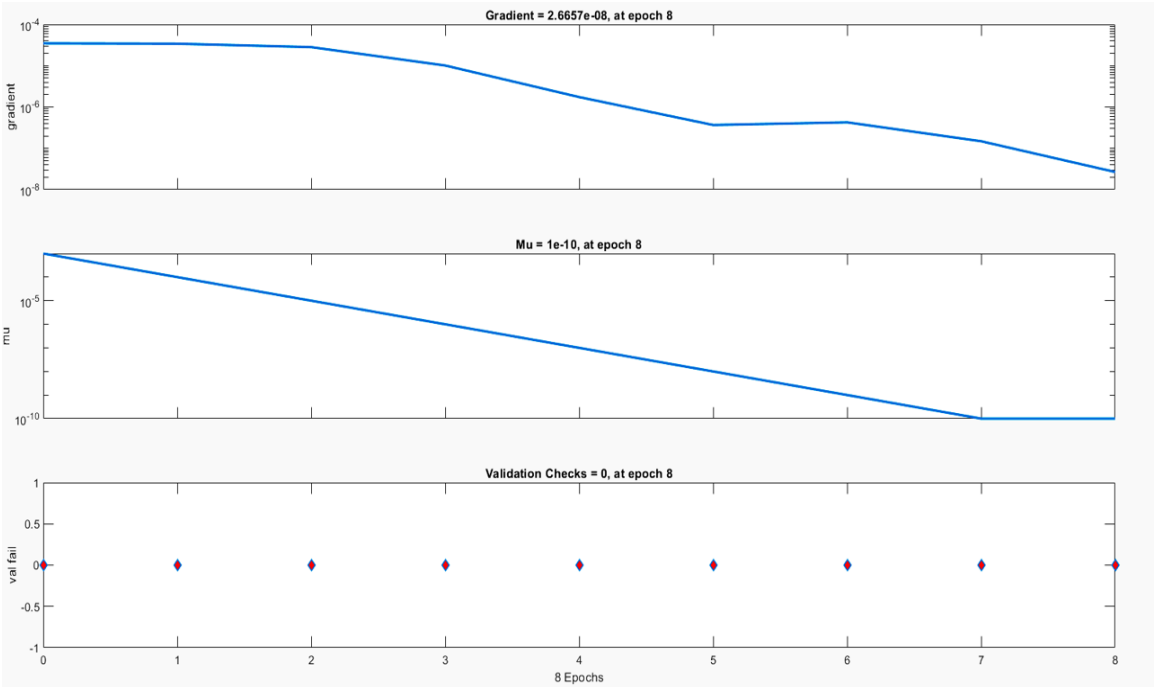

(b)

Figure (5.52). NARX performance for 16QAM after the end of training for (a) real part (b) imaginary part

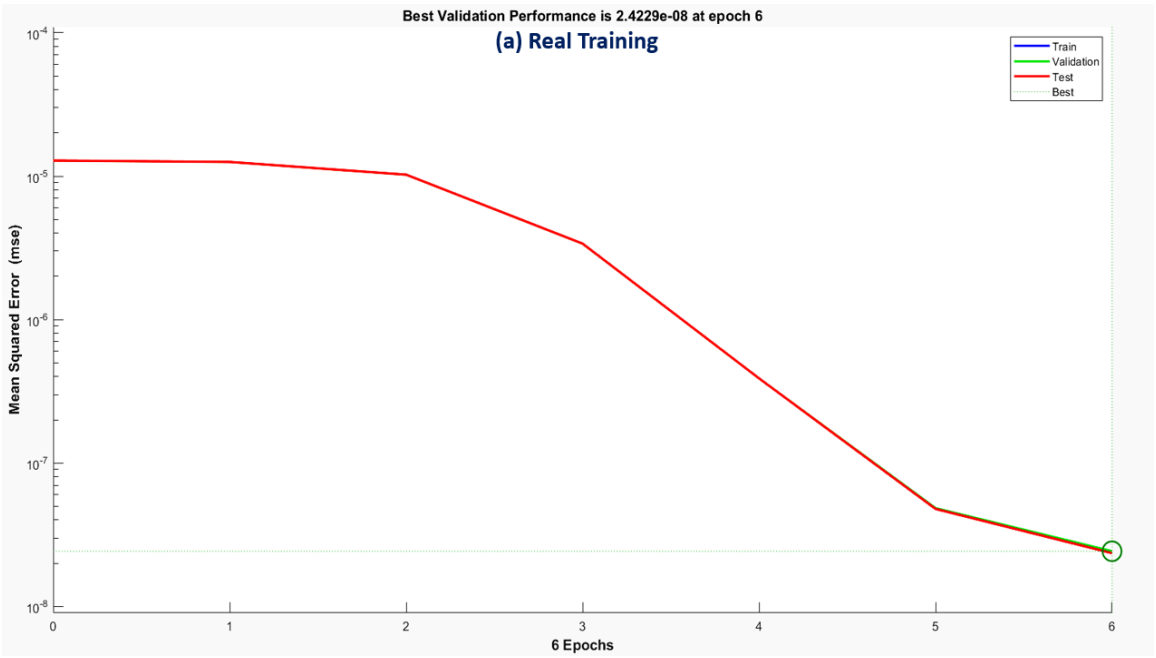

(a)

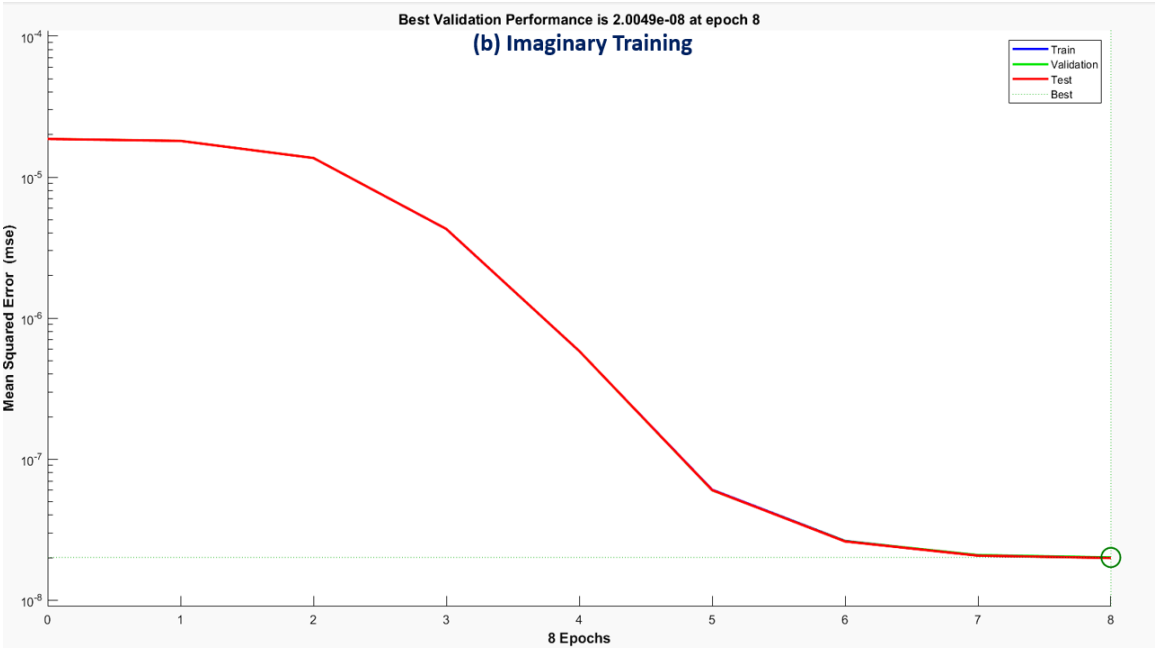

(b)

Figure (5.53). MSE vs. number of epochs for (a) real part (b) imaginary part

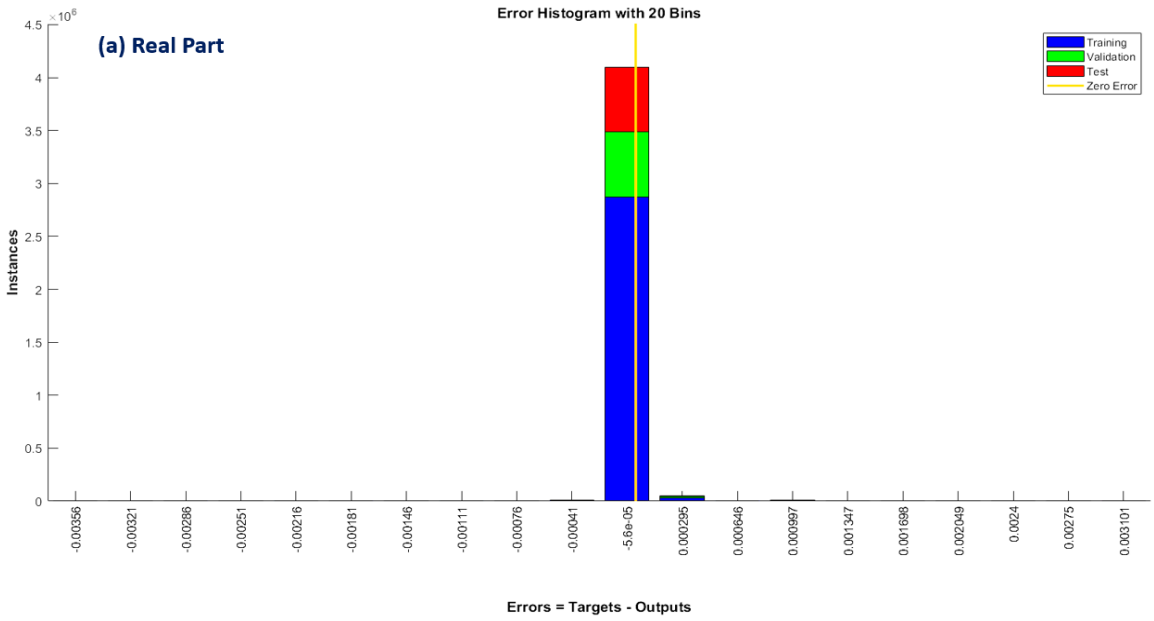

(a)

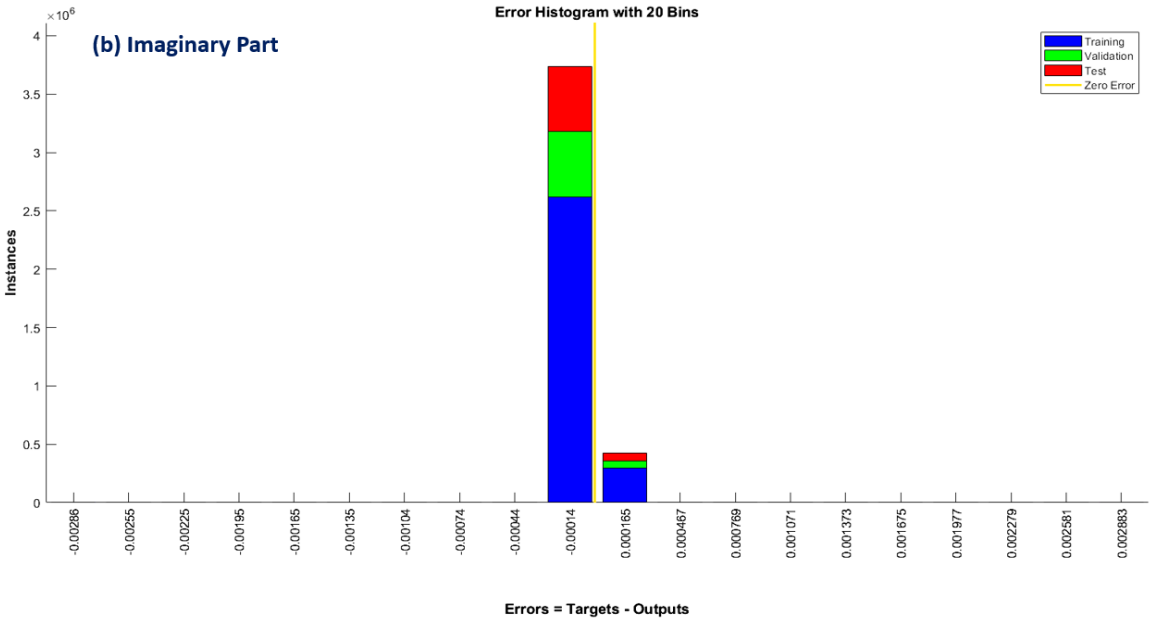

(b)

Figure (5.54). Error histogram with 20 Bins (a) real training (b) imaginary training

Overall, the results of the NARX machine learning model demonstrate its effectiveness in accurately modeling the nonlinearity of optical fibers and compensating for distortions in the optical signal. To demonstrate NARX's

effectiveness on the proposed system, the obtained results will be shown in the next section.

5.7.2 Results of Implementation NARX-16QAM

The results obtained from applying the NARX time series to a 16-QAM modulation scheme have been presented. The NARX machine learning model demonstrates its efficacy by precisely predicting the nonlinearity of optical fibers and adjusting for aberrations in the optical signal. By examining the performance metrics of BER, Q-factor, and EVM, it will be possible to acquire insights into the efficacy of the NARX algorithm in adjusting for nonlinearity effects and optimizing signal transmission within the 16-QAM modulation scheme.

In Appendix B, Table (B.19) illustrates the BER with Q-factor and EVM over 1000 km at first, middle, and last channels at different signal power. As can be seen from the table results, the best value in terms of the quality of the signal received at 5 dBm. The effect of the NARX algorithm was present and able to process the fiber impairments at all the channels and obtain the same quality of the received signal. Therefore, a signal power of 5 dBm will be used to study and evaluate the performance of the proposed system at a variety of fiber lengths by altering the number of spans in order to determine how effective the NARX compensating method is. The bit error rate was presented at various span connections for the first, middle, and last channels illustrated in figure (5.55).

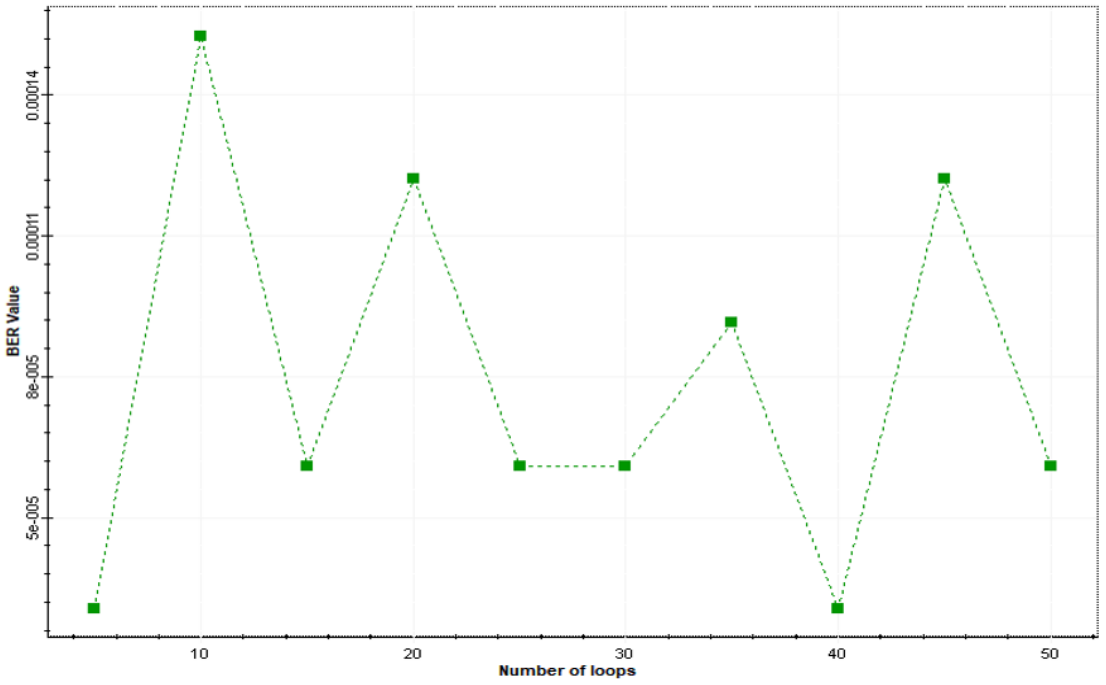
BER Value
0.00014
0.00011
8e-005
5e-005
10
20
30
40
50
Number of loops

(a)

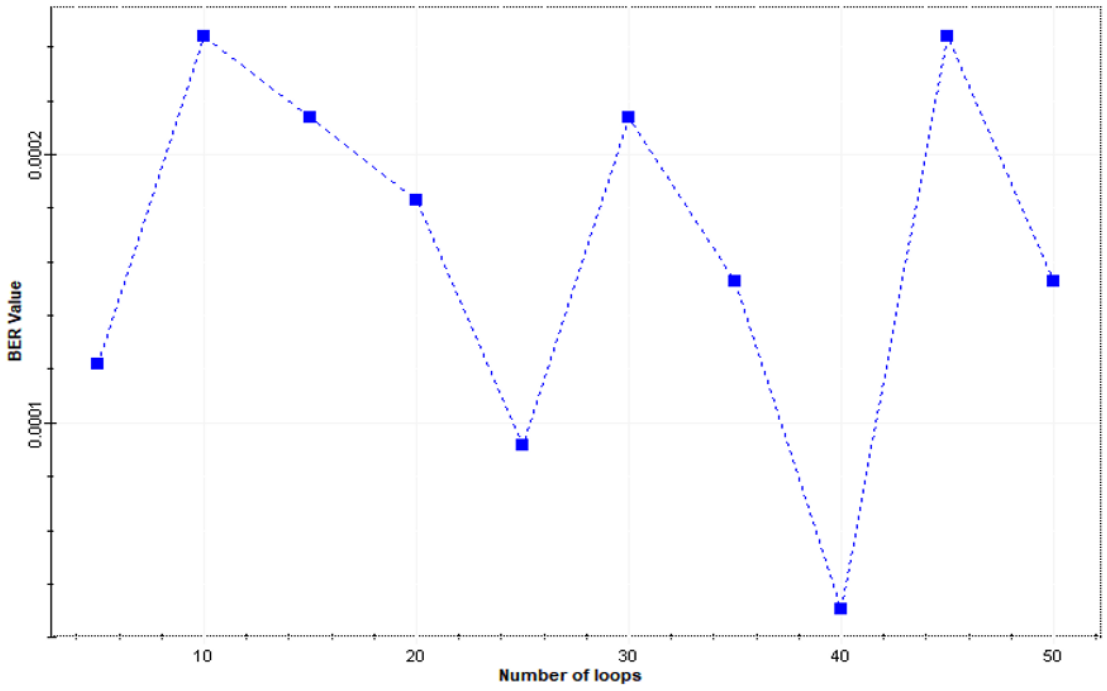
BER Value
0.0002
0.0001
10
20
30
40
50
Number of loops

(b)

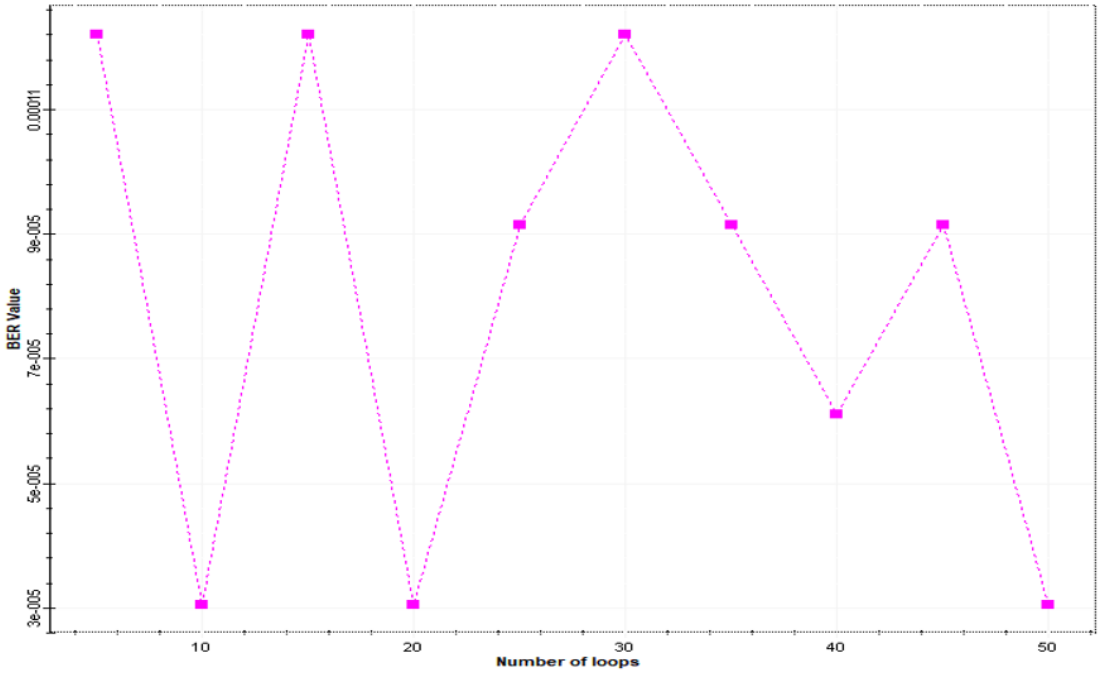

(c)

Figure (5.55). BER patterns in 16QAM-NARX algorithm for (a) Ch.1 (b) Ch.8 (c) Ch.16

The obtained results indicate that the observed minor variations in BER values are not influenced by the increase in the transmission distance and kept their values within the required limits, which gain valuable insights into the behavior and performance of the NARX algorithm in addressing nonlinearity effects and ensuring reliable signal transmission in fiber optic communication systems. The Q-factor, error vector magnitude, and constellation diagram for channels 1, 8, and 16 are depicted respectively in Figures (5.56), (5.57), and (5.58). The fact that the transmission achieved a value that was higher than the HD-FEC limit, as shown by the results of the Q-factor for all three channels, provides a favorable impression regarding this method of compensation.

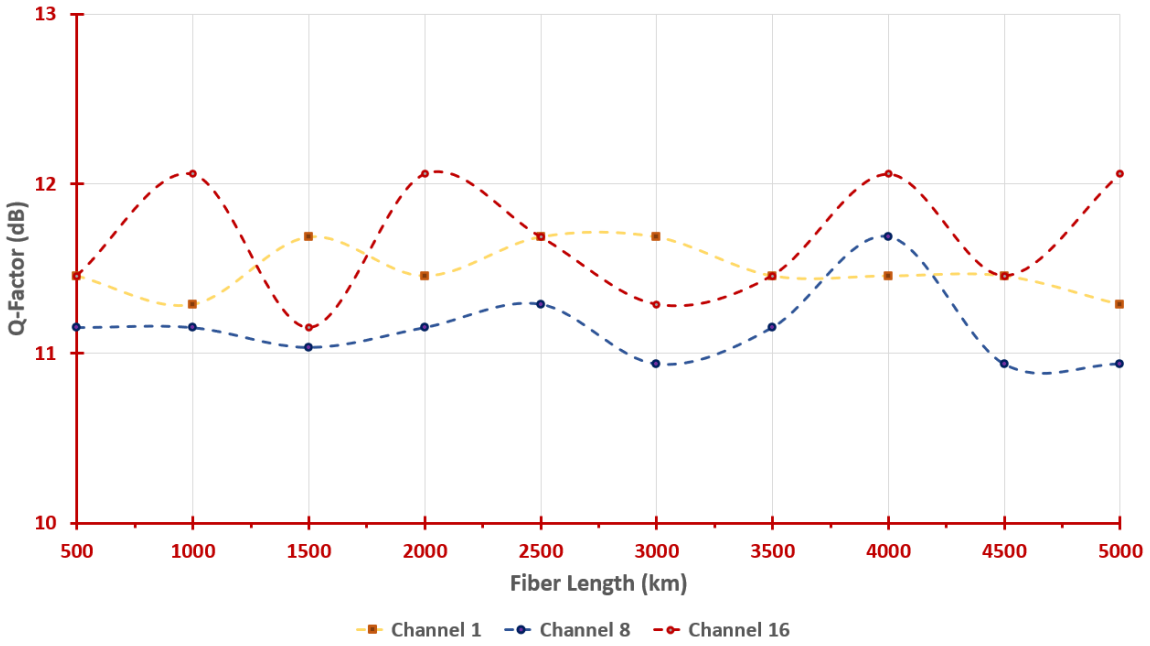

Figure (5.56). Q-factor in 16QAM based on NARX algorithm for three channels

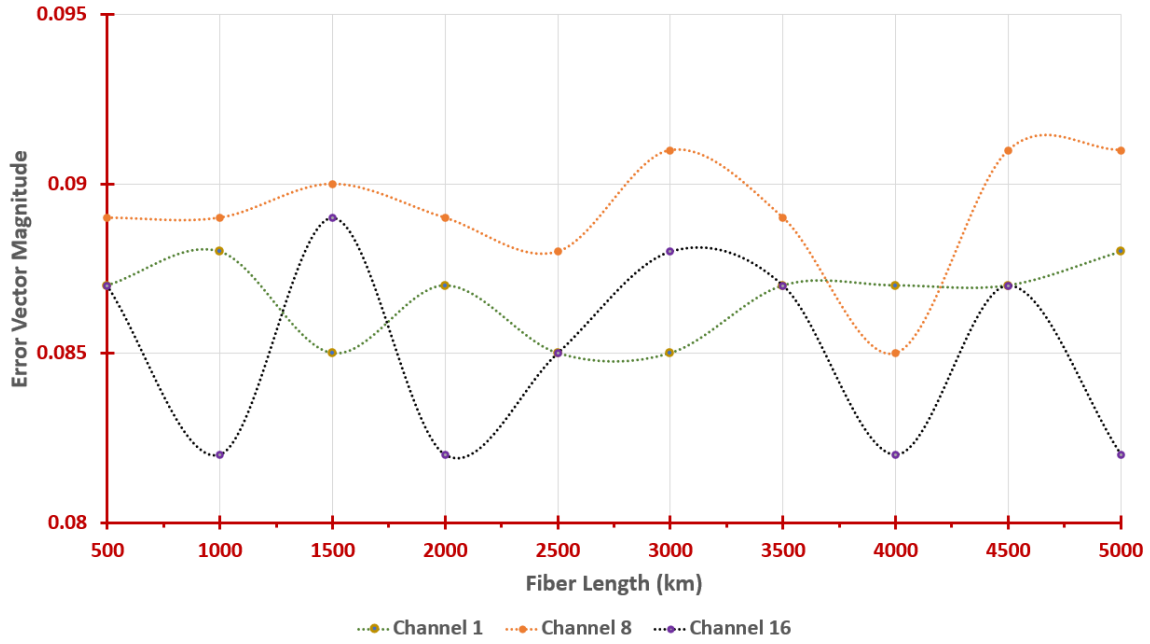

Figure (5.57). Error vector magnitude (EVM) in 16QAM based on NARX algorithm for three channels

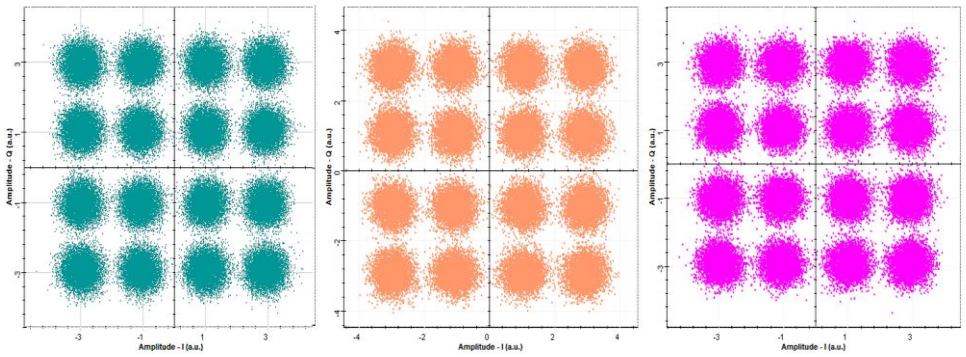

(a) **(b)** **(c)**

Figure (5.58). Constellation diagram in 16QAM based on NARX algorithm for (a) Ch.1 (b) Ch.8 (c) Ch.16

The obtained results demonstrate the capability of the NARX algorithm to mitigate the nonlinearity effects and maintain a high-quality signal transmission. The BER patterns in multichannel scenarios indicate that the NARX network can effectively handle the nonlinearity induced impairments, resulting in reliable signal reception. It is worth noting that the examination of the Q-factor, constellation diagram, and EVM values offers insights into the level of distortion or interference present in the transmission and reception process and measures the effectiveness of the NARX time series algorithm.

5.7.3 Compensation of Fiber Impairment for Single Polarization 64QAM

In this section, it will investigate into the results obtained from the application of the NARX algorithm to a 64-QAM modulation scheme. Building upon the effectiveness demonstrated in the previous evaluation of NARX with 16-QAM, it will be exploring its performance with a higher order modulation scheme. The unique properties of 64-QAM, such as the increased number of symbol constellations and tighter signal spacing, pose additional challenges in accurately estimating and compensating for nonlinearity-induced impairments. As was mentioned in the previous section, it will also be

implemented single polarization but with sixty-four quadrature amplitude modulation (SP-64QAM) based DWDM over a transmission distance of 5000 km with a data rate of 120 Gb/s for each channel.

The NARX module has a total of 10 hidden neurons, which is considered the optimal number for training purposes. The training function is called "trainlm," and the size of the dataset is determined to be (sps × 10979), where sps is the sample per frame and is equal to 192 from 64QAM. 70% of the dataset is used for training, and the remaining is split evenly between testing and validation. Figure (5.59) displays the results of the NARX machine learning model. The figure illustrates that an increase in network coverage as a consequence of minimum gradients being obtained requires 1000 and 263 epochs, respectively, for the real and imaginary parts, which leads to an increase in overall performance (MSE). At this moment, the value of the gradient was equal to 1.60 E-5 and 1.60e-3, while the value of mu reached 1e-7 both for the real and imaginary sections. As can be seen in figure (5.60), the optimal performance for the real and imaginary parts is equal to 2.8753E-5 at epoch 1000 and 2.7643E-5 at epoch 257, respectively. At this stage in the training phase, this seems that the network was able to converge and arrive at a stable solution.

It is possible to view the error histogram for the suggested model in figure (5.61), which has 20 different bins. According to the figure, the majority of data points of error with the minimum equal to -0.02608 and -0.02906, while the maximum error is equal to 0.02551 and 0.02912 for the real and imaginary parts, respectively.

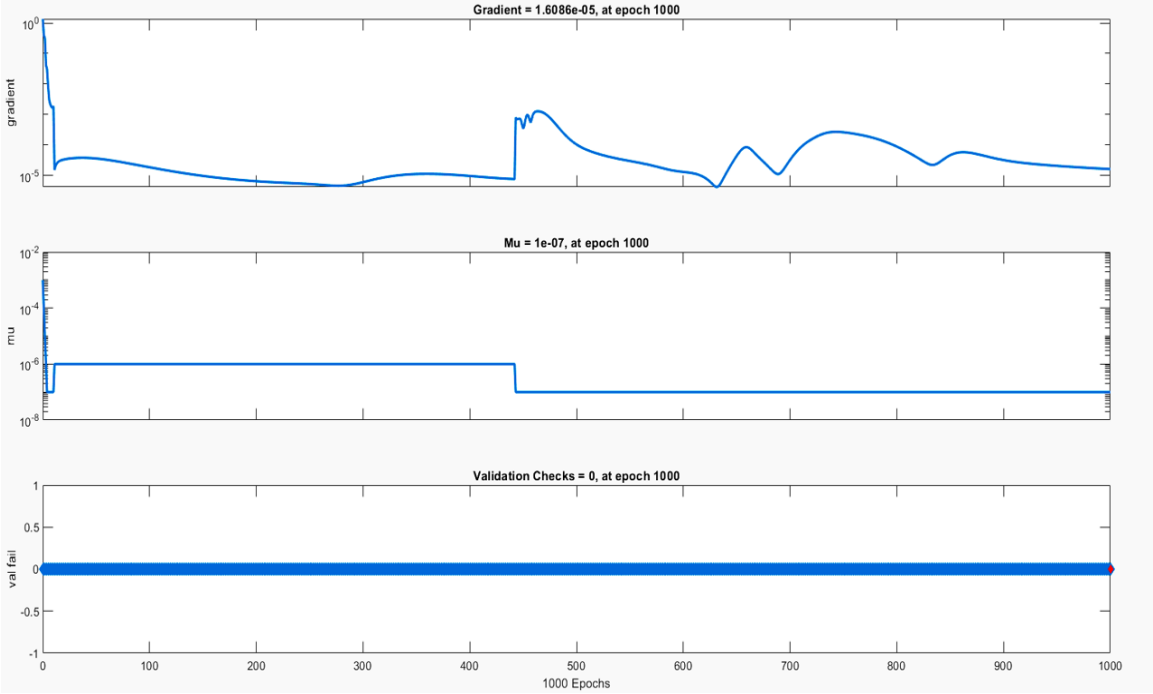

(a)

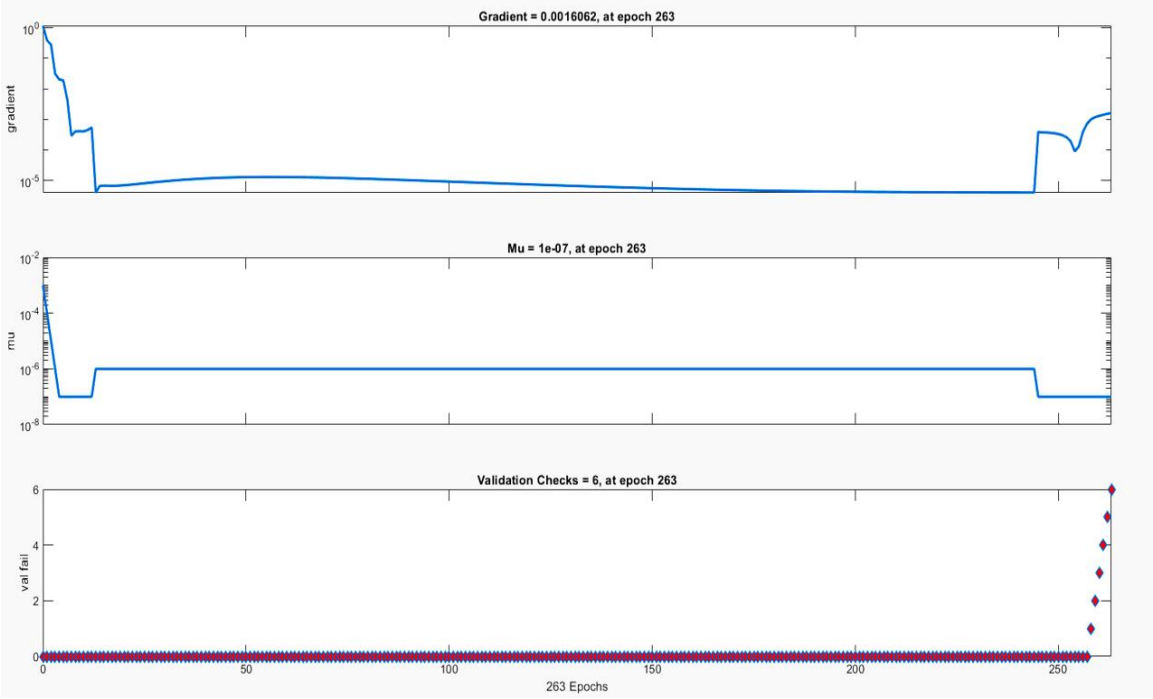

(b)

Figure (5.59). NARX performance for 64QAM after the end of training for (a) real part (b) imaginary part

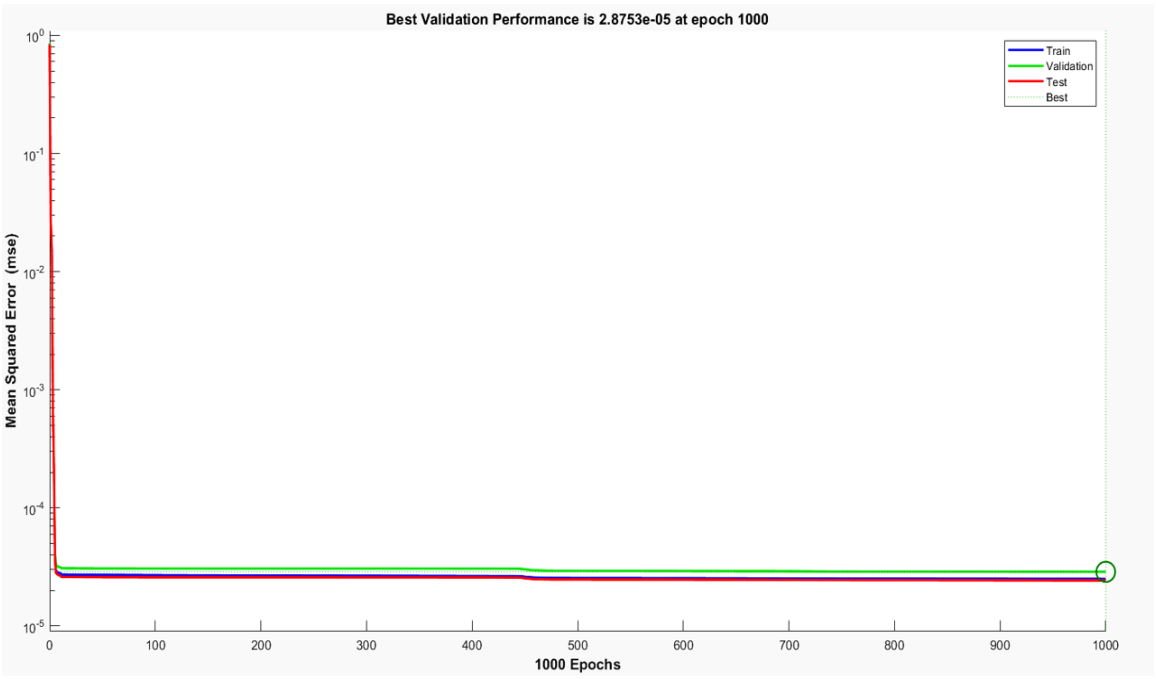

(a)

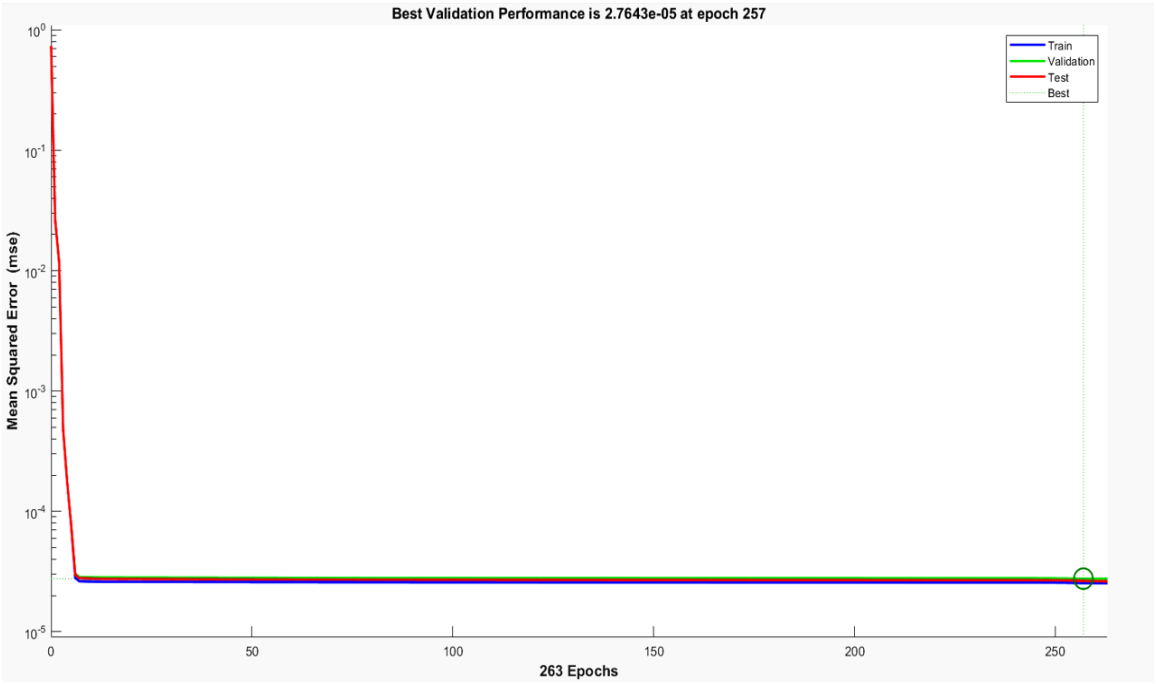

(b)

Figure (5.60). MSE vs. number of epochs for (a) real part (b) imaginary part

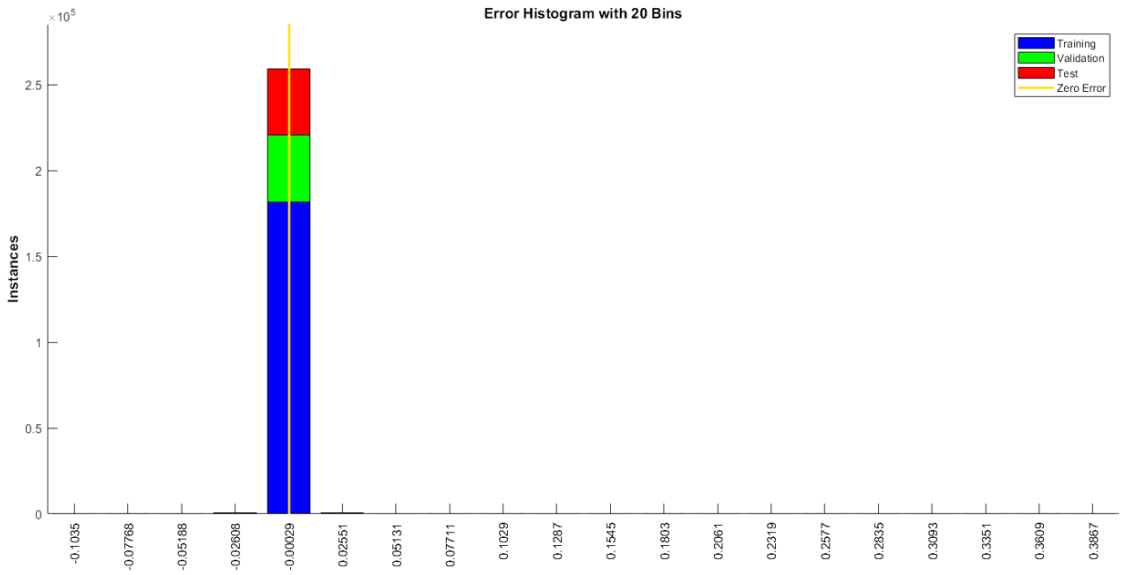

(a)

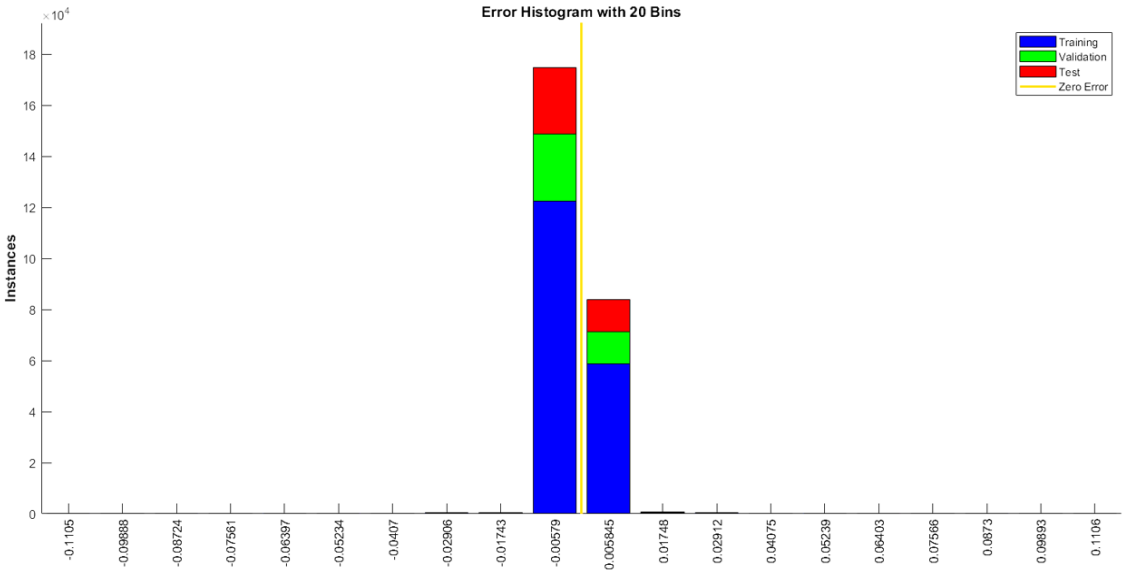

(b)

Figure (5.61). Error histogram with 20 Bins (a) real training (b) imaginary training

The results obtained from the training investigation reveal the robustness of the NARX technique potential for nonlinear impairment compensation, as will be clarified in the subsequent section of the results that have been reached, which will give a full impression of the effectiveness of the NARX algorithm in solving the problems of the optical fiber.

5.7.4 Results of Implementation NARX-64QAM

This section shows NARX time series results with 64-QAM modulation. Analyzing BER, Q-factor, and EVM will reveal the NARX algorithm's ability to adjust for nonlinearity effects and maximize signal transmission in 64-QAM modulation. In Appendix B, Table (B.20) shows the first, eighth, and sixteenth channels' parameters at 1000 km at different signal powers. Table data shows that 10 dBm provides the best received signal. All channels used the NARX algorithm to analyze fiber impairments and achieve the same signal quality. Thus, a signal power of 10 dBm will be utilized to test the proposed system at different fiber lengths by adjusting the number of spans to determine how well the NARX compensating approach works. This will assess the proposed system's performance at various fiber lengths. BER at various span connections for the first, middle, and final channels is shown in Figure (5.62).

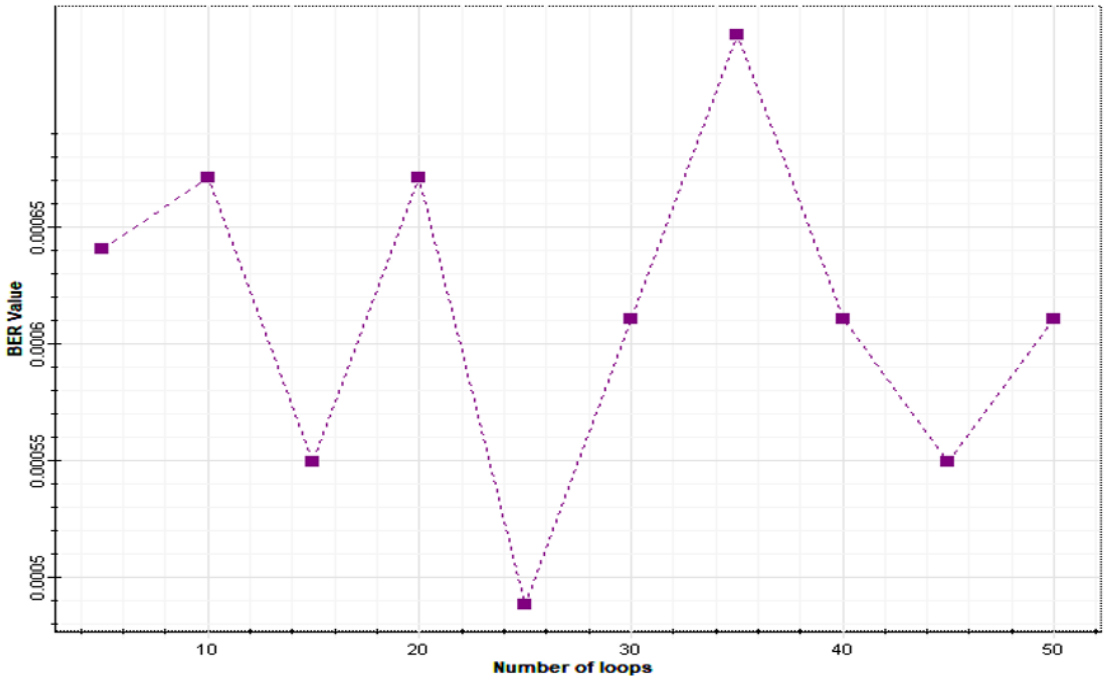

(a)

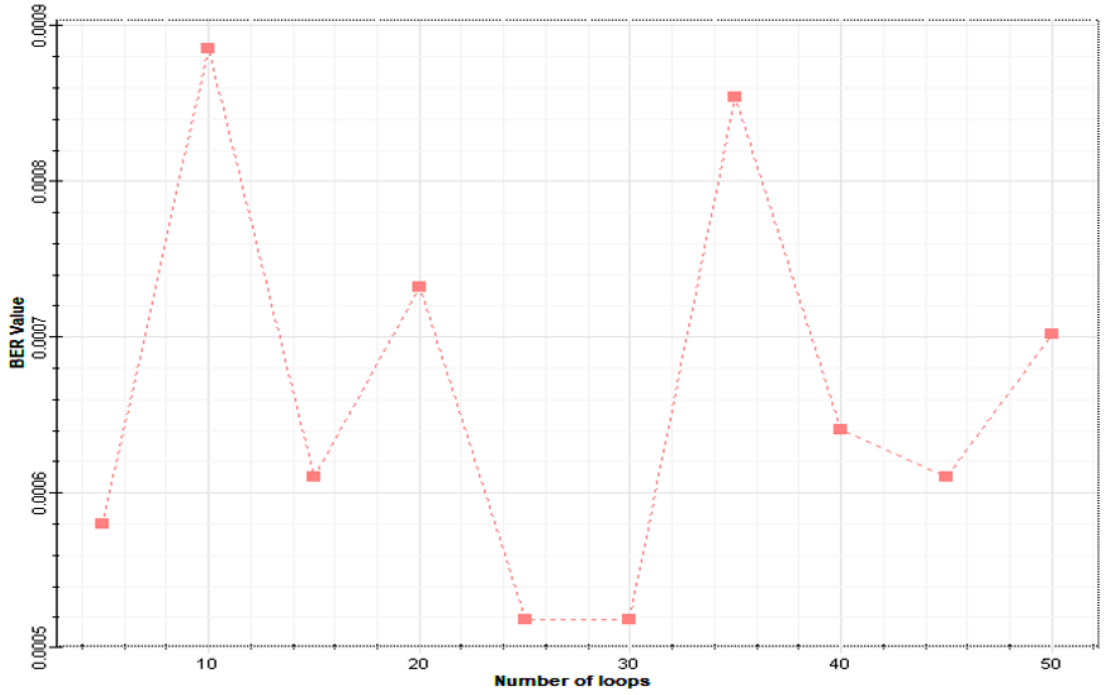

(b)

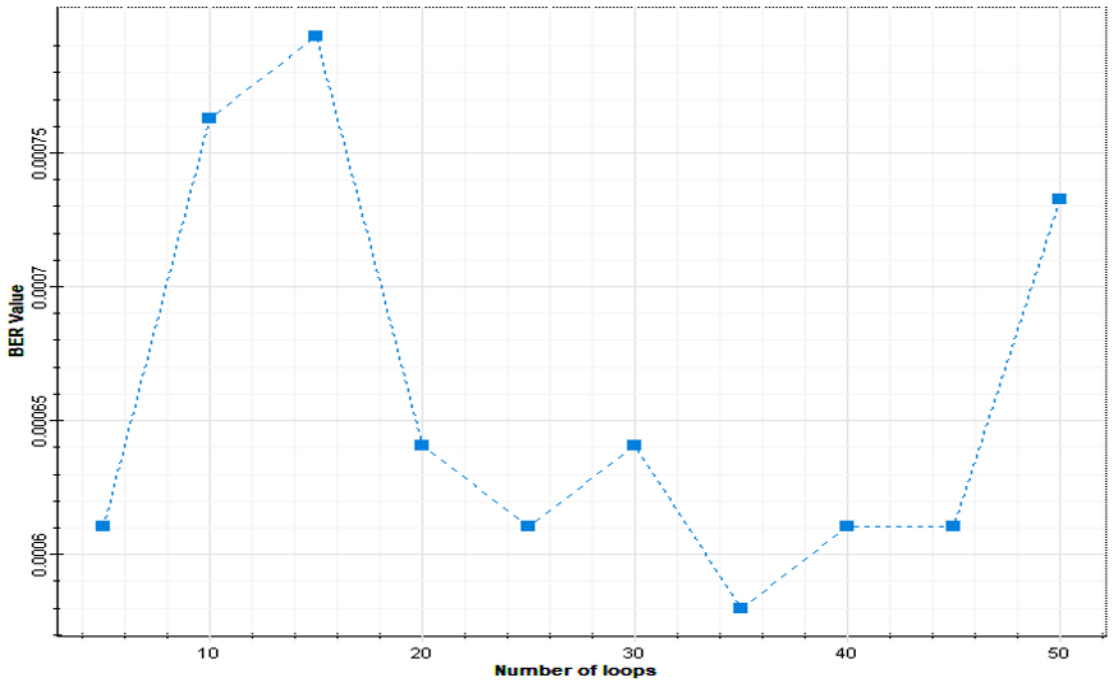

(c)

Figure (5.62). BER patterns in 64QAM-NARX algorithm for (a) Ch.1 (b) Ch.8 (c) Ch.16

The BER, which measures the quality of the received signal, indicates that the network is able to maintain a high-quality signal despite the nonlinearity effects of the communication channel. In light of the data presented, it can be reaching the inference that the quality of the signal received, as measured by the BER, has vastly improved in comparison to the situation in which the NARX-NLC was not utilized. Additionally, it should be pointed out that extending the transmission distance does not have an effect on the received signal, nor does it degrade its quality. This is possible owing to the unique qualities of NARX time series neural networks, which have the ability to anticipate and solve issues that arise in the channel. The Q-factor, error vector magnitude, and constellation diagram for channels 1, 8, and 16 are depicted respectively in Figures (5.63), (5.64), and (5.65). The fact that the transmission achieved a value that was higher than the HD-FEC limit, as shown by the results of the Q-factor for all three channels, provides a favorable impression regarding this method of compensation.

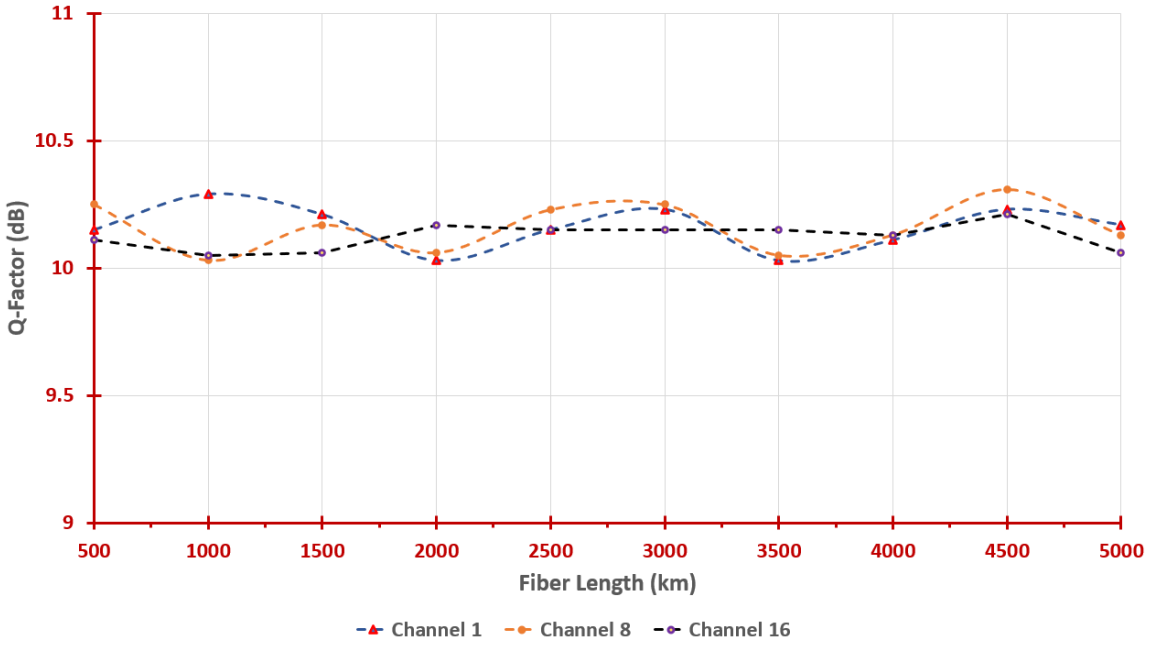

Figure (5.63). Q-factor in 64QAM based on NARX algorithm for three channels

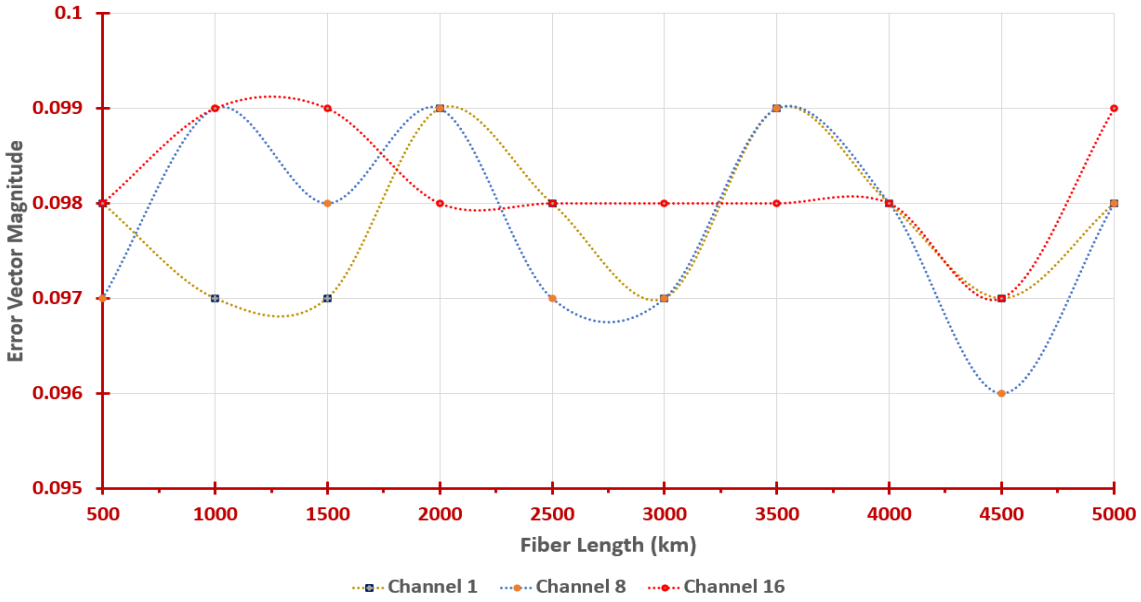

Figure (5.64). Error vector magnitude (EVM) in 64QAM based on NARX algorithm for three channels

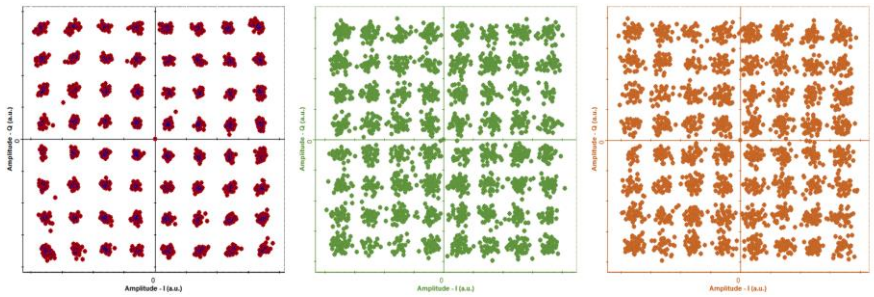

(a) **(b)** **(c)**

Figure (5.65). Constellation diagram in 64QAM based on NARX algorithm for (a) Ch.1 (b) Ch.8 (c) Ch.16

Overall, the utilization of the Nonlinear Autoregressive with exogenous input technique has demonstrated its effectiveness in compensating for nonlinearities in DWDM systems. By leveraging the capabilities of the NARX algorithm, the model has been able to accurately capture and mitigate the distortions caused by nonlinear impairments in the optical signal. By comprehensively analyzing BER, Q-factor, and EVM, gaining valuable insights into the behavior and performance of the NARX algorithm in ensuring reliable signal transmission in fiber optic communication systems.

5.8 Summarization and Contributions of Machine Learning Method Based on Neural Network Algorithms

At the end of the investigation of machine learning compensation based on two efficient algorithms that were employed in this work to address and solve the problems that the optical fiber suffers from, table (5.8) provides a comparison of the current study with previously published works for the last four years of different machine learning compensation methods illustrating the main points of contributions. The results obtained showed the quality of the received signal based on BER was 10^{-6} in the case of 16 QAM and 10^{-4} in the case of 64 QAM which is higher than HD-FEC (BER=3.8×10^{-3}), which is the best compared to previous studies in terms of multiplexing technique, transmission distance, number of channels, and data transfer rate.

Table (5.8). Comparison of proposed work with previously published work

No. of Ref.	Type of compensation	Method of compensation	Multiplexing type	Modulation format	No. of channel	Total Data rate	Transmission distance (km)	BER
[120]	Nonlinear effects	Support Vector Machine (SVM)	----------	SP-64QAM	Single	54 Gb/s	100	3.1×10^{-6}
[121]	Nonlinear effects	Recurrent neural network (RNN)	WDM/ 62.5 GHz	PDM-16 QAM	3	324 Gb/s	2400	7×10^{-3}
[122]	Kerr effects	Siamese Neural Networks (SNN)	WDM/ 100 GHz	DP-16 QAM	2	200 Gb/s	3200	2×10^{-3}
[123]	SPM	Logistic Regression	----------	16 QAM	Single	56 Gb/s	100	4.27×10^{-4}
[34]	Nonlinear effects	Convolutional Neural Network (CNN)	WDM	DP-64 QAM	8	960 Gb/s	375	1×10^{-3}
[36]	Nonlinear effects	Deep Neural Network (DNN)	----------	DP-16QAM	Single	-------	1200	5.4×10^{-3}
My proposed work	Linear and Nonlinear effects	Convolutional Neural Network (CNN) + Nonlinear Auto Regressive with exogenous inputs (NARX)	DWDM/ 50 GHz	SP-16QAM SP-64QAM	16	1.920 Tb/s	5000	61.03×10^{-6} 5.18×10^{-4}

Chapter Six

Conclusions and Future Works

6.1 Conclusion

Mitigation and compensation of fiber impairments in advanced optical fiber communication systems have been investigated and analyzed based on two different methods of implementation. The first compensation approach was implemented on the transmission link of fiber called optical phase conjugation. The second compensation method was implemented on the received side based on advanced machine learning techniques. Both techniques of compensation are used with a multichannel system using dense wavelength division multiplexing. From the present work on compensation techniques, the following conclusions can be drawn as follows:

1- System performance against fiber impairment was improved by the proposed compensating techniques. This increased wire communication power, distance, and data rate by over 1 Tbps.
2- This work encourages installing OPC modules at strategic locations along fiber spans to boost the functionality of communication systems over long fiber optic links.
3- The results show that the BER performance and transmission range can be improved by using multiple OPC modules instead of a single mid OPC module.
4- The hybrid backward Raman amplifier with OPC gives better performance compared to conventional or hybrid with DCF.

5- Machine learning based on two different algorithms for compensating fiber impairments yields the best results in highly complex models and environments without having to build a physical model to meet the challenges of the complexity of optical transmission.
6- CNN and NARX have different strengths and limitations in compensating nonlinearities and assessing performance. Due to their differing patterns and performance predictions, the two approaches yielded different results. CNN algorithm uses feature detection, while NARX estimates channel impulsivity.
7- NARX neural networks gave more accurate and higher results than CNNs due to the CNN algorithm has more layers, which increases training time, power consumption, and computational power compared to the NARX algorithm.

6.2 Recommendations for Future Works

While the present study has provided valuable insights into the performance of OPC, CNN, and NARX networks in compensating for nonlinearity in optical communication systems, there are several areas that warrant further investigation and offer opportunities for future research. These potential future directions include:

1- The investigated system is capable of being extended to include additional modulation schemes, such as 128 QAM and 256 QAM, or a hybrid mQAM with OFDM, which would result in an increase in the amount of data rate with reduced channel spacing.
2- The impacts of fiber impairments employing OPC approaches or machine learning networks are analyzed theoretically. Experimental research will play a crucial role in the future to verify the accuracy of

the theoretical models and to evaluate the efficacy of the compensation scheme.

3- There are other neural network architectures that can be explored for nonlinearity compensation in optical communication systems. Long Short-Term Memory (LSTM) networks, or transformer-based models may provide new insights and potentially improve performance.

4- Hyperparameters and network designs greatly affect neural network performance. More research can optimize these parameters to improve CNN and NARX networks' nonlinearity compensation. Techniques such as grid search, evolutionary algorithms, or Bayesian optimization can be employed for this purpose.

5- Combining multiple techniques and approaches can often lead to improved performance. Future work could investigate the potential benefits of hybrid approaches that integrate machine learning techniques with traditional compensation methods or digital signal processing algorithms. This could potentially enhance the overall performance of the optical communication system.

References

[1] X. Liu, "Evolution of fiber-optic transmission and networking toward the 5G era," *Iscience,* vol. 22, pp. 489-506, 2019.

[2] U. Cisco, "Cisco annual internet report (2018–2023) white paper. 2020," *Acessado em,* vol. 10, no. 01, pp. 1-35, 2021.

[3] P. J. Winzer, "Scaling optical fiber networks: Challenges and solutions," *Optics and Photonics News,* vol. 26, no. 3, pp. 28-35, 2015.

[4] E. Yamazaki, M. Tomizawa, and Y. Miyamoto, "100-Gb/s optical transport network and beyond employing digital signal processing," *IEEE communications magazine,* vol. 50, no. 2, pp. s43-s49, 2012.

[5] R. J. Essiambre, Robert W. Tkach, "Capacity trends and limits of optical communication networks," presented at the Proceedings of the IEEE, 2012.

[6] P. J. Winzer, D. T. Neilson, and A. R. Chraplyvy, "Fiber-optic transmission and networking: the previous 20 and the next 20 years," *Optics express,* vol. 26, no. 18, pp. 24190-24239, 2018.

[7] A. Khanna and S. Kaur, "Internet of things (IoT), applications and challenges: a comprehensive review," *Wireless Personal Communications,* vol. 114, pp. 1687-1762, 2020.

[8] I. P. Kaminow, T. Li, and A. E. Willner, *Optical fiber telecommunications VB: systems and networks*. Elsevier, 2010.

[9] O. Vassilieva, I. Kim, and T. Ikeuchi, "Enabling technologies for fiber nonlinearity mitigation in high capacity transmission systems," *Journal of Lightwave Technology,* vol. 37, no. 1, pp. 50-60, 2019.

[10] J. Mata *et al.*, "Artificial intelligence (AI) methods in optical networks: A comprehensive survey," *Optical switching and networking,* vol. 28, pp. 43-57, 2018.

[11] R. T. Jones, "Machine learning methods in coherent optical communication systems," *International Series of Monographs on Physics; Technical University of Denmark: Kongens Lyngby, Denmark,* 2019.

[12] R.-J. Essiambre, G. Kramer, P. J. Winzer, G. J. Foschini, and B. Goebel, "Capacity limits of optical fiber networks," *Journal of Lightwave Technology,* vol. 28, no. 4, pp. 662-701, 2010.

[13] R.-J. Essiambre and R. W. Tkach, "Capacity trends and limits of optical communication networks," *Proceedings of the IEEE,* vol. 100, no. 5, pp. 1035-1055, 2012.

[14] I. Kim, O. Vassilieva, Y. Akasaka, P. Palacharla, and T. Ikeuchi, "Enhanced spectral inversion for fiber nonlinearity mitigation," *IEEE Photonics Technology Letters,* vol. 30, no. 23, pp. 2040-2043, 2018.

[15] T. Sabapathi and R. Poovitha, "Mitigation of nonlinearities in fiber optic DWDM system," *Optik,* vol. 185, pp. 657-664, 2019.

[16] M. Ajmani, P. Singh, and P. Kaur, "Hybrid dispersion compensating modules: a better solution for mitigating four-wave mixing effects," *Wireless Personal Communications,* vol. 107, pp. 959-971, 2019.

[17] T. Huszaník, J. Turán, and L. u. Ovseník, "On mitigation of four-wave mixing in high capacity ultra-DWDM system," in *2019 20th International Carpathian Control Conference (ICCC)*, 2019: IEEE, pp. 1-4.

[18] B. Foo, M. Karlsson, K. Vijayan, M. Mazur, and P. A. Andrekson, "Analysis of nonlinearity mitigation using phase-sensitive optical parametric amplifiers," *Optics Express,* vol. 27, no. 22, pp. 31926-31941, 2019.

[19] P. M. Kaminski *et al.*, "All-optical nonlinear pre-compensation of long-reach unrepeatered systems," in *2020 European Conference on Optical Communications (ECOC)*, 2020: IEEE, pp. 1-4.

[20] I. Amiri, A. N. Z. Rashed, and P. Yupapin, "Comparative simulation study of multi stage hybrid all optical fiber amplifiers in optical communications," *Journal of Optical Communications,* 2020.

[21] J. Wang, Y. Du, C. Liang, Z. Li, and J. Fang, "Performance Evaluation of Highly Nonlinear Fiber (HNLF) Based Optical Phase Conjugation (OPC) in Long Haul Transmission of 640 Gbps 16-QAM CO-OFDM," in *Photonics*, 2021, vol. 8, no. 2: MDPI, p. 45.

[22] L. N. Venkatasubramani, A. Sobhanan, A. Vijay, R. D. Koilpillai, and D. Venkitesh, "Optical phase conjugation using nonlinear SOA for nonlinearity and dispersion compensation of coherent multi-carrier lightwave systems," *IEEE Access,* vol. 9, pp. 44059-44068, 2021.

[23] M. Tan *et al.*, "Distributed Raman amplification for fiber nonlinearity compensation in a mid-link optical phase conjugation system," *Sensors,* vol. 22, no. 3, p. 758, 2022.

[24] V. Gordienko, F. M. Ferreira, V. Ribeiro, and N. Doran, "Design of an interferometric fiber optic parametric amplifier for the rejection of unwanted four-wave mixing products," *Optics Express,* vol. 31, no. 5, pp. 8226-8239, 2023.

[25] W. Cao, "Improved compensation of intrachannel four-wave mixing in dispersion-managed transmission links with mid-span optical phase conjugation," *Optics Communications,* vol. 530, p. 129185, 2023.

[26] M. Närhi, L. Salmela, J. Toivonen, C. Billet, J. M. Dudley, and G. Genty, "Machine learning analysis of extreme events in optical fibre modulation instability," *Nature communications,* vol. 9, no. 1, p. 4923, 2018.

[27] O. Sidelnikov, A. Redyuk, and S. Sygletos, "Nonlinear equalization in long haul transmission systems using dynamic multi-layer perceptron networks," in *2018 European Conference on Optical Communication (ECOC)*, 2018: IEEE, pp. 1-3.

[28] S. Zhang *et al.*, "Field and lab experimental demonstration of nonlinear impairment compensation using neural networks," *Nature communications,* vol. 10, no. 1, p. 3033, 2019.

[29] M. Schaedler, C. Bluemm, M. Kuschnerov, F. Pittalà, S. Calabrò, and S. Pachnicke, "Deep neural network equalization for optical short reach communication," *Applied Sciences,* vol. 9, no. 21, p. 4675, 2019.

[30] O. Kotlyar, M. Pankratova, M. Kamalian-Kopae, A. Vasylchenkova, J. E. Prilepsky, and S. K. Turitsyn, "Combining nonlinear Fourier transform and neural network-based processing in optical communications," *Optics letters,* vol. 45, no. 13, pp. 3462-3465, 2020.

[31] M. M. Melek and D. Yevick, "Nonlinearity mitigation with a perturbation based neural network receiver," *Optical and Quantum Electronics,* vol. 52, pp. 1-10, 2020.

[32] O. Sidelnikov, A. Redyuk, S. Sygletos, M. Fedoruk, and S. Turitsyn, "Advanced convolutional neural networks for nonlinearity mitigation in long-haul WDM transmission systems," *Journal of Lightwave Technology,* vol. 39, no. 8, pp. 2397-2406, 2021.

[33] N. Hattori, J. Shiomi, Y. Masuda, T. Ishihara, A. Shinya, and M. Notomi, "Neural Network Calculations at the Speed of Light Using Optical Vector-Matrix Multiplication and Optoelectronic Activation," *IEICE Transactions on Fundamentals of Electronics, Communications and Computer Sciences,* vol. 104, no. 11, pp. 1477-1487, 2021.

[34] C. Li *et al.*, "Convolutional neural network-aided DP-64 QAM coherent optical communication systems," *Journal of Lightwave Technology,* vol. 40, no. 9, pp. 2880-2889, 2022.

[35] P. He *et al.*, "Unsupervised-learning neural network for fiber nonlinearity compensation," in *2021 International Conference on Optical Instruments and Technology: Optical Communication and Optical Signal Processing*, 2022, vol. 12278: SPIE, pp. 110-116.

[36] F. Li, X. Zhou, Y. Gao, J. Huo, R. Li, and K. Long, "The DNN-based DBP scheme for nonlinear compensation and longitudinal monitoring of optical fiber links," *Digital Communications and Networks,* 2023.

[37] C. Costa *et al.*, "Self-phase modulation and inter-polarization cross-phase modulation mitigation in single-channel DP-16QAM coherent PON employing 4D clustering," *Optical Fiber Technology,* vol. 75, p. 103186, 2023.

[38] G. P. Agrawal, "Nonlinear fiber optics," 6 ed.: Academic Press, Springer, 2019, pp. 717-728.

[39] A. Newell, *Nonlinear optics*. CRC Press, 2018.

[40] G. Keiser and G. Keiser, "Optical Signal Attenuation and Dispersion," *Fiber Optic Communications,* pp. 93-145, 2021.

[41] H. Murata, *Handbook of optical fibers and cables*. CRC Press, 2020.

[42] Y. Tamura *et al.*, "The first 0.14-dB/km loss optical fiber and its impact on submarine transmission," *Journal of Lightwave Technology,* vol. 36, no. 1, pp. 44-49, 2018.

[43] S. Kaushal and J. Azaña, "Group-velocity dispersion compensation of telecom data signals using compact discrete phase filters in silicon," in *2022 Optical Fiber Communications Conference and Exhibition (OFC)*, 2022: IEEE, pp. 1-3.

[44] P. Günter, *Nonlinear optical effects and materials*. Springer, 2012.

[45] V. G. Dmitriev, G. G. Gurzadyan, and D. N. Nikogosyan, *Handbook of nonlinear optical crystals*. Springer, 2013.

[46] L. S. Schanner, C. Mineto, L. G. Riveros, F. D. Simões, T. Sutili, and R. C. Figueiredo, "Low-Complexity Method for Optical Fiber Nonlinear Coefficient Measurement," in *2021 SBMO/IEEE MTT-S International Microwave and Optoelectronics Conference (IMOC)*, 2021: IEEE, pp. 1-3.

[47] M. Seimetz and M. Seimetz, "Fiber Propagation Effects," *High-order modulation for optical fiber transmission,* vol. 143, pp. 143-154, 2009.

[48] M. F. Ferreira, *Nonlinear effects in optical fibers*. John Wiley & Sons, 2011.

[49] R. R. Alfano, Y. Shen, and G.-Z. Yang, "Theory of self-phase modulation and spectral broadening," *The Supercontinuum Laser Source: The Ultimate White Light,* pp. 1-32, 2016.

[50] K. Vijayan, B. Foo, M. Karlsson, and P. A. Andrekson, "Cross-phase modulation mitigation in phase-sensitive amplifier links," *IEEE Photonics Technology Letters,* vol. 31, no. 21, pp. 1733-1736, 2019.

[51] M. K. Azad and M. Islam, "Performance limitations of WDM optical transmission system due to cross-phase modulation in presence of chromatic dispersion," in *2009 11th International Conference on Advanced Communication Technology*, 2009, vol. 3: IEEE, pp. 1877-1881.

[52] R. Kaler and R. Kaler, "Investigation of four wave mixing effect at different channel spacing," *optik,* vol. 123, no. 4, pp. 352-356, 2012.

[53] J. Ahmed, A. Hussain, M. Siyal, H. Manzoor, and A. Masood, "Parametric analysis of four wave mixing in DWDM systems," *Optik,* vol. 125, no. 7, pp. 1853-1859, 2014.

[54] B. Goebel and N. Hanik, "Analytical calculation of the number of Four-Wave-Mixing products in optical multichannel communication system," *Technische Universität München, Technical, German,* 2008.

[55] G. C. Baldwin, *An introduction to nonlinear optics*. Springer Science & Business Media, 2012.

[56] Y.-D. Lin, R.-H. Hwang, and F. Baker, *Computer networks: an open source approach*. 2012, p. 768.

[57] M. Cvijetic and I. Djordjevic, *Advanced optical communication systems and networks*. Artech House, 2013.

[58] S. Kumar and M. J. Deen, *Fiber optic communications: fundamentals and applications*. John Wiley & Sons, 2014.

[59] S. Bhatt and S. Jhaveri, "A review of dense wavelength division multiplexing and next generation optical internet," *International Journal of Engineering Science and Innovative Technology (IJESIT) Volume,* vol. 2, 2013.

[60] A. Bahrami, A. Lord, and T. Spiller, "Quantum key distribution integration with optical dense wavelength division multiplexing: a review," *IET Quantum Communication,* vol. 1, no. 1, pp. 9-15, 2020.

[61] J. M. Simmons, *Optical network design and planning*. Springer, 2014.

[62] J. Zyskind and A. Srivastava, *Optically amplified WDM networks*. Academic Press, 2011.

[63] S. Singh and R. Kaler, "Comparison of pre-, post-and symmetrical compensation for 96 channel DWDM system using PDCF and PSMF," *Optik,* vol. 124, no. 14, pp. 1808-1813, 2013.

[64] A. Naji *et al.*, "Review of Erbium-doped fiber amplifier," *International Journal of the Physical Sciences,* vol. 6, no. 20, pp. 4674-4689, 2011.

[65] L. Sirleto and M. A. Ferrara, "Fiber amplifiers and fiber lasers based on stimulated Raman scattering: a review," *Micromachines,* vol. 11, no. 3, p. 247, 2020.

[66] V. Supradeepa, Y. Feng, and J. W. Nicholson, "Raman fiber lasers," *Journal of Optics,* vol. 19, no. 2, p. 023001, 2017.

[67] P. Rosa *et al.*, "Unrepeatered 240-km 64-QAM transmission using distributed raman amplification over SMF fiber," *Applied Sciences,* vol. 10, no. 4, p. 1433, 2020.

[68] M. B. Hossain, A. Adhikary, and T. Z. Khan, "Performance investigation of different dispersion compensation methods in optical fiber communication," *Asian Journal of Research in Computer Science,* vol. 5, no. 2, pp. 36-44, 2020.

[69] S. Kheris and B. Bouabdallah, "Analysis three dispersion compensation techniques using DCF," *Journal of Optical Communications,* 2021.

[70] S. Ramachandran, *Fiber based dispersion compensation*. Springer Science & Business Media, 2007.

[71] S. T. Le, Vahid Aref, Henning Buelow, "Nonlinear signal multiplexing for communication beyond the Kerr nonlinearity limit," *Nature Photonics,* vol. 11, no. 9, pp. 570-576, 2017.

[72] T. Xu, Nikita A. Shevchenko, Yunfan Zhang, Cenqin Jin, Jian Zhao, Tiegen Liu, "Information rates in Kerr nonlinearity limited optical fiber communication systems," *Optics Express,* vol. 29, no. 11, pp. 17428-17439, 2021.

[73] S. L. Olsson, Bill Corcoran, Carl Lundström, Tobias A. Eriksson, Magnus Karlsson, Peter A. Andrekson, "Phase-sensitive amplified transmission links for improved sensitivity and nonlinearity tolerance," *Journal of Lightwave Technology,* vol. 33, no. 3, pp. 710 - 721, 2014.

[74] B. Y. Zel'Dovich, Nikolai F. Pilipetsky, Vladimir Vasil′evich Shkunov, *Principles of phase conjugation*. Springer, 2013.

[75] N. D. Binh, Nguyen Van Dien, Nguyen Quang Nhu Quynh, Ho Phuoc Tien, Nguyen Van Tuan, Nguyen Tan Hung, "Impact of Frequency Shift on Nonlinear Compensation Using Optical Phase Conjugation for M-QAM Signals," *REV Journal on Electronics and Communications,* vol. 9, no. 3, pp. 55-62, 2020.

[76] F. Sun, Feng Wen, Baojian Wu, Yun Ling, Kun Qiu, "Optical phase conjugation conversion through a nonlinear bidirectional semiconductor optical amplifier configuration," *Photonics,* vol. 9, no. 3, p. 164, 2022. MDPI.

[77] S.-R. Lee, "Dispersion management and optical phase conjugation in optical transmission links with a randomly distributed single-mode fiber length," *Journal of information and communication convergence engineering,* vol. 11, no. 1, pp. 1-6, 2013.

[78] M. P. Yankov, Pawel M. Kaminski, Francesco Da Ros, "Four-wave mixing conversion efficiency requirements for optical phase conjugation based fiber nonlinearity compensation," presented at the CLEO: Science and Innovations 2020, Washington, DC United States, 2020.

[79] I. A. M. Ali Hayder Abdul Kareem, "Investigation of Fiber Impairment Mitigation Based on Optical Phase Conjugation Technique," *International Journal of Microwave and Optical Technology,* vol. 18, no. 2, pp. 184-194, 2023.

[80] M. E. Marhic, Peter A. Andrekson, Periklis Petropoulos, Stojan Radic, Christophe Peucheret, Mahmoud Jazayerifar, "Fiber optical parametric amplifiers in optical communication systems," *Laser & photonics reviews,* vol. 9, no. 1, pp. 50-74, 2015.

[81] Z. Chen, Xiaojie Guo, Xuelei Fu, Chester Shu, Zhaohui Li, "Investigation of four-wave-mixing crosstalk in phase-sensitive fiber optical parametric amplifier," *Journal of Lightwave Technology,* vol. 36, no. 22, pp. 5113-5120, 2018.

[82] N. Othman, NS Mohd Shah, K. G. Tay, N. A. Cholan, R. Talib, "The effect of pump parameters on dual-pump fiber optical parametric amplifier," *MATEC Web of Conferences,* vol. 150, no. 01010, p. 3, 2018.

[83] S. Rahbarfam, Shiva Kumar, "Nonlinear phase noise reduction using digital back propagation and midpoint optical phase conjugation," *Optics Express,* vol. 27, no. 6, pp. 8968-8982, 2019.

[84] H. Hu, Robert M. Jopson, "Fiber Nonlinearity Mitigation Using Multiple Optical Phase Conjugations," *Asia Communications and Photonics Conference,* p. Su4A.1, 2017. Optica Publishing Group.

[85] B. N. Due, Nguyen Van Dien, Hung Nguyen Tan, Quang Nguyen-The, "Nonlinearity compensation in DWDM metro systems using optical phase conjugation,"

2019 International Conference on Advanced Technologies for Communications (ATC), vol. IEEE, pp. 193-197, 2019.

[86] J. Mata, Ignacio de Miguel, Ramon J. Duran, Noemí Merayo, Sandeep Kumar Singh, Admela Jukan, Mohit Chamania, "Artificial intelligence (AI) methods in optical networks: A comprehensive survey," *Optical switching and networking,* vol. 28, pp. 43-57, 2018.

[87] I. H. Sarker, "Machine learning: Algorithms, real-world applications and research directions," *SN computer science,* vol. 2, no. 3, p. 160, 2021.

[88] S. Wang, Wanpracha Chaovalitwongse, Robert Babuska, "Machine learning algorithms in bipedal robot control," *IEEE Transactions on Systems, Man, and Cybernetics, Part C (Applications and Reviews),* vol. 42, no. 5, pp. 728-743, 2012.

[89] Y. Bengio, Aaron C. Courville, Pascal Vincent, "Unsupervised feature learning and deep learning: A review and new perspectives," *CoRR,* vol. 1, no. 2665, p. 30, 2012.

[90] C. Sun, Eurika Kaiser, Steven L. Brunton, J. Nathan Kutz, "Deep reinforcement learning for optical systems: A case study of mode-locked lasers," *Machine Learning: Science and Technology,* vol. 1, no. 4, p. 045013, 2020.

[91] C. A. Charu, *Neural networks and deep learning: a textbook*. Spinger, 2018, p. 506.

[92] A. L. Caterini, Dong Eui Chang, *Deep neural networks in a mathematical framework*. Berlin/Heidelberg, Germany: Springer International Publishing, 2018.

[93] A. V. d. Oliveira, Márcia Cristina Schiavi Dazzi, Anita Maria da Rocha Fernandes, Rudimar Luis Scaranto Dazzi, Paulo Ferreira, Valderi Reis Quietinho Leithardt, "Decision Support Using Machine Learning Indication for Financial Investment," *Future Internet,* vol. 14, no. 11, p. 304, 2022.

[94] A. D. Rasamoelina, Fouzia Adjailia, Peter Sinčák, "A review of activation function for artificial neural network," *2020 IEEE 18th World Symposium on Applied Machine Intelligence and Informatics (SAMI),* vol. 1, pp. 281-286, 2020.

[95] Y. Gao, Weiqiang Liu, Fabrizio Lombardi, "Design and implementation of an approximate softmax layer for deep neural networks," *2020 IEEE international symposium on circuits and systems (ISCAS),* vol. 1, pp. 1-5, 2020.

[96] R. Rojas, *Neural networks: a systematic introduction*. Springer Science & Business Media, 2013, p. 509.

[97] P. N. Suganthan, Rakesh Katuwal, "On the origins of randomization-based feedforward neural networks," *Applied Soft Computing,* vol. 105, p. 107239, 2021.

[98] C. Wu, Junwei Wang, Juntao Liu, Wenyu Liu, "Recurrent neural network based recommendation for time heterogeneous feedback," *Knowledge-Based Systems,* vol. 109, pp. 90-103, 2016.

[99] S. Dargan, Munish Kumar, Maruthi Rohit Ayyagari, Gulshan Kumar, "A survey of deep learning and its applications: a new paradigm to machine learning," *Archives of Computational Methods in Engineering,* vol. 27, pp. 1071-1092, 2020.

[100] T. Doan, *Convolutional Neural Network in classifying scanned documents*. GRIN Verlag, 2016, p. 40.

[101] L. Alzubaidi, Jinglan Zhang, Amjad J. Humaidi, Ayad Al-Dujaili, Ye Duan, Omran Al-Shamma, José Santamaría, Mohammed A. Fadhel, Muthana Al-Amidie, Laith Farhan, "Review of deep learning: Concepts, CNN architectures, challenges, applications, future directions," *Journal of big Data,* vol. 8, pp. 1-74, 2021.

[102] Y.-N. Chen, Kuo-Chin Fan, Yang-Lang Chang, Toshifumi Moriyama, "Special Issue Review: Artificial Intelligence and Machine Learning Applications in Remote Sensing," *Remote Sensing,* vol. 15, no. 3, p. 569, 2023.

[103] V. E. Balas, Raghvendra Kumar, Rajshree Srivastava, eds, *Recent trends and advances in artificial intelligence and internet of things*. Cham: Springer International Publishing, 2020.

[104] A. Zafar, Muhammad Aamir, Nazri Mohd Nawi, Ali Arshad, Saman Riaz, Abdulrahman Alruban, Ashit Kumar Dutta, Sultan Almotairi, "A comparison of pooling methods for convolutional neural networks," *Applied Sciences,* vol. 12, no. 17, p. 8643, 2022.

[105] S. S. Basha, Shiv Ram Dubey, Viswanath Pulabaigari, Snehasis Mukherjee, "Impact of fully connected layers on performance of convolutional neural networks for image classification," *Neurocomputing,* vol. 378, pp. 112-119, 2020.

[106] J. D. Kelleher, *Deep learning*. MIT press, 2019, p. 296.

[107] J. I. G. Heaton, Yoshua Bengio, Aaron Courville, "Deep learning: The MIT Press," *Genetic programming and evolvable machines,* vol. 19, no. 1, pp. 305-307, 2016.

[108] I. K. M. Jais, Amelia Ritahani Ismail, Syed Qamrun Nisa, "Adam optimization algorithm for wide and deep neural network," *Knowledge Engineering and Data Science,* vol. 2, no. 1, pp. 41-46, 2019.

[109] A. K. Tyagi, Ajith Abraham, eds, *Recurrent Neural Networks: Concepts and Applications*. CRC Pr I Llc, 2022, p. 413.

[110] H. Hewamalage, Christoph Bergmeir, Kasun Bandara, "Recurrent neural networks for time series forecasting: Current status and future directions," *International Journal of Forecasting,* vol. 37, no. 1, pp. 388-427, 2021.

[111] L. A. Tavares, Petrus EOGB Abreu, Luis A. Aguirre, "Nonlinearity compensation based on identified NARX polynomials models," *Nonlinear Dynamics,* vol. 107, no. 1, pp. 709-725, 2022.

[112] M. Zhao, Ruhui Zhang, Cheng Lin, Hui Zhou, Junhui Shi, "Stochastic model predictive control for dual-motor battery electric bus based on signed Markov chain Monte Carlo method," *IEEE Access,* vol. 1, 8, pp. 120785-120797, 2020.

[113] D. A. Kumar, S. Murugan, "Performance analysis of NARX neural network backpropagation algorithm by various training functions for time series data," *International Journal of Data Science,* vol. 3, no. 4, pp. 308-325, 2018.

[114] M. C. Phan, Mark H. Beale, Martin T. Hagan, "A procedure for training recurrent networks," presented at the The 2013 International Joint Conference on Neural Networks (IJCNN), Dallas, TX, USA, 2013.

[115] S. Lahmiri, "On simulation performance of feedforward and NARX networks under different numerical training algorithms," in *Handbook of research on computational simulation and modeling in engineering*: IGI Global, 2016, pp. 171-183.

[116] V. Kaleeswaran, S. Dhamodharavadhani, R. Rathipriya, "A comparative study of activation functions and training algorithm of NAR neural network for crop prediction,"

presented at the 2020 4th International Conference on Electronics, Communication and Aerospace Technology (ICECA), Coimbatore, 2020.

[117] T. Xu *et al.*, "Digital nonlinearity compensation in high-capacity optical communication systems considering signal spectral broadening effect," *Scientific reports,* vol. 7, no. 1, p. 12986, 2017.

[118] M. Berbineau *et al.*, "All-Optical Nonlinear Pre-Compensation of Long-Reach Unrepeatered Systems," in *2021 IEEE 93rd Vehicular Technology Conference*, 2022: IEEE.

[119] F. Sun, F. Wen, B. Wu, Y. Ling, and K. Qiu, "Optical phase conjugation conversion through a nonlinear bidirectional semiconductor optical amplifier configuration," in *Photonics*, 2022, vol. 9, no. 3: MDPI, p. 164.

[120] R. Weixer, J. Koch, P. Plany, S. Ohlendorf, and S. Pachnicke, "Mitigation of nonlinear impairments by using support vector machine and nonlinear volterra equalizer," *Applied Sciences,* vol. 9, no. 18, p. 3800, 2019.

[121] Y. Zhao *et al.*, "Low-complexity fiber nonlinearity impairments compensation enabled by simple recurrent neural network with time memory," *IEEE Access,* vol. 8, pp. 160995-161004, 2020.

[122] M. M. Melek and D. Yevick, "Fiber nonlinearity mitigation with a perturbation based Siamese neural network receiver," *Optical Fiber Technology,* vol. 66, p. 102641, 2021.

[123] R. A. de Paula *et al.*, "Mitigation of nonlinear phase noise in single-channel coherent 16-QAM systems employing logistic regression," *Optical and Quantum Electronics,* vol. 53, pp. 1-14, 2021.

Appendix A

Optisystem Version 19

Optisystem is a comprehensive software design suite that enables users to plan, test, and simulate optical links in the transmission layer of modern optical networks. It is a system level simulator based on the realistic modeling of fiber optic communication systems. A comprehensive Graphical User Interface (GUI) controls the optical component layout and net list, component models, and presentation graphics as in figure (A-1).

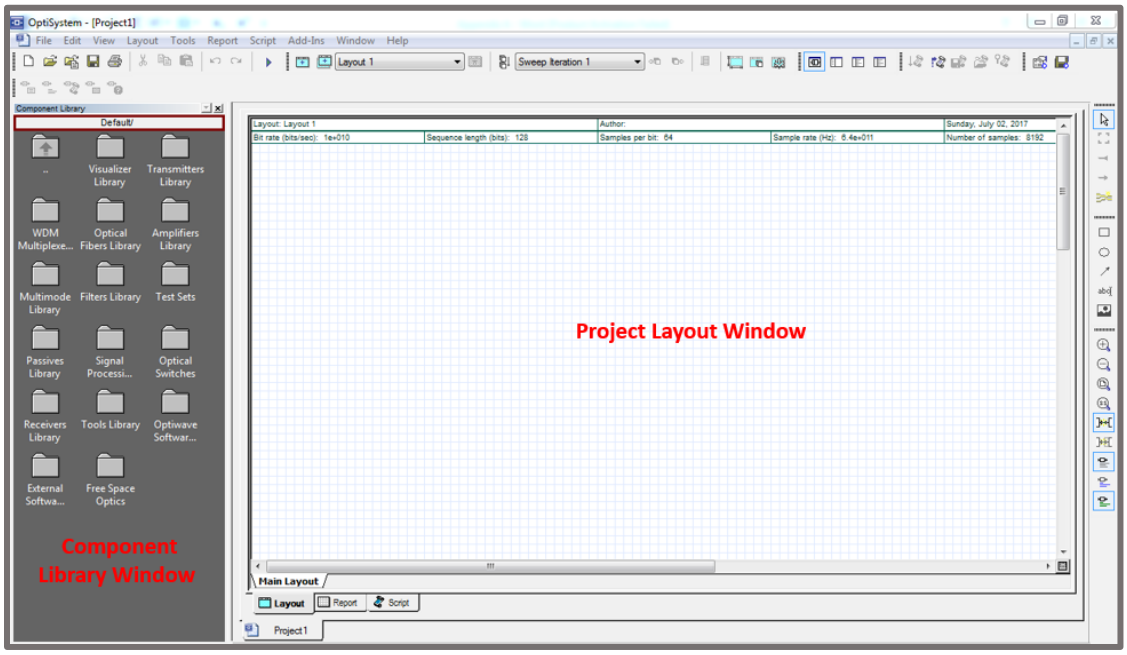

Fig. A.1: Optisystem Graphical User Interface (GUI).

Optisystem allows for the design automation of virtually any type of optical link in the physical layer, and the analysis of a broad spectrum of optical networks, from long haul networks to Metropolitan Area Networks (MANs) and Local Area Networks (LANs). Optisystem includes an extensive library of optical sample design (.osd) files that can be used as templates for optical design projects for learning and demonstration purposes.

MATLAB R2022b

MATLAB is a programming platform that has been specifically designed for analyzing data, developing algorithms, designing models, and applications. The matrix-based MATLAB language is the world's most natural way to express computational mathematics. Built-in graphics make it easy to visualize and gain insights from data. MATLAB code can be integrated with other languages, enabling to deploy algorithms and applications within web, enterprise, and production systems.

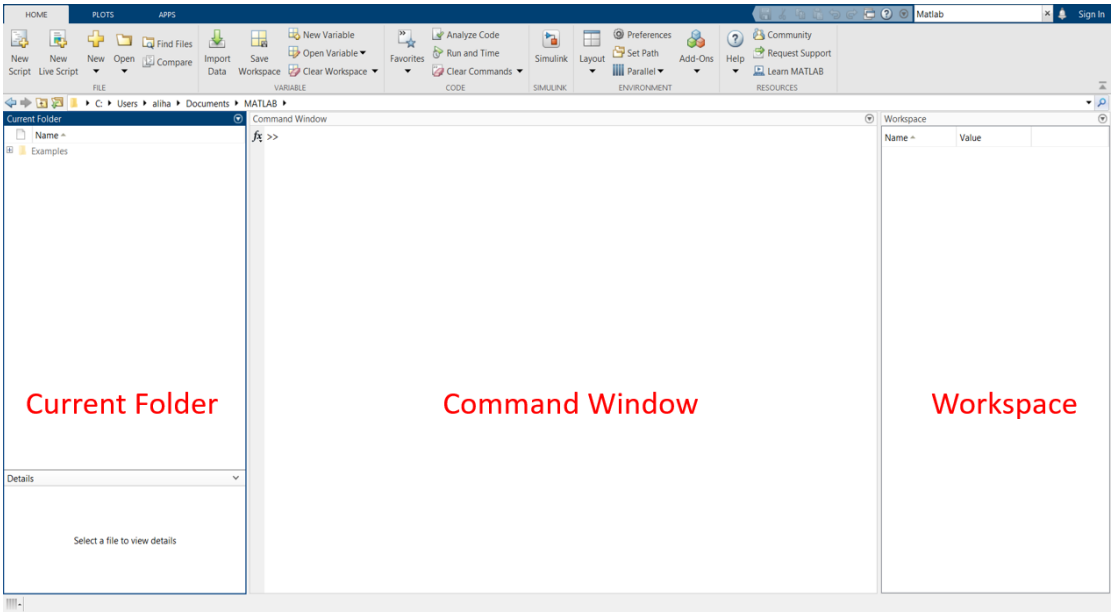

Fig. A.2: Default layout of MATLAB program.

The layout includes these panels:

- **Current Folder:** Access user files.
- **Command Window:** Enter commands at the command line, indicated by the prompt (>>).
- **Workspace:** Explore data that user creates or import from files.

Appendix B

Tables of Results

Table (B.1). BER for channels (1, 8, and 16) with conventional mid OPC

Power (dBm)	Channel 1	Channel 8	Channel 16
-10	9.11 E-3	9.01 E-3	6.99 E-3
-9	3.08 E-3	3.06 E-3	3.00 E-3
-8	1.39 E-3	1.38 E-3	1.34 E-3
-7	3.04 E-4	3.02 E-4	3.01 E-4
-6	1.07 E-4	1.07 E-4	1.04 E-4
-5	3.32 E-5	3.31 E-5	3.32 E-5
-4	3.48 E-7	3.41 E-7	1.49 E-6
-3	5.88 E-9	5.71 E-9	1.83 E-8
-2	5.21 E-12	7.10 E-11	5.84 E-11
-1	1.53 E-12	1.77 E-10	2.05 E-10
0	3.19 E-12	3.11 E-10	4.78 E-10
1	5.35 E-11	2.87 E-9	3.15 E-9
2	4.45 E-10	1.36 E-8	1.44 E-8
3	3.77 E-9	5.83 E-8	6.02 E-8
4	8.06 E-8	4.87 E-7	4.90 E-7
5	1.91 E-6	5.03 E-6	4.97 E-6
6	3.18 E-5	4.75 E-5	4.69 E-5
7	2.77 E-4	3.12 E-4	3.05 E-4
8	1.32 E-3	1.28 E-3	1.27 E-3
9	2.41 E-3	2.23 E-3	2.23 E-3
10	4.00 E-3	3.64 E-3	3.63 E-3

Table (B.2). BER for channel (1, 8, and 16) with hybrid mid OPC and DCF

Power (dBm)	Channel 1	Channel 8	Channel 16
-10	2.97 E-3	2.66 E-3	2.65 E-3
-9	1.35 E-3	1.27 E-3	1.26 E-3
-8	4.80 E-4	4.79 E-4	4.77 E-4
-7	3.25 E-4	3.15 E-4	3.13 E-4
-6	2.22 E-4	2.20 E-4	2.13 E-4
-5	1.48 E-5	2.10 E-5	2.06 E-5
-4	9.44 E-8	3.34 E-7	3.16 E-7
-3	3.87 E-11	1.39 E-9	1.20 E-9
-2	1.80 E-14	1.14 E-12	1.53 E-12
-1	1.16 E-15	1.40 E-13	1.23 E-13
0	8.27 E-17	1.69 E-15	1.77 E-15
1	6.30 E-18	2.08 E-16	1.05 E-16
2	5.83 E-19	2.88 E-17	1.26 E-17
3	2.54 E-16	4.13 E-14	2.52 E-14
4	7.73 E-15	6.07 E-13	4.35 E-13
5	1.01 E-13	3.37 E-11	2.62 E-11
6	7.29 E-12	4.57 E-10	3.87 E-10
7	1.76 E-9	1.71 E-8	1.54 E-8
8	3.84 E-6	3.40 E-6	1.06 E-6
9	1.07 E-4	1.01 E-4	1.01 E-4
10	3.90 E-4	3.89 E-4	3.88 E-4

Table (B.3). BER for channels (1, 8, and 16) with mid OPC with Raman

Power (dBm)	Channel 1	Channel 8	Channel 16
-10	1.60 E-4	1.54 E-4	1.95 E-4
-9	5.33 E-5	5.20 E-5	6.41 E-5
-8	3.23 E-5	3.07 E-5	3.84 E-5
-7	1.47 E-5	1.34 E-5	1.72 E-5
-6	7.21 E-7	5.16 E-7	7.45 E-7
-5	1.50 E-9	7.01 E-8	1.21 E-8
-4	6.12 E-11	4.55 E-11	4.74 E-11
-3	2.64 E-14	2.34 E-14	2.27 E-14
-2	1.95 E-18	3.05 E-17	4.31 E-17
-1	5.88 E-22	3.63 E-22	2.33 E-22
0	1.15 E-29	8.04 E-27	3.88 E-27
1	1.11 E-29	1.07 E-29	2.94 E-29
2	1.32 E-28	3.36 E-24	1.74 E-24
3	2.06 E-27	9.78 E-23	5.51 E-23
4	4.39 E-24	2.20 E-20	1.51 E-20
5	2.52 E-22	7.86 E-18	5.89 E-18
6	2.45 E-20	3.59 E-16	2.90 E-16
7	4.85 E-17	1.53 E-13	1.38 E-13
8	2.43 E-14	1.23 E-11	1.29 E-11
9	4.34 E-11	1.18 E-9	1.29 E-9
10	1.11 E-6	2.18 E-6	2.28 E-6

Table (B.4). BER for channels (1, 8, and 16) with conventional multiple OPC

Power (dBm)	Channel 1	Channel 8	Channel 16
-10	3.14 E-3	2.92 E-3	2.23 E-3
-9	2.73 E-3	2.00 E-3	1.84 E-3
-8	4.37 E-4	2.25 E-4	2.04 E-4
-7	8.00 E-5	3.88 E-5	1.05 E-4
-6	1.07 E-5	1.02 E-5	1.00 E-5
-5	4.43 E-6	3.54 E-6	3.15 E-6
-4	7.55 E-8	3.87 E-8	2.20 E-7
-3	3.37 E-9	2.37 E-9	1.68 E-8
-2	9.85 E-11	9.82 E-11	8.85 E-10
-1	2.03 E-13	1.32 E-12	1.20 E-12
0	6.31 E-14	5.60 E-14	2.83 E-14
1	1.24 E-13	9.34 E-12	2.43 E-12
2	3.05 E-12	3.65 E-10	2.90 E-10
3	2.80 E-11	2.07 E-9	1.54 E-9
4	1.48 E-10	6.20 E-9	5.55 E-9
5	4.60 E-10	2.05 E-8	1.30 E-8
6	1.68 E-9	2.76 E-8	2.37 E-8
7	1.82 E-8	2.70 E-7	2.01 E-7
8	9.71 E-7	8.88 E-7	1.05 E-6
9	6.85 E-6	2.54 E-5	1.79 E-5
10	3.98 E-4	2.72 E-4	2.01 E-4

Table (B.5). BER for channels (1, 8, and 16) with hybrid multiple OPC with DCF

Power (dBm)	Channel 1	Channel 8	Channel 16
-10	3.91 E-4	2.96 E-4	2.09 E-4
-9	7.28 E-5	6.42 E-5	6.38 E-5
-8	2.02 E-5	1.04 E-5	1.02 E-5
-7	1.49 E-6	1.44 E-6	1.34 E-6
-6	9.87 E-8	2.03 E-7	1.13 E-7
-5	5.51 E-9	5.33 E-9	4.43 E-9
-4	6.69 E-10	6.10 E-10	6.03 E-10
-3	3.98 E-11	2.24 E-11	2.16 E-11
-2	8.76 E-14	7.90 E-14	1.05 E-13
-1	2.30 E-17	1.56 E-17	1.48 E-17
0	8.20 E-21	7.30 E-21	6.81 E-21
1	3.28 E-25	2.64 E-25	1.30 E-25
2	1.95 E-26	1.84 E-26	1.56 E-26
3	1.26 E-23	1.12 E-23	1.02 E-23
4	2.15 E-20	1.91 E-20	1.18 E-20
5	3.02 E-17	2.72 E-17	1.91 E-17
6	2.61 E-14	2.39 E-14	1.88 E-14
7	9.01 E-12	8.48 E-12	8.17 E-12
8	1.38 E-9	1.31 E-9	1.19 E-9
9	6.37 E-8	6.14 E-8	5.80 E-8
10	1.12 E-6	1.09 E-6	1.05 E-6

Table (B.6). BER for channels (1, 8, and 16) with hybrid multiple OPC with Raman

Power (dBm)	Channel 1	Channel 8	Channel 16
-10	6.84 E-5	5.92 E-5	5.02 E-5
-9	7.05 E-6	6.25 E-6	6.18 E-6
-8	1.69 E-6	1.63 E-6	1.61 E-6
-7	3.88 E-7	3.77 E-7	3.76 E-7
-6	8.21 E-8	7.40 E-8	7.32 E-8
-5	2.61 E-9	1.66 E-9	1.62 E-9
-4	8.20 E-14	7.55 E-14	7.08 E-14
-3	2.29 E-19	1.32 E-19	1.23 E-19
-2	3.73 E-26	3.59 E-26	2.55 E-26
-1	5.40 E-32	4.85 E-32	4.28 E-32
0	4.30 E-34	3.83 E-34	3.72 E-34
1	8.61 E-35	6.60 E-35	5.40 E-35
2	2.77 E-31	2.75 E-31	1.23 E-31
3	3.83 E-29	2.18 E-29	1.02 E-29
4	7.96 E-26	7.01 E-26	6.80 E-26
5	4.11 E-23	3.99 E-23	3.73 E-23
6	8.98 E-21	6.04 E-21	5.43 E-21
7	2.03 E-18	1.17 E-18	1.00 E-18
8	8.75 E-15	7.45 E-15	6.61 E-15
9	3.52 E-12	2.74 E-12	2.50 E-12
10	6.64 E-10	6.02 E-10	5.62 E-10

Table (B.7). BER, Q-factor, and EVM for SP-8QAM for mid OPC with channels (1, 8, and 16)

Power	Channel one			Channel eight			Channel sixteen		
	BER	Q-factor	EVM	BER	Q-factor	EVM	BER	Q-factor	EVM
-15	11.95E-2	1.41	0.709	12.5E-2	1.21	0.826	12.74E-2	1.12	0.892
-12	9.91E-2	2.18	0.458	10.5E-2	1.95	0.512	10.81E-2	1.84	0.543
-9	9.56E-2	2.32	0.431	9.6E-2	2.30	0.434	9.57E-2	2.31	0.432
-6	9.17E-2	2.47	0.404	9.33E-2	2.42	0.413	9.37E-2	2.39	0.418
-3	8.71E-2	2.65	0.377	9.15E-2	2.48	0.403	9.21E-2	2.45	0.408
0	8.01E-2	2.94	0.340	8.1E-2	2.90	0.344	8.51E-2	2.74	0.364
3	7.51E-2	3.15	0.317	7.64E-2	3.09	0.323	7.70E-2	3.07	0.325
6	7.88E-2	3.00	0.333	7.98E-2	2.95	0.338	7.99E-2	2.95	0.338
9	8.27E-2	2.83	0.353	8.3E-2	2.82	0.354	8.34E-2	2.80	0.357
12	8.49E-2	2.74	0.364	8.59E-2	2.70	0.370	8.60E-2	2.70	0.370
15	8.83E-2	2.61	0.383	8.97E-2	2.56	0.390	9.00E-2	2.54	0.393

Table (B.8). BER, Q-factor, and EVM for SP-8QAM for mid OPC with Raman amplifier for channels (1, 8, and 16)

Power	Channel one			Channel eight			Channel sixteen		
	BER	Q-factor	EVM	BER	Q-factor	EVM	BER	Q-factor	EVM
-15	6.53E-2	3.58	0.27	7.33E-2	3.23	0.30	7.40E-2	3.19	0.31
-12	5.31E-2	4.16	0.24	6.45E-2	3.62	0.27	6.47E-2	3.61	0.27
-9	4.33E-2	4.67	0.21	5.11E-2	4.26	0.23	5.19E-2	4.22	0.23
-6	3.45E-2	5.18	0.19	4.06E-2	4.82	0.20	4.11E-2	4.79	0.20
-3	2.60E-2	5.77	0.17	3.41E-2	5.21	0.19	3.45E-2	5.18	0.19
0	2.01E-2	6.23	0.16	2.47E-2	5.86	0.17	2.52E-2	5.82	0.17
3	1.53E-2	6.69	0.14	1.86E-2	6.37	0.15	1.91E-2	6.32	0.15
6	2.01E-3	6.23	0.16	2.19E-2	6.08	0.16	2.22E-2	6.06	0.16
9	2.53E-2	5.82	0.17	2.6E-2	5.77	0.17	2.69E-2	5.70	0.17
12	2.90E-2	5.55	0.18	3.28E-2	5.29	0.19	3.33E-2	5.26	0.19
15	3.99E-2	4.86	0.20	4.26E-2	4.71	0.21	4.35E-2	4.66	0.21

Table (B.9). BER, Q-factor, and EVM for SP-8QAM conventional multiple OPC for channels (1, 8, and 16)

Power	Channel one			Channel eight			Channel sixteen		
	BER	Q-factor	EVM	BER	Q-factor	EVM	BER	Q-factor	EVM
-15	6.53E-2	3.36	0.29	7.33E-2	3.29	0.30	7.40E-2	3.24	0.30
-12	5.31E-2	3.64	0.27	6.45E-2	3.57	0.28	6.47E-2	3.45	0.29
-9	4.33E-2	4.20	0.23	5.11E-2	4.17	0.24	5.19E-2	3.90	0.25
-6	3.45E-2	4.73	0.21	4.06E-2	4.66	0.21	4.11E-2	4.47	0.22
-3	2.60E-2	4.96	0.20	3.41E-2	4.85	0.20	3.45E-2	4.83	0.20
0	2.01E-2	5.15	0.19	2.47E-2	4.97	0.20	2.52E-2	4.94	0.20
3	1.53E-2	5.39	0.18	1.86E-2	5.28	0.19	1.91E-2	5.22	0.19
6	2.01E-3	5.40	0.18	2.19E-2	5.30	0.18	2.22E-2	5.26	0.19
9	2.53E-2	5.06	0.19	2.6E-2	4.96	0.20	2.69E-2	4.91	0.20
12	2.90E-2	4.78	0.21	3.28E-2	4.69	0.21	3.33E-2	4.65	0.21
15	3.99E-2	4.45	0.22	4.26E-2	4.33	0.23	4.35E-2	4.30	0.23

Table (B.10). BER, Q-factor, and EVM for SP-8QAM hybrid multiple OPC with Raman amplifier for channels (1, 8, and 16)

Power	Channel one			Channel eight			Channel sixteen		
	BER	Q-factor	EVM	BER	Q-factor	EVM	BER	Q-factor	EVM
-15	2.09E-2	6.17	0.16	2.13E-2	6.13	0.16	2.19E-2	6.08	0.16
-12	1.57E-2	6.65	0.15	1.62E-2	6.60	0.15	1.69E-2	6.53	0.15
-9	1E-2	7.32	0.13	1.05E-2	7.25	0.13	1.11E-2	7.18	0.14
-6	6.95E-3	7.81	0.12	7.18E-3	7.77	0.12	7.23E-3	7.76	0.12
-3	4.04E-3	8.45	0.11	4.25E-3	8.40	0.12	4.33E-3	8.38	0.12
0	2.22E-3	9.07	0.11	2.43E-3	8.99	0.11	2.52E-3	8.95	0.11
3	1.60E-3	9.38	0.10	1.752-3	9.32	0.10	1.88E-3	9.24	0.10
6	1.37E-3	9.52	0.10	1.42E-3	9.49	0.10	1.55E-3	9.41	0.10
9	1.87E-3	9.24	0.10	1.97E-3	9.19	0.10	2.07E-3	9.14	0.11
12	2.71E-3	8.88	0.11	2.89E-3	8.81	0.11	3E-3	8.77	0.11
15	4.06E-3	8.45	0.11	4.24E-3	8.40	0.12	4.39E-3	8.36	0.12

Table (B.11). BER, Q-factor, and EVM for DP-16QAM conventional mid OPC for channels (1, 8, and 16)

Power	Channel one			Channel eight			Channel sixteen		
	BER	Q-factor	EVM	BER	Q-factor	EVM	BER	Q-factor	EVM
-15	7.97E-2	2.95	0.33	8.58E-2	2.70	0.37	8.61E-2	2.69	0.37
-12	7.55E-2	3.12	0.32	7.76E-2	3.04	0.32	7.85E-2	3.01	0.33
-9	6.83E-2	3.44	0.29	6.89E-2	3.42	0.29	7.47E-2	3.38	0.29
-6	6.31E-2	3.67	0.27	6.46E-2	3.61	0.27	6.54E-2	3.57	0.28
-3	5.98E-2	3.83	0.26	6.12E-2	3.76	0.26	6.16E-2	3.75	0.26
0	5.64E-2	3.99	0.25	5.78E-2	3.93	0.25	5.82E-2	3.91	0.25
3	5.41E-2	4.10	0.24	5.45E-2	4.08	0.24	5.54E-2	4.04	0.24
6	5.77E-2	3.93	0.25	5.84E-2	3.90	0.25	5.95E-2	3.85	0.25
9	6.19E-2	3.73	0.26	6.23E-2	3.72	0.26	6.29E-2	3.69	0.27
12	6.59E-2	3.55	0.28	6.63E-2	3.53	0.28	6.69E-2	3.50	0.28
15	6.99E-2	3.37	0.29	7.04E-2	3.35	0.29	7.12E-2	3.32	0.30

Table (B.12). BER, Q-factor, and EVM for DP-16QAM hybrid mid OPC with DCF for channels (1, 8, and 16)

Power	Channel one			Channel eight			Channel sixteen		
	BER	Q-factor	EVM	BER	Q-factor	EVM	BER	Q-factor	EVM
-15	6.25E-2	3.71	0.26	6.49E-2	3.59	0.27	6.53E-2	3.58	0.27
-12	5.35E-2	4.13	0.24	5.59E-2	4.01	0.24	5.62E-2	4.00	0.25
-9	4.70E-2	4.46	0.22	4.73E-2	4.45	0.22	4.75E-2	4.44	0.22
-6	4.04E-2	4.82	0.20	4.06E-2	4.82	0.20	4.08E-2	4.80	0.20
-3	3.56E-2	5.11	0.19	3.60E-2	5.09	0.19	3.65E-2	5.06	0.19
0	2.93E-2	5.52	0.18	2.98E-2	5.48	0.18	3.01E-2	5.47	0.18
3	2.76E-2	5.64	0.17	2.81E-2	5.61	0.17	2.83E-2	5.59	0.17
6	3.16E-2	5.37	0.18	3.20E-2	5.34	0.18	3.22E-2	5.35	0.18
9	3.63E-2	5.07	0.19	3.67E-2	5.05	0.19	3.69E-2	5.03	0.19
12	4.04E-2	4.83	0.20	4.08E-2	4.80	0.20	4.10E-2	4.80	0.20
15	4.56E-2	4.54	0.22	4.62E-2	4.51	0.22	4.65E-2	4.49	0.22

Table (B.13). BER, Q-factor, and EVM for DP-16QAM hybrid mid OPC with backward Raman amplifier for channels (1, 8, and 16)

Power	Channel one			Channel eight			Channel sixteen		
	BER	Q-factor	EVM	BER	Q-factor	EVM	BER	Q-factor	EVM
-15	3.04E-2	5.45	0.183	3.15E-2	5.37	0.186	3.19E-2	5.34	0.187
-12	5.45E-2	5.67	0.176	2.76E-2	5.64	0.177	2.81E-2	5.61	0.178
-9	2.37E-2	5.93	0.168	2.41E-2	5.90	0.169	2.45E-2	5.87	0.170
-6	1.97E-2	6.26	0.159	2.04E-2	6.21	0.161	2.06E-2	6.18	0.161
-3	1.70E-2	6.52	0.153	1.73E-2	6.48	0.154	1.75E-2	6.46	0.154
0	1.33E-2	6.91	0.144	1.36E-2	6.87	0.145	1.38E-2	6.84	0.146
3	1.05E-2	7.24	0.138	1.17E-2	7.10	0.140	1.19E-2	7.07	0.141
6	1.37E-2	6.86	0.145	1.45E-2	6.77	0.147	1.48E-2	6.74	0.148
9	1.67E-2	6.55	0.152	1.71E-2	6.50	0.153	1.76E-2	6.46	0.154
12	1.95E-2	6.28	0.159	2.01E-2	6.22	0.160	2.04E-2	6.20	0.161
15	2.38E-2	5.92	0.168	2.41E-2	5.90	0.169	2.43E-2	5.88	0.170

Table (B.14). BER, Q-factor, and EVM for DP-16QAM conventional multiple OPC for channels (1, 8, and 16)

Power	Channel one			Channel eight			Channel sixteen		
	BER	Q-factor	EVM	BER	Q-factor	EVM	BER	Q-factor	EVM
-15	2.44E-3	8.98	0.111	2.54E-3	8.94	0.111	2.57E-3	8.93	0.111
-12	2.12E-3	9.12	0.109	2.23E-3	9.07	0.110	2.26E-3	9.05	0.110
-9	1.73E-3	9.31	0.107	1.90E-3	9.22	0.108	1.95E-3	9.20	0.108
-6	1.59E-3	9.38	0.106	1.62E-3	9.37	0.106	1.68E-3	9.33	0.107
-3	1.36E-3	9.52	0.105	1.40E-3	9.50	0.105	1.45E-3	9.47	0.105
0	1.13E-3	9.69	0.103	1.20E-3	9.64	0.103	1.24E-3	9.61	0.104
3	9.91E-4	9.80	0.102	1.07E-3	9.73	0.102	1.10E-3	9.71	0.102
6	1.14E-3	9.68	0.103	1.25E-3	9.60	0.104	1.27E-3	9.58	0.104
9	1.32E-3	9.56	0.104	1.40E-3	9.50	0.105	1.45E-3	9.47	0.105
12	1.58E-3	9.45	0.105	1.54E-3	9.42	0.106	1.59E-3	9.38	0.106
15	1.65E-3	9.36	0.106	1.67E-3	9.34	0.107	1.71E-3	9.32	0.107

Table (B.15). BER, Q-factor, and EVM for DP-16QAM hybrid multiple OPC with DCF for channels (1, 8, and 16)

Power	Channel one			Channel eight			Channel sixteen		
	BER	Q-factor	EVM	BER	Q-factor	EVM	BER	Q-factor	EVM
-15	6.95E-4	10.09	0.099	7.22E-4	10.06	0.099	7.30E-4	10.05	0.099
-12	5.88E-4	10.22	0.097	6.18E-4	10.18	0.098	6.29E-4	10.16	0.098
-9	7.49E-4	10.34	0.096	5.11E-4	10.32	0.096	5.26E-4	10.30	0.097
-6	7.81E-4	10.52	0.095	4.28E-4	10.45	0.095	4.44E-4	10.42	0.095
-3	3.05E-4	10.69	0.093	3.51E-4	10.59	0.094	3.59E-4	10.57	0.094
0	2.53E-4	10.82	0.092	2.91E-4	10.72	0.093	3.02E-4	10.70	0.093
3	2.32E-4	10.88	0.091	2.51E-4	10.82	0.092	2.64E-4	10.78	0.092
6	2.41E-4	10.85	0.092	2.68E-4	10.78	0.092	2.79E-4	10.75	0.093
9	2.73E-4	10.77	0.092	3.00E-4	10.70	0.093	3.16E-4	10.66	0.093
12	3.06E-4	10.69	0.093	3.39E-4	10.62	0.094	3.52E-4	10.59	0.094
15	3.51E-4	10.59	0.094	3.81E-4	10.53	0.094	3.94E-4	10.51	0.095

Table (B.16). BER, Q-factor, and EVM for DP-16QAM hybrid multiple OPC with Raman for channels (1, 8, and 16)

Power	Channel one			Channel eight			Channel sixteen		
	BER	Q-factor	EVM	BER	Q-factor	EVM	BER	Q-factor	EVM
-15	17.85E-6	12.32	0.081	19.00E-6	12.29	0.081	19.48E-6	12.28	0.081
-12	13.83E-6	12.44	0.080	13.86E-6	12.42	0.080	14.88E-6	12.40	0.080
-9	10.35E-6	12.57	0.079	10.78E-6	12.55	0.079	11.14E-6	12.54	0.079
-6	8.17E-6	12.68	0.078	16.93E-6	12.67	0.078	8.81E-6	12.64	0.079
-3	6.28E-6	12.80	0.078	6.56E-6	12.78	0.078	6.82E-6	12.76	0.078
0	4.79E-6	12.91	0.077	5.02E-6	12.89	0.077	5.31E-6	12.87	0.077
3	3.70E-6	13.02	0.076	3.85E-6	13	0.077	4.11E-6	12.98	0.077
6	3.50E-6	13.04	0.076	3.64E-6	13.02	0.076	3.89E-6	13	0.077
9	4.89E-6	12.91	0.077	5.00E-6	12.90	0.077	5.25E-6	12.87	0.077
12	6.44E-6	12.78	0.078	6.62E-6	12.77	0.078	6.90E-6	12.75	0.078
15	7.69E-6	12.70	0.078	8.11E-6	12.68	0.078	8.49E-6	12.66	0.078

Table (B.17). BER, Q-factor, and EVM for SP-16QAM based CNN-NLC for channels (1, 8, and 16)

Power	Channel one			Channel eight			Channel sixteen		
	BER	Q-factor	EVM	BER	Q-factor	EVM	BER	Q-factor	EVM
-15	3.17×10^{-3}	8.72	0.114	2.19×10^{-3}	9.09	0.110	2.68×10^{-3}	8.89	0.112
-10	4.63×10^{-3}	8.30	0.120	2.19×10^{-3}	9.09	0.110	4.15×10^{-3}	8.42	0.118
-5	3.66×10^{-3}	8.56	0.116	2.19×10^{-3}	9.09	0.110	3.41×10^{-3}	8.64	0.115
0	1.46×10^{-3}	9.47	0.105	2.19×10^{-3}	9.09	0.110	7.32×10^{-4}	10.05	0.099
5	7.32×10^{-4}	10.05	0.099	7.32×10^{-4}	10.05	0.099	7.32×10^{-4}	10.05	0.099
10	7.32×10^{-4}	10.05	0.099	2.19×10^{-3}	9.09	0.110	7.32×10^{-4}	10.05	0.099
15	7.32×10^{-4}	10.05	0.099	2.19×10^{-3}	9.09	0.110	7.32×10^{-4}	10.05	0.099

Table (B.18). BER, Q-factor, and EVM for SP-64QAM based CNN-NLC for channels (1, 8, and 16)

Power	Channel one			Channel eight			Channel sixteen		
	BER	Q-factor	EVM	BER	Q-factor	EVM	BER	Q-factor	EVM
-15	6.83×10^{-3}	7.84	0.127	1.07×10^{-2}	7.23	0.138	2.31×10^{-2}	6.01	0.166
-10	4.63×10^{-3}	8.30	0.120	1.00×10^{-2}	7.33	0.136	1.87×10^{-2}	6.36	0.157
-5	3.17×10^{-3}	8.72	0.114	6.59×10^{-3}	7.88	0.126	1.53×10^{-2}	6.69	0.149
0	3.05×10^{-3}	8.88	0.112	5.85×10^{-3}	8.02	0.124	1.39×10^{-2}	6.84	0.146
5	7.32×10^{-4}	10.05	0.099	4.88×10^{-3}	8.24	0.121	8.78×10^{-3}	7.51	0.133
10	7.32×10^{-4}	10.05	0.099	7.32×10^{-4}	10.05	0.099	8.31×10^{-4}	9.94	0.100
15	7.32×10^{-4}	10.05	0.099	1.22×10^{-3}	9.63	0.103	1.22×10^{-3}	9.63	0.103

Table (B.19). BER, Q-factor, and EVM for SP-16QAM based NARX-NLC for channels (1, 8, and 16)

Power	Channel one			Channel eight			Channel sixteen		
	BER	Q-factor	EVM	BER	Q-factor	EVM	BER	Q-factor	EVM
-15	7.32×10^{-4}	10.05	0.099	1.07×10^{-2}	7.23	0.138	2.24×10^{-2}	6.04	0.165
-10	7.32×10^{-4}	10.05	0.099	1.02×10^{-2}	7.30	0.136	1.90×10^{-2}	6.33	0.157
-5	7.32×10^{-4}	10.05	0.099	7.32×10^{-3}	7.75	0.129	1.85×10^{-2}	6.38	0.156
0	7.32×10^{-4}	10.05	0.099	6.83×10^{-3}	7.83	0.127	1.51×10^{-2}	6.71	0.149
5	1.22×10^{-4}	11.28	0.088	1.52×10^{-4}	11.15	0.089	7.32×10^{-4}	10.05	0.099
10	7.32×10^{-4}	10.05	0.099	3.41×10^{-3}	8.64	0.115	6.34×10^{-3}	7.93	0.126
15	7.32×10^{-4}	10.05	0.099	4.39×10^{-3}	8.36	0.119	7.32×10^{-3}	7.75	0.129

Table (B.20). BER, Q-factor, and EVM for SP-64QAM based NARX-NLC for channels (1, 8, and 16)

Power	Channel one			Channel eight			Channel sixteen		
	BER	Q-factor	EVM	BER	Q-factor	EVM	BER	Q-factor	EVM
-15	4.63×10^{-3}	8.30	0.120	2.75×10^{-2}	5.65	0.176	4.73×10^{-2}	4.46	0.224
-10	3.41×10^{-3}	8.64	0.115	1.83×10^{-2}	6.39	0.156	3.27×10^{-2}	5.30	0.188
-5	1.46×10^{-3}	9.47	0.105	1.07×10^{-2}	7.23	0.138	1.78×10^{-2}	6.44	0.155
0	7.32×10^{-4}	10.05	0.099	3.90×10^{-3}	8.49	0.117	6.59×10^{-3}	7.88	0.126
5	7.32×10^{-4}	10.05	0.099	7.32×10^{-4}	10.05	0.099	7.32×10^{-4}	10.05	0.099
10	5.34×10^{-4}	10.29	0.097	7.47×10^{-4}	10.03	0.099	7.32×10^{-4}	10.05	0.099
15	7.32×10^{-4}	10.05	0.099	1.46×10^{-3}	9.47	0.105	1.46×10^{-3}	9.47	0.105

الخلاصة

نمت الاتصالات الضوئية بشكل ملحوظ بسبب ارتفاع معدلات البيانات ومسافات الإرسال الطويلة. البنية التحتية الحالية للألياف تحد من الأداء، وتتطلب تكنولوجيا جديدة لتلبية الطلب المستقبلي. يمكن لاستراتيجية التخفيف من ضعف الألياف أن تزيد من سعة شبكة الاتصالات الضوئية وتقلل من معدل خطأ البت.

ركزت هذه الأطروحة على التعويض في اللاخطية متعددة القنوات باستخدام تقنية تعدد الإرسال بتقسيم الطول الموجي الكثيف مع تباعد بين القنوات يبلغ 50 جيجا هرتز.

تنقسم الأطروحة إلى قسمين رئيسيين على أساس تقنية التعويض المستخدمة. في الجزء الأول، تمت دراسة اقتران الطور في الألياف غير الخطية لتكوينين مختلفين؛ عملية اقتران الطور البصري (OPC) المتوسط والمتعدد. تم التحقيق في هذا العمل باستخدام ثلاث طرق؛ تقليدي، هجين مع ألياف تعويض التشتت، وهجين مع مضخم رامان. في الجزء الثاني، تم استخدام أسلوب التعلم الآلي بالاعتماد على خوارزميتين عصبيتين مختلفتين؛ الشبكة العصبية التلافيفية (CNN) والانحدار التلقائي غير الخطي مع المدخلات الخارجية (NARX).

أظهرت النتائج أن OPC الهجين مع مضخم رامان هو الأمثل لمسافة تزيد عن 800 كم وأن OPC المتعدد أفضل من المتوسط لستة عشر قناة. يمكن أن يصل عامل جودة الاشارة إلى 12.29 ديسيبل بمعدل نقل بيانات كلي يبلغ 800 جيجابت/ثانية لنظام تضمين نوع (DP-NRZ-OOK). أدى استخدام (SP-8QAM) بمعدل بيانات 1.72 تيرا بايت/ثانية إلى زيادة جودة الإشارة، حيث وصل معدل الخطأ في البت إلى 1.3×10^{-3}. وأخيرًا، حققت طريقة التعويض (DP-16QAM) بمعدل 3.58 تيرابايت/ثانية زيادة قدرها 5 ديسيبل في قوة الإطلاق وعامل جودة قدره 13 ديسيبل.

في المقابل، أظهرت نتائج الشبكات العصبية أن خوارزمية NARX تتفوق على CNN في المعالجة والأداء وسهولة التدريب على مسافة تزيد عن 5000 كم بمعدل بيانات (16×120) جيجابت/ثانية. خوارزمية NARX حسنت عامل الجودة ومعدل الخطأ في البت إلى 11.15 ديسيبل و10^{-6} في SP-16 QAM وفي SP-64 QAM إلى 10.29 ديسيبل و10^{-4} متجاوزًا تصحيح الخطأ المسماة (HD-FEC).

تم تنفيذ المحاكاة الضوئية باستخدام برنامج Optisys (V.19) وتم تنفيذ ومحاكاة خوارزميات الذكاء الاصطناعي باستخدام MATLAB (V.2022b). وتم ربط البرنامجين باستخدام المحاكاة المشتركة للتأكد من صحة النتائج التي تم الحصول عليها.

جمهورية العراق

وزارة التعليم العالي والبحث العلمي

جامعة بابل / كلية الهندسة

التعويض البصري في الألياف الضوئية اللاخطية في نظام فائق السعة

أطروحة

مقدمة إلى كلية الهندسة في جامعة بابل

كجــزء من متطلبات الحصول على درجة الدكتوراه فلسفة في الهندسة / الهندسة الكهربائية / الكترونيك واتصالات

من قبل

علي حيدر عبد الكريم عبد الرضا

بإشراف

الأستاذ الدكتور إبراهيم عبد الله مرداس

تشرين الأول 2023 ***ربيع الأول 1445***